Modélisation des particules organiques dans l'atmosphère

Florian Couvidat

Cerea

Centre d'Enseignement et de Recherche en Environnement Atmosphérique

Thèse de doctorat de l'Université Paris-Est

Présentée et soutenue publiquement le 15 novembre 2012 par

Florian COUVIDAT

pour l'obtention du diplôme de docteur
de l'Université Paris-Est

Spécialité : Sciences et techniques de l'environnement

Modélisation des aérosols organiques dans l'atmosphère

Jury composé de

Dr Céline Mari	LA, Université Paul Sabatier	Examinatrice et présidente du jury
Pr Anne Monod	LCE, Université Aix-Marseilles	rapporteur
Pr Spyros Pandis	Carnegie Mellon University, USA and University of Patras, Greece	rapporteur*
Dr Isabelle Coll	LISA, Université Paris-Est	examinatrice
Dr Nathalie Poisson	ADEME	invitée
Dr Karine Sartelet	CEREA, École des Ponts ParisTech	Invitée
Pr Christian Seigneur	CEREA, École des Ponts ParisTech	directeur de thèse

* Absent de la soutenance

Remerciements

Je remercie en premier lieu l'École des Ponts ParisTech et l'Agence De l'Environnement et de Maîtrise de l'Énergie pour avoir financé cette thèse et sans qui cette thèse n'aurait pas été possible.

Je remercie très fortement Christian Seigneur pour m'avoir offert ce sujet qui s'est révélé prenant et passionnant et pour m'avoir dirigé pendant ces trois ans. J'ai pu apprécier sa grande disponibilité malgré son activité bouillonnante, ses qualités scientifiques et la confiance qu'il m'a accordée. Tout cela a fait que ma thèse s'est déroulée dans des conditions optimales et je l'en remercie profondément.

Je remercie également Karine Sartelet pour le grand intérêt et la curiosité qu'elle a portés à mes travaux et c'est avec grand plaisir que je les continue avec elle sur les suites de cette thèse.

Je remercie les membres du jury : Spyros Pandis pour avoir été relu cette thèse et qui n'a malheureusement pas pu se déplacer pour ma soutenance ; Anne Monod pour avoir accepté à la fois d'être rapporteur de cette thèse, mais aussi d'être membre de tous les comités de pilotages et avoir ainsi apporté des commentaires très utiles ; Céline Mari, examinatrice et présidente du jury, pour avoir fait le déplacement depuis Toulouse pour assister à la soutenance ; Isabelle Coll, examinatrice avec qui j'ai eu le plaisir de travailler et avec qui j'espère avoir des collaborations fructueuses et enfin Nathalie Poisson, ingénieur ADEME, pour avoir suivi l'évolution de cette thèse.

Je remercie Jean Sciare et Nicolas Marchand pour avoir participé à l'étude du chapitre 4 en apportant leurs commentaires sur les mesures utilisées dans cette partie. Je remercie Youngseob Kim pour toute l'aide qu'il m'a apportée durant cette thèse, Édouard Debry avec qui j'ai travaillé sur le module d'aérosols organiques et Antoine Waked pour les travaux que l'on a effectué ensemble sur le Liban.

Je remercie enfin la commande "activity" sous Linux testée par Régis Briant, Jérôme Drevet, Hilel Dergaoui et Marion Devilliers qui ont tous été impressionné par cet outil. Ce programme a permis entre autre le lancement du programme GITC testé par Laëtitia Girault en période d'essai de son contrat au CEREA avec les autres membres du laboratoire.

Je n'oublierai pas ces années passées au CEREA où des gens aux personnalités très différentes se sont côtoyés. Certains sont passés à l'ennemi, d'autres ne partiront jamais et une personne est revenue parce que c'est une vraie geek et qu'au fond, ça lui plait bien de travailler sur un ordinateur tant qu'il y a du café et tant que l'on peut se parler à travers la paroi. Je remercie tous ces gens (dans le désordre) : Yelva Roustan, Damien Garaud, Victor Winiarek, la

RATP (pour toutes les fois où je me suis fait snober par un RER), Pierre Tran, Sylvain Doré, Marc Bocquet (cherche désespérement le chocolat en poudre poulain ancienne recette), Bertrand Carissimo, Vivien Mallet, Nicolas Cherin (au fait, j'ai vu "les avengers" et je n'ai pas trouvé cela terrible), Elsa Real (source inépuisable d'informations sur la vie d'un labo même quand elle n'en fait plus partie), Eve Lecoeur (merci encore pour les quiches), Luc Musson Genon, Vincent Loizeau, Véronique Dehlinger, Jérôme Drevet (pour toutes les fois où on est allé manger au chinois après la muscu), Nicolas Yan, Laëtitia Girault (lovely bones), Nora Duhanyan (steak haché, frites), Régis Briant (dont Nora Duhanyan est secrètement amoureuse), Giuliana Becerra ("le bio, ça fait du bien"), Stéphanie Deschamps, Yiguo Wang , Masoud Fallah Shorshani, Marion Devilliers (chips !) et Hilel Dergaoui (adhérent UMP). Je remercie également tous mes amis, qui, de toutes façons, ne liront jamais ces remerciements. Juste une petite pensée pour Shaodong Zhang, un ami d'école d'ingénieurs : on aura finalement commencé et fini nos thèses les mêmes jours.

Je remercie aussi Bruno Sportisse, ancien directeur du CEREA, que je n'ai pas eu le plaisir de rencontrer, mais qui a heureusement une date de naissance très facile à se souvenir et feu Jean Bricard pour décorer mon bureau.

Je remercie tout particulièrement Irène Korsakissok qui trouvait que je ressemblais à un adolescent au début de ma thèse, commentaire qui fut suivi quelques jours après par celui d'une presque-inconnue qui pensait que j'avais plus de trente ans. Faut croire que pendant ces trois ans de thèse, j'ai vieilli de 12 ans soit une moyenne de quatres années de chercheur par années civiles. Si j'extrapole cette cinétique de vieillissement (en supposant la cinétique d'ordre zéro) et en supposant que l'âge de départ à la retraite reste de 62 ans, j'atteindrai un âge de chercheur suffisant pour partir à la retraite à l'âge de 33 ans.

Pour finir, un labo (ou la vie en général) c'est comme un aérosol qui se concentrerait autour d'un noyau. Il y a des arrivées (condensation) et des départs (évaporation) de gens avec des noms (formules chimiques) plus ou moins compliqués. Ces gens selon les affinités et les interactions avec les autres membres du labo peuvent rester plus ou moins longtemps et vieillir à l'intérieur du CEREA (oxydation). Une fois saturés, ils se volatilisent. Il y a même parfois séparation de phases, le CEREA est un bon exemple avec ses trois sites (phases) où les gens sont répartis selon leurs affinités, ces trois phases constituant la grosse particule qu'est le CEREA. Il y a même parfois un peu de gêne stérique à l'intérieur du RER pour rentrer chez soi et même réactions chimiques avec productions de nouvelles molécules qui viendront peut-être un jour alimenter le CEREA à condition que ce soit un choix par passion (réactivité). Car finalement, la recherche, c'est avant tout une histoire de passion : "dream life and live dream".

Résumé

La formation des aérosols organiques dans l'atmosphère est étudiée via le développement d'un nouveau modèle de formation d'aérosols organiques secondaires nommé H^2O (Hydrohilic/Hydrophobic Organics). Dans un premier temps, une paramétrisation de la formation d'aérosols via l'oxydation de l'isoprène est développée. Cette paramétrisation prend notamment en compte l'influence des concentrations d'oxydes d'azote sur la formation d'aérosols et leurs propriétés hydrophiles. Ensuite, H^2O incluant cette paramétrisation et d'autres développements est évalué par comparaison aux mesures de carbone organique sur l'Europe. Prendre en compte les émissions de composés semi-volatils primaires gazeux (qui peuvent former des aérosols organiques secondaires après oxydation ou se condenser lors de baisses de température) améliore les performances du modèle de manière significative. En revanche, si les émissions de ces composés ne sont pas prises en compte, il en résulte une très forte sous-estimation des concentrations d'aérosols organiques en hiver. La formation d'aérosols organiques secondaires sur l'Île-de-France durant la campagne d'été de Megapoli (juillet 2009) a aussi été simulée pour évaluer les performances du modèle en zone urbaine. H^2O donne de bons résultats sur l'Île-de-France bien que le modèle prévoit un pic d'aérosols organiques, provenant des émissions du trafic durant les heures de pointe, qui n'apparaît pas dans les mesures. La présence de ce pic dans les résultats du modèle peut être due à la sous-estimation de la volatilité des composés semi-volatils primaires. Il est aussi possible que les composés organiques primaires et les composés organiques secondaires ne se mélangent pas et que les composés semi-volatils primaires ne peuvent pas se condenser sur un aérosol organique majoritairement secondaire et très oxydé. Enfin, l'impact de la chimie aqueuse est étudié. Le mécanisme utilisé inclue notamment, la formation d'aérosols organiques secondaires dans la phase aqueuse des nuages par oxydation du glyoxal, du méthylglyoxal, de la méthacroleine et de la méthyl-vinyl-cétone, la formation de méthyltétrols dans la phase aqueuse des particules ou des gouttes d'eau des nuages et le vieillissement des aérosols organiques dans un nuage. L'impact des dépôts humides sur la formation d'aérosols est aussi étudié pour mieux caractériser l'impact des nuages sur les concentrations d'aérosols organiques.

Abstract

Organic aerosol formation in the atmosphere is investigated via the developpement of a new model named H^2O (Hydrohilic/Hydrophobic Organics). First, a parameterization is developped to take into account secondary organic aerosol formation from isoprene oxidation. It takes into account the effect of nitrogen oxides on organic aerosol formation and the hydrophilic properties of the aerosols. This parameterization is then implemented in H^2O along with some other developments and the results of the model are compaired to organic carbon measurements over Europe. Model performance is greatly improved by taking into account emissions of primary semi-volatile compounds, which can form secondary organic aerosols after oxidation or can condense when temperature decreases. If those emissions are not taken into account, a significant underestimation of organic aerosol concentrations occurs in winter. The formation of organic aerosols over an urban area was also studied by simulating organic aerosols concentration over the Paris area during the summer campaign of Megapoli (July 2009). H^2O gives satisfactory results over the Paris area, although a peak of organic aerosol concentrations from traffic, which does not appear in the measurements, appears in the model simulation during rush hours. It could be due to an underestimation of the volatility of organic aerosols. It is also possible that primary and secondary organic compounds do not mix well together and that primary semi volatile compounds do not condense on an organic aerosol that is mostly secondary and highly oxidized. Finally, the impact of aqueous-phase chemistry was studied. The mechanism for the formation of secondary organic aerosol includes in-cloud oxydation of glyoxal, methylglyoxal, methacrolein and methylvinylketone, formation of methyltetrols in the aqueous phase of particles and cloud droplets, and the in-cloud aging of organic aerosols. The impact of wet deposition is also studied to better estimate the impact of clouds on organic aerosol concentrations.

Table des matières

Chapitre 1

Introduction

Sommaire

1.1 Les particules atmosphériques

Les aérosols sont des particules sous forme de matière solide ou liquide en suspension dans l'atmosphère. Ces particules peuvent avoir un effet néfaste sur la santé (elles sont réglementées depuis 1997 aux États-Unis et la commission européenne a émis en 2008 une directive pour leur réglementation dans l'Union Européenne). Par ailleurs, ces particules ont un effet direct sur le climat par diffusion et absorption du rayonnement solaire et un effet indirect par le rôle que ces particules jouent dans la formation des nuages qui interceptent une partie du rayonnement solaire.

L'effet des particules sur la santé varie selon leur taille. En effet, les particules ayant un diamètre supérieur à 10 μm sont peu susceptibles de pénétrer dans le système respiratoire. Les particules ayant un diamètre supérieur à 2.5 μm ($PM_{2.5}$) pénètrent plus difficilement dans le système respiratoire que les particules ayant un diamètre inférieur à 2.5 μm. Ces dernières pénètrent profondément dans le système respiratoire jusque dans les poumons où elles peuvent causer des problèmes respiratoires, des irritations, des inflammations et des cancers. Elles peuvent aussi franchir la barrière physiologique et atteindre d'autres organes. Pour ces raisons, les législations sur les particules portent sur les $PM_{2.5}$ et sur les particules ayant un diamètre inférieur à 10 μm (PM_{10}).

1.1.1 Réglementations des particules

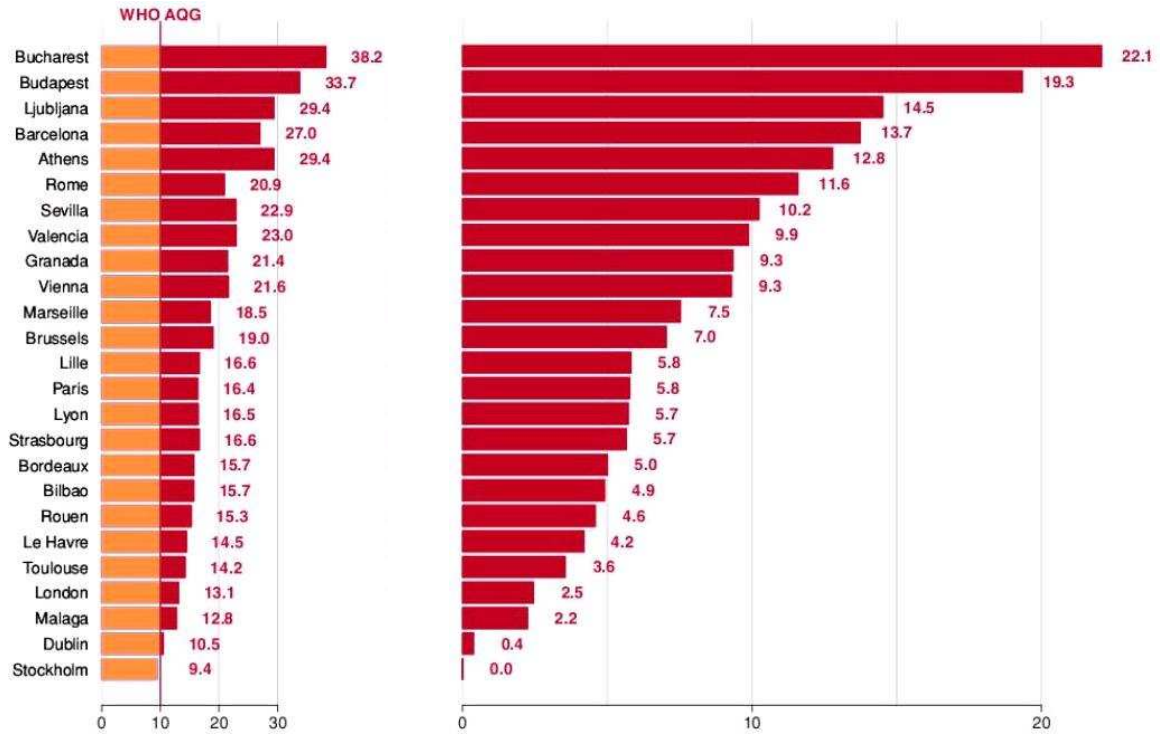

Concentrations annuelles de $PM_{2.5}$ Gain d'espérance de vie (en mois)

FIGURE 1.1 – Concentrations annuelles de $PM_{2.5}$ et gain d'espérance de vie pour une personne de 30 ans si la recommandation de l'OMS (concentration annuelle de $PM_{2.5}$ inférieure à 10 $\mu g.m^{-3}$) était respectée sur 25 des plus grandes villes européennes. Source : *Aphekom* [2011].

Pour minimiser l'effet des particules sur la santé, l'organisation mondiale de la santé (OMS)

recommande que les concentrations annuelles de particules ne dépassent pas 20 μg.m^{-3} pour les PM_{10} et 10 μg.m^{-3} pour les $PM_{2.5}$, et que les concentrations journalières ne dépassent pas 50 μg.m^{-3} plus de 3 jours par an pour les PM_{10} et 25 μg.m^{-3} plus de 3 jours par an pour les $PM_{2.5}$. Cependant, la plupart des grandes villes européennes ne respectent pas les recommandations de l'OMS comme le montre la figure 1.1. Seule Stockholm est en dessous de la valeur guide de l'OMS.

Les valeurs limites pour les effets sanitaires fixées par les réglementations de l'Union Européenne et des États-Unis sont encore bien supérieures aux recommandations de l'OMS. Le tableau 1.1 montre les valeurs limites à ne pas dépasser dans les pays de l'Union Européenne et aux États-Unis. Les valeurs fixées pour les États-Unis sont valables pour des stations de fond urbain ou suburbain (stations en milieu urbain mais éloignées des sources de pollution) alors que celles fixées pour l'Union Européenne sont aussi valables pour les stations de proximité des sources (par exemple proche d'une route).

Actuellement, la France ne respecte pas les réglementations européennes fixées pour les concentrations de PM_{10} (source : europa.eu). Les réglementations de $PM_{2.5}$ n'entrant en vigueur qu'à partir de 2015, mais certaines stations en bordure de route dépasseraient la valeur limite. Pour respecter les réglementations européennes et se rapprocher des recommandations de l'OMS, il est nécessaire de bien comprendre les processus de formation de particules et leurs origines pour pouvoir évaluer efficacement les politiques de réduction des émissions.

Polluant	Zone géographique	Durée de Prélévement	Concentration
PM_{10}	Union Européenne	1 an	40 μg.m^{-3} [a]
		1 jour	50 μg.m^{-3} [a]
	États-Unis	1 jour	150 μg.m^{-3} [b]
$PM_{2.5}$	Union Européenne	1 an	25 μg.m^{-3} en 2015 [a] 20 μg.m^{-3} en 2020 [a]
	États-Unis	1 an	15 μg.m^{-3} [b]
		1 jour	35 μg.m^{-3} [b]

a) Concentrations aux stations de fond et à proximité des sources.
b) Concentrations aux stations de fond.

TABLE 1.1 – Valeurs limites pour les effets sanitaires dans les pays de l'Union-Européenne (Directive européenne transcrite dans le code de l'environnement) aux États-Unis (Clean Air Act et réglementations de l'U.S. Environmental Protection Agency

1.1.2 Les impacts des particules

En plus des impacts sur la santé, les particules ont aussi un impact sur la visibilité, sur la détérioration du bâti et sur le climat.

La dégradation de la visibilité peut être perçue comme un indicateur de la mauvaise qualité de l'air et possède donc un effet esthétique nocif qui peut porter préjudices aux activités touristiques. Cette baisse de visibilité (ou de la portée visuelle) est due à la capacité des particules fines d'absorber (notamment le carbone suie) et de diffuser le rayonnement lumineux qui rend ainsi plus difficile de distinguer les objets à distance.

L'impact des dépôts de particules sur le bâti se traduit par l'apparition de salissures qui détériorent l'aspect esthétique des bâtiments voire même fragilisent l'édifice. La formation de ces salissures a donc un coût économique car la restauration et le traitement chimique du bâtiment peuvent s'avérer nécessaires.

Les particules ont enfin un effet direct et un effet indirect sur le climat. L'effet direct est dû aux propriétés radiatives des particules qui peuvent absorber ou diffuser le rayonnement lumineux selon la composition chimique de la particule. L'effet indirect est dû aux propriétés hygroscopiques (faculté à absorber de l'eau) des particules qui peuvent mener à la formation de nuages. Les particules influencent donc la distribution granulométrique des gouttelettes des nuages et, par conséquent, les propriétés radiatives et la durée de vie de ces nuages. De manière générale, selon le Groupe d'experts intergouvernemental sur l'évolution du climat (GIEC), les effets direct et indirect des particules auraient tendance à refroidir le climat (voir Figure 1.2). Les particules sont la première source d'incertitude sur l'évolution du climat et il est nécessaire d'améliorer les connaissances sur la composition des particules et leurs propriétés radiatives et hygroscopiques pour améliorer notre connaissance sur l'évolution du climat.

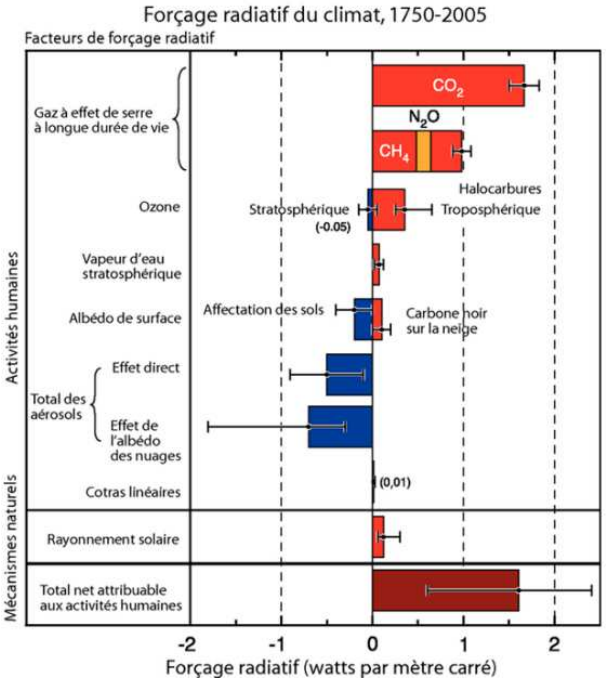

FIGURE 1.2 – Facteurs influençant le forcage radiatif du climat (pour les années 1750 à 2005). Source : GIEC.

1.1.3 Composition et origine des particules

Les particules sont constituées de composés primaires (qui sont directement émis sous forme de particules) et de composés secondaires (formés par réactions chimiques dans l'atmosphère). Les sels marins, les poussières minérales, le carbone élémentaire sont des particules primaires. Les particules de sulfate (formées par l'oxydation du dioxyde de soufre), de nitrate (formées par l'oxydation du dioxyde d'azote) et d'ammonium (formées par condensation de l'ammoniac émis dans l'atmosphère) sont d'origine secondaire. Les particules atmosphériques peuvent également être d'origine anthropique (provenant des activités humaines) ou d'origine naturelle comme les sels marins, les particules émises par les volcans ou les particules d'origine biogénique (provenant des émissions de la végétation). Les sources de particules sont donc nombreuses et diverses. La

composition des $PM_{2.5}$ sur un site de fond urbain et un site de fond rural de la région parisienne est présentée dans la figure 1.3.

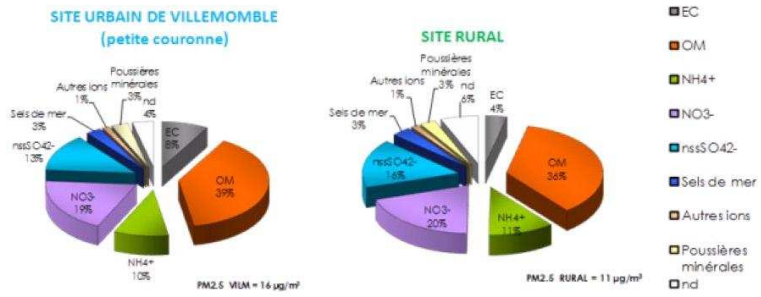

FIGURE 1.3 – Composition des $PM_{2.5}$ sur un site de fond urbain et un site de fond rural de la région parisienne (source : *Airparif* [2011])

Les particules organiques constituent une fraction significative des $PM_{2.5}$ (environ 35% des $PM_{2.5}$ en région parisienne). Elles sont à la fois d'origine primaire et d'origine secondaire (composés formés par l'oxydation de nombreux composés organiques volatils émis dans l'atmosphère) et peuvent provenir à la fois de sources naturelles (notamment les sources biogéniques) et de sources anthropiques. La formation de la matière organique particulaire est donc complexe, elle peut provenir de sources locales (au niveau d'une ville) mais aussi de sources lointaines (matière organique provenant du transport sur de longues distances de particules).

1.1.4 Formation des aérosols organiques secondaires

La formation de matière organique particulaire dans l'atmosphère est due à la présence de composés organiques suffisamment peu volatils pour former des particules. On parle alors de composés semi-volatils si ces composés sont à la fois présents dans la phase gazeuse et la phase particulaire et de composés non-volatils s'ils sont entièrement dans la phase particulaire. Ces composés peu volatils peuvent être formés par l'oxydation des composés organiques volatils (COV) par les différents oxydants de l'atmosphère (l'ozone, les radicaux hydroxyle et nitrate) dans l'air ou dans la phase aqueuse des nuages.

Les précurseurs peuvent être d'origine anthropique comme les alcénes, les alcanes, les composés aromatiques, les hydrocarbures aromatiques polycycliques ou d'origine biogénique comme l'isoprène (le composé biogénique émis en plus grande quantité après le méthane), les monoterpènes, molécules constituées de deux blocs d'isoprène (comme l'α-pinène, le β-pinène ou le limonène), et les sesquiterpènes, molécules composées de trois blocs d'isoprène (comme l'humulène). Les COV biogéniques sont généralement issus de la photosynthèse. Les émissions de ces composés sont donc importantes quand celle-ci est favorisée, c'est-à-dire lorsque les températures et le rayonnement solaire sont élevés. Les émissions de COV biogéniques sont donc plus importantes en été. La formation d'aérosols organiques secondaires (AOS) biogéniques est donc favorisée en été.

L'oxydation des précurseurs peut être très complexe et dépend généralement du régime d'oxydation : oxydation par l'ozone, par les radicaux hydroxyles (HO) ou par les radicaux nitrates. De plus, selon que les concentrations d'oxydes d'azote NO_x sont faibles (on parle alors de régime bas-NO_x) ou élevées (régime haut-NO_x), les quantités d'aérosols formés peuvent être très différentes. La structure moléculaire des composés formés, d'où d'écoulent certaines propriétés physico-chimiques à prendre en compte, peut elle aussi être différente selon les concentrations de

NO_x. Par exemple dans le cas de l'oxydation d'un alcane, l'alcane réagira avec HO pour former un radical :

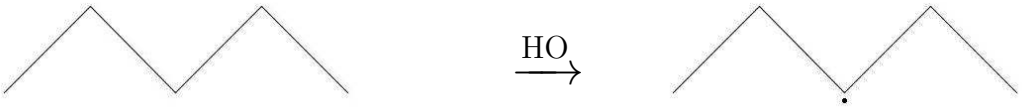

Si ce radical réagit avec le radical hydroperoxyle HO_2 (en régime bas-NO_x), il formera un hydroperoxide :

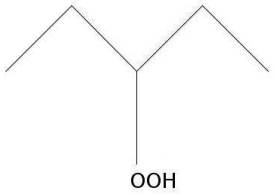

Si le radical réagit avec le monoxyde d'azote NO, il formera une cétone :

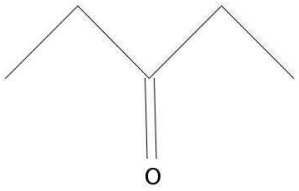

Les composés organiques semi-volatils présents en phase gazeuse peuvent aussi être oxydés pour former d'autres composés plus ou moins volatils, on parle alors de vieillissement. Une partie des composés formés peut être plus volatile, on parle alors de composés formés par fragmentation (le composé semi-volatil s'est séparé en plusieurs molécules de plus petites tailles). L'autre partie, moins volatile, est formée par functionnalisation (de nouveaux groupes fonctionnels se sont ajoutés à la molécule d'origine). Prendre en compte le vieillissement des composés semi-volatils peut être important, car cela influe sur la volatilité des composés (soit la capacité à former des aérosols) et leur degré d'oxydation (et donc la masse totale de l'aérosol).

1.2 Thermodynamique des aérosols organiques

La formation d'aérosols organiques est due à la présence de composés semi-volatils et non-volatils dans l'atmosphère. Pour bien représenter la formation des aérosols organiques, il est donc nécessaire de représenter le partage des composés semi-volatils entre la phase gazeuse et la phase particulaire. L'objectif de ce chapitre est de décrire les aspects thermodynamiques du partage de ces composés.

1.2.1 Cas général : Loi de Raoult et équilibre liquide-gaz

Les aérosols organiques sont formés par absorption de composés organiques de faibles volatilités dans une phase liquide qui peut aussi bien être organique ou aqueuse. La volatilité d'un composé peut être reliée à sa pression de vapeur saturante (pression partielle du composé à laquelle le gaz devient saturé, les molécules du composé en excès vont alors chercher à se condenser). Plus la pression de vapeur saturante d'un composé sera faible, moins le composé sera volatil et plus il

formera de masse particulaire. La pression de vapeur saturante d'un composé est un paramètre intrinsèque à un composé qui varie avec la température, le composé devenant moins volatil si la température diminue.

La quantité d'un composé dans l'aérosol peut être calculée à l'aide de la loi de Raoult qui relie les concentrations dans la phase liquide aux concentrations dans la phase gazeuse, en supposant ces deux concentrations à l'équilibre. La loi de Raoult s'écrit dans un cas général :

$$\gamma_{G,i}\left(P_i\right) P_i = \gamma_{L,i}\left(x_i\right) x_i P_i^0 \tag{1.1}$$

avec P_i la Pression partielle d'un composé i dans la phase gazeuse, x_i la fraction molaire du composé i dans la phase liquide, P_i^0 la pression de vapeur saturante du composé i, $\gamma_{G,i}$ le coefficient d'activité du composé dans la phase gazeuse et $\gamma_{L,i}$ le coefficient d'activité du composé dans la phase liquide.

Les coefficients d'activité caractérisent un écart à l'idéalité, l'idéalité étant un état de référence pour lequel un composé i interagit avec un composé j (force d'interaction F_{ij}) de la même manière que s'il interagissait avec lui-même (force d'interaction F_{ii}). Pour un mélange dit "idéal", on a donc :

$$F_{ij} = F_{ii} = F_{jj} \tag{1.2}$$

Pour un mélange idéal, les coefficients d'activité sont égaux à 1. En supposant la phase gazeuse et la phase liquide idéaux, la loi de Raoult s'écrit alors :

$$P_i = x_i P_i^0 \tag{1.3}$$

La pression partielle dans la phase gazeuse est alors directement proportionnelle à la fraction molaire du composé dans la phase liquide. Un exemple de mélange idéal est le mélange toluène-benzène. Comme le benzène et le toluène ont des structures moléculaires très similaires, les interactions entre le benzène et le toluène sont similaires aux interactions benzène-benzène et toluène-toluène d'où l'idéalité du mélange.

En pratique, dans l'atmosphère, la solution aqueuse ou organique des aérosols est rarement idéale, car elle résulte du partage de nombreux composés d'origines différentes et aux structures moléculaires variées. Cependant, dans les conditions atmosphériques, le mélange gazeux est idéal, car les interactions entre les différentes molécules de gaz sont très faibles contrairement à une phase liquide condensée. La notion de non-idéalité (solution qui s'écarte du comportement idéal) s'applique donc en chimie de l'atmosphère uniquement à la phase particulaire. La loi de Raoult s'écrira alors :

$$P_i = \gamma_i x_i P_i^0 \tag{1.4}$$

Plus γ_i est faible, plus le composé est stable dans la phase liquide et plus il a d'affinité avec les autres composés constituant la phase liquide. Au contraire, plus γ_i est élevé, plus le composé est instable et moins il a d'affinité avec les autres composés. Si γ_i est inférieur à 1, le composé est stabilisé par la présence de certains composés dans le mélange. Si γ_i est supérieur à 1, le composé est déstabilisé.

1.2.2 Absorption dans une phase organique : modèle de Pankow

Pankow [1994a] développa un modèle à partir de la loi de Raoult pour calculer le partage d'un composé organique entre la phase gazeuse et une phase organique. Ce modèle suppose que la matière organique particulaire est consituée d'une seule et unique phase bien qu'il soit possible que la matière organique particulaire soit constituée de plusieurs phases dans un mélange

complexe constitué de molécules ayant peu d'affinités entre elles. Pankow définit une constante de partage gas-particule $K_{p,i}$ tel que :

$$K_{p,i}M_o = \frac{A_{p,i}}{A_{g,i}} \tag{1.5}$$

avec $K_{p,i}$ en $m^3.\mu g^{-1}$, M_o la concentration de la phase organique en $\mu g.m^{-3}$, $A_{g,i}$ la concentration du composé i dans l'air et $A_{p,i}$ la concentration de i dans la phase organique.
En utilisant la loi de Raoult, on peut calculer la constante de partage du composé i de la manière suivante :

$$K_{p,i} = \frac{760 \times 8.202 \times 10^{-5} \times T}{M_{ow} \times \gamma_i \times 10^6 \times P_i^0} \tag{1.6}$$

avec $K_{p,i}$ en $m^3.\mu g^{-1}$, T la température en Kelvin, M_{ow} la masse molaire moyenne de la phase organique en $g.mol^{-1}$, γ_i le coefficient d'activité du composé i dans la phase organique et P_i^0 la pression de vapeur saturante du composé i en torr.

1.2.3 Absorption dans la phase aqueuse des particules : loi de Henry

On peut définir par analogie à la loi de Raoult, la loi de Henry pour calculer l'absorption d'un composé dans une phase aqueuse. Le partage d'un composé dans une phase aqueuse pure se fera selon la loi suivante :

$$C_i = H_i \times P_i \tag{1.7}$$

avec C_i la concentration de i dans la phase aqueuse, H_i la constante de Henry en $mol.L^{-1}.atm^{-1}$ et P_i la pression partielle de i. La loi de Henry est un cas particulier de la loi de Raoult s'appliquant à un composé infiniment dilué dans de l'eau (le composé i est uniquement entouré par des molécules d'eau et interagit uniquement avec celles-ci). En appliquant la loi de Raoult et la loi de Henry a un composé infiniment dilué dans l'eau, on obtient :

$$H_i = \lim_{C_i \to 0}(\frac{C_i}{P_i}) = \frac{\rho_{eau}}{M_{eau} \times \gamma_i^\infty \times P_i^0} \tag{1.8}$$

avec ρ_{eau} la masse volumique de l'eau en $g.L^{-1}$ (égal à 1000 $g.L^{-1}$ dans les conditions standards de température et de pression), M_{eau} la masse molaire de l'eau en $g.mol^{-1}$ (égal à 18 $g.mol^{-1}$), P_i^0 la pression de vapeur saturante du composé i (en atm) et γ_i^∞ le coefficient d'activité à dilution infinie dans l'eau qui correspond au coefficient d'activité du composé i entouré uniquement de molécules d'eau. On a donc :

$$\gamma_i^\infty = \lim_{x_i \to 0}(\gamma_i(x_i)) \tag{1.9}$$

Le coefficient d'activité à dilution infinie symbolise l'affinité d'un composé avec l'eau. La constante de Henry combine donc la pression de vapeur saturante symbolisant la volatilité du composé au coefficient d'activité à dilution infinie symbolisant l'affinité avec l'eau pour déterminer l'aptitude d'un composé à être absorbé dans une phase aqueuse. Pour être absorbé dans une phase aqueuse, un composé doit être peu volatil et/ou avoir une grande affinité avec l'eau.

Dans l'atmosphère, la phase aqueuse des particules n'est cependant pas pure et les composés absorbés dans la phase aqueuse ne sont pas infiniment dilués. On peut définir un coefficient d'activité ζ_i comme coefficient d'activité dans la phase aqueuse et comme écart à la dilution infinie :

$$\zeta_i = \frac{\gamma_i}{\gamma_i^\infty} \tag{1.10}$$

Dans le cas d'une phase aqueuse qui s'écarte de la dilution infinie, la loi de Raoult s'écrit alors :

$$C_i = \frac{H_i \times P_i}{\zeta_i} \tag{1.11}$$

De manière similaire au modèle de Pankow, on peut alors définir une constante de partage $K_{aq,i}$ d'un composé dans l'eau :

$$K_{aq,i}LWC = \frac{A_{aq,i}}{A_{g,i}} \tag{1.12}$$

avec $K_{aq,i}$ en $m^3.\mu g^{-1}$ LWC, la teneur liquide en eau en $\mu g.m^{-3}$, $A_{g,i}$ la concentration du composé i dans l'air et $A_{aq,i}$ la concentration de i dans la phase aqueuse. D'après la loi de Henry, la constante de partage $K_{aq,i}$ s'écrit alors :

$$K_{aq,i} = \frac{H_i \times R \times T}{\rho_{eau}\zeta_i \times 1.013 \times 10^{11}} \tag{1.13}$$

avec R la constante des gaz parfaits (égale à 8,314 $J.mol^{-1}.K^{-1}$).

1.2.4 Déplacement de l'équilibre : dissociation des acides et oligomérisation

Certaines réactions peuvent déplacer l'équilibre gaz-particule vers la formation de particules. Ce sont par exemple les équilibres de dissociation des acides dans une phase aqueuse et les réactions d'oligomérisation. On peut alors prendre en compte ces phénomènes pour la formation des particules en modifiant les constantes de partages.

Dans le cas d'un monoacide HA, l'équilibre de dissociation en ions A^- et H^+ s'écrit de la manière suivante :

$$[A^-] = K_a[HA]/[H^+] \tag{1.14}$$

avec K_a la constante de dissociation de l'acide (en $mol.L^{-1}$) et $[H^+]$, la concentration en proton. En nommant A_{tot} la concentration de l'acide dans la phase aqueuse (somme de HA et A-) et M la masse molaire de l'acide, on a :

$$\frac{A_{tot}}{A_g} = \frac{A_{aq}}{A_g} \times \left(1 + \frac{K_a}{[H^+]} \times \frac{M-1}{M}\right) = K_{aq,i}LWC \times \left(1 + \frac{K_a}{[H^+]} \times \frac{M-1}{M}\right) \tag{1.15}$$

De manière similaire pour un diacide ayant deux constantes de dissociation K_{a1} et K_{a1}, le partage gaz-particule s'écrira :

$$\frac{A_{tot}}{A_g} = K_{aq,i}LWC \times \left(1 + \frac{K_{a1}}{[H^+]} \times \frac{M-1}{M} + \frac{K_{a1}K_{a2}}{[H^+]^2} \times \frac{(M-1)(M-2)}{M^2}\right) \tag{1.16}$$

Dans le cas de l'oligomérisation, on définit une constante d'oligomérisation K_{oligo} telle que :

$$K_{oligo} = \frac{\text{masse d'oligomères}}{\text{masse de monomères}} \tag{1.17}$$

Le partage s'écrit alors :

$$\frac{A_{tot}}{A_g} = K_{p,i}M_o \times (1 + K_{oligo}) \tag{1.18}$$

Cette constante d'oligomérisation peut être plus ou moins complexe selon le mécanisme d'oligomérisation. Par exemple, dans le cas de l'oligomérisation en phase aqueuse des aldéhydes, *Pun et Seigneur* [2007] ont proposé la formule suivante pour la constante d'oligomérisation :

$$K_{oligo} = 0.1 \left(\frac{a(H^+)}{10^{-6}}\right)^{1.91} \tag{1.19}$$

avec $a(H^+)$ l'activité des ions H^+ dans la solution.

1.2.5 Effet de la température sur les constantes de partage

Il est important de prendre en compte l'effet de la température sur les constantes de partage des composés. En effet, un composé deviendra moins volatil si la température diminue et sera alors plus susceptible de former des particules. Généralement, une constante de partage est connue pour une température donnée. La valeur d'une constante de partage à une température T entre une phase gazeuse et une phase particulaire (aqueuse ou organique) peut être déterminée à partir de la constante de partage connue à une température de référence T_{ref} via la formule suivante :

$$\frac{K_p(T)}{K_p(T_{ref})} = \frac{T}{T_{ref}} \exp\left[\frac{\Delta H_{vap}}{RT}\left(\frac{1}{T} - \frac{1}{T_{ref}}\right)\right] \tag{1.20}$$

1.2.6 Calcul des coefficients d'activité

Les coefficients d'activité peuvent être calculés à l'aide de modèles thermodynamiques d'équilibre liquide-gaz. De nombreux modèles existent pour l'étude de systèmes binaires (comme le modèle de van Laar et le modèle de Margules) utilisant des paramètres d'interactions entre les composés généralement déterminés expérimentalement. Cependant, ces modèles thermodynamiques ne peuvent pas s'appliquer à des systèmes multi-composants avec des molécules chimiques qui ont rarement été étudiées. Pour calculer les coefficients d'activité dans un aérosol atmosphérique, il est donc nécessaire d'utiliser un modèle semi-prédictif qui pourra déterminer les coefficients d'activité des composés en fonction de leur structure chimique.

Le modèle le plus adapté à la modélisation des aérosols organiques est le modèle thermodynamique UNIversal Functional group Activity Coefficient (UNIFAC) [*Fredenslund et al.*, 1975]. Ce modèle découpe une molécule en groupes fonctionnels. À l'aide de paramètres d'interactions entre les groupes fonctionnels, UNIFAC estime les interactions entre les différents groupes présents et en déduit les interactions entre les différentes molécules. Une liste des paramètres d'UNIFAC pour de très nombreux groupes (alkyles, oléfines, aromatiques, carboxyliques, alcools, carbonyles, éther, amine et beaucoup d'autres groupes en plus du groupe H_2O pour les interactions avec les molécules d'eau) est disponible sur le site suivant :

http ://www.aim.env.uea.ac.uk/aim/info/UNIFACgroups.html

1.3 Les modèles de formation des particules organiques

1.3.1 Approche "Odum" : SORGAM

Les premiers modèles de formation d'aérosols organiques secondaires tels le modèle SORGAM (Secondary Organic Aerosol Model) utilisent une approche basée sur les constantes de partage. *Odum et al.* [1996a] décrivent une méthode pour développer des paramètrisations pour la formation d'aérosols organiques secondaires. Ils définissent la notion de rendement Y :

$$Y = \frac{\text{Masse d'aérosols formée}}{\text{Masse de précurseur oxydée}} \tag{1.21}$$

En supposant que la masse d'aérosol organique secondaire se forme par la condensation de n composés formés avec un rendement massique α_i qui se partagent entre gaz et particule selon le modèle de *Pankow* [1994a], le rendement peut s'écrire sous la forme suivante :

$$Y = \sum_{i=1}^{n} \frac{\alpha_i K_{p,i} M_o}{1 + K_{p,i} M_o} \tag{1.22}$$

Pour développer des paramètrisations, *Odum et al.* [1996a] proposent d'utiliser les résultats des expériences en chambre de simulation. Cela permet d'obtenir, pour l'oxydation d'un précurseur pour le régime d'oxydation étudié, le rendement en fonction de la masse d'organique M_o. On peut alors caler sur ces résultats les paramètres de l'équation (1.22), $K_{p,i}$ et α_i, en supposant que deux composés suppléants (composés utilisés pour représenter le comportement de l'aérosol) sont formés (n=2). Par exemple dans le cas de la formation d'aérosols organiques secondaires à partir de l'oxydation de l'α-pinène, *Odum et al.* [1996a] donne dans la figure 1.4 les courbes d'Odum (courbe du rendement en fonction de la masse d'organique) expérimentales et calées.

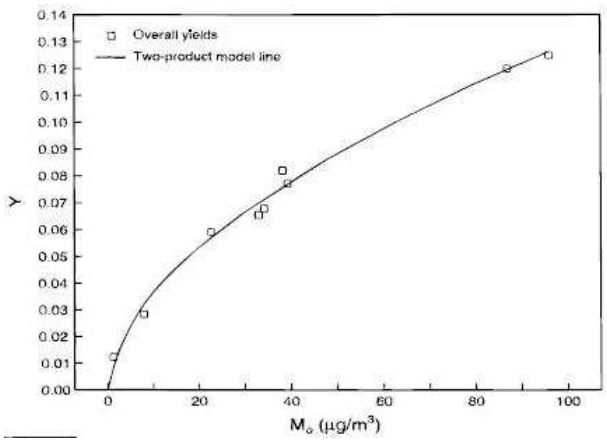

FIGURE 1.4 – Courbes d'Odum expérimentales calées pour l'oxydation de l'α-pinène (source : *Odum et al.* [1996a]).

SORGAM fut développé en utilisant cette méthodologie pour l'oxydation en régime haut-NO_x de certains précurseurs anthropiques (toluène, xylène, alcanes et alcènes à longues chaines) et biogéniques (les monoterpènes). Ce modèle est très simple, et pose plusieurs problèmes. Les constantes de partage calées sur les expériences dépendent du coefficient d'activité et de la masse molaire moyenne de la phase organique. Ces deux paramètres peuvent être très différents dans l'atmosphère et dans la chambre de simulation. Les coefficients d'activité des composés dans la chambre de simulation devraient être proches de 1, car les composés formés devraient avoir des structures similaires vu qu'ils proviennent de la même source. Dans l'atmosphère, la phase organique est constituée de composés venant de sources très diverses et avec des structures moléculaires pouvant être très différentes, les coefficients d'activité devraient dans ce cas être très différents de 1.

1.3.2 Approche "volatilité" : Volatility-Basis-Set (VBS)

VBS a été développé à l'origine pour prendre en compte le vieillissement des composés semi-volatils dans l'atmosphère. Ce modèle regroupe les composés qui ont des constantes de partage similaires et les regroupe en une seule espèce dans une même boîte de volatilité. Au lieu de caler deux constantes de partage et deux rendements massiques sur une courbe d'Odum pour bien représenter les expériences, les rendements massiques de chaque boîte de volatilité sont calés. Ce modèle estime donc les concentrations dans l'atmosphère de chaque boîte de volatilité. Pour prendre le vieillissement des composés semi-volatilité, ce modèle suppose qu'une oxydation donnera seulement des composés moins volatils (pas de fragmentation) et qu'une oxydation réduit d'un facteur 10 la volatilité (passage d'une boîte de volatilité à une autre). Le vieillissement est

schématisé par la figure 1.5.

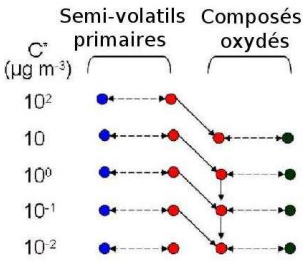

FIGURE 1.5 – Évolution des composés organiques semi-volatils primaires dans VSB (source : *Tsimpidi et al.* [2011]). C* est l'inverse de la constante de partage K_p.

VBS ne prend cependant pas en compte l'influence de la non-idéalité sur le partage des composés semi-volatils et le mécanisme de vieillissement des aérosols ne repose pas sur des résultats d'expèrience. En effet, la durée des expériences en chambre de simulation est de quelques heures à cause des dépôts sur les parois, ce qui ne permet pas d'étudier le vieillissement des composés semi-volatils. Par ailleurs, ce modèle suppose qu'il n'y a pas de fragmentation des molécules lors d'une oxydation. Cela peut conduire à une forte surestimation des concentrations d'aérosols organiques notamment dans le cas du vieillissement des monoterpènes où une surestimation du modèle par un facteur 2 à 3 est observée [*Donahue*, 2011].

1.3.3 Approche couplée volatilité-degré d'oxydation : "VBS-2D"

L'approche couplée volatilité-degré d'oxydation est une amélioration de l'approche précédente qui regroupe les composés ayant une volatilité similaire. Dans cette approche, les composés sont regroupés selon leurs volatilités et leurs degrés d'oxydation et, lors d'une oxydation, à la fois la volatilité et le degré d'oxydation d'un composé évoluent.

En ajoutant le degré d'oxydation, le VBS-2D permet par exemple de prendre en compte la non-idéalité de l'aérosol en évaluant les interactions entre un atome d'oxygène et un atome de carbone [*Donahue et al.*, 2011] et le pourcentage d'un composé organique semi-volatil qui subira une fragmentation [*Donahue*, 2011].

1.3.4 Approche moléculaire : AEC, MPMPO et H^2O

Dans l'approche moléculaire, la formation d'aérosols est représentée via des composés suppléants (composés choisis judicieusement pour représenter la formation d'aérosol) auxquels sont attachés des structures moléculaires. Cela permet de prendre en compte divers processus qui dépendent de la structure moléculaire des composés comme la non-idéalité de l'aérosol, l'absorption dans la phase aqueuse des aérosols, la dissociation des acides en phase aqueuse et l'hygroscopicité (absorption d'eau par l'aérosol).

AEC (AER/EPRI/Caltech) et H^2O (Hydrophylic Hydrophobic Organics, un modèle basé sur AEC qui a été développé durant cette thèse) sont des modèles qui utilisent l'approche moléculaire pour distinguer composés hydrophiles (c'est-à-dire composés qui se condensent principalement sur la phase aqueuse des particules) et composés hydrophobes (c'est-à-dire composés qui se condensent uniquement sur la phase organique des particules). Le modèle MPMPO [*Griffin et al.*, 2003] utilise une approche similaire, mais les composés peuvent se condenser à la fois sur la phase aqueuse et sur la phase organique. L'absorption dans la phase organique est alors calculée avec les équations 1.5 et 1.6 et l'absorption dans la phase aqueuse est calculée avec l'équation

1.11. Les coefficients d'activité doivent être calculés avec un modèle thermodynamique comme UNIFAC. Les concentrations d'eau particulaire et le pH de l'aérosol (nécessaire pour le partage des composés acides dans la phase aqueuse) doivent être calculées avec un modèle de formation d'aérosols inorganiques comme le modèle ISORROPIA [*Nenes et al.*, 1998].

C'est cette dernière approche qui sera utilisée ici pour modéliser les aérosols organiques.

1.4 Simulation des aérosols atmosphériques avec un logiciel de qualité de l'air

Pour simuler la formation d'aérosols organiques secondaires dans l'atmosphère, il est nécessaire d'implémenté un modèle de formation d'aérosols organiques dans un modèle de chimie transport pour déterminer la qualité de l'air. Ce type de modèle utilise différentes données comme les champs météorologiques (température, pression, direction du vent, rayonnement lumineux), les taux d'émissions des différents composés, les données d'occupation des sols, les conditions initiales (concentrations des composés au début de la simulation) et les conditions aux limites (concentrations aux bords du domaine) pour déterminer le transport et l'évolution chimique des composés gazeux et particulaires. Le modèle de formation d'aérosols doit de plus être couplé à un mécanisme chimique de la phase gazeuse, par exemple CB05 [*Luecken et al.*, 2008] ou RACM2 [*Goliff and Stockwell*, 2008] pour calculer les concentrations des oxydants et l'évolution chimique des précurseurs et à un modèle de dynamique des aérosols, par exemple SIREAM [*Debry et al.*, 2007a].

Les simulations 3D présentées dans cette thèse ont toutes été effectuées avec le modèle de qualité de l'air Polair3D/Polyphemus [*Mallet et al.*, 2007] utilisant l'approche eulérienne. Les données nécessaires pour effectuer une simulation avec Polyphemus sont présentées ci-dessous :

Les données d'utilisation des sols :

Les données de couverte du sol LUC (land use cover) déterminent le type de terrain dans une région donnée (régions urbaines, forêts, surfaces agricoles, étendues d'eau). Ces données sont nécessaires pour déterminer les vitesses de dépôts des composés et déterminer les émissions. Elles sont extraites des données USGS sur le monde entier (United States Geological Survey) et des données CORINE (Coordination of information on the environment) pour l'Europe.

Émissions anthropiques :

Les émissions anthropiques sont fournies par des cadastres d'émissions par classe d'activité économique. Ces cadastres d'émissions permettent de recenser l'ensemble des émissions gazeuses et particulaires d'une zone géographique avec leurs distributions spatiale et temporelle. En Europe, les émissions anthropiques sont fournies par le réseau EMEP (European Monitoring and Evaluation Program) sur un maillage de 50 km x 50 km. Pour des modélisations à petite échelle (résolution de quelques kilomètres), il faut des cadastres d'émissions plus fins avec des résolutions spatiales entre 1 et 5 km. En Île-de-France, le réseau AIRPARIF (Association agréée de surveillance de la qualité de l'air) fournit les émissions anthropiques avec une résolution spatiale de l'ordre de 1 km.

Émissions biogéniques :

Les émissions biogéniques peuvent être calculées avec un modèle d'émissions biogéniques comme le modèle MEGAN (Model of Emissions of Gases and Aerosols from Nature, *Guenther*

et al. [2006]) qui les détermine en fonction du rayonnement lumineux, de la température, du type de végétation et de l'indice de surface folaire (ratio de la surface totale supérieure des feuilles sur la surface du sol au-dessus de laquelle la végétation se développe).

Données météorologiques :

Ces données sont fournies par les modèles météorologiques et sont projetées sur le maillage du modèle de chimie-transport. Plusieurs variables météorologiques sont ainsi modélisées (par exemple la vitesse et direction du vent, la température, la pression, l'humidité et la hauteur de la couche limite). Les modèles météorologiques tel que WRF, ont besoin de données d'entrée de modèles globaux comme celles fournies par le National Centers of Environmental Prediction (NCEP) avec une résolution spatiale de 1 °.

Conditions aux limites :

Dans un modèle de chimie-transport (CTM), les concentrations de polluants aux limites du domaine (conditions aux limites) sont nécessaires pour connaître la composition chimique de l'air entrant dans le domaine. Les conditions aux limites sont obtenues grâce aux résultats de modèles de chimie-transport globaux comme MOZART (Model for OZone And Related chemical Tracers).

1.5 Objectifs et plan de la thèse

L'objectif est d'améliorer la représentation des particules organiques dans les modèles de qualité de l'air pour améliorer la prévision des concentrations de particules par les modèles, pouvoir effectuer des études d'impacts fiables (par exemple des études d'impacts des émissions dues au trafic routier ou à l'utilisation du chauffage au bois sur les concentrations de particules atmosphérique) et étudier l'efficacité des politiques de réductions des émissions sur la réduction des concentrations de particules. L'objectif est aussi d'étudier et de comprendre les processus influençant la formation de particules organiques : d'où proviennent les aérosols organiques ? L'aérosol organique est-il plutôt d'origine anthropique ou d'origine biogénique ? Est-il formé localement ou provient-il du transport de composés sur de longues distances ? Quels sont les phénomènes influençant la formation d'aérosols organiques ?

La thèse est composée de 4 parties :

Pour pouvoir bien modéliser la formation d'aérosols organiques, il est important de bien représenter la formation d'aérosols organiques secondaires venant des principaux précurseurs. Or, l'isoprène, le COV biogénique émis en plus grande quantité après le méthane, peut former après oxydation des aérosols, mais la seule paramétrisation précédemment développée ne prend pas en compte le fait que les aérosols formés par oxydation de l'isoprène ont une forte affinité avec l'eau. Ainsi, dans un premier temps, une nouvelle paramétrisation prenant en compte les propriétés hydrophiles des aérosols issus de l'oxydation de l'isoprène est développée et présentée dans le Chapitre 2.

Dans le Chapitre 3, cette paramétrisation est implémentée avec d'autres développements dans le modèle de formation d'aérosols organiques H^2O développé dans le cadre de cette thèse. Le modèle est ensuite évalué avec les données disponbles aux stations de mesure européennes en fond rural du réseau EMEP.

Dans le Chapitre 4, le modèle est évalué sur l'Île-de-France pour étudier la formation et l'origine de l'aérosol organique en zone urbaine ainsi que l'influence des coefficients d'activité

sur la condensation des composés organiques primaires semi-volatils émis par le trafic.

Dans le Chapitre 5, l'impact de la chimie de la phase aqueuse des nuages et des particules sur la formation d'aérosols (oxydation de certains COV dans les nuages, formation d'aérosols dans la phase aqueuse des particules, vieillissement des aérosols dans les nuages) et le dépôt des composés organiques solubles dans l'eau sont étudiés.

Un résumé des résultats de cette thèse et des perspectives pour des futurs travaux sont présentés dans le Chapitre 6.

Chapitre 2

Modélisation des aérosols organiques secondaires formés par oxydation de l'isoprène en conditions sèches et humides

Résumé

L'isoprène, composé organique volatil biogénique émis en plus grande quantité dans l'atmosphère après le méthane, a longtemps été considéré comme étant trop volatil pour former des aérosols organiques après oxydation [*Pandis et al.*, 1991]. Cependant, des études menées en Amazonie par *Claeys et al.* [2004] et par *Edney et al.* [2005] ont permis d'identifier des composés comme le méthyltétrol ayant le même squelette carboné que l'isoprène, ce qui a suggéré que l'isoprène peut, en fait, contribuer à la formation d'aérosols organiques. D'autres études en chambre de simulation (réacteur utilisé pour étudier l'oxydation de composés dans des conditions expérimentales proches des conditions atmosphèriques) ont ensuite confirmé la formation d'aérosols organiques secondaires par oxydation de l'isoprène. Ces études ont aussi montré que la formation d'aérosols est fortement liée aux concentrations d'oxydes d'azote (NO_x) et qu'elle est influencée par la formation d'oligomères [*Kroll et al.*, 2006; *Surratt et al.*, 2006].

Pour bien mo déliser la formation des aérosols organiques, il est important de bien représenter la formation d'aérosols organiques secondaires via l'oxydation des principaux précurseurs gazeux et donc de représenter la formation d'aérosols formés par oxydation de l'isoprène de manière aussi complète et détaillée que possible. Une première paramétrisation a été développée par *Henze et Seinfeld* [2006] pour prendre en compte la formation d'aérosols venant de l'isoprène. Cette paramètrisation suppose que des composés hydrophobes (qui se condensent uniquement sur une phase organique et ont peu d'affinités avec l'eau) sont formés alors que, d'après une étude de modélisation menée par *Pun* [2008], les composés formés par oxydation de l'isoprène ont une grande affinité avec l'eau et sont donc suceptibles de se condenser sur une phase aqueuse. De plus, cette paramètrisation ne prend pas en compte l'influence des concentrations d'oxydes d'azote sur la formation d'aérosols.

Le but de cette étude est de développer une nouvelle paramètrisation qui prend en compte les propriétés hydrophiles des aérosols et l'influence du régime d'oxydation. La formation d'aérosols sous trois régimes d'oxydation de l'isoprène est étudiée : oxydation par les radicaux nitrates, oxydation par les radicaux hydroxyles en régime bas-NO_x et en régime haut-NO_x. Pour développer

le modèle de formation d'aérosols, la chimie gazeuse de l'isoprène est simulée avec le mécanisme RACM2 (Regional Atmospheric Chemistry Mechanism, version 2) qui est modifié pour prendre en compte la formation d'aérosols organiques. Les différents paramètres sont calés par rapport à des expériences en chambre de simulation en conditions sèches (car peu d'études ont porté sur l'oxydation de l'isoprène en conditions humides). La paramètrisation est ensuite extrapolée aux conditions humides en prenant en compte les propriétés hydrophiles des aérosols.

Lorsque l'isoprène est oxydé par les radicaux nitrates, des organonitrates sont formés dont un composé trinitrate qui est ici utilisè comme composé suppléant. Le rendement de formation de ce composé et sa pression de vapeur saturante sont calés sur les résultats de *Ng et al.* [2008].

Lorsque l'isoprène est oxydé par les radicaux hydroxyles en régime bas-NO_x, *Kroll et al.* [2006] observent que la quantité d'aérosols formée augmente rapidement dans un premier temps puis atteint un maximum avant de diminuer fortement et d'atteindre un palier. De fortes concentrations d'aérosols sont donc formées de manière transitoire et une plus petite quantité est formée de manière "permanente". Un composé suppléant ayant la structure d'un dihydroxy-dihydroperoxide est utilisé pour prendre en compte la formation transitoire d'aérosols, en supposant que ce composé puisse être photolysé. Un autre composé suppléant ayant la structure d'un méthyltétrol est utilisé pour la formation "permanente" d'aérosols organiques. Les rendements de formations de ces composés, leurs pressions de vapeur saturante et la cinétique de photolyse du premier composé sont calés sur les résultats de *Kroll et al.* [2006].

En régime haut-NO_x, l'isoprène forme l'acide méthylglycerique et son dérivé nitrate [*Surratt et al.*, 2006]. *Surratt et al.* [2010] et *Chan et al.* [2010a] ont montré que ces deux composés sont formés par l'oxydation d'une molècule de type peroxyacétyl nitrate (PAN) provenant de l'oxydation de la méthacroléine (composé de premiére génération d'oxydation de l'isoprène). Il en résulte une dépendance complexe des concentrations de monoxide et de dioxide d'azotes, car le rapport de ces deux oxides d'azote influence fortement la concentration d'aérosols. Deux composés suppléants sont utilisés, l'un ayant la structure de l'acide méthylglycerique et l'autre ayant la structure du dérivé nitrate. Les rendements de formation de ces composés et leurs constantes de partage gas-particule prenant en compte l'oligomérisation (via estérification) de ces composés sont calés sur les résultats de *Kroll et al.* [2006] et de *Surratt et al.* [2006] sous différentes concentrations de monoxyde et de dioxyde d'azote, afin de bien représenter l'influence de ces oxydes sur la formation d'aérosols.

La paramètrisation étant basée sur des expériences en conditions sèches, la formation d'aérosols organiques est extrapolée aux conditions humides en estimant la constante de Henry des composés suppléants pour déterminer leur condensation sur la phase aqueuse des aérosols. La constante de Henry d'un composé peut être calculée avec la pression de vapeur saturante et le coefficient d'activité à dilution infinie (qui représente l'affinité du composé avec l'eau). Le coefficient d'activité à dilution infinie de chacun des composés a été estimé en utilisant le modèle thermodynamique UNIFAC, qui estime les coefficients d'activités en fonction de la structure moléculaire des composés.

Une fois, les constantes de Henry estimées, il est possible de déterminer si un composé est plutôt hydrophile (c'est-à-dire, il se condense principalement sur la phase aqueuse des particules) ou plutôt hydrophobe (c'est-à-dire, il se condense uniquement sur la phase organique des particules). En utilisant des concentrations représentatives de l'atmosphère d'isopréne, de particules aqueuses et d'aérosols organiques (avec une structure moléculaire représentative des composés primaires organiques), on détermine sur quelle phase un composé va se condenser. Le composé trinitrate formé par oxydation de l'isoprène par les radicaux nitrates et le dérivé nitrate formé en régime haut-NO_x sont des composés hydrophobes, peu susceptibles de se condenser sur la phase aqueuse des particules. En régime bas-NO_x, les composés formés sont très hydrophiles et se condensent seulement sur la phase aqueuse des particules. L'acide méthylglycérique semble

pouvoir se condenser sur les deux phases, mais se condensent principalement sur la phase aqueuse des particules.

Ce chapitre est constitué de :
Couvidat, F. et Seigneur, C. (2011). **Modeling secondary organic aerosol formation from isoprene oxidation under dry and humid conditions**, Atmos. Chem. Phys., 11 : 893-909.

Sommaire

Abstract

A new model for the formation of secondary organic aerosol (SOA) from isoprene was developed. This model uses surrogate molecular species (hydroxy-hydroperoxides, tetrols, methylglyceric acid, organic nitrates) to represent SOA formation. The development of this model used available experimental data on yields and molecular composition of SOA from isoprene and methacrolein oxidation. This model reproduces the amount of particles measured in smog chambers under both low-NO_x and high-NO_x conditions. Under low-NO_x conditions, the model reproduces the transitional formation of hydroxy-hydroperoxides particles, which are photolyzed and lead to SOA mass decrease after reaching a maximum. Under high-NO_x conditions, particles are assumed to be formed mostly from the photo-oxidation of a PAN-type molecule derived from methacrolein (MPAN). This model successfully reproduces the complex NO_x-dependence of isoprene oxidation and suggests a possible yield increase under some high-NO_x conditions. Experimental data correspond to dry conditions (RH $<$ 10 %). However, particles formed from isoprene are expected to be highly hydrophilic, and isoprene oxidation products would likely partition between an aqueous phase and the gas phase at high humidity in the atmosphere. The model was extended to take into account the hydrophilic properties of SOA, which are relevant under atmospheric conditions, and investigate the effect of particulate liquid water on SOA formation. An important increase in SOA mass was estimated for humid conditions due to the hydrophilic properties. Experiments under high relative humidity conditions should be conducted to confirm the results of this study, which have implications for SOA modeling.

2.1 Introduction

Atmospheric fine particles are known to have effects on health, atmospheric visibility, materials and climate. Among those particles, particulate organic matter (POM) represents a large fraction of the particulate mass, typically between 20 and 60% [*Kanakidou et al.*, 2005; *Yu et al.*, 2007; *Zhang et al.*, 2007a]. Those particles are either primary (directly emitted as particles) or secondary (particles formed by chemical reactions in the atmosphere). In the latter case, secondary organic aerosols (SOA) are formed by the gas-to-particle partitioning of the oxidation products of volatile organic compounds (VOCs). VOCs are emitted by both anthropogenic and biogenic sources. However, SOA formation is poorly understood due to the numerous and complex chemical phenomena involved (successive VOC oxidation steps, NO_x chemistry, compounds partitioning between several phases, SOA degradation, interactions between compounds in the particle, oligomerization).

The complexity of SOA formation makes chemical modeling of particulate matter (PM) difficult. To model SOA formation, most air quality models use simple parameterizations based on yields estimated from smog chamber measurements conducted under specific conditions, which can be different from atmospheric conditions (for example, oxidation under dry conditions). Those parameterizations rarely represent the effects of the NO_x level or oligomerization, whereas those effects have been shown to greatly affect the level of SOA predicted (e.g. *Ng et al.* [2007a,b]; *Pun and Seigneur* [2007]). Therefore, it is necessary to develop a parameterization that gathers all those phenomena.

Isoprene (2-methylbutadiene) is the biogenic VOC, which has the largest emission rate of all the non-methane VOCs, estimated at 600 $Tg.yr^{-1}$ [*Guenther et al.*, 2006]. Until recently, isoprene was believed not to be a major SOA precursor, despite its large emission flux, due in part to the high volatility of its first generation oxidation products such as methacrolein and methyl vinyl ketone [*Pandis et al.*, 1991]. Furthermore, some smog chamber studies initially showed that no significant aerosol growth was observed from isoprene photooxidation under high-NO_x

conditions [*Pandis et al.*, 1991]. However, during field studies in Amazonia, compounds like tetrols with the same carbon skeleton as isoprene were identified [*Claeys et al.*, 2004; *Edney et al.*, 2005], suggesting that isoprene could in fact contribute to SOA formation. SOA formation was then confirmed by several chamber studies and has been intensively investigated [*Kroll et al.*, 2006; *Surratt et al.*, 2006; *Ng et al.*, 2008; *Carlton et al.*, 2009; *Jang et al.*, 2002].

Therefore, it is important to take isoprene-SOA into account in air quality modeling. Chamber experiments led to the identification of species composing isoprene SOA like tetrols and methylglyceric acid [*Surratt et al.*, 2006; *Kleindienst et al.*, 2009]. As those products are rather small organic molecules (number of carbon atoms ≤ 5) and with numerous functional groups, they are expected to be highly hydrophilic. Then, those compounds would likely partition between an aqueous phase and the gas phase at high humidity in the atmosphere. It has been shown that taking into account the hydrophilic properties of isoprene SOA increases greatly the amount of SOA formed [*Pun*, 2008], whereas the parameterization of *Zhang et al.* [2007b] used currently in most air quality models does not take those effects into account.

The objective of this work is to develop a new model for the formation of SOA from isoprene, which takes into account NO_x chemistry, the hydrophilic properties of molecular species and oligomerization. First, a model is developed based on results from experiments conducted under dry conditions. Next, the model is extended to humid conditions by taking into account gas-aqueous phase partitioning.

2.2 Model development

2.2.1 Method

To develop the model for SOA formation from isoprene oxidation, the experimental results of *Kroll et al.* [2006] and *Surratt et al.* [2006] were used. Those experiments were done in the Caltech experimental chamber under both low-NO_x and high-NO_x conditions. A complete description of the facility is given by *Cocker III et al.* [2001]. The gas-phase chemistry was simulated with RACM2 [*Goliff and Stockwell*, 2008], which includes a mechanism for isoprene oxidation. This mechanism has been shown to perform well for oxidant formation [*Kim et al.*, 2009]. The mechanism was modified to take into account the formation of the surrogate species to represent SOA formation as described below. The ROS2 algorithm [*Verwer et al.*, 1999] was used to solve the chemical kinetic equations.

The experiments of *Kroll et al.* [2006] and *Surratt et al.* [2006] used blacklights, which emit in the ultraviolet between 300 and 400 nm with a maximum at 354 nm [*Kroll et al.*, 2006]. Under those conditions, nitrate radical (NO_3) and ozone (O_3) photolysis hardly occurs [*Carter et al.*, 2005] and their photolysis rates are almost negligible. The rate given by *Kroll et al.* [2006] was used for H_2O_2 photolysis, which leads to hydroxy radical (HO) formation in the chamber. As the evolution of isoprene concentrations as a function of time was in good agreement with the isoprene degradation observed by *Kroll et al.* [2006], we consider that the HO concentrations are correctly simulated by the gas-phase mechanism and the impact of HO concentrations was not studied. The photolysis rate for NO_2 photolysis was chosen so that the maximum ozone concentration matches the results from *Kroll et al.* [2006]. O_3, NO_3 and HONO photolysis rates were then calculated using the photolysis rates relative to NO_2 given by *Carter et al.* [2005].

As those experiments were done under dry conditions (RH $< 10\%$), partitioning between the gas phase and an organic liquid phase was assumed. The partitioning was calculated using the model of *Pankow* [1994a,b], which defines the absorption equilibrium constant ($K_{p,i}$) according to Raoult's law as :

$$K_{om,i} = \frac{F_{i,om}}{A_i \; M_o} = \frac{760 \; R \; T}{MW_{om} \; 10^6 \; \zeta_i \; p^o_{L,i}} \tag{2.1}$$

where A_i is the gas-phase concentration of compound i (ng.m^{-3}), $F_{i,om}$ is the concentration of the compound i in the absorbing organic phase (ng.m^{-3}), M_o is the absorbing organic mass concentration (μg.m^{-3}), R is the ideal gas constant (8.206×10^{-5} m^3.atm.mol^{-1}.K^{-1}), T is the temperature (K), MW_{om} is the mean molecular weight of the absorbing organic phase (g.mol^{-1}), ζ_i is the activity coefficient of compound i in the organic phase, and $p^o_{L,i}$ is the saturation vapor pressure of the absorbed compound (torr). The thermodynamic model UNIFAC (UNIversal Functional group Activity Coefficient) was used to calculate activity coefficients [*Fredenslund et al.*, 1975]. The missing UNIFAC parameters (for the functional groups nitrate and hydroperoxide) were taken from *Compernolle et al.* [2009]. An iterative method was used to calculate activity coefficients and the partitioning.

The effect of temperature was taken into account according to the Clausius-Clapeyron equation using enthalpies of vaporization. *Kleindienst et al.* [2009] measured the effective enthalpies of vaporization of SOA formed from isoprene oxidation for both low-NO_x and high-NO_x conditions. Those values were used in this study : a value of 38.4 kJ.mol^{-1} for compounds formed under low-NO_x conditions (tetrols, hydroxy-hydroperoxides) and a value of 43.2 kJ.mol^{-1} for compounds formed under high-NO_x conditions (methyl-glyceric acid, organic nitrates). The use of experimental effective enthalpies of vaporization instead of theoretically estimated values for specific SOA compounds is appropriate because SOA surrogates may represent a lumping of several individual compounds.

Stoechiometric coefficients of condensable products, saturation vapor pressure (for low-NO_x conditions), effective partitiong constant (for high-NO_x conditions) of the different surrogate species were selected to reproduce the results of experiments. The reactions added to RACM2 for SOA formation from isoprene are listed in Table 2.1. The first six reactions dominate under low-NO_x conditions whereas the last two reactions dominate under high-NO_x conditions. Propertes of surrogate species (molecular structure, saturation vapor pressures, molar mass and enthalpies of vaporization) are listed in Table 2.2.

The model development for SOA formation via oxidation of isoprene by NO_3 and HO is presented next. Although SOA formation occurs via oxidation of isoprene by O_3 [*Kamens et al.*, 1982; *Kleindienst et al.*, 2007; *Nguyen et al.*, 2010], this pathway was not taken into account here because of insufficient quantitative and mechanism information to develop a model at this point.

2.2.2 Oxidation of isoprene by NO_3

The results of *Ng et al.* [2008] were used to model oxidation of isoprene by NO_3. In their study, a C_5-hydroxy-trinitrate ($C_5H_9N_3O_{10}$) compound (structure of the compound shown in Table 2.2) was found to be predominant in the "typical experiment" of *Ng et al.* [2008] (experiment relevant to atmospheric conditions). Therefore, it was used as a surrogate compound for SOA formation for oxidation by NO_3.

Isoprene reacts with NO_3 to form the surrogate ISON in RACM2 (which groups all compounds formed from the oxidation of isoprene with NO_3) by this reaction :

$$ISO + NO_3 \Rightarrow ISON \tag{R 2.1}$$

(with a kinetic constant k = 6.61×10^{-13} molecule^{-1}.cm^3.s^{-1}). However, there is no oxidation of this compound by NO_3 in RACM2. The following reaction was added to RACM2 to take into

account the formation of C_5-hydroxy-trinitrate :

$$\mathrm{ISON} + \mathrm{NO_3} \Rightarrow ... \Rightarrow \alpha_{\mathrm{NO3}}\ \mathrm{C_5H_9N_3O_{10}} \qquad \text{(R 2.2)}$$

where α_{NO3} is the stoichiometric coefficient of the C_5-hydroxy-trinitrate. A kinetic constant of 7.0×10^{-14} molecule^{-1}.cm^3.s^{-1} was taken from *Rollins et al.* [2009].

The method of *Odum et al.* [1996a] with aerosol yields was used by *Ng et al.* [2008] with

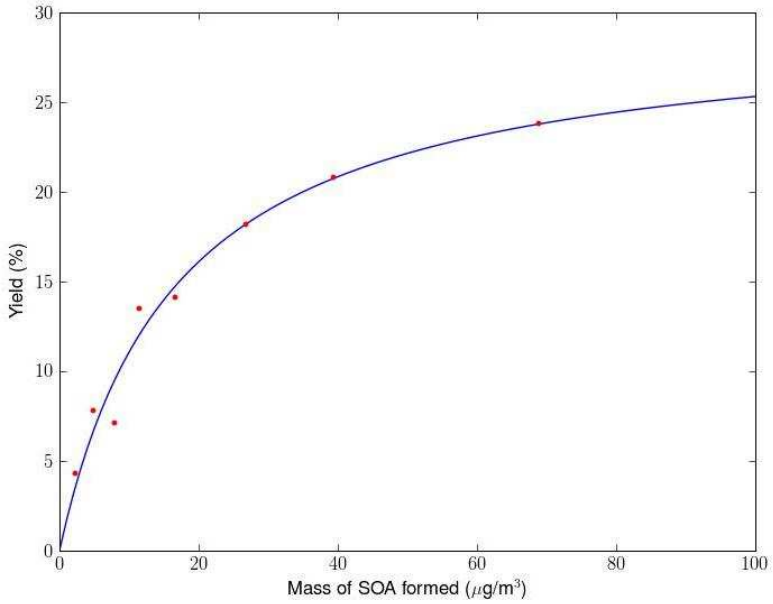

FIGURE 2.1 – SOA yield data and yield curve for isoprene-NO_3 reaction using one surrogate compound.

two surrogate compounds to estimate SOA formation parameters. Here, the same method was used but with only one surrogate compound because one surrogate compound is sufficient to reproduce the results of *Ng et al.* [2008] as shown in Fig. 2.1. A stoichiometric coefficient α_{NO3} of 0.074 was estimated with a saturation vapor pressure of 1.12×10^{-6} torr.

It should be noted that the formation of $C_5H_9N_3O_{10}$ may be a minor pathway for SOA formation in the atmosphere because there is probably not enough NO_3 in the atmosphere to form much C_5-hydroxy-trinitrate (C_5-dihydroxy-dinitrate is more likely). Reaction R2.2 could then overestimate SOA formation from ISON oxidation. However, this reaction could be used to deduce whether or not oxidation of isoprene by NO_3 can lead to a significant quantity of SOA. In this study, this reaction was used to make sure that NO_3 does not contribute significantly to SOA formation in environmental chambers.

2.2.3 Oxidation of isoprene by HO : Formation of methyl-tetrols and hydroxy-hydroperoxides under low-NO_x conditions

Methyl-tetrols and hydroxy-hydroperoxides are expected to be the two main compounds formed from the photo-oxidation of isoprene under low-NO_x conditions. Whereas tetrols have been explicitly identified in chamber experiments [*Kleindienst et al.*, 2009], the structure of hydroxy-hydroperoxides is still unknown and has not been conclusively identified [*Kroll et al.*, 2006]. Nevertheless, it is expected to be a key-component for SOA formation [*Kroll et al.*, 2006; *Surratt*

et al., 2006] and *Surratt et al.* [2006] confirmed that peroxides constitute a large fraction of SOA under low-NO_x conditions. Under the conditions of *Kroll et al.* [2006], the RO_2 (organic radical) chemistry is dominated by RO_2 + HO_2 reactions. Hydroxy-hydroperoxides are expected to be formed by those reactions. In RACM2, the formation of the radical (noted ISOP) from the oxidation of isoprene by HO can lead to the formation of first-generation hydroxy-hydroperoxides (noted ISHP) by the following chemical reactions :

$$\text{ISO} + \text{HO} \Rightarrow \text{ISOP} \tag{R 2.3}$$

$$\text{ISOP} + \text{HO}_2 \Rightarrow \text{ISHP} \tag{R 2.4}$$

However, the surrogate compound ISHP is too volatile to form SOA (the group contribution method SIMPOL.1 [*Pankow and Asher*, 2008] gives a saturation vapor pressure of 6.09×10^{-3} torr). Only one of the isoprene double bonds has been oxidized to form ISHP. If hydroxy-hydroperoxides SOA are formed, it can be assumed that ISHP is a key intermediate in their formation. So, it was assumed that hydroxy-hydroperoxides are formed from the oxidation of the ISHP double bond by HO and a subsequent RO_2 + HO_2 reaction :

$$\text{ISHP} + \text{HO} \Rightarrow ... \Rightarrow ... + \alpha\ \text{BiPER} + \beta\ \text{BiDER} \tag{R 2.5}$$

where BiPER is a dihydroxy-dihydroperoxide, which may undergo photolysis, BiDER is another product with structure unknown, which is not photolyzed, α and β are respectively the stoichiometric coefficients of BiPER and BiDER. Because of lack of data, molar mass and molecular structure of BiDER were assumed to be those of tetrols but the saturation vapor pressure was chosen to be different from the tetrol saturation vapor pressure in order to fit the experimental data (the sensitivity of the model to this assumption is investigated below). A rate constant of 3.0×10^{-11} molecule^{-1}.cm^3.s^{-1} was chosen for reaction R2.5 (kinetics supposed similar to the kinetics of the MACR + HO reaction in RACM2 [*Goliff and Stockwell*, 2008]).

TABLE 2.1 – Reactions and products added to RACM2.

Reactions	kinetic rate parameters (molecule^{-1}.cm^3.s^{-1})
ISHP + HO ⇒ ... + 0.28 BiPER + 0.030 BiDER	3.0×10^{-11}
2 ISOP ⇒ 2 MACR + HCHO + HO_2 + 0.16 DIOL	2.0×10^{-12}
ISOP + MO_2 ⇒ ... + 0.16 DIOL	3.40×10^{-14} exp(221/T)
ISOP + ACO_3 ⇒ ... + 0.16 DIOL	8.40×10^{-14} exp(221/T)
DIOL + HO ⇒ 0.16 BiMT + HO*	1.30×10^{-10}
ISON + NO_3 ⇒ 0.074 $C_5H_9N_3O_{10}$	6.61×10^{-13}
MPAN + HO ⇒ ... + 0.063 BiMGA + 0.046 BiNGA	3.20×10^{-11}

(*) Oxidant HO is added as both reactant and product in order not to modify HO prediction by RACM2.

After reaching a maximum, the SOA mass was observed to decrease rapidly in the experiments of *Kroll et al.* [2006] under low-NO_x conditions. The decrease stopped immediately when

TABLE 2.2 – Properties of the selected SOA surrogate species.

Surrogate species	Saturation vapor pressure (torr)	Molar Mass ($g.mol^{-1}$)	ΔH_{vap} ($kJ.mol^{-1}$)	Formula
BiMT	1.12×10^{-6} at 294 K	136	38.4	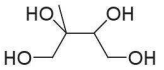
BiPER[a]	2.61×10^{-6} at 298 K[b]	168	38.4	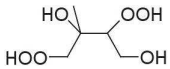
BiDER	4.1×10^{-7} at 298 K[b]	136[b]	38.4	unspecified
$C_5H_9N_3O_{10}$	1.12×10^{-6} at 294 K	271	38.4	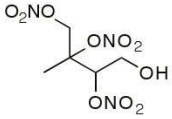
BiMGA	1.40×10^{-5} at 298 K[c]	120	43.2	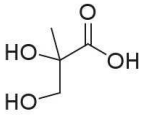
BiNGA	1.39×10^{-5} at 298 K[c]	165	43.2	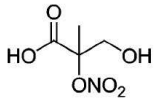

(a) Can undergo degradation due to photolytic reactions ($k_{degradation} = 2.0\times10^{-4}$ s^{-1}).
(b) Value obtained by using tetrols as BiDER structure. Results may change with an other structure (change mainly due to different molar mass, see text).
(c) Can undergo oligomerization. Calculated partitioning constant with this saturation vapor pressure has to be changed to take into account oligomerization with Equation 2.3. K_{oligo} = 64.2.

the lights were turned off. It indicates that the loss is due to photolytic activity and not to wall losses. To our knowledge, rapid loss of SOA has not been observed in the photo-oxidation of another compound.

The mechanism for SOA loss has not been completly elucidated. The loss of SOA could be due to either gas-phase reactions (consumption of the partitioning compounds may drive equilibrium away from the particle phase) or particle-phase reactions [*Kroll et al.*, 2006]. For example, SOA loss could be due to gas-phase reaction with HO or photolysis. *Kroll et al.* [2006] assumed that the compounds accountable for the rapid SOA loss may be organic hydroperoxides as this loss is only seen under low-NO_x conditions. The pathway by which this SOA loss occurs should be clarified (particle-phase reaction, gas-phase reaction, photolysis) by further experimental studies.

Because of the uncertainties of the SOA loss mechanism, modeling the loss by a global BiPER degradation kinetics (degradation into both particulate and gas phases) was chosen :

$$\text{BiPER} \Rightarrow \text{Unknown Products} \qquad \text{(R 2.6)}$$

Tetrols are assumed to be formed from the oxidation of diols which can be formed from RO_2 + RO_2 reactions. Under low-NO_x conditions, RO_2 + RO_2 reactions become predominant when concentrations of isoprene become high but can contribute slightly to SOA formation in *Kroll et al.* [2006]. RACM2 does not take into account the diol formation from isoprene. However, *Ruppert and Becker* [2000] give a yield for diol formation between 7.1% and 9.3%. A yield of

8.0% was assumed here. Based on data of *Ruppert and Becker* [2000], a rate constant for the oxidation of diols by HO of 13.0×10^{-11} molecule^{-1}.cm^3.s^{-1} was chosen. Under the conditions of *Ruppert and Becker* [2000], diols (noted here DIOL) can be expected to be formed from an ISOP + ISOP reaction, as follows :

$$2\ \mathrm{ISOP} \Rightarrow 2\ \mathrm{MACR} + \mathrm{HCHO} + \mathrm{HO_2} + 0.16\ \mathrm{DIOL} \qquad (\mathrm{R}\,2.7)$$

The ISOP + ISOP reaction has been taken from *Pöschl et al.* [2000] and DIOL formation was added to this reaction (the yield was multiplied by two because two radicals from isoprene react in this reaction). ISOP can also be oxidized by radicals MO_2 and ACO_3. The following reactions have been added to RACM2 :

$$\mathrm{ISOP} + \mathrm{MO_2} \Rightarrow ... + 0.16\ \mathrm{DIOL} \qquad (\mathrm{R}\,2.8)$$

$$\mathrm{ISOP} + \mathrm{ACO_3} \Rightarrow ... + 0.16\ \mathrm{DIOL} \qquad (\mathrm{R}\,2.9)$$

$$\mathrm{DIOL} + \mathrm{HO} \Rightarrow \gamma\ \mathrm{BiMT} + \mathrm{HO} \qquad (\mathrm{R}\,2.10)$$

where BiMT is the surrogate compound for tetrols and γ is the corresponding stoichiometric coefficient of BiMT. The group contribution method SIMPOL.1 gives similar saturation vapor pressures for tetrols and C_5-hydroxy-trinitrate. Accordingly, the saturation vapor pressure of tetrols was taken identical to that of C_5-hydroxy-trinitrate. A value for γ of 0.16 was used (assuming that the second oxidation has the same yield as the oxidation of the first double bond).

In the atmosphere, concentrations of ISOP are not typically sufficient for reaction R2.7 to be dominant. Inside environmental chambers, reactions R2.8 and R2.9 probably do not produce high quantity of DIOL due to the low concentrations of radicals MO_2 and ACO_3. However, those radicals are likely to be in higher concentrations in the atmosphere and BiMT could be formed by this pathway.

The stoichiometric coefficients α and β, the degradation rate of BiPER (reaction R2.6) and the saturation vapor pressures of BiPER and BiDER were selected to minimize the error between modeled and experimental results by a least square method for both maximal and final mass of SOA. A mean temperature of 25°C was assumed. However, to be able to solve the system, one of the parameters has to be set. According to *Kroll et al.* [2006], the SOA loss is about 0.006-0.018 min^{-1}. A mean value of 0.012 min^{-1} was then taken for reaction R2.6. Optimization gives the values of the parameters presented in Table 2.3. Results of the comparison between modeled and measured SOA formation are shown in Table 2.4 and Fig. 2.2. Fig.2.3a shows the results of a simulation for 63.6 ppb of isoprene.

The model reproduces well the results from *Kroll et al.* [2006] but there are still uncertainties, in particular in the mechanism for SOA degradation and in the values for the yield and the saturation vapor pressure of methyl-tetrols. Under the conditions of *Kroll et al.* [2006], tetrols only represent a small part of SOA (simulation for the oxidation of 63.6 ppb of isoprene gives 8% of tetrols). But tetrols would represent a larger fraction of SOA with a larger quantity of oxidized isoprene because the ISOP + ISOP reaction would then be competitive with the ISOP + HO_2 reaction. This is confirmed by a simulation done with 500 ppb where tetrols represent about 40% of SOA formed (Fig. 2.3b).

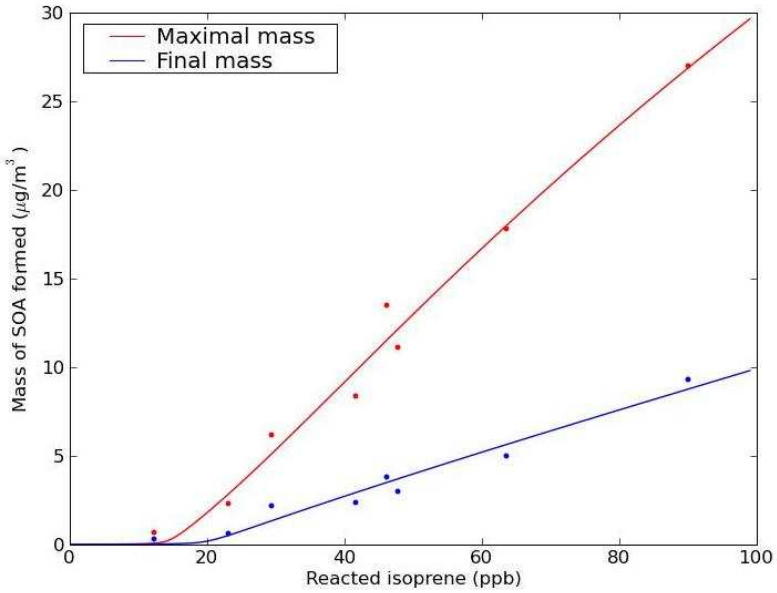

FIGURE 2.2 – SOA growth versus isoprene reacted. Dots correspond to measurements from *Kroll et al.* [2006]. Lines correspond to results from the model for T = 298 K.

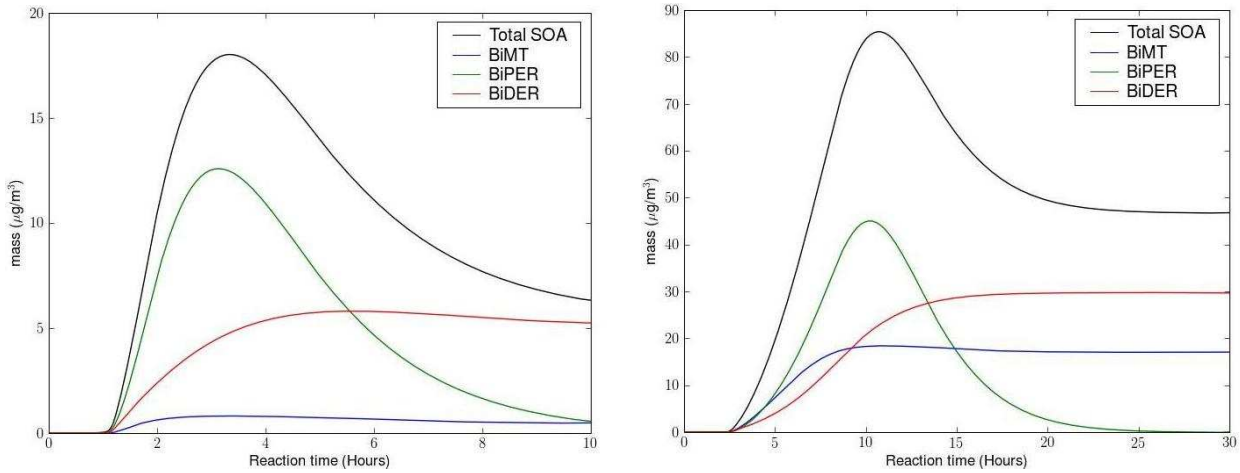

(a) Initial concentration of isoprene : 63.6 ppb (b) Initial concentration of isoprene : 500 ppb

FIGURE 2.3 – Evolution of the calculated mass of SOA formed from isoprene photooxidation as a function of time at T = 298 K (a) for an initial isoprene concentration of 63.6 ppb (b) for an initial isoprene concentration of 500 ppb.

2.2.4 Oxidation of isoprene by HO : Formation of methyl-glyceric acid under high-NO_x conditions

Under high-NO_x conditions, *Surratt et al.* [2006] showed that methyl-glyceric acid (MGA) and its nitrate derivative can oligomerize and form substantial amount of SOA. Recent studies showed that MGA is formed from the oxidation of MPAN (PAN-type molecule derived from the oxidation of methacrolein) [*Surratt et al.*, 2010; *Chan et al.*, 2010a] and that MGA strongly depends on the initial $[NO_2]/[NO]$ ratio (because MPAN formation is favored under high NO_2 conditions).

TABLE 2.3 – Values of the optimized parameters used for low-NO_x conditions at 298 K.

Parameter	Value
α	0.28
β	0.030
BiPER degradation	2.0×10^{-4} s^{-1}
BiPER saturation vapor pressure	2.6×10^{-6} torr
BiDER saturation vapor pressure	4.1×10^{-7} torr

To model SOA formation under high-NO_x conditions, we assumed that SOA formation comes mainly from MGA and its nitrate derivative formation via MPAN oxidation. Currently, there is not enough information to distinguish MGA formation from its nitrate derivative formation in the model. However, experiments by *Surratt et al.* [2006] show that the two molecules are formed in equivalent quantities when isoprene is oxidized under high-NO_x conditions. We assumed that MPAN oxidation leads to the same overall mass (particle + gas) of MGA and its nitrate derivative. It means that there is 1.375 (molecular weight ratio of the two compounds) times as much MGA as nitrate :

$$\text{MPAN} + \text{HO} \Rightarrow ... + 1.375\ \lambda\ \text{BiMGA} + \lambda\ \text{BiNGA} \qquad \text{(R 2.11)}$$

where BiMGA represents MGA, BiNGA represents its nitrate derivative and λ is the stoichiometric coefficient for BiNGA. However, when methacrolein is directly oxidized, a higher quantity of nitrate derivative is formed. This fact could be due to faster MPAN formation when methacrolein is directly oxidized : more NO_x is available to react with MPAN, which leads to higher nitrate derivative concentrations. When isoprene is oxidized, methacrolein is formed first and MPAN formation occurs latter in the oxidation process. Then, there is more time for NO_x to be consumed to form HNO_3. As the nitrate derivative has a higher molecular weight than MGA and a priori a similar saturation vapor pressure, the hypothesis made could lead to underestimation of the SOA mass in environmental chamber under some conditions.

Oligomerization can impact strongly the formation of SOA (e.g. *Gao et al.* [2004]; *Jang et al.* [2005]; *Liggio et al.* [2005]). It is then important to take it into account. To take into account oligomerization, a simple parameterization was developed :

$$K_{oligo} = \frac{A_{oligomer}}{A_{monomer}} \qquad (2.2)$$

where K_{oligo} represents the ratio of the oligomer mass ($A_{oligomer}$) to the monomer mass ($A_{monomer}$). With this simple parameterization, an effective partitioning coefficient can be calculated as follows :

$$K_{eff,om,i} = K_{om,i}(1 + K_{oligo}) \qquad (2.3)$$

where $K_{om,i}$ is the absorption equilibrium constant of the monomer. It was calculated by using the saturation vapor pressures obtained with the SIMPOL.1 method for MGA and its nitrate derivative. The same parameter K_{oligo} was applied for both BiMGA and BiNGA.

The parameters λ and K_{oligo} were selected to minimize the error between the model and the results from *Kroll et al.* [2006] and *Surratt et al.* [2006] by a least-square method. A mean temperature of 298 K and a relative humidity of 5 % were assumed. Optimization gives $\lambda = 0.046$

TABLE 2.4 – Comparison of measured[a] and modeled[b] SOA formation (ΔM_o) for NO_x-free conditions : maximum ΔM_o and final ΔM_o.

Initial isoprene (ppb)	Measured ΔM_o (max) ($\mu g.m^{-3}$)	Calculated ΔM_o (max) ($\mu g.m^{-3}$)	Measured ΔM_o (final) ($\mu g.m^{-3}$)	Calculated Δ M_o (final) ($\mu g.m^{-3}$)
90.0	27.0 ± 0.5	26.9	9.3 ± 0.4	8.6
46.1	13.5 ± 0.6	11.5	3.8 ± 0.5	3.4
23.0	2.3 ± 0.5	2.8	0.6 ± 0.3	0.5
12.2	0.7 ± 0.1	0.07	0.3 ± 0.1	0.02
63.6	17.8 ± 0.5	18.0	5.0 ± 0.5	5.6
29.4	6.2 ± 0.8	5.1	2.2 ± 0.5	1.3
47.8	11.1 ± 0.5	12.2	3.0 ± 0.4	3.7
41.6	8.4 ± 0.4	9.8	2.4 ± 0.5	2.9

(a) Measured values taken from *Kroll et al.* [2006].
(b) With T = 298 K.

TABLE 2.5 – Comparison of measured and modeled[a] SOA formation (ΔM_o) for high-NO_x conditions.

	Initial reagent (ppb)	Initial NO (ppb)	Initial NO_2 (ppb)	Measured ΔM_o ($\mu g.m^{-3}$)	Calculated ΔM_o ($\mu g.m^{-3}$)
Kroll et al. [2006] (isoprene)	46.7	242	24	6.3 ± 1.0	6.0
	43.5	496	30	2.9 ± 1.2	3.3
	42.7	98	31	6.7 ± 1.3	5.9
	49.1	51	27	5.6 ± 1.3	7.0
	42.7	337	68	4.6 ± 1.0	4.7
	42.0	708	37	1.7 ± 1.1	1.5
Surratt et al. [2006] (isoprene)	500	827	34	74	90
	500	759	112	73	93
	500	805	87	104	92
	500	825	80	111	91
	500	891	74	95	90
Surratt et al. [2006] (methacrolein)	500	791	60	181	136
	500	898	30	197	121

(a) With T = 298 K and RH = 5 %.

and K_{oligo} = 64.2. Results are presented in Table 2.5. Fig. 2.4 shows the results of a simulation for 42.7 ppb of isoprene, 98 ppb of NO and 31 ppb of NO_2. The slight difference between the BiMGA and BiNGA concentrations is due to the slightly different activity coefficients of the two compounds.

The model successfully reproduces the results of *Kroll et al.* [2006] within the uncertainties of the experiments except for one experiment, (the lowest quantity of NO_x, the model gives a result (7.0 $\mu g.m^{-3}$) close to the upper value (6.9 $\mu g.m^{-3}$)). This slight overestimation could be attributed to a calculated quantity of radical HO_2 too important or the fact that some reactions (the radical formed from ISHP + HO could react with NO and forms less SOA) are missing in

the gas-phase mechanism. For high isoprene experiments, the model gives relative errors from 5 to 20%, but the model is less sensitive to NO_x conditions than observed in the experiments. This lack of sensitivity of the model may be due to the fact that the BiMGA/BiNGA ratio in the model does not vary with NO_x conditions. It may also explain the underestimation of SOA formed when methacrolein is directly oxidized (which leads to a lower BiMGA/BiNGA ratio [*Surratt et al.*, 2006]).

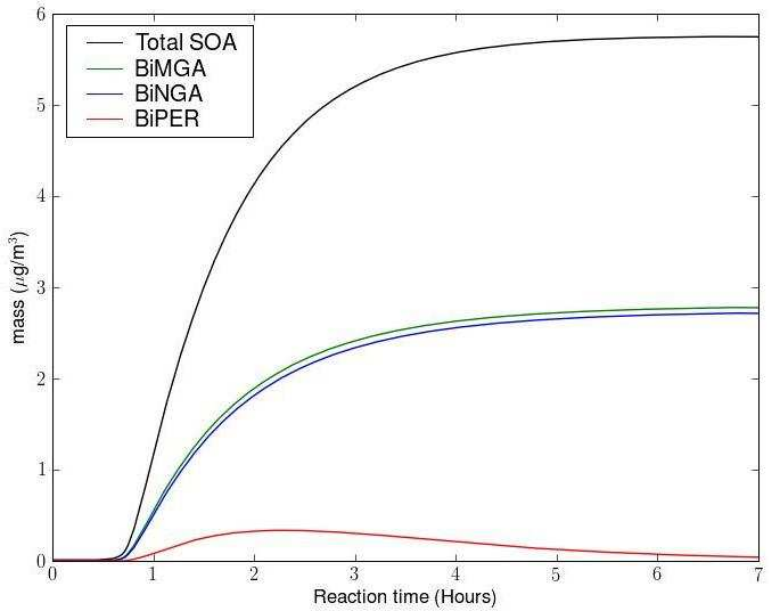

FIGURE 2.4 – Evolution of the calculated mass of SOA formed from the photooxidation of isoprene as a function of time for initial concentrations of 42.7 ppb of isoprene, 98 ppb of NO and 31 ppb of NO_2 at 298 K.

2.3 Influence of parameters

2.3.1 Influence of NO_x level and NO_2/NO ratio

Based on the experiments of *Kroll et al.* [2006], the SOA yield seems to be maximal for an oxidation of 300 ppb of NO_x and seems to decrease for higher concentrations. The recent study of *Chan et al.* [2010a] shows that under high-NO_x conditions, the SOA yield strongly depends on the $[NO_2]/[NO]$ ratio due to MPAN chemistry (MPAN formation is favored under high NO_2 conditions).

To study the impact of the NO_x level, the amount of SOA formed was calculated as a function of initial NO_x concentrations (Fig. 2.5) for different $[NO_2]/[NO]$ initial ratios (the ratio may change with time). According to the model results, the amount of SOA decreases strongly only for low $[NO_2]/[NO]$ ratio (Fig. 2.5 for $[NO_2]/[NO]$=0.1) and is below the amount of SOA formed in no-NO_x conditions (3.5 $\mu g.m^{-3}$) for very high concentrations of NO_x (more than 500 ppb of NO_x for 45 ppb of oxidized isoprene and an initial $[NO_2]/[NO]$ ratio of 0.1). The inhibition of SOA formation for low $[NO_2]/[NO]$ ratios is due to the MPAN chemistry. Fig. 2.4 shows that SOA begin to form nearly 1 hour after the beginning of oxidation. To observe high concentration of SOA, MPAN formation must be favored after 1 hour and so, a high $[NO_2]/[NO]$ ratio after

1 hour must be observed. For an initial $[NO_2]/[NO]$ ratio of 0.1, the ratio after 1 hour is : 53 for 100 ppb, 52 for 200 ppb, 31 for 300 ppb and 7 for 400 ppb. The decrease of SOA for a NO_x concentration greater than 200 ppb is due to the drop of NO_2 during oxidation.

For higher $[NO_2]/[NO]$ ratios, it seems that the SOA yield is higher under high-NO_x condi-

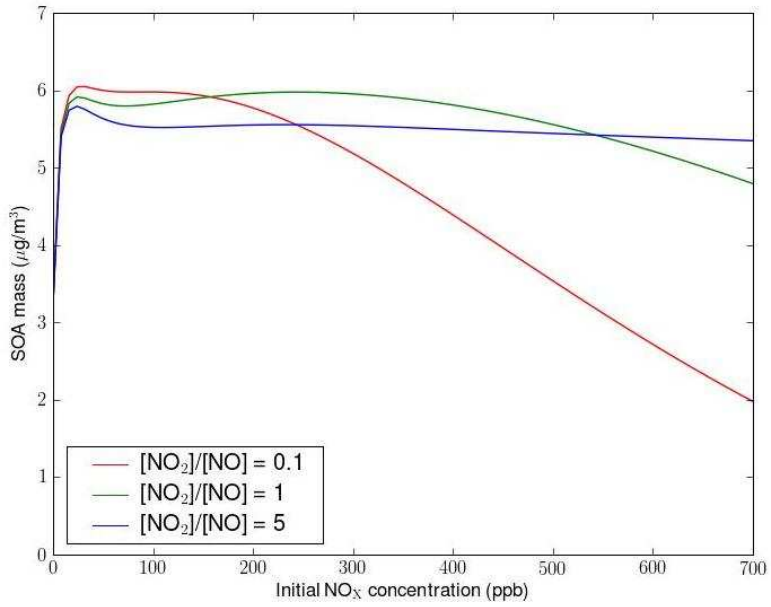

FIGURE 2.5 – Evolution of calculated SOA mass with NO_x for 45 ppb of oxidized isoprene and different initial $[NO_2]/[NO]$ ratios.

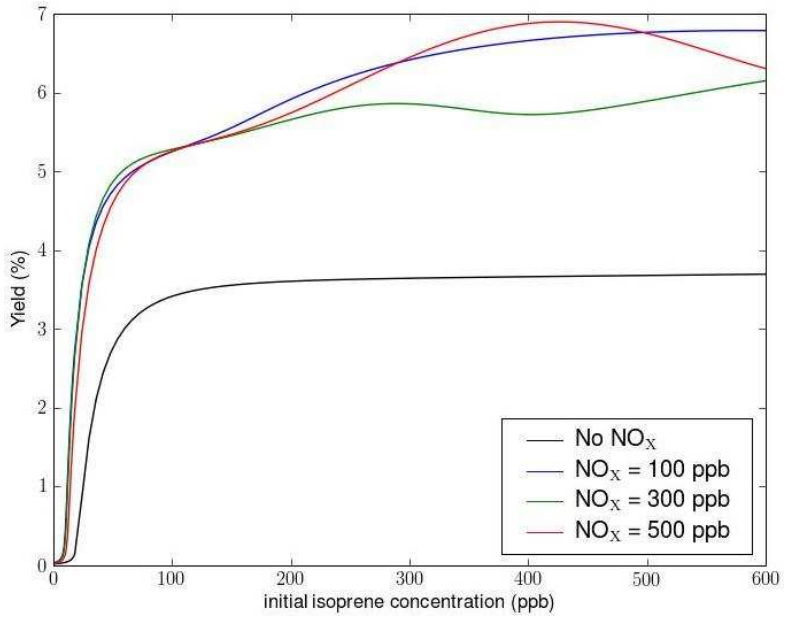

FIGURE 2.6 – Evolution of calculated yield with isoprene concentration for different NO_x concentrations with a $[NO_2]/[NO]$ ratio of 1.

tions than under low-NO_x conditions. For an initial $[NO_2]/[NO]$ ratio of 5, the quantity of SOA formed appears insensitive to the NO_x quantity. However, in reality, a stronger sensitivity may be observed if the BiMGA/BiNGA ratio were sensitive to NO_x concentrations.

For a $[NO_2]/[NO]$ ratio of 1, the final SOA yield (when there is no more SOA growth or loss) was calculated as a function of initial isoprene concentration for several initial concentrations of NO_x (Fig. 2.6). For the no-NO_x simulation, the yield increases and stabilizes at about 3.75%. In this case, a typical SOA yield curve is obtained. For high-NO_x simulations, the evolution of the yield is more complex because of the MPAN chemistry. Yields can vary from 5 to 7% if more than 100 ppb of isoprene is oxidized. For 300 ppb of NO_x, the yield decreases slightly between 300 and 400 ppb of oxidized isoprene and increases for higher concentrations of isoprene.

It is difficult to deduce a general pattern for isoprene SOA formation in presence of NO_x because of the complex effects of the gas-phase chemistry. Depending on NO_x concentrations and the $[NO_2]/[NO]$ ratio, the yield can be lower or as much as twice higher than the no-NO_x SOA yield. However, for atmospheric conditions (NO_x and isoprene concentrations generally inferior to 100 ppb), the yield should be higher under high-NO_x conditions than under low-NO_x conditions, when SOA formation occurs in an organic phase.

2.3.2 Influence of temperature

Fig. 2.7 shows the effect of temperature on the amount of SOA formed for different $[NO_2]/[NO]$ ratios. In all cases, a decrease of the temperature by 20°C leads to an increase of SOA mass by about 2 $\mu g.m^{-3}$. This result can be explained by an increase in SOA volatility when the temperature increases. The temperature affects SOA partitioning more than the kinetics of the reactions leading to the formation of SOA. However, the activation energy was not used for all the reactions due to a lack of data and the chemical kinetics could be in reality more sensitive to temperature.

2.3.3 Influence of the BiDER molecular structure

To investigate the impact of the BiDER molecular structure (which could be very different from the structure of tetrols) on the results of the model optimization, we substitute its structure by that of another compound. We used the peroxy-hemiacetal that could be formed by the particle phase reaction [*Kroll and Seinfeld*, 2008] of a trihydroxy-hydroperoxide with glyoxal. This compound has a molar mass of 224 $g.mol^{-1}$ (instead of 136 $g.mol^{-1}$ for tetrols). Using this compound, the optimization gives the same yield for BiPER (0.28) but a slightly different saturation vapor pressure (2.2×10^{-6} torr instead of 2.6×10^{-6} torr). Results obtained for BiPER are not very sensitive then to the choice of the BiDER structure. The results obtained by assuming that BiDER has the structure of tetrols should give a good estimation of BiPER yield and saturation vapor pressure.

For BiDER, the molar yield is lower (0.018 instead of 0.030 but the mass yield is the same) and the saturation vapor pressure is lower (2.5×10^{-7} torr instead of 4.1×10^{-7} torr). Therefore, BiDER volatility may be underestimated in the model.

2.4 Extension of the model to humid conditions

The model described above applies to dry conditions. However, it is important to implement in an air quality model an SOA model that covers the full range of atmospheric conditions including high humidity conditions. Consequently, a parameterization for SOA formation must take into account humid conditions. Moreover, the SOA compounds produced from isoprene photooxidation may be highly hydrophilic due to their structural composition, i.e., short compounds

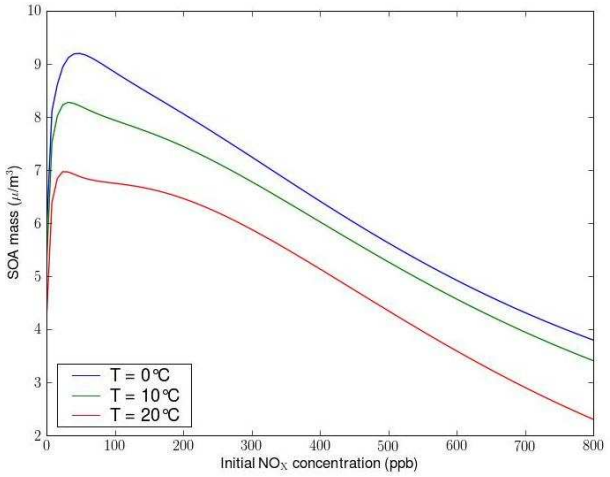

(a) $[NO_2]/[NO]$ ratio of 0.1

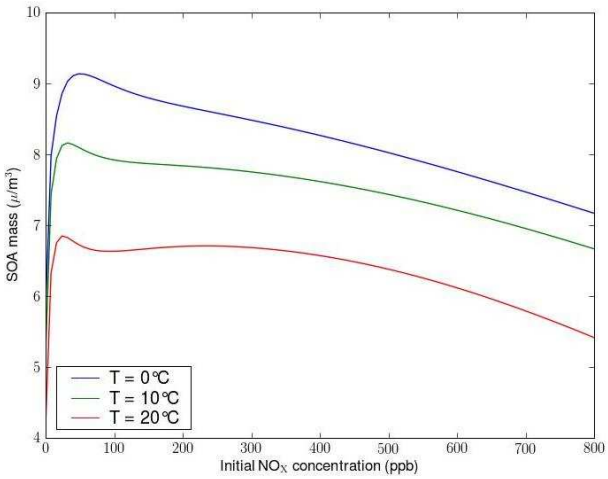

(b) $[NO_2]/[NO]$ ratio of 1

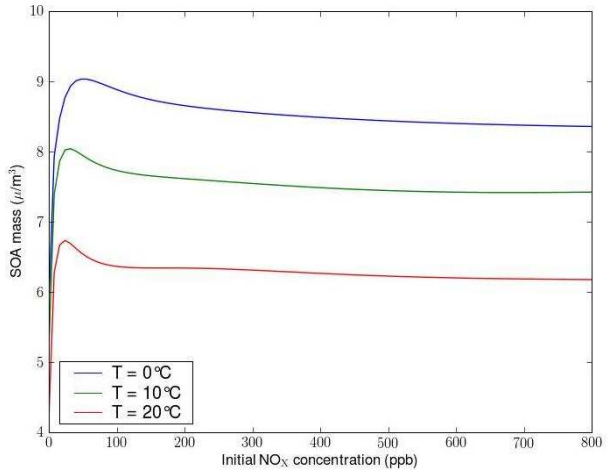

(c) $[NO_2]/[NO]$ ratio of 5

FIGURE 2.7 – Evolution of SOA with NO_x for 45 ppb of oxidized isoprene at different temperatures for : (a) $[NO_2]/[NO]$ ratio of 0.1, (b) $[NO_2]/[NO]$ ratio of 1, (c) $[NO_2]/[NO]$ ratio of 5.

(number of carbons ≤ 5) with several functional groups. Under humid conditions, in presence of both an aqueous phase and an organic liquid phase, isoprene SOA surrogates may partition mostly between the aqueous phase and the gas phase rather than the organic phase and the gas phase.

Several methods have been used to account for the influence of water on SOA formation. On one hand, one can treat the atmospheric particles as internal mixtures (all particles of a same size have the same chemical composition) and solve he thermodynamics with possible phase separation (e.g., mostly organic and aqueous phases) as performed by *Pun* [2008] and *Zuend et al.* [2010]. On the other hand, one can treat the atmospheric particles as external mixtures with aqueous (mostly inorganic) particles being distinct from hydrophobic (mostly organic) particles as performed by *Pun et al.* [2002a, 2006]. The latter approach is used here.

For the extension to humid conditions, a parameterization for the partitioning between the gas phase and the aqueous phase was added to the model described above. It was assumed that all surrogate SOA compounds can partition between the gas phase and any liquid phase

(aqueous phase and organic phase). *Surratt et al.* [2010] showed that under low-NO_x conditions, an epoxidiol intermediate should be formed from reaction R2.5 with a high yield (about 75%). This epoxidiol can lead to methyl-tetrol and other components formation in the presence of an acid aerosol. However, the study of aqueous-phase reactions [*Ervens et al.*, 2008; *Volkamer et al.*, 2009] was considered outside the scope of this work and was not modeled here.

2.4.1 Parameterization of the partitioning between an aqueous phase and the gas phase

To extend the model to humid conditions, the partitioning between the gas phase and the aqueous phase is calculated with a modified Henry's law [*Pun et al.*, 2002a] :

$$H_i = \frac{A_i \ \zeta_i}{M_i \ LWC \ p_i} \tag{2.4}$$

with H_i the Henry's law constant of compound i ($\mu M.atm^{-1}$), p_i the partial pressure of compound i in the gas phase (atm), LWC the liquid water content (L_{water}/m^3 of air), M_i the molar mass of compound i and ζ_i the activity coefficient of compound i in the aqueous phase defined by reference to the infinite dilution. ζ_i can be computed by using the UNIFAC model :

$$\zeta_i = \frac{\gamma_i}{\gamma_i^\infty} \tag{2.5}$$

where γ_i is the activity coefficient of the compound i in the aqueous phase computed with UNIFAC and γ_i^∞ is the activity coefficient of compound i at infinite dilution computed with UNIFAC.

Different methods can be used to determine the Henry's law constant. Functional group methods give very high values for the Henry's law constant of BiMT (2.7×10^{16} $M.atm^{-1}$ and 1.66×10^{16} $M.atm^{-1}$ with the methods of *Meylan and Howard* [2000] and *Suzuki et al.* [1992] respectively). On the contrary, the HENRYWIN bond contribution method of *Meylan and Howard* [2000, 1991] predicts a lower value for BiMT : 2.45×10^6 $M.atm^{-1}$. However, according to the data available in *Raventos-Duran et al.* [2010], the HENRYWIN bond contribution method seems to underestimate the Henry's law constant for compounds with several hydroxy groups (for example, for propane-1,3-diol, this method predicts a Henry's law constant of 6.31×10^3 $M.atm^{-1}$ whereas the experimental value is 1.0×10^6 $M.atm^{-1}$). SPARC online [*Hilal et al.*, 2008] seems then to provide the best estimation for Henry's constants (3.38×10^{10} $M.atm^{-1}$ for BiMT and 5.25×10^8 $M.atm^{-1}$ for BiMGA). However, SPARC online does not provide algorithms to calculate the Henry's law constants of the other compounds.

We chose to calculate the other Henry's law constants by reference to either BiMT or BiMGA using the following equation :

$$H_i = \frac{\gamma_j^\infty P_j^o}{\gamma_i^\infty P_i^o} H_j \tag{2.6}$$

where j is the compound of reference (BiMT or BiMGA) and i is the compound for which the Henry's law constant is wanted. The Henry's law constants for BiPER, BiDER and $C_5H_9N_3O_{10}$ were calculated by reference to BiMT. The Henry's law constant for BiNGA was calculated by reference to BiMGA. The saturation vapor pressures used in the model for dry conditions were used for the calculation. The calculated values at 298 K are presented in Table 2.6.

TABLE 2.6 – Calculated Henry's law constants for SOA surrogate species.

Surrogate species	H_i at 298K ($M.atm^{-1}$)
BiMT	3.30×10^{10}
$C_5H_9N_3O_{10}$	4.75×10^{6}
BiMGA	5.25×10^{8}
BiNGA	3.73×10^{7}
BiPER	8.09×10^{9}
BiDER	8.91×10^{10}

2.4.2 Influence of an aqueous phase on SOA formation

The partitioning of the surrogate compounds under atmospheric conditions was calculated for four different cases. In the first case, SOA partition between the gas phase and an organic phase constituted by primary organic aerosols (POA). A mean value of 5 $\mu g.m^{-3}$ for POA concentrations was chosen as follows : 40% of C23H47COOH, 5% of C8H17CH=CHC7H14COOH, 15% of 4-(2-propio)-syringone, 12% of C29H60 and 28% of 2-carboxybenzoic acidic (EPRI, 1999). In the second case, SOA partition between the gas phase and an aqueous phase. A value of 50 $\mu g.m^{-3}$ of liquid water was used in the second case. The aqueous aerosol was supposed to be too acid for BiMGA and BiNGA to dissociate. In the third case, SOA can condense on 5 $\mu g.m^{-3}$ of POA and on 50 $\mu g.m^{-3}$ of liquid water. In the fourth case, surrogates can condense on an organic phase assumed to be ideal (activity coefficients equal to 1).

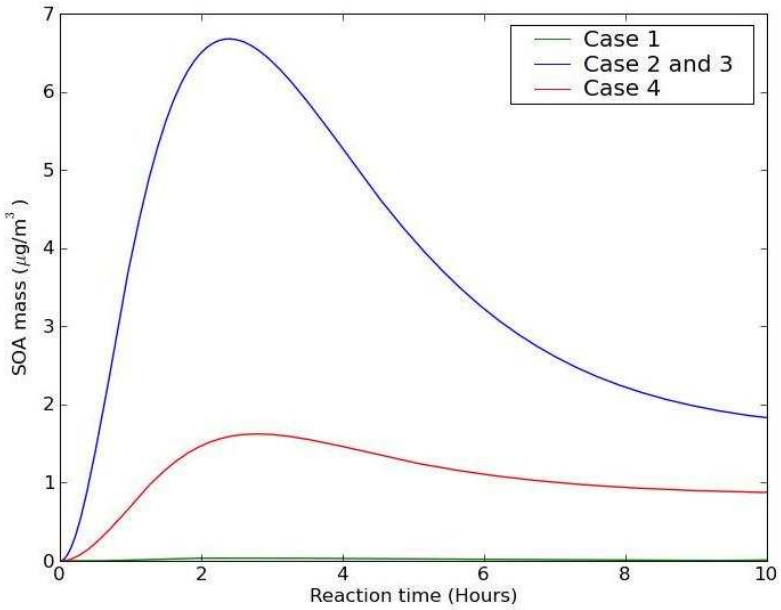

FIGURE 2.8 – Effect of an aqueous phase on SOA formation under no-NO_x conditions for 10 ppb of initial isoprene concentration for different cases. Case 1 : Condensation on 5 $\mu g.m^{-3}$ of POA. Case 2 : Condensation on 50 $\mu g.m^{-3}$ of liquid water. Case 3 : Condensation on 5 $\mu g.m^{-3}$ of POA and on 50 $\mu g.m^{-3}$ of liquid water. Case 4 : Condensation on 5 $\mu g.m^{-3}$ of an ideal organic phase.

Under no-NO_x conditions ([NO]=[NO_2]=0.0), no substantial amount of SOA is formed in the first case (maximum of SOA formed is 0.027 $\mu g.m^{-3}$) whereas a significant amount is formed in the second case. The low amount of SOA formed in the first case is due to low affinity of the surrogate compounds formed under those conditions (mainly BiPER and BiDER) with POA. In the second and third case, the same amount of SOA is formed (because all SOA compounds seem to partition only in the aqueous phase). Fig. 2.8 shows the evolution of SOA formed for the second and third cases. A substantial amount of isoprene is formed (1.6 $\mu g.m^{-3}$ at the end of the oxidation and a maximum at 6.7 $\mu g.m^{-3}$). The amount of SOA formed is even greater than in the case where SOA would condense on an ideal organic phase, which gives much greater concentrations than the non-ideal organic phase case. This result shows the importance of taking into account the non-ideality of particles for SOA partitioning. Furthermore, SOA formed from isoprene photooxidation under low-NO_x conditions are not likely to condense on POA (due to non-ideality of the organic phase), it would more likely condense efficiently on an aqueous phase. It should be noted that, whereas surrogates do not condense on POA, they condense almost entirely on the aqueous phase (only 1% of BiPER remains in the gas phase).

Under high-NO_x conditions ([NO]=[NO_2]=50 ppb), all the components formed are not highly hydrophilic. Fig. 2.9 shows the quantity of SOA formed for the different cases under high-NO_x conditions. There is still a lower quantity of SOA (0.16 $\mu g.m^{-3}$) formed when SOA condense on POA than when they condense on an aqueous phase (0.59 $\mu g.m^{-3}$). But, contrary to the low-NO_x conditions, the third case shows that a non-negligible part of the surrogates condense on the organic phase. The fourth case (ideal organic phase) strongly increases the mass of SOA. The difference between low-NO_x and high-NO_x conditions is due to lower Henry's law constants of the surrogate species, which dominate under high-NO_x conditions. Whereas, the measured SOA yield was higher for dry conditions under high-NO_x conditions (but for concentrations of NO_x less than 300 ppb) than under low-NO_x conditions, it is possible that in the atmosphere under high-NO_x conditions, less SOA could be formed due to lower water solubility of the corresponding SOA. The increase in SOA mass under humid conditions is commensurate with the results obtained by *Pun* [2008] who estimates, using a different approach, an increase by a factor of five of SOA mass by taking into account the hydrophilic properties of SOA from isoprene.

To explain the absorption of surrogates in the organic phase in high-NO_x but not in low-NO_x, the distribution of the SOA (formed from the oxidation of 10 ppb of isoprene with 50 ppb of NO and NO_2) between the organic and aqueous phases for different $M_{water}/M_{organic}$ ratios is shown in Fig. 2.10. BiMT, BiPER and BiDER (compounds formed under low-NO_x conditions) are only present in the aqueous phase and do not condense significantly in the organic phase. BiMGA (formed under high-NO_x) does not condense on the aqueous as efficiently as the surrogates formed under low-NO_x conditions. However, for an $M_{water}/M_{organic}$ ratio of 1, 60% of particulate BiMGA is in the aqueous phase and around 95% for a ratio of 10. When, the $M_{water}/M_{organic}$ ratio is superior to 1 in the atmosphere, BiMGA should partition preferably between the aqueous phase and the gas phase. BiNGA and C_5-hydroxy-trinitrate seem to be hydrophobic because even for an $M_{water}/M_{organic}$ ratio of 10, they condense preferably on the organic phase. The condensation of SOA on the organic phase under high-NO_x conditions is then due to the hydrophobic properties of BiNGA (only a small quantity of C_5-hydroxy-trinitrate is formed under the conditions considered here).

The AER/EPRI/Caltech model (AEC) [*Pun et al.*, 2002a, 2003, 2006] is a model for SOA formation that takes into account the hydrophilic and hydrophobic properties of surrogates. It distinguishes compounds into two types : hydrophilic compounds (which are absorbed only in an aqueous particle) and hydrophobic compounds (which are absorbed only in an organic particle). In AEC, a compound cannot condense on both phases simultaneously ; we investigate here the uncertainty associated with this formulation. According to the distribution of the surrogates,

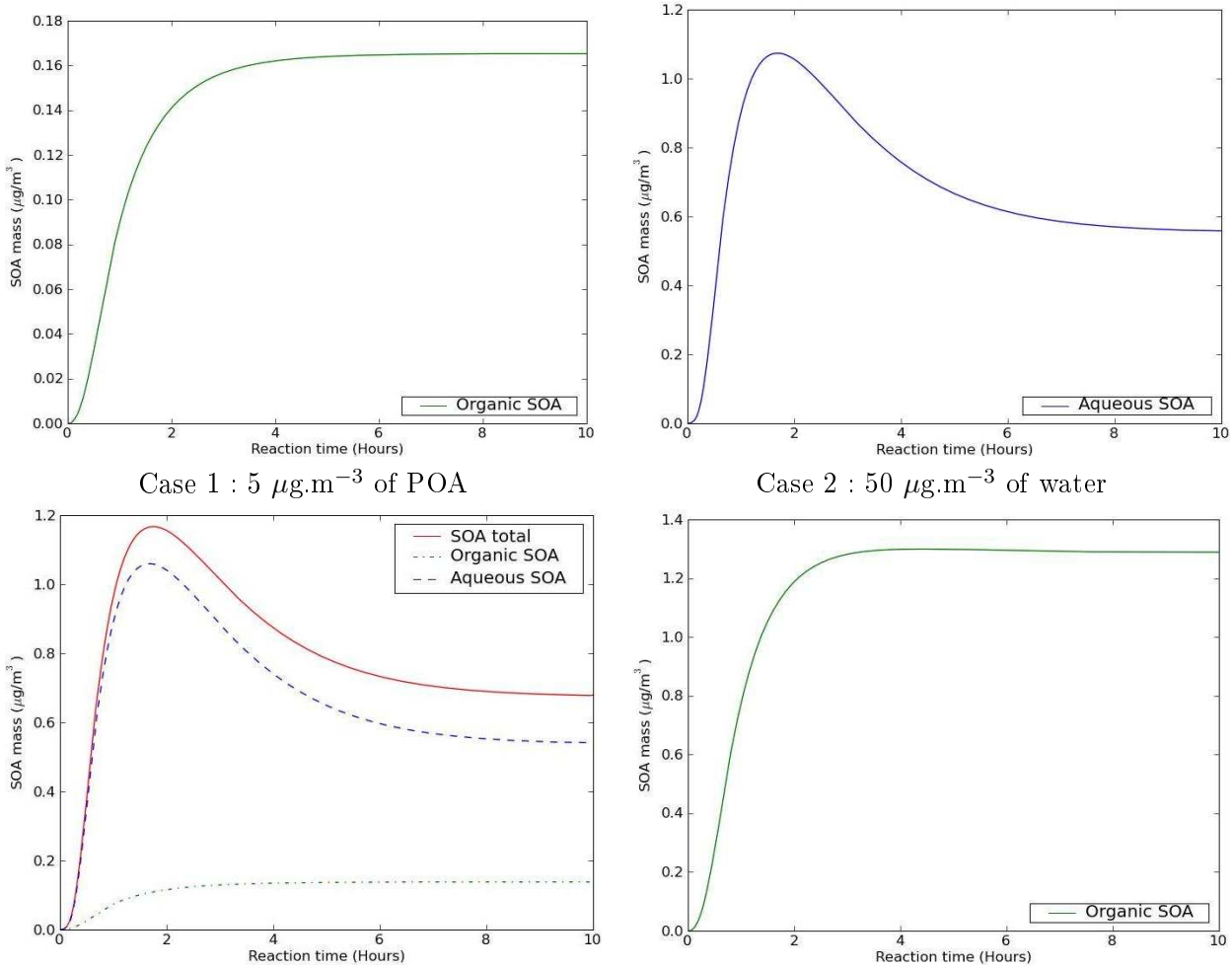

Case 1 : 5 μg.m^{-3} of POA

Case 2 : 50 μg.m^{-3} of water

Case 3 : 5 μg.m^{-3} of POA and 50 μg.m^{-3} of water

Case 4 : 5 μg.m^{-3} of POA Ideal Organic Phase

FIGURE 2.9 – Effect of an aqueous phase on SOA formation under high-NO_x conditions ([ISO]=10 ppb, [NO]=[NO_2]=50 ppb). Case 1 : Condensation on 5 μg.m^{-3} of POA. Case 2 : Condensation on 50 μg.m^{-3} of liquid water. Case 3 : Condensation on 5 μg.m^{-3} of POA and on 50 μg.m^{-3} of liquid water. Case 4 : Condensation on 5 μg.m^{-3} of an ideal organic phase.

BiMT, BiPER, BiDER and BiMGA may be considered hydrophilic compounds and BiNGA and $C_5H_9N_3O_{10}$ hydrophobic compounds. Under low-NO_x conditions, as the compounds formed are highly hydrophilic and condense almost entirely on aqueous particles, the hypothesis of AEC does not change the results significantly. Fig. 2.11 shows the evolution of SOA formed with time for the high-NO_x case, assuming that surrogates are only hydrophilic or only hydrophobic. The difference between the case where all compounds can partition among all the phases (see Fig. 2.9) and the case with the hypothesis of AEC is greater for high-NO_x conditions because BiMGA and BiNGA (major components formed under high-NO_x conditions) are neither totally hydrophilic nor hydrophobic. In this case, the mass of SOA is underestimated by the AEC hypothesis by 11% : 0.61 μg.m^{-3} (Fig. 2.11) with the AEC hypothesis against 0.68 μg.m^{-3} (Fig. 2.9) without the AEC hypothesis.

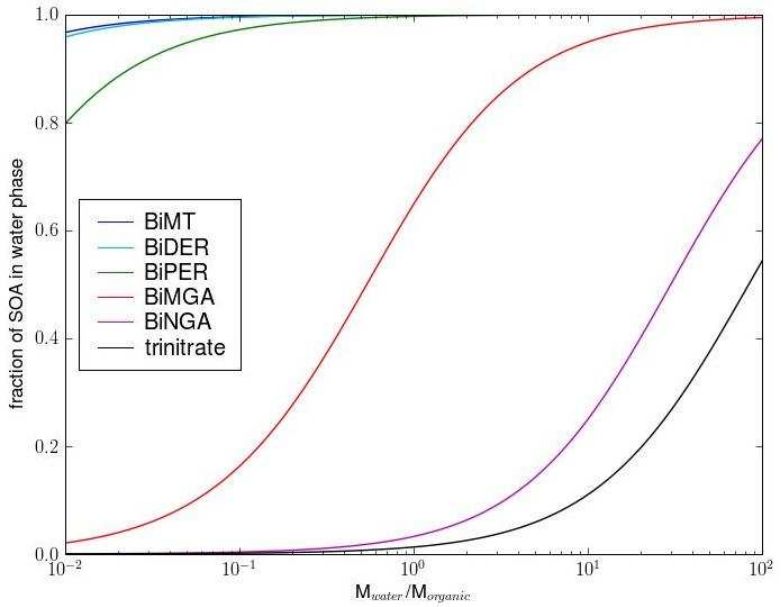

FIGURE 2.10 – Distribution of the absorbed surrogates between the aqueous phase and the organic phase for different $M_{water}/M_{organic}$ ratios if oligomerization only happens in the organic phase.

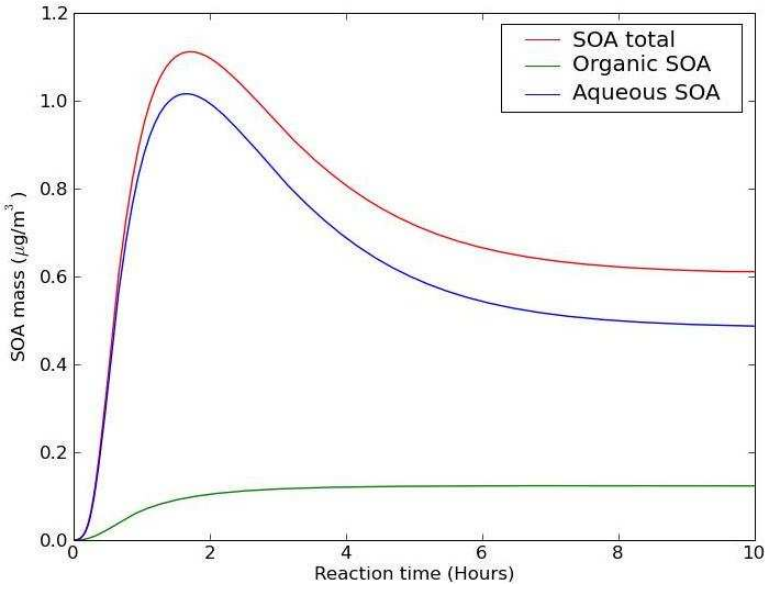

FIGURE 2.11 – Simulated SOA concentration in aqueous and organic phases for 10 ppb of isoprene and high-NO_x conditions ([NO]=[NO_2]=50 ppb) assuming all the surrogates are hydrophilic except for BiNGA and $C_5H_9N_3O_{10}$.

2.4.3 Influence of oligomerization and particle pH on partitioning

SOA surrogates have been separated between hydrophobic and hydrophilic compounds, however, calculated partitioning can change whether oligomerization is taken into account in the

computation or not. We assumed that esterification does not occur in the aqueous phase, although *Altieri et al.* [2008] observed formation of oligoesters in an aqueous phase. Additional absorption of acidic SOA species (BiMGA and BiNGA) occurs by dissociation in an aqueous phase. For a pH superior to pKa (pKa = 4 estimated for BiMGA with SPARC online), BiMGA and BiNGA would, therefore, dissociate and would be more efficiently absorbed. On the other hand, oligomerization in the organic phase could be less important in the atmosphere due to less concentrated monomers. The amount of SOA formed (for 10 ppb of isoprene, 50 ppb of NO, 50 ppb of NO_2, 5 $\mu g.m^{-3}$ of POA and 50 $\mu g.m^{-3}$ of liquid water) was simulated to investigate the sensitivity of the system to additional absorption due to acid dissociation and oligomerization.

To investigate the effect of potential oligomerization in the aqueous phase and pH, an effective Henry's law constant for BiMGA and BiNGA was used :

$$H_{eff,i} = H_i(1 + K_{oligo}) \tag{2.7}$$

where K_{oligo} is the same constant as the one in Eq. 2.3 (it supposes that additional absorption due to dissociation and oligomerization occurs with the same extent in both phases). Fig. 2.12a shows the evolution of the SOA mass. Additional absorption of BiMGA and BiNGA greatly increases the amount of SOA formed (1.7 $\mu g.m^{-3}$ against 0.68 $\mu g.m^{-3}$ without additional absorption). Moreover, there is almost no condensation on POA : all the condensation occurs on the aqueous phase. Fig. 2.13a shows the distribution of the surrogates between the two condensed phases for different $M_{water}/M_{organic}$ ratios. For an $M_{water}/M_{organic}$ ratio of 1, almost all the particulate BiMGA is in the aqueous phase and nearly 80% of the particulate BiNGA is in the aqueous phase. Contrary to the case where there is no additional absorption in the aqueous phase (see Fig. 2.10), BiNGA can then be considered hydrophilic when its additional absorption is accounted for.

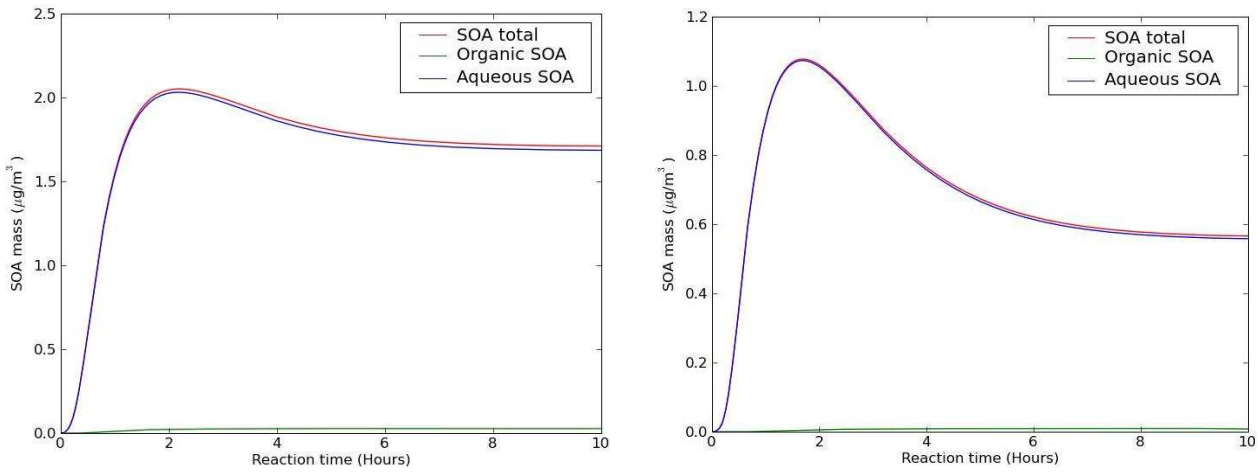

(a) additional absorption in the aqueous phase (acid dissociation and oligomerization)

(b) no additional absorption in the aqueous phase and no oligomerization in the organic phase

FIGURE 2.12 – Evolution with time of the mass of SOA formed : (a) with additional absorption in the aqueous phase (acid dissociation and oligomerization) and (b) with no additional absorption in the aqueous phase and no oligomerization in the organic phase.

To investigate the possible absence of oligomerization in the organic phase, $K_{oligo} = 0$ was used. Fig. 2.12b shows the evolution of the SOA mass without oligomerization in the organic

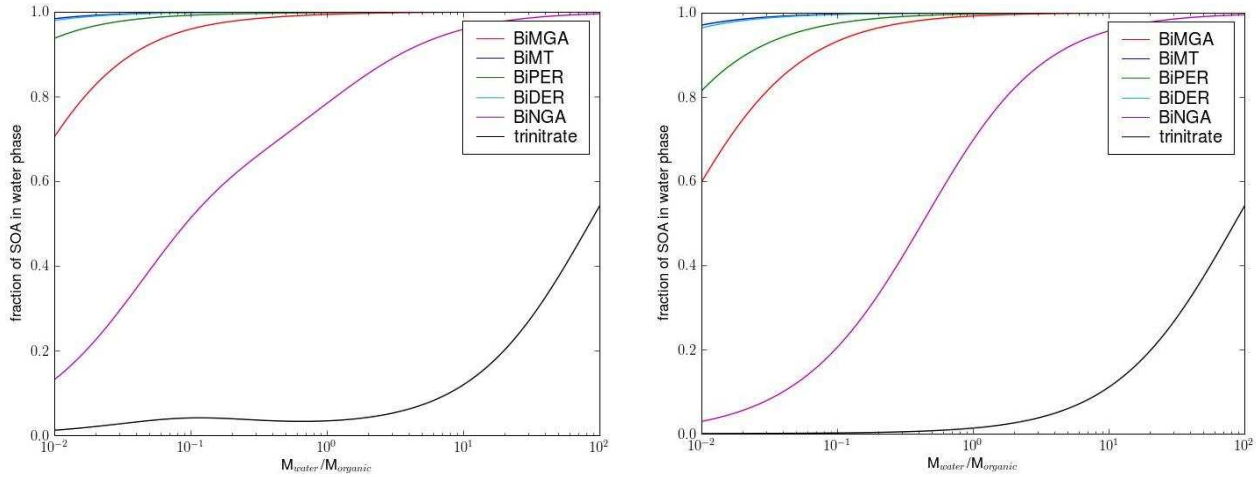

(a) additional absorption in the aqueous phase (acid dissociation and oligomerization)

(b) no additional absorption in the aqueous phase and no oligomerization in the organic phase

FIGURE 2.13 – Distribution of the absorbed surrogates between the aqueous phase and the organic phase for different $M_{water}/M_{organic}$ ratios : (a) with additional absorption in the aqueous phase (acid dissociation and oligomerization) and (b) with no additional absorption in the aqueous phase and no oligomerization in the organic phase.

phase. The final SOA mass is reduced by 16% (0.57 $\mu g.m^{-3}$ without oligomerization against 0.68 $\mu g.m^{-3}$ with oligomerization). There is no significant absorption of the surrogates on the organic phase. Fig. 2.13b shows the distribution of the surrogates between the two phases. As in the previous case, BiNGA partitions more efficiently between the aqueous phase and the gas phase and can be considered hydrophilic when its oligomerization in the organic phase is not accounted for.

Whether BiNGA condenses on POA or an aqueous phase depends on potential additional absorption in the aqueous phase by potential oligomerization and dissociation and on the extent of oligomerization in the organic phase. Most of the components can be classified as hydrophilic (BiMT, BiPER, BiDER and BiMGA) but BiNGA can be considered either as hydrophobic or hydrophilic, depending on oligomerization in the organic phase or additional absorption in the aqueous phase.

2.4.4 Sensitivity of the model to Henry's law constants

One of the main uncertainties of the model is the values of Henry's law constants. The constants used here were estimated using the saturation vapor pressure and the activity coefficient at infinite dilution ; however, as discussed above, other methods may lead to quite different results. For that reason, a sensitivity study was conducted to evaluate the impact of those uncertainties on liquid-gas partitioning.

Under low-NO_x conditions, the partitioning is not very sensitive to the values. If Henry's law constants are divided by 2, 1.76 $\mu g.m^{-3}$ of SOA are formed instead of 1.83 $\mu g.m^{-3}$ (for 50 $\mu g.m^{-3}$ of liquid water and 10 ppb of initial isoprene). If the Henry's law constants are divided by 10, 0.92 $\mu g.m^{-3}$ is formed (i.e. half of SOA previously formed). On the contrary, when Henry's law constants are multiplied by 10, the quantity of SOA does not change significantly (1.86 $\mu g.m^{-3}$ instead of 1.83 $\mu g.m^{-3}$) because most of the SOA species are already present in the

condensed phase. So, for BiMT, BiPER and BiDER, the amount of SOA formed does not change significantly for a small decrease of the Henry's law constants or for an important increase of the Henry's law constant. Of course, the impact of Henry's law constant values is more important for lower quantity of liquid water, but even at 5 μg.m^{-3} of liquid water, Henry's law constant values have a small impact on SOA formation : 1.46 μg.m^{-3} of SOA for Henry's law constants divided by two, and 1.86 μg.m^{-3} for Henry's law constants multiplied by ten instead of 1.73 μg.m^{-3}. If the structure of the peroxy-hemiacetal that could be formed by the particle phase reaction [*Kroll and Seinfeld*, 2008] of a trihydroxy-hydroperoxide with glyoxal, the Henry's law constant of BiDER should be higher (less volatile and more affinity with water) by about a factor 4. But, as the formation of SOA is not very sensitive to Henry's law constants, the impact of the uncertainty of the BiDER structure should be limited.

Under high-NO_x conditions, the partitioning is more sensitive. However, it was shown previously that using effective Henry's law constants taking into account additional absorption due to oligomerization and dissociation greatly influences the partitioning of the surrogates. The main uncertainty for BiMGA and BiNGA partitioning is then the extent of the additional absorption rather than the actual Henry's law constants for BiMGA and BiNGA.

For $C_5H_9N_3O_{10}$ formed by oxidation of isoprene by NO_3 radicals, as the component seems hydrophobic, the value of its Henry's law constant does not impact its partitioning noticeably.

2.5 Conclusions

A model for SOA formation from isoprene oxidation that takes into account different chemical regimes and the hydrophilic properties of SOA has been developed. For low-NO_x conditions, SOA was found to be highly hydrophilic and it is likely that components formed would condense on an aqueous phase rather than on an organic phase. For high-NO_x conditions, methyl glyceric acid (BiMGA) was found to be hydrophilic whereas the nitrate derivative (BiNGA) can be considered as hydrophilic or hydrophobic depending on the hypothesis formulated.

A major conclusion is the importance of the hydrophilic properties of SOA formed from isoprene oxidation. Because the parameterizations derived from smog chambers experiments apply to dry conditions, SOA formation could be underestimated in current models.

This SOA model can be implemented in an air quality model to evaluate the amount of isoprene-SOA formed in the atmosphere. However, several questions remain before implementing this model. Are all the pathways described here important for SOA formation ? The formation of C_5-hydroxy-trinitrate may not be relevant in the atmosphere and in any case, it could be a minor pathway for the formation of SOA in the atmosphere. If 3D simulations show that those compounds do not contribute significantly to the SOA burden, this pathway could be removed from the model. Can the number of surrogates be reduced ? Some surrogates like BiMT and BiDER have similar thermodynamic properties (same molecular structure and high Henry's law constants), and they could perhaps be merged into a single surrogate.

To develop this model, several assumptions hwere made. Readers should be aware of these assumptions and that several uncertainties remain. Which molecular structure for BiDER should be chosen ? Can the products formed in experimental chambers be formed under all conditions in the atmosphere ? For example, if BiDER is formed by reaction in an organic phase, it is possible that it is not formed when the compounds tend to condense on liquid water. To what extent does the oligomerization occur in the atmosphere for BiMGA and BiNGA. Are the estimated Henry's law constants and saturation vapor pressures reliable enough for extrapolation to atmospheric conditions ? For example, *Barley and McFiggans* [2010] showed that results of models of SOA formation are very sensitive to saturation vapor pressures.

It should be noted that the main uncertainties of the model concern the high-NO_x regime.

However, isoprene is emitted by biogenic sources in remote areas where concentrations of NO_x are low. Most of SOA should, therefore, be formed under low-NO_x conditions and the impact of the uncertainties of the high-NO_x regime should be limited.

Chapitre 3

Développement et évaluation d'un module de formation d'aérosols organiques secondaires

Résumé

La paramétrisation développée pour prendre en compte la formation d'aérosols organiques secondaires formés par oxydation de l'isoprène peut être introduite dans un modèle de formation d'aérosols organiques pour améliorer ses performances. Cette paramétrisation a été implémentée dans le modèle AEC (AER/EPRI/Caltech) dévéloppé à l'origine par *Pun et al.* [2002a], puis modifié en une version davantage sur les données expérimentales par *Pun et al.* [2006]. Ce modèle utilise l'approche moléculaire (chaque espèce du modèle est reliée à une structure chimique pour évaluer les interactions entre les différents composés) et distingue composés hydrophiles, qui ont une grande affinité avec l'eau et qui se condensent donc principalement sur la phase aqueuse des particules, et composés hydrophobes, qui se condensent uniquement sur la phase organique du fait de leur faible affinité avec l'eau. La formation d'aérosols organiques sur l'Europe par oxydation de l'isoprène a été simulée du 15 juillet au 15 août 2001 dans l'étude présentée en Annexe 1 : "Comparison of different gas-phase mechanisms and aerosol modules for simulating particulate matter formation" [*Kim et al.*, 2011a]. Cette étude compare l'approche hydrophobe de la formation d'aérosols organiques secondaires par oxydation de l'isoprène typiquement utilisée dans la plupart des modèles (les aérosols se forment par condensation sur une phase organique) à l'approche hydrophile présentée dans le Chapitre 2. En moyenne sur l'Europe, 0,15 μg.m^{-3} d'aérosols sont formés avec l'approche hydrophobe contre 0,35 μg.m^{-3} avec l'approche hydrophile. Cela confirme les conclusions du Chapitre 2 disant que les concentrations d'aérosols organiques secondaires provenant de l'oxydation de l'isoprène sont probablement sous-estimées par l'approche hydrophobe et qu'il est important de prendre en compte les propriétés hydrophiles des aérosols.

Dans cette étude utilisant le modèle AEC, d'autres processus qui influencent la formation d'aérosols ont été étudiés comme l'ajout de certains précurseurs (66% d'aérosols organiques en plus, l'isoprène comptant pour 44%), l'impact du traitement des régimes bas-NO_X et haut-NO_X (de 32 à 122% d'aérosols organiques en plus), celui de l'oligomérisation des aldéhydes (60% d'aérosols organiques en plus) et l'effet du calcul des coefficients d'activité sur le partage des composés semi-volatils (9% d'aérosols organiques en plus).

Puisque l'étude de *Kim et al.* [2011a] a montré que le régime d'oxydation des précurseurs

et les interactions des composés entre eux ou avec l'eau influent fortement sur la formation d'aérosols, il est important d'intègrer ces phénomènes dans le traitement des aérosols organiques utilisé pour la simulation de la qualité de l'air. Par conséquent, un nouveau module, nommé H^2O (Hydrophilic-Hydrophobic Organics), basé sur le concept d'AEC, a été développé. Ce module corrige le calcul des coefficients d'activité pour les composés hydrophiles, utilise des enthalpies de vaporisation plus en accord avec les résultats d'expériences et utilise un schéma chimique de formation d'aérosols actualisé : des rendements de formation d'aérosols différents selon le type de monoterpènes, la formation d'organonitrates par oxydation des monoterpènes avec le radical nitrate, la distinction des régimes haut-NO_X et bas-NO_X pour les composés anthropiques et la paramétrisation développée au Chapitre 1 pour la formation d'aérosols organiques secondaires par oxydation de l'isoprène.

De plus, H^2O considère que les aérosols organiques primaires ne sont pas des composés non-volatils mais, au contraire, des composés organiques semi-volatils présents à la fois en phase gazeuse et en phase particulaire, comme les expériences en laboratoire de *Schauer et al.* [1999] et de *Robinson et al.* [2007]. Cette distinction est importante, car la quantité d'aérosols organiques primaires dépend de la température (les composés semi-volatils primaires devenant moins volatils si la température diminue, ils forment plus d'aérosols) et les composés semi-volatils en phase gazeuse peuvent être oxydés pour former plus d'aérosols.

Une fois le modèle développée, il est important d'évaluer ses performances pour savoir si le modèle estime la formation d'aérosols correctement et savoir à quel point les résultats du modèle sont fiables. Le modèle a donc été implémenté dans le modèle de qualité de l'air Polyphemus/ Polair3D et la formation d'aérosols organiques a été simulée de Juillet 2002 à Juillet 2003 sur l'Europe. Les résultats du modèle ont été comparés aux mesures de carbone organique réalisées sur 12 des stations du réseau EMEP (European Monitoring and Evaluation Programme).

Les émissions biogéniques (émissions de monoterpènes, de sesquiterpènes et d'isoprène) ont été estimées avec le modèle MEGAN [*Guenther et al.*, 2006] qui estime ces émissions en fonction de la couverture végétale, du rayonnement solaire et de la température (les émissions biogéniques devenant plus importantes à fort rayonnement lumineux et à forte température du fait de la photosynthèse). Ces émissions ont déjà utilisées avec Polyphemus sur l'Europe et l'Amérique du nord dans l'étude présentée en Annexe 2 : "Impact of biogenic emissions on air quality over Europe and North America" [*Sartelet et al.*, 2012]. Cette étude montre notamment que la formation d'aérosols organiques secondaires biogéniques est influencée par les émissions anthropiques. Si les émissions anthropiques sont plus faibles, les concentrations d'oxydants et la masse d'aérosols organiques sur lesquels les composés peuvent se condenser deviennent plus faibles. Il en résulte une diminution des concentrations d'aérosols organiques secondaires biogèniques. Supprimer toutes les émissions anthropiques mènerait à une diminution des concentrations d'aérosols organiques secondaires biogèniques d'environ 15 % sur l'Europe.

Les inventaires d'émissions d'EMEP et de *Junker et Liousse* [2008] ont été utilisés pour les émissions anthropiques de particules organiques. Cependant, ces inventaires donnent uniquement la quantité d'aérosols organiques primaires et non pas la quantité totale de composés organiques semi-volatils émis. Il est donc nécessaire d'évaluer les émissions de composés semi-volatils à partir des émissions d'aérosols organiques primaires. D'après la courbe de dilution de *Robinson et al.* [2007] pour les véhicules diesel, environ 20% des composés semi-volatils primaires serait en phase particulaire en conditions ambiantes. En supposant que les aérosols organiques émis par différentes sources suivent la même courbe de dilution, les émissions d'aérosols organiques primaires données par les inventaires sont multipliées par 5 pour obtenir les émissions de composés organiques semi-volatils.

D'après la comparaison aux mesures, H^2O donne des résultats corrects sur la plupart des stations, avec de meilleurs résultats en utilisant l'inventaire d'émissions d'EMEP qu'avec l'in-

ventaire d'émissions de *Junker et Liousse* [2008]. Bien que le modèle ait tendance à sous-estimer les concentrations d'aérosols organiques, en utilisant l'inventaire d'EMEP, H^2O donne des statistiques pour les concentrations d'aérosols organiques (erreur égale à 47 %, biais égale à -33 %) respectant les scores de performance (erreur inférieure à 75 %, biais compris entre ± 60 %) et atteignant presque les buts de performance (erreur inférieure à 50 %, biais compris entre ± 30 %) définis par *Boylan et Russel* [2006] pour les concentrations totales de particules.

La sous-estimation des résultats est plus importante en hiver. Or, il apparait que l'erreur entre le carbone organique mesuré et le carbone organique modélisé est bien corrélée à l'erreur entre le carbone élémentaire mesuré et le carbone élémentaire modélisé. Cela montre que si les sources d'émissions anthropiques étaient mieux représentées, les performances du modèle seraient améliorées et l'écart entre modèle et mesures serait fortement réduit. La sous-estimation en hiver est donc probablement due à la sous-estimation des émissions anthropiques. D'ailleurs, en supposant que les aérosols organiques primaires sont non-volatils et sans prendre en compte les composés semi-volatils primaires en phase gazeuse, les concentrations d'aérosols organiques diminuent très fortement. Cela montre que la quantité de composés semi-volatils primaires dans la phase gazeuse est très importante, car elle peut former des aréosols secondaires, ou se condenser en hiver lorsque les températures sont faibles. D'après le modèle, l'aérosol organique est d'ailleurs majoritairement constitué en hiver d'aérosols organiques primaires et d'aérosols organiques secondaires venant de l'oxydation en phase gazeuse des composés organiques semi-volatils primaires. Même en été, l'aérosol organique est constitué en grande partie d'aérosols organiques secondaires venant de l'oxydation des composés organiques semi-volatils, le reste de l'aérosol organique estival étant surtout constitué d'aérosols organiques biogéniques (provenant majoritairement de l'oxydation des monoterpènes). Utiliser des émissions non-volatiles d'aérosols organiques conduit donc à une très forte sous-estimation de l'aérosol organique en hiver, mais aussi, dans une moindre mesure, en été.

Le modèle permet d'évaluer le rapport matière organique/ carbone organique (noté OM/OC). Le modèle donne des rapports entre 1,55 et 1,65 en été ; ce rapport semble faible pour un site rural (*Turpin and Lim* [2001] ont mesuré des rapports OM/OC de l'ordre de 1,6 pour un site urbain et de l'ordre de 2,1 pour un site rural). Il est donc probable que le modèle sous-estime globalement le degré d'oxydation des aérosols organiques. Par exemple, l'absence de mécanisme de vieillissement des aérosols organiques pourrait expliquer ce faible rapport.

L'impact du calcul des coefficients d'activité a aussi été étudié plus en détails. Prendre en compte les coefficients d'activité conduit globalement à une diminution des concentrations d'aérosols organiques hydrophobes (les composés hydrophobes sont globalement déstabilisés par la présence d'autres composés dans la phase organique) mais conduit, au contraire, à une augmentation des concentrations d'aérosols organiques hydrophiles (un composé organique est généralement plus stable dans un mélange d'eau et de composés organiques que dans un milieu quasiment entièrement constitué d'eau).

Ce chapitre est constitué de :
Couvidat, F., Debry, É, Sartelet, K. et Seigneur, C. (2012). **A hydrophilic/hydrophobic organic (H^2O) aerosol model : Model development, evaluation, and sensitivity analysis**, J. Geophys. Res., 117 : D10304.

Sommaire

Abstract

A new secondary organic aerosol (SOA) model, the Hydrophilic/Hydrophobic Organic model (H^2O), is presented and evaluated over Europe. H^2O uses surrogate organic molecules to represent the myriad of SOA species and distinguishes two kinds of surrogate species : hydrophilic species (which condense preferentially on an aqueous phase) and hydrophobic species (which condense only on an organic phase). These surrogates species are formed from the oxidation in the atmosphere of Volatile Organic Compounds. H^2O includes several important processes, including the effect of NO_X on SOA formation, the dissociation of acids into an aqueous phase, the oligomerization of aldehydes, the non-ideality of the particulate phase and the hygroscopicity of organics. Concentrations of organic aerosols were simulated over Europe from July 2002 to July 2003 for comparison with measurements of the European Monitoring Evaluation Program (EMEP). In H^2O, POA are considered as semi-volatile organics compounds (SVOC) present in both the gas phase and the particle phase. Taking into account the gas-phase fraction of SVOC increases significantly organic PM concentrations, particularly in winter. The impact of ideality, of the choice of the parameterization for isoprene SOA formation, and of the OM/OC ratio of the model were also investigated. Assuming ideality in H^2O was found to lead to a small decrease in OM. Compared to a two-product parameterization, the parameterization of *Couvidat and Seigneur* [2011] for SOA formation from isoprene oxidation leads to a significant increase in isoprene SOA by taking into account their hydrophilic properties and suggests that most models may currently underestimate isoprene SOA.

3.1 Introduction

Fine particulate matter (PM) with an aerodynamic diameter less than 2.5 μm ($PM_{2.5}$) is regulated because of its impact on human health. Furthermore, $PM_{2.5}$ degrades atmospheric visibility and influences climate change. Three-dimensional air quality models, which estimate $PM_{2.5}$ formation, tend to underestimate organic aerosol concentrations due to the complexity of the phenomena involved (gas and particle phase chemistry, oligomerization, hygroscopicity, non-ideality of particulate solutions) and to the large number of organic species involved originating from diverse anthropogenic and biogenic sources. Particulate organic matter (OM) represents a large fraction of the particulate mass, typically between 20 and 60% [*Kanakidou et al.*, 2005; *Yu et al.*, 2007; *Zhang et al.*, 2007a]. Therefore, efforts have to be made to represent OM as accurately as possible in models. Organic PM is either primary (directly emitted as particles) or secondary (formed in the atmosphere by the condensation of the low-volatility oxidation products of gaseous species into an organic phase or by condensation of species with a high affinity for water into an aqueous phase) [*Kanakidou et al.*, 2005; *Hallquist et al.*, 2009]. Both primary organic aerosols (POA) and secondary organic aerosols (SOA) are currently poorly understood [*Kanakidou et al.*, 2005; *Hallquist et al.*, 2009; *Jimenez et al.*, 2009].

Five years ago, models used to consider POA as non-volatile whereas experimental studies [*Robinson et al.*, 2007] have shown that some POA are in fact condensed semi-volatile organic compounds (SVOC), which exist in both the gas phase and the particle phase. Consequently, the amount of POA depends on the dilution of the aerosol, temperature (if the temperature decreases, the volatility of SVOC decreases) and SVOC present in the gas phase, which can be oxidized to form less volatile compounds. For example, SVOC oxidation in the gas phase was shown to be an important source of SOA in several modeling studies concerning the MILAGRO campaign [*Dzepina et al.*, 2011; *Hodzic et al.*, 2010; *Tsimpidi et al.*, 2011; *Shrivastava et al.*, 2011]. The representation of POA in emission inventories (which typically suppose that POA are non-volatile) has therefore to be rethought because they are based on PM measurements

after some significant dilution of the emissions and do not account for the gaseous fraction of the SVOC present in POA.

SOA can be modeled with different approaches. One approach is the two lumped product method [*Odum et al.*, 1996b; *Schell et al.*, 2001], which is based on empirical data obtained in smog chambers. Another approach is the volatility basis set [*Donahue et al.*, 2006], which treats the chemical evolution of an aggregate distribution of semi-volatile material according to their volatilities. Finally, the molecular approach [*Pun et al.*, 2002a, 2006; *Griffin et al.*, 2003; *Tulet et al.*, 2006] associates experimental data with several molecular structures, which are surrogates of a large number of SOA species, to extrapolate SOA formation from smog chambers to the atmosphere. In the molecular approach, several processes, which are often not taken into account in the other approaches can be readily estimated (e.g., condensation into an aqueous phase, oligomerization, hygroscopicity, non-ideality) and treated explicitly in the model.

In this work, a model based on the molecular approach is presented : The Hydrophilic/-Hydrophobic Organic model (H^2O). This model includes primary SVOC, oxidation of several precursors (aromatics, isoprene, monoterpenes, sesquiterpenes) under several conditions (oxidation by OH under high-NO_X and low-NO_X conditions, oxidation by O_3 and by NO_3) and several processes (condensation into an organic phase or an aqueous phase, oligomerization, hygroscopicity and non-ideality). The model formulation is described first. Next, this model is evaluated over Europe with measurements available for a one-year period and the results are discussed. Finally, the sensitivity of the model to several key parameters is investigated.

3.2 Model development

3.2.1 Overview

Previous work based on analysis of experimental data [*Saxena et al.*, 1995] and modeling [*Chang et al.*, 2010] has suggested the importance of the absorption of organic species into aqueous particles. Accordingly, H^2O, which is based on the conceptual approach of the AER/EPRI/Caltech (AEC) model [*Pun et al.*, 2002a, 2003, 2006; *Kim et al.*, 2011a], distinguishes two types of surrogate SOA species : hydrophilic species (which condense mainly into an aqueous phase) and hydrophobic species (which condense only into an organic phase due to their low affinity with water). Hydrophilic species may condense into an organic phase in the absence of aqeuous particles, i.e. at very low relative humidities (see Table 3.1). Distinction between hydrophobic and hydrophilic compounds is based on their octanol/water coefficient [*Pun et al.*, 2006] or their partitioning between the organic and the aqueous phases [*Couvidat and Seigneur*, 2011]. Highly oxygenated compounds (like tetrols), organic acids (which can dissociate in an aqueous phase) and aldehydes (which can be hydrated in water and undergo oligomerization [*Jang et al.*, 2005; *Pun and Seigneur*, 2007]) are generally hydrophilic. Lowly oxygenated compounds with long carbon chains and aromatics are generally hydrophobic. As H^2O uses molecular structures, the organic carbon (OC) can be estimated directly from the organic matter for the comparison between the model and OC measurements (see Section 3).

H^2O uses the same conceptual structure as AEC as described by *Pun et al.* [2002a]. Activity coefficients are computed with the UNIversal Functional group Activity Coefficient (UNIFAC) thermodynamic model [*Fredenslund et al.*, 1975] but does not take into account the impact of inorganic species on the activity coefficients of hydrophilic organic species. Hygroscopicity is computed with the Zdanovskii-Stokes-Robinson (ZSR) method as used by [*Meng et al.*, 1998]. However, H^2O was optimized to be computationally efficient by using the parameters of *Liu and Zhang* [2008] for the method of Newton-Raphson presented in *Pun et al.* [2002a] and by removing useless but time consuming data in the call of UNIFAC. It includes also more organic

species than AEC (coming mainly from isoprene and primary SVOC oxidation) and accounts for processes that had not been identified when AEC was developed (oligomerization, impact of NO_X on the chemistry of SOA formation). The hydrophilic module was also corrected to take into account infinite dilution as reference for partitioning instead of the mixture dilution (i.e., the mixture of water and the other organic compounds) when Henry's law is used.

To simulate OM formation, H^2O is implemented in the Polair3D air quality model [*Sartelet et al.*, 2007] of the Polyphemus air quality platform [*Mallet et al.*, 2007] and is coupled with the Carbon Bond 05 model (CB05) [*Sarwar et al.*, 2008] for the gas-phase chemistry, ISORROPIA [*Nenes et al.*, 1998] for the formation of inorganic aerosol and the SIze REsolved Aerosol Model (SIREAM) [*Debry et al.*, 2007a] for simulating the dynamics of the aerosol size distribution. The amount of liquid water and the pH computed with ISORROPIA are used to compute the partitioning of hydrophilic compounds between the gas phase and the aqueous phase as done by *Pun et al.* [2002a]. CB05 was modified to take into account SOA formation [*Kim et al.*, 2011b].

3.2.2 Secondary organic aerosol module

In H^2O, SOA are formed from 4 classes of precursors : aromatic compounds, isoprene, monoterpenes and sesquiterpenes. For theses classes of precursors, which include a great number of species, only a few surrogate precursor species are used to represent all the species as customary in gas-phase chemical mechanisms (for example, the compound noted HUM, for humulene, is used to represent all sesquiterpenes). Properties of the surrogate SOA species and reactions added to CB05 are listed in Tables 3.1 and 3.2, respectively.

The following nomenclature is used to name the model species. The species names begin either by "Bi" for biogenic compounds or by "An" for anthropogenic compounds. The suffix of the name corresponds to the species type. "A2D" and "A1D" mean that the species are hydrophilic and are respectively a diacid and a monoacid. "A0D" means that the species is hydrophilic and non-dissociative. "NIT" and "NIT3" mean that the compound is an hydrophobic nitrate or trinitrate. "BlP", "BmP" and "ClP" mean that the compounds are hydrophobic and are more or less volatile (lP and mP for low and medium saturation vapor pressure, respectively). AnBlP, AnBmP and AnClP are formed by oxidation of aromatic species (B and C refer to semi-volatile and non-volatile organic compouds, respectively). BiA0D, BiA1D, BiA2D and BiNIT are formed by oxidation of monoterpenes, BiBlP and BiBmP by oxidation of sesquiterpenes. Finally, BiMGA, BiNGA are acids formed by oxidation of isoprene under high-NO_X conditions ; BiMT, BiPER and BiDER are formed under low-NO_X conditions and BiNIT3 by oxidation of isoprene by the nitrate radical NO_3 (see *Couvidat and Seigneur* [2011] for details).

For aromatic compounds, toluene (TOL) and xylene (XYL) are used as precursors. The precursors react with OH to form oxidation products (TOLP and XYLP, respectively). These radicals may then react preferentially with HO_2, MO_2 (methylperoxy radical) or C_2O_3 (peroxyacetyl radical) under low-NO_X conditions or with NO or NO_3 under high-NO_X conditions. Note that all reaction pathways are simulated but some prevail under low-NO_X conditions whereas others prevail under high-NO_X conditions ; they may contribute similarly in the NO_X transition regime. AnBlP and AnBmP are formed by oxidation of aromatic compounds under high-NO_X conditions and AnClP (which is assumed to be non-volatile based on data from *Ng et al.* [2007b]) is formed under low-NO_X conditions. These compounds are hydrophobic. Their stoichiometric coefficients and saturation vapor pressures are estimated from the experiments of *Ng et al.* [2007b]. *Svendby et al.* [2008] found an enthalpy of vaporization between 40 $kJ.mol^{-1}$ and 60 $kJ.mol^{-1}$. A mean value of 50 $kJ.mol^{-1}$ is used here for the enthalpy of vaporization of AnBlP and AnBmP.

For SOA formation from isoprene oxidation, a previously developed model [*Couvidat and Seigneur*, 2011] is included. It takes into account SOA formation under different conditions (oxi-

TABLE 3.1 – Properties of the different surrogate SOA species.

Species	Type[a]	Molecular structure	MW[b]	H [c]	P^{0} [d]	ΔH[e]	Comments
BiMT	A	methyl tetrol	136	0.805	1.45×10^{-6}	38.4	-
BiPER	A	methyl dihydroxy dihydroperoxide	168	0.111	2.61×10^{-6}	38.4	-
BiDER	A	methyl tetrol	136	2.80	4.10×10^{-7}	38.4	-
BiMGA	A	methyl glyceric acid (MGA)	120	1.13×10^{-2}	1.4×10^{-5}	43.2	pK$_a$ = 4.0
BiNGA	B	nitrate derivative of MGA	165	-	1.4×10^{-5}	43.2	See Eq. 3.1
BiNIT3	B	methyl hydroxy trinitrate butane	272	-	1.45×10^{-6}	38.4	-
BiA0D	A	pinonaldehyde	168	4.82×10^{-5}	2.70×10^{-4}	50	See Eq. 3.2
BiA1D	A	norpinic acid	170	2.73×10^{-3}	2.17×10^{-7}	50	pK$_a$ = 3.2
BiA2D	A	pinic acid	186	6.52×10^{-3}	1.43×10^{-7}	50	pK$_{a1}$ = 3.4, pK$_{a2}$ = 5.1, DRH[f]=0.79
BiNIT	A	Nitrooxy-limonene-1-ol	215	-	2.5×10^{-6}	109	-
BiBlP	B	C15 hydroxy nitrate aldehyde	298	-	6.0×10^{-10}	175	-
BiBmP	B	C15 oxo aldehyde	236	-	3.0×10^{-7}	175	-
AnBlP	B	methyl nitro benzoic acid	167	-	6.8×10^{-8}	50	-
AnBmP	B	methyl hydroxy benzoic acid	152	-	8.4×10^{-6}	50	-
AnClP	C	No structure	167	-	-	-	-

a) Type A : hydrophilic species, type B : hydrophobic species, type C : hydrophobic non-volatile species, which is not used to compute activity coefficients
b) Molecular weight [g.mol^{-1}]
c) Henry's law constant [(μg/μg water)/(μg/m^3)] at 298K
d) Saturation vapor pressure [torr] at 298K
e) Enthalpy of vaporization [kJ.mol^{-1}]
f) Deliquescence relative humidity : if RH < DRH, the species is solid (Type B), if RH > DRH, the species is liquid (Type A)

dation by OH under low-NO_X and high-NO_X conditions and oxidation by NO_3) and hydrophilic properties of the various compounds. The compound named BiNGA formed under high-NO_X conditions can undergo oligomerization with an effective partitioning constant :

$$K_{p,eff} = K_p(1 + K_{oligo}) \tag{3.1}$$

where $K_{p,eff}$ is the effective partitioning constant, K_p is the monomer partitioning constant as defined by *Pankow* [1994a], and K_{oligo} represents the ratio of the oligomer mass to the monomer mass (equal to 64.2).

For monoterpenes, the oxidation scheme is based on *Pun et al.* [2006]. Three precursors are used : API (for α-pinene and sabinene), BPI (for β-pinene and Δ^3-carene) and LIM (for limonene and other monoterpenes and terpenoïds). For oxidation by OH and O_3, the reaction scheme is

TABLE 3.2 – Reactions leading to SOA formation[a].

Reaction	Kinetic rate parameter (s^{-1} or $molecule^{-1}.cm^3.s^{-1}$)
ISOP + OH → ISOR + OH	$2.54 \times 10^{-11} \times \exp(\frac{408}{T})$
ISOP + NO_3 → ISON + NO_3	$3.03 \times 10^{-12} \times \exp(\frac{-448}{T})$
ISOR + HO_2 → 0.282 BiPER + 0.030 BiDER + HO_2	$2.05 \times 10^{-13} \times \exp(\frac{1300}{T})$
ISOR + C_2O_3 → 0.026 BiMT + 0.219 MACR + C_2O_3	$8.40 \times 10^{-14} \times \exp(\frac{221}{T})$
ISOR + MeO_2 → 0.026 BiMT + 0.219 MACR + MeO_2	$3.40 \times 10^{-14} \times \exp(\frac{221}{T})$
ISOR + NO → 0.418 MACR + 0.046 ISON + NO	$2.43 \times 10^{-12} \times \exp(\frac{360}{T})$
ISOR + NO_3 → 0.438 MACR + NO_3	1.20×10^{-12}
ISON + OH → OH	1.30×10^{-11}
ISON + NO_3 → 0.074 BiNIT3 + NO_3	6.61×10^{-13}
MACR + NO → NO	$2.54 \times 10^{-12} \times \exp(\frac{360}{T})$
MACR + HO_2 → HO_2	$1.82 \times 10^{-13} \times \exp(\frac{1300}{T})$
MACR + MeO_2 → MeO_2	$3.40 \times 10^{-14} \times \exp(\frac{221}{T})$
MACR + NO_2 → MPAN + NO_2	$2.80 \times 10^{-12} \times \exp(\frac{181}{T})$
MPAN → MACR	$1.60 \times 10^{16} \times \exp(\frac{-13486}{T})$
MPAN + OH → 0.067 BiMGA + 0.047 BiNGA + OH	3.20×10^{-11}
MPAN + NO_3 → 0.067 BiMGA + 0.047 BiNGA + NO_3	3.20×10^{-11}
BiPER + hν → Degradation products	50 times faster than photolysis of H_2O_2
API + OH → 0.30 BiA0D + 0.17 BiA1D + 0.10 BiA2D + OH	$1.21 \times 10^{-11} \times \exp(\frac{440}{T})$
API + O_3 → 0.18 BiA0D + 0.16 BiA1D + 0.05 BiA2D + O_3	$5.00 \times 10^{-16} \times \exp(\frac{-530}{T})$
API + NO_3 → 0.70 BiA0D + 0.10 BiNIT + NO_3	$1.19 \times 10^{-12} \times \exp(\frac{-490}{T})$
BPI + OH → 0.07 BiA0D + 0.08 BiA1D + 0.06 BiA2D + OH	$2.38 \times 10^{-11} \times \exp(\frac{357}{T})$
BPI + O_3 → 0.09 BiA0D + 0.13 BiA1D + 0.04 BiA2D + O_3	1.50×10^{-17}
BPI + NO_3 → 0.02 BiA0D + 0.63 BiNIT + NO_3	2.51×10^{-12}
LIM + OH → 0.35 BiA0D + 0.20 BiA1D + 0.0035 BiA2D + OH	$4.20 \times 10^{-11} \times \exp(\frac{401}{T})$
LIM + O_3 → 0.09 BiA0D + 0.10 BiA1D + O_3	$2.95 \times 10^{-15} \times \exp(\frac{783}{T})$
LIM + NO_3 → 0.69 BiA0D + 0.27 BiNIT + NO_3	1.22×10^{-11}
HUM + OH → 0.74 BiBmP + 0.26 BiBlP + OH	2.93×10^{-10}
TOL + OH → ... + 0.25 TOLP	$1.80 \times 10^{-12} \times \exp(\frac{355}{T})$
TOLP + HO_2 → 0.78 AnClP + HO_2	$3.75 \times 10^{-13} \times \exp(\frac{980}{T})$
TOLP + C_2O_3 → 0.78 AnClP + C_2O_3	$7.40 \times 10^{-13} \times \exp(\frac{765}{T})$
TOLP + MeO_2 → 0.78 AnClP + MeO_2	$3.56 \times 10^{-14} \times \exp(\frac{708}{T})$
TOLP + NO → 0.097 AnBlP + 0.748 AnBmP + NO	$2.70 \times 10^{-12} \times \exp(\frac{360}{T})$
TOLP + NO_3 → 0.097 AnBlP + 0.748 AnBmP + NO_3	1.2×10^{-12}
XYL + OH → ... + 0.274 XYLP	1.70×10^{-11} x $\exp(\frac{116}{T})$
XYLP + HO_2 → 0.71 AnClP + HO_2	$3.75 \times 10^{-13} \times \exp(\frac{980}{T})$
XYLP + C_2O_3 → 0.71 AnClP + C_2O_3	$7.40 \times 10^{-13} \times \exp(\frac{765}{T})$
XYLP + MeO_2 → 0.71 AnClP + MeO_2	$3.56 \times 10^{-14} \times \exp(\frac{708}{T})$
XYLP + NO → 0.063 AnBlP + 0.424 AnBmP + NO	$2.70 \times 10^{-12} \times \exp(\frac{360}{T})$

a) Oxidants may be present as both reactants and products so that a reaction added to CB05 will not affect the original photochemical oxidant concentrations. MeO_2 and C_2O_3 are respectively the methylperoxy radical and the peroxyacetyl radical.

taken from *Pun et al.* [2006] with the same species and the same properties. Only the enthalpies of vaporization of BiA0D and BiA1D are decreased to 50 $kJ.mol^{-1}$ [*Svendby et al.*, 2008]. For

oxidation by NO_3, the reaction scheme is based on several studies where organonitrates and aldehydes were formed [*Hallquist et al.*, 1999; *Spittler et al.*, 2006]. BiA0D and BiNIT are used to represent, respectively, the formation of aldehydes and organonitrates. Yields of *Hallquist et al.* [1999] for aldehydes formed from the oxidation of different monoterpenes are used as yields for BiA0D. Yields of aerosols from *Hallquist et al.* [1999] and *Spittler et al.* [2006] are used to determine the stoichiometric coefficients and the saturation vapor pressure of BiNIT. BiA0D undergoes oligomerization via an effective Henry's law constant [*Pun and Seigneur*, 2007] :

$$H_{eff} = H\left(1 + 0.1\left(\frac{a(H^+)}{10^{-6}}\right)^{1.91}\right) \tag{3.2}$$

where H_{eff} is the effective Henry's law constant of BiA0D, H is the monomer Henry's law constant of BiA0D, and $a(H^+)$ is the activity of protons in the aqueous phase. As the parameterization used an effective Henry's law constant, the formation of oligomers could strongly vary with the pH and the amount of water. However, fine particles are generally very acidic [*Ludwig and Klemm*, 1990; *Keene et al.*, 2004] and oligomer formation from BiA0D will then in fact appear as an irreversible process, even though the parameterization is formulated as a reversible process.

Formation of SOA from sesquiterpene oxidation is determined as in *Pun et al.* [2006]. HUM represents all sesquiterpenes and two hydrophobic compounds are formed from its oxidation : BiBmP and BiBlP .

3.2.3 Primary and aged organic aerosol module

Primary organic compounds are treated as SVOC. Their concentrations in the particle phase depend on the amount of organic matter into which SVOC will condense and temperature (which influences the volatility of compounds). To treat POA as SVOC, the curve of dilution of POA from diesel exhaust of *Robinson et al.* [2007] was fitted to represent the dilution with three molecules : POAlP for compounds of a low volatility, POAmP for compounds of medium volatility and POAhP for compounds of high volatility. Based on this fitting, POAlP, POAmP and POAhP represent respectively 25%, 32% and 43% of "non-diluted" POA emissions from diesel vehicles with partitioning constants of 1.1 $m^3.\mu g^{-1}$, 0.0116 $m^3.\mu g^{-1}$ and 0.00031 $m^3.\mu g^{-1}$, respectively. Properties of primary SVOC are listed in Table 3.3. The least volatile compound (POAlP) does not condense entirely on the particle phase at low concentrations of OM. Areas with low concentrations of organic aerosols should then be sensitive to the value of the partitioning constant of POAlP. To study POA dilution, *Robinson et al.* [2007] used mostly data at concentrations greater than 20 $\mu g.m^{-3}$. There is therefore large uncertainties on the partitioning of SVOC at concentrations typical of ambient conditions. As a result, POA evaporation could then be overestimated (in that case SOA, formation from SVOC oxidation may be overestimated) or underestimated (in that case, SOA formation from primary SVOC oxidation may be underestimated). Information on the amount of POA at very low concentrations of OM is needed to know if there is a significant fraction of non-volatile POA and how SVOC partition.

By default and due to the lack of data, we suppose that SVOC emitted from other sources have the same dilution behavior as diesel exhaust. *Shrivastava et al.* [2006] show a very similar dilution behavior between diesel exhaust and wood smoke. A mean organic matter (OM)/organic carbon (OC) ratio of 1.3 for primary SVOC (ratio typical of hydrocarbon aerosols) is chosen.

SVOC in the gas phase can be oxidized, form less volatile compounds and a significant amount of SOA [*Robinson et al.*, 2007; *Grieshop et al.*, 2009]. For one oxidation step, we supposed, following *Grieshop et al.* [2009], that SVOC volatility is reduced by a factor of 100 and that the molar mass of the SVOC is increased by 40% due to oxygen addition. However, following *Pye and Seinfeld* [2010], SVOC were supposed to undergo only one oxidation step for the

following reasons. First, chamber experiments are conducted on short time scales and provide information only on the first oxidation steps. Second, this reduction of volatility could be less valid for later generations of oxidation for which molecular fragmentation becomes more important. Thus, aging of primary aerosol is taken into account with the following three reactions in the gas phase, which were added to CB05 :

$$\mathrm{POAlP} + \mathrm{HO} \xrightarrow{k} \mathrm{SOAlP} \quad \text{(R 3.1)}$$

$$\mathrm{POAmP} + \mathrm{HO} \xrightarrow{k} \mathrm{SOAmP} \quad \text{(R 3.2)}$$

$$\mathrm{POAhP} + \mathrm{HO} \xrightarrow{k} \mathrm{SOAhP} \quad \text{(R 3.3)}$$

with k the kinetic rate constant equal to 2×10^{-11} molecules^{-1}.cm^3.s^{-1} [*Grieshop et al.*, 2009]. SOAlP, SOAmP and SOAhP are the aged SVOC. Properties of aged SVOC are listed in Table 3.3.

TABLE 3.3 – Properties of primary and aged SVOC.

Surrogate	MW[a]	K_p [b]	ΔH_{vap} [c]	OM/OC [d]
POAlP	280	1.1	106	1.3
POAmP	280	0.0116	91	1.3
POAhP	280	0.00031	79	1.3
SOAlP	392	110	106	1.82
SOAmP	392	1.16	91	1.82
SOAhP	392	0.031	79	1.82

a) Molecular weight [g.mol^{-1}]
b) Partitioning constant [m^3.μg^{-1}] at 298K obtained by fitting to *Robinson et al.* [2007]
c) Enthalpy of vaporization [kJ.mol^{-1}] from *Robinson et al.* [2007]
d) Ratio of organic mass and organic carbon mass based on data from *Grieshop et al.* [2009]

Unlike SOA surrogate compounds, no molecular structure is associated with primary and aged SVOC. Their partitioning between the gas phase and the organic particle phase is calculated with a partitioning constant K_p (values in Table 3.3) whereas for SOA surrogate compounds the partitioning constant depends on the mean molecular weight of the organic phase and the activity coefficient of the molecule. For the computation of activity coefficients of SOA surrogate compounds, a molecular structure is needed for POAlP, POAmP, POAhP, SOAlP, SOAmP and SOAhP. They are represented by a single POA species with an "average" structure representative of atmospheric PM. This average structure is constituted of 40% of $C_{23}H_{47}COOH$, 5% of $C_8H_{17}CH{=}CHC7H_{14}COOH$, 15% of 4-(2-propio)-syringone, 12% of $C_{29}H_{60}$ and 28% of 2-carboxybenzoic acid based on *EPRI* [1999]. This is a simplifying assumption as each source of primary organic aerosol emits different molecules with different structures. Some attempts have been made to use molecular surrogates to represent various POA emissions (e.g., *Pun* [2008]; *Lee-Taylor et al.* [2011]). However, there is still considerate uncertainty due to a lack of complete molecular data for POA and, consequently, we selected this simple POA representation. Moreover, it is possible that two organic aerosols emitted from two different sources have little affinity with each other, do not mix and evolve separately. In that case, instead of treating aerosols as an internal mixture (all particles in a given size range having the same composition),

it would be necessary to treat aerosols as an external mixture (each aerosol group having its own composition). This part of the model can be refined as more experimental data become available on the chemical composition of major POA sources. The molecular structure used for the mixture of POAlP, POAmP, POAhP, SOAlP, SOAmP and SOAhP is not used to compute activity coefficients of these individual compounds (their partitioning uses a simple partitioning constant assuming constant activity coefficients) but to estimate the impact of these anthropogenic SVOC on the partitioning of other SVOC.

Robinson et al. [2007] also argue for the presence of Intermediate Volatility Organic Compounds (IVOC). IVOC were taken into account in several studies using the VBS framework and lead to improvement in the urban to regional ratio of OM [*Robinson et al.*, 2007; *Shrivastava et al.*, 2008]. However, IVOC were not taken into account here for several reasons. First, the amount of emitted IVOC is highly uncertain (1 to 3 times the amount of emitted SVOC, and there is already, a large uncertainty on emissions of SVOC). Second, there is also a large uncertainty on the oxidation mechanism of IVOC. To have a better representation of IVOC oxidation, *Pye and Seinfeld* [2010] used naphthalene as a surrogate for IVOC and used the yields from smog chamber experiments [*Chan et al.*, 2009; *Kautzman et al.*, 2010] to develop a mechanism of oxidation of IVOC. They found only minor concentrations of SOA from IVOC (only 5% of total OM and 14% of SOA from SVOC). However, *Pye and Seinfeld* [2010] discussed the fact that naphthalene may not be an appropriate candidate for lumping IVOC. We consider that more work should be done on IVOC emissions and the associated oxidation mechanism before their incorporation in the model.

3.3 Simulation of organic aerosols over Europe

3.3.1 Description of the simulation configurations

OM was simulated over Europe from July 2002 to July 2003. During this period, OC was measured one day per week at 12 monitoring stations from the EMEP network. Locations and names of the stations are shown in Fig. 3.1. OC concentrations simulated by the model are estimated using the OM/OC ratios of the surrogate compounds and are evaluated by comparison to measurements.

Input data to Polair3D/Polyphemus were prescribed as follows. Meteorology was obtained from the European Centre for Medium-Range Weather Forecasts (ECMWF) model. Boundary conditions for gaseous species were obtained from the Model for OZone And Related chemical Tracers (Mozart v2.0 [*Horowitz et al.*, 2003]) and boundary conditions for particles from ECHAM5-HAMMOZ [*Pozzoli et al.*, 2011]. Anthropogenic emissions of gases and particles were taken from the EMEP inventory [*Vestreng*, 2003], except for POA and EC, which were taken from *Junker and Liousse* [2008]. Biogenic emissions were estimated with the Model of Emissions of Gases and Aerosols from Nature (MEGAN) [*Guenther et al.*, 2006].

Because the inventory of *Junker and Liousse* [2008] only provides emissions of EI-POA (emission inventory POA measured solely as PM and traditionnally assumed to be non-volatile) and does not take into account that a part of SVOC ais present in the gas phase and is missing from the inventory. Here, the model does not use EI-POA emissions and all primary compounds are supposed to be SVOC. SVOC emissions are estimated by applying a SVOC/EI-POA ratio to transform EI-POA emissions into emissions of SVOC. *Junker and Liousse* [2008] use an emission factor of 0.5 g/kg-fuel for diesel POA whereas *Robinson et al.* [2007] give an emission factor of non-diluted POA of 2.5 g/kg-fuel indicating that at least 80% of diesel SVOC are in the gas phase. Therefore, for the reference simulation, a SVOC/EI-POA ratio of 5 for all sources of SVOC is chosen. It is, however, possible that some of the difference may be due to different

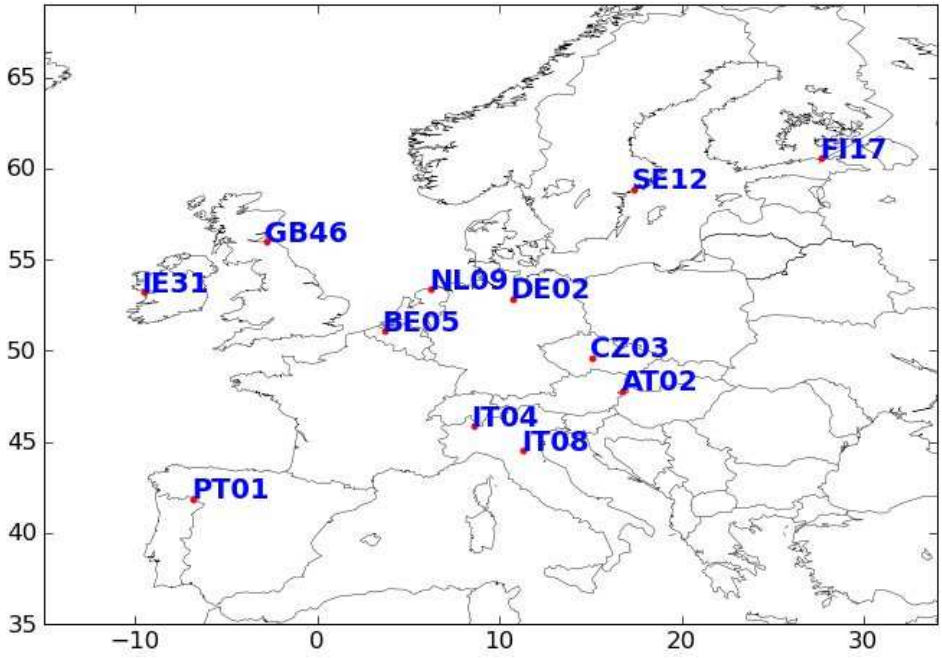

FIGURE 3.1 – Locations and names of OC monitoring stations.

types of engines and experimental conditions. *Junker and Liousse* [2008] used a OC/EC ratio of 0.5 and determined the OC emission factor from the EC emission factor. This ratio is derived from U.S. emission sampling experiments [*Cooke et al.*, 1999] where the dilution of the vehicule exhaust is at least by a factor of 100 [*Schauer et al.*, 1999]. *Chirico et al.* [2011] studied the evolution of the OM/BC ratio (which is approximately equal to 1.3 × OC/EC) at low organic loading in a tunnel. They found that a OC/EC ratio of 0.5 can only be obtained at low organic loading (from 10 to 20 μg.m^{-3}). The emission factor of OC used in Junker and Liousse should then correspond to low organic loading and probable missing emissions should be accounted for. Although different sources could have different SVOC/EI-POA ratios with different dilution behaviors, available experimental data [*Shrivastava et al.*, 2006] suggest that a large part of SVOC can be in the gas phase even at low dilution ratios. At this point, an average ratio of 5 seems to be a reasonable estimate. The uncertainty associated with this parameter is tested below.

For biomass burning emissions, the inventory of *Liousse et al.* [2010] is used. This inventory does not provide information on injection heights, which is a potentially significant source of uncertainty for air quality modeling. A parameterization was developed to estimate injection heights depending on PM emissions. First, the burned area is estimated by using the emission factors of *Wiedinmyer et al.* [2006] for different land covers. Once the burned area has been estimated, emissions are injected between two heights (Htop and Hbottom), which depend on the burned area, based on the method of *WRAP* [2008]. Injections heights are listed in Table 3.4.

TABLE 3.4 – Injection heights as a function of the fire size class.

Class	1	2	3	4	5
Size (acres)	0-10	10-100	100-1000	1000-5000	> 5000
Hbottom (m)	0	324	1238	2168	2430
Htop (m)	25.6	864	3600	5202	6480

Results from four different simulations (noted SimRef, SimFire, Sim7, and SimEMEP) are presented and evaluated. The first simulation (SimRef) is the reference simulation ; it does not include fire emissions, uses the inventory of *Junker and Liousse* [2008] for anthropogenic carbonaceous emissions and a SVOC/EI-POA ratio of 5. The other simulations differ from the reference simulation via one of these components : fire emissions for SimFire, a SVOC/EI-POA ratio of 7 for Sim7 (which is the ratio for a very low concentration of OM of 1 μg.m^{-3} in the dilution sampler and, therefore can be considered as the highest possible ratio) and POA and EC anthropogenic emissions from EMEP for SimEMEP (see Table 3.5 for details of simulation configurations).

TABLE 3.5 – Configurations of the different simulations.

Name	SimRef	SimFire	Sim7	SimEMEP
SVOC/EI-POA ratio	5	5	7	5
Fire emissions	No	Yes	No	No
OC & EC inventory	*Junker and Liousse* [2008]	*Junker and Liousse* [2008]	*Junker and Liousse* [2008]	EMEP

3.3.2 Simulation results

Performance statistics (RMSE : Root Mean Square Error, MNE : Mean Normalized Error, MNB : Mean Normalized Bias, NME : Normalized Mean Error, NMB : Normalized Mean Bias, MFE : Mean Fractional Error and MFE : Mean Fractional Bias) for the four model simulations are shown in Tables 3.6 and 3.7. Comparisons between observed and simulated OC at the twelve EMEP monitoring stations over the entire year are shown in Fig. 3.2 for two of these simulations, SimRef and SimFire.

In the four simulations, OC is underestimated both in summer (from May to October) and in winter (from November to April). Correlations are higher in summer (0.67 for SimRef) than in winter (0.48 for SimRef). In winter, correlations are higher when the station PT01 is not taken into account (0.55 against 0.48 for SimRef). This station has a negative annual correlation for SimRef due to the low concentrations given by the model in winter whereas very high concentrations (between 5 and 35 μg.m^{-3}) are observed at the station (as shown in Fig. 3.2). This observed high OC concentration at PT01 is unexplained by the model and by other models [*Simpson et al.*, 2007; *Bessagnet et al.*, 2008]. It may be due to missing emissions in the inventory or the presence of local pollution sources in winter near the station.

Adding forest fires does not improve overall model results significantly as there is no significant change in the global RMSE (3.68 μg.m^{-3} for SimRef against 3.64 μg.m^{-3} for SimFire). The RMSE even increases and the correlation decreases at several stations (CZ03, DE02, FI17, SE12). At station SE12, SimFire simulates a large unobserved peak (as shown in Fig. 3.2). This peak may be due to a low fire injection height given by the algorithm for a forest fire of medium intensity (Class 2 or 3), which may actually have been emitted above the planetary boundary layer. On the contrary, some big fires may not contribute significantly to the ground-level OC concentrations due to an injection height above the planetary boundary layer. Even if the results of the model does not improve significantly on average, fires seem to contribute locally to OC in April and May as shown in Fig. 3.2. Further work on implementation of forest fires emissions with emphasis on the injection heights is needed to minimize this source of uncertainty in air quality modeling.

Using the emissions of *Junker and Liousse* [2008] with a SVOC/EI-POA ratio of 7 or EMEP inventory emissions leads to improved results with higher annual correlations (0.53 for Sim7 and

TABLE 3.6 – OC Statistics for the different simulations at individual EMEP stations. Concentrations and the root mean-square error (RMSE) are in $\mu g.m^{-3}$.

	SimRef				SimFire			
Stations	mean measured OC	mean modeled OC	RMSE	correlation	mean measured OC	mean modeled OC	RMSE	correlation
AT02	5.57	3.75	3.18	0.57	5.57	4.09	3.13	0.53
BE05	4.12	1.68	2.86	0.76	4.12	1.78	2.74	0.79
CZ03	4.54	3.35	2.35	0.69	4.54	3.80	2.49	0.65
DE02	4.30	2.24	2.97	0.84	4.30	2.51	3.02	0.70
FI17	2.08	1.14	1.68	0.68	2.08	1.30	1.70	0.57
GB46	1.53	0.66	1.13	0.76	1.53	0.71	1.06	0.78
IE31	1.20	0.46	1.15	0.89	1.20	0.57	1.03	0.76
IT04	7.79	2.83	8.32	0.13	7.79	3.07	8.17	0.15
IT08	5.92	2.48	4.58	0.24	5.92	2.71	4.45	0.21
NL09	2.59	1.32	1.80	0.75	2.59	1.41	1.71	0.76
PT01	4.10	0.77	5.72	-0.02	4.10	0.88	5.67	-0.02
SE12	2.12	1.12	1.49	0.83	2.12	1.33	1.76	0.49
	SimRef				SimFire			
Stations	mean measured OC	mean modeled OC	RMSE	correlation	mean measured OC	mean modeled OC	RMSE	correlation
AT02	5.57	4.85	3.50	0.57	5.57	4.10	2.48	0.67
BE05	4.12	4.54	2.30	0.76	4.12	3.42	1.69	0.72
CZ03	4.54	4.54	2.74	0.68	4.54	3.28	2.16	0.72
DE02	4.30	2.89	2.33	0.85	4.30	2.60	3.21	0.62
FI17	2.08	1.34	1.61	0.63	2.08	1.73	1.86	0.39
GB46	1.53	0.82	0.96	0.79	1.53	1.05	0.77	0.81
IE31	1.20	0.56	0.99	0.90	1.20	0.60	0.92	0.92
IT04	7.79	3.51	7.70	0.31	7.79	4.91	6.77	0.43
IT08	5.92	3.05	4.11	0.33	5.92	4.07	3.35	0.42
NL09	2.59	1.72	1.50	0.77	2.59	1.96	1.64	0.61
PT01	4.10	0.84	5.66	0.03	4.10	1.38	5.20	0.32
SE12	2.12	1.31	1.36	0.78	2.12	1.47	1.41	0.68

0.63 for SimEMEP) and lower RMSE (3.46 $\mu g.m^{-3}$ for Sim7 and 3.10 $\mu g.m^{-3}$ for SimEMEP) in particular in winter. Improvements in model performance are due to higher carbonaceous emissions with the EMEP inventory or the use of a higher SVOC/EI-POA ratio in Sim7. Moreover, in winter, OC is essentially constituted of anthropogenic primary SVOC (POAlP, POAmP and POAhP) and their oxidation products (SOAlP, SOAmP and SOAhP). These results indicate that OC concentrations in winter are very sensitive to anthropogenic primary SVOC emissions (concentrations of SOA from the oxidation of biogenic precursors and aromatics are low) and that the underestimation of OC in the model may be due to missing anthropogenic primary SVOC emissions and, therefore, missing SOA from SVOC oxidation. Results in summer are also better for both simulations (SimEMEP and Sim7). This is supported by Fig. 3.3 showing the relative error in OC as a function of the relative error in EC (used here as a tracer of anthropogenic primary emissions) during winter. This figure shows that these two errors are correlated (r = 0.45) and that we might expect OC concentrations to improve if anthropogenic primary

TABLE 3.7 – OC statistics for the different simulations averaged over all EMEP stations.

		Overall		Winter		Summer	
Configuration		with PT01	without PT01	with PT01	without PT01	with PT01	without PT01
SimRef	mean measured OC[a]	3.78	3.75	4.33	4.23	3.19	3.23
	mean modeled OC[a]	1.78	1.87	1.84	1.97	1.71	1.77
	correlation	0.52	0.58	0.48	0.55	0.67	0.67
	RMSE[a]	3.68	3.43	4.60	4.21	2.33	2.33
	MNE	53%	52%	58%	55%	49%	49%
	MNB	-48%	-46%	-50%	-47%	-45%	-45%
	NME	57%	54%	62%	58%	49%	48%
	NMB	-53%	-50%	-58%	-53%	-46%	-45%
	MFE	77%	73%	84%	78%	69%	68%
	MFB	-73%	-69%	-80%	-73%	-66%	-68%
SimFire	mean measured OC[a]	3.78	3.75	4.33	4.23	3.19	3.23
	mean modeled OC[a]	1.97	2.07	2.29	2.15	1.85	1.79
	correlation	0.50	0.55	0.43	0.5	0.67	0.67
	RMSE[a]	3.64	3.38	4.56	4.16	2.28	2.28
	MNE	52%	51%	57%	55%	47%	46%
	MNB	-41%	-39%	-40%	-36%	-42%	-42%
	NME	55%	52%	60%	56%	48%	47%
	NMB	-48%	-45%	-51%	-46%	-44%	-43%
	MFE	71%	68%	78%	72%	65%	64%
	MFB	-65%	-61%	-69%	-62%	-61%	-60%
Sim7	mean measured OC[a]	3.78	3.75	4.33	4.23	3.19	3.23
	mean modeled OC[a]	2.26	2.39	2.55	2.74	1.94	2.02
	correlation	0.53	0.59	0.48	0.55	0.68	0.69
	RMSE[a]	3.46	3.18	4.34	3.90	2.16	2.14
	MNE	48%	46%	51%	48%	44%	43%
	MNB	-36%	-33%	-33%	-28%	-38%	-37%
	NME	51%	48%	55%	50%	45%	44%
	NMB	-40%	-36%	-41%	-35%	-39%	-37%
	MFE	53%	59%	67%	60%	60%	58%
	MFB	-55%	-50%	-56%	-47%	-55%	-53%
SimEMEP	mean measured OC[a]	3.78	3.75	4.33	4.23	3.19	3.23
	mean modeled OC[a]	2.52	2.63	2.73	2.86	2.30	2.37
	correlation	0.63	0.69	0.60	0.68	0.72	0.72
	RMSE[a]	3.10	2.82	3.90	3.47	1.90	1.90
	MNE	42%	41%	46%	44%	37%	37%
	MNB	-22%	-19%	-18%	-14%	-26%	-25%
	NME	44%	41%	48%	44%	38%	37%
	NMB	-33%	-30%	-37%	-32%	-28%	-27%
	MFE	50%	47%	53%	49%	46%	45%
	MFB	-37%	-33%	-36%	-30%	-38%	-36%

a) in μg.m^{-3}

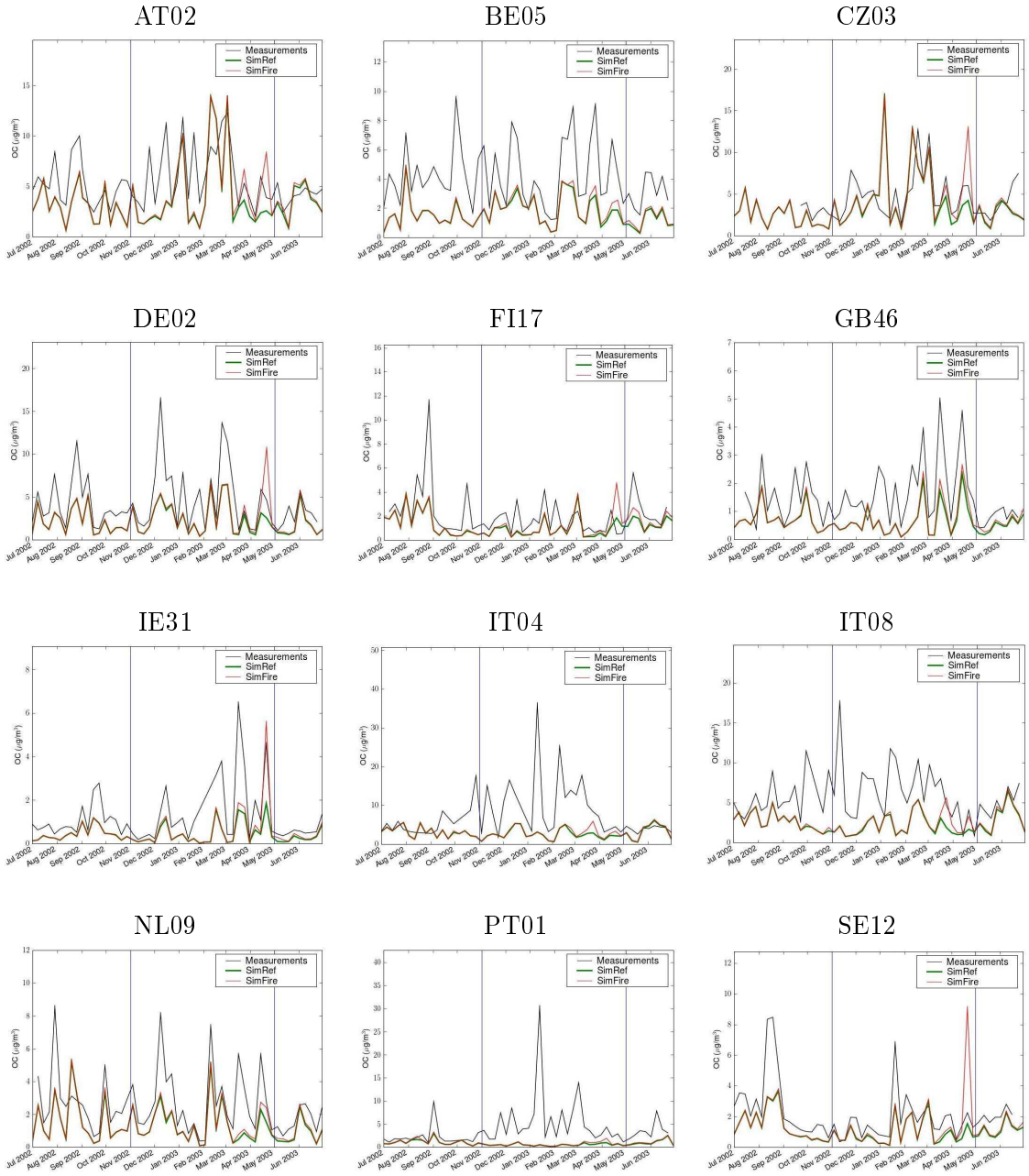

FIGURE 3.2 – Comparisons between observed and simulated OC at EMEP monitoring stations for SimRef and SimFire (as defined in Table 3.5). Vertical lines separate the winter and summer periods used to calculate statistics in Table 3.7.

carbonaceous emissions are improved.

OM concentrations are shown over Europe in Fig. 3.4 for August 2002 and February 2003. In August 2002, concentrations are higher with SimEMEP than with SimRef. SimEMEP shows greater concentrations of OM over urban areas and over the Mediterranean and the North Sea due to higher emissions from the marine traffic. For February 2003, SimRef shows very high and localized concentrations over central Europe whereas concentrations are significantly lower over the rest of Europe. SimEMEP shows high concentrations of OM over all Europe. The Mean Fractional Error (MFE) and the Mean Fractional Bias (MFB) averaged over EMEP stations

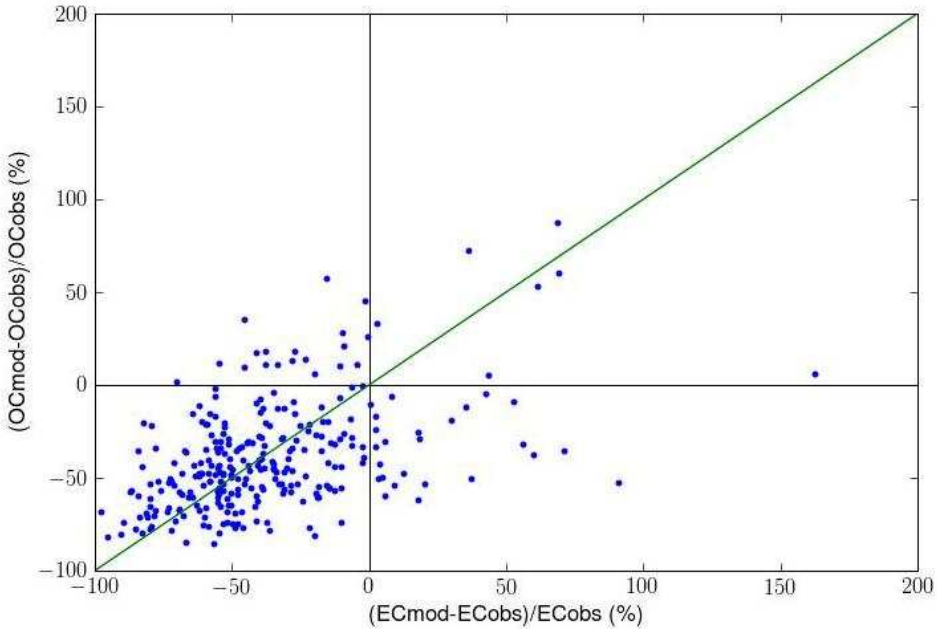

FIGURE 3.3 – Scatter diagram of errors (%) in OC and EC for all EMEP monitoring stations in winter (correlation = 0.45) ; mod and obs stand for modeled and observed.

(excluding PT01) are, respectively, 47% and -33% for SimEMEP and 73% and -69% for SimRef.

With SimEMEP, the model performance criteria proposed by *Boylan and Russell* [2006] (MFE less than 75% and MFB within ± 60%) are met for OM concentrations and almost meet the model goal criteria (MFE less than 50% and MFB within ± 30%). Furthermore, the MNE obtained with SimEMEP (42%) is lower than obtained by *Bessagnet et al.* [2008] (between 46% and 79% at EMEP stations). Correlations are similar between SimEMEP and *Bessagnet et al.* [2008] at some stations (BE05, DE02, GB46, IE31 and NL09) but are much higher at the other stations with SimEMEP (e.g., 0.67 against 0.11 at AT02). These correlations are also higher than those obtained by *Simpson et al.* [2007]. The differences between SimEMEP and those earlier studies lie mostly in the treatment of POA as SVOC. *Bessagnet et al.* [2008] found indeed low concentrations of OC in winter, which are consistent with the concentrations obtained here when non-volatile emissions of EI-POA (i.e, without SVOC emissions) are used, as shown below.

As H^2O uses a molecular approach, it is straightforward to estimate the contribution of the different precursors to OM contributions and determine the nature of the aerosol (biogenic or anthropogenic). Fig. 3.5 shows the contributions of precursors and SOA surrogates to OM concentrations over Europe calculated with SimEMEP. In summer, the main contributors are monoterpenes, aged anthropogenic SVOC and, to a smaller extent, isoprene. However, *Bessagnet et al.* [2008] simulated a very large fraction of SOA originating from isoprene oxidation in summer. One reason is that the periods compared are different (summer 2002 in this study against summer 2003 in *Bessagnet et al.* [2008]) ; the period studied by *Bessagnet et al.* [2008] was hotter and, consequently, with higher biogenic emissions. For example, isoprene emissions are 40% higher in 2003 than in 2002, whereas terpene emissions only increased by 15% from 2002 to 2003 based on MEGAN. In winter, the main contributors are primary and aged anthropogenic SVOC. The higher contribution of POA in winter is due to the decrease of volatility of SVOC (because of colder conditions), as well as the lower emissions of biogenic precursors. Aromatics and sesquiterpenes are found to be only a minor source of SOA. The low concentration of SOA from aromatics oxidation over Europe has been reported in earlier modeling studies [*Bessagnet*

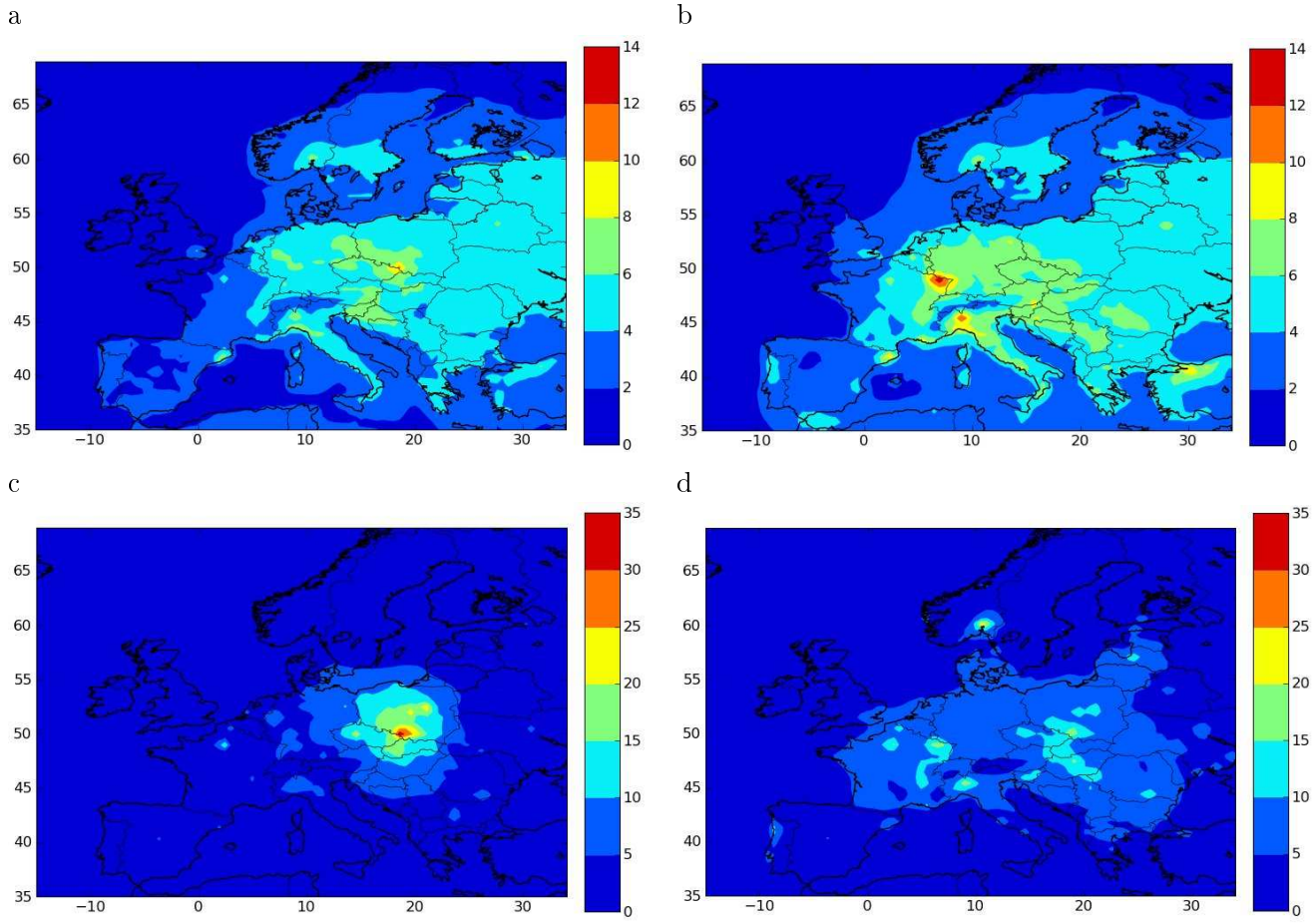

FIGURE 3.4 – Concentrations of OM over Europe in August 2002 (top) and February 2003 (bottom) for SimRef (left) and SimEMEP (right).

et al., 2008; *Henze et al.*, 2008]. However, compounds formed by oxidation of aromatics remain mostly in the gas phase and it is possible that further oxidation could occur leading to additional SOA formation, which is not taken into account in the model. Overall, sesquiterpenes are a minor precursor of SOA, nevertheless, SOA from sesquiterpene oxidation represent locally up to 0.5 μg.m^{-3} in August 2002, which is not insignificant. The contribution of sesquiterpenes to OM concentrations over Europe is low because of the low emission rates obtained with the emission model [*Guenther et al.*, 2006] (around 6% of monoterpene emissions). This low emission rates of sesquiterpenes over Europe is consistent with the results of *Karl et al.* [2009].

Fig. 3.6 shows the fraction of biogenic organic aerosols calculated with SimEMEP for August 2002 and February 2003. In summer, most of Europe is covered by an organic aerosol, which is mostly biogenic (from 50% to 90%). Only the area around the English Channel is mostly anthropogenic due to the proximity of megacities (London and Paris) and high anthropogenic marine emissions. Organic aerosols from the north of Europe are highly biogenic due to high monoterpene emissions. The large fraction of anthropogenic organic aerosol over the Atlantic ocean is due in part to missing marine emissions of organic aerosols and to the fact that organic aerosols coming from boundary conditions were classified by default as anthropogenic. In winter, the organic aerosol is almost entirely anthropogenic due to low biogenic emissions except in Portugal and in southern Europe where a small fraction of the aerosol is biogenic (around 20%).

Aerosols formed from isoprene and monoterpene oxidation are mainly hydrophilic [*Pun*

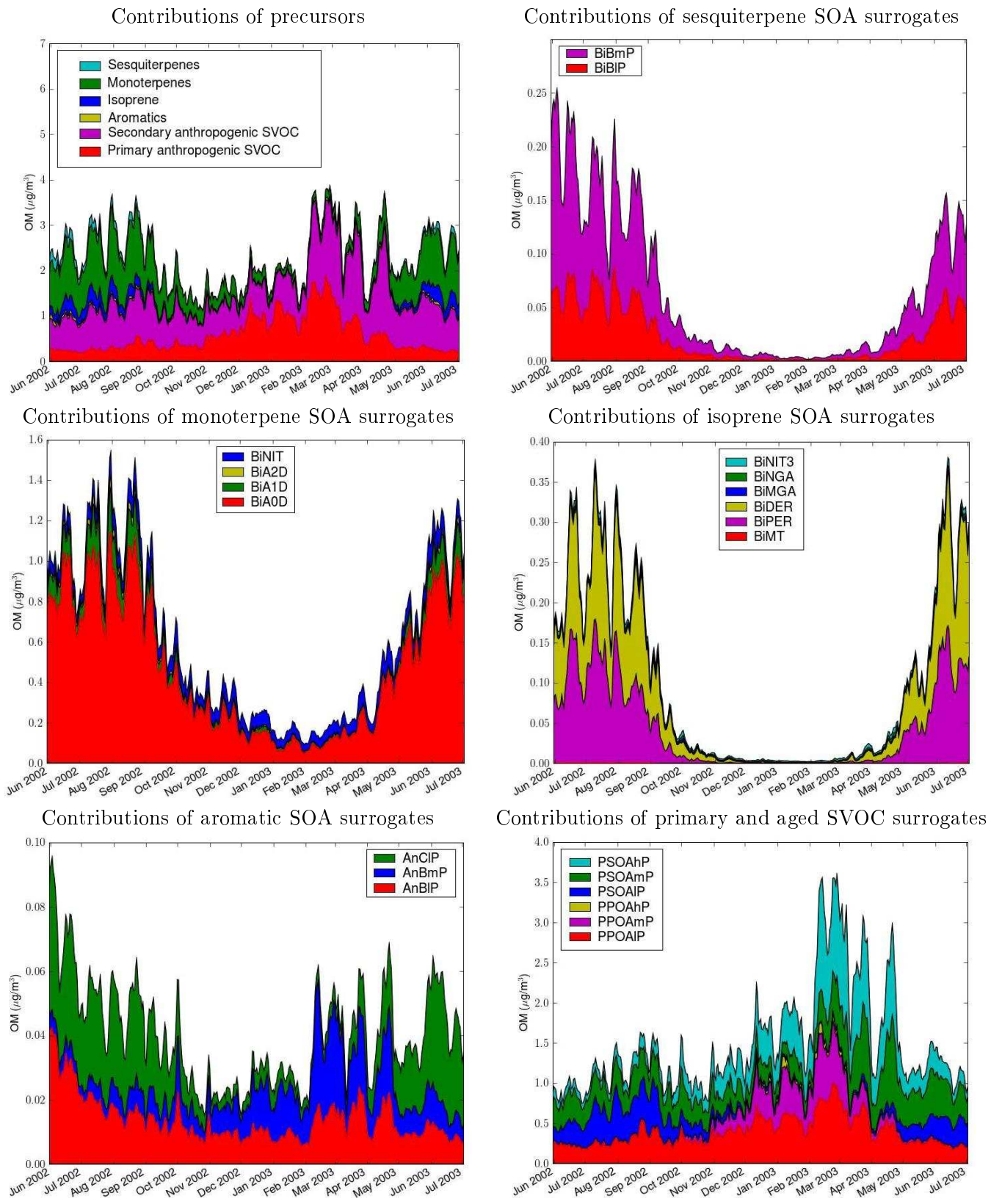

FIGURE 3.5 – Contributions of precursors (VOC and SVOC) and surrogate species to OM concentrations averaged over Europe (land and sea) calculated with SimEMEP.

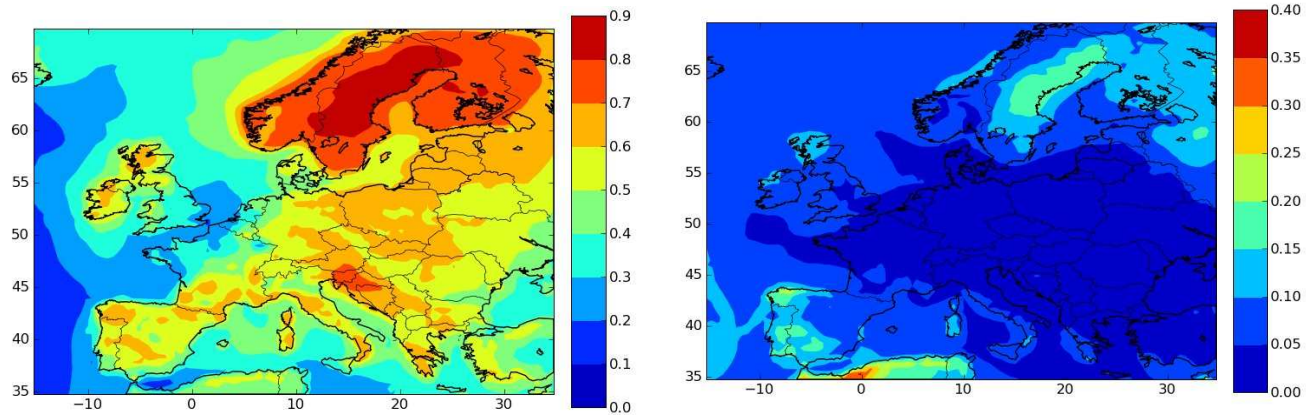

FIGURE 3.6 – Fraction of biogenic organic aerosol over Europe calculated with SimEMEP for August 2002 (left) and February 2003 (right).

et al., 2006; *Couvidat and Seigneur*, 2011] whereas other precursors lead in the model to hydrophobic compounds. Hydrophilic compounds should then be produced during summer when biogenic emissions are high. In August 2002, 95% and 92% of SOA formed from isoprene and monoterpene oxidation are found to be hydrophilic. In this model, 45% of organic aerosols are then constituted of hydrophilic compounds. However, this fraction could be underestimated because this model does not account for aging of aerosols with several oxidation steps. Aging will produce more oxygenated species that could become hydrophilic at some point and SOA found initially to be hydrophobic (SOA formed from oxidation of primary SVOC, aromatics and sesquiterpenes) could then become in part hydrophilic.

As OM is necessary to estimate PM concentrations (and not OC, which is measured), the OM/OC ratio should be evaluated to understand how well the model performs. In that respect, Fig. 3.7 shows the OM/OC ratio calculated with SimEMEP for August 2002 and February 2003. In summer, the calculated ratio is between 1.55 and 1.65 over most of Europe. The ratio decreases in winter to 1.35-1.55 due to the higher contribution of POA (which are less volatile in winter due to the decrease in temperature) and lower contributions of biogenic SOA. This ratio does not exceed 1.8 ; this value seems low compared to the ratio of 2.1 estimated by *Turpin and Lim* [2001] for rural areas. This low ratio is probably due to the low ratios of major SOA compounds, which are between 1.4 and 1.8 for monoterpene SOA compounds and 1.8 for aged anthropogenic SVOC. This ratio can be increased by adding the formation of highly oxidized species in the model with high OM/OC ratios. For this purpose, several processes can contribute significantly : aqueous-phase oxidation, additional oxidation steps or formation of organosulfates. Clearly, such processes should be studied in greater detail and possibly incorporated in future modeling studies. Fig. 3.7 shows the OM/OC ratio calculated with SimEMEP for August 2002 and February 2003. In summer, the OM/OC ratio is slightly lower with SimRef than with SimEMEP. This is due to higher emissions of primary SVOC in SimEMEP that become oxidized with a high OM/OC ratio. On the contrary, the OM/OC ratio in winter is higher with SimRef than with SimEMEP. In winter, the primary SVOC are oxidized more slowly and the contribution of primary compounds with a low OM/OC ratio is higher. In SimEMEP, as the concentration of OM is higher, primary SVOC condense more easily than with SimRef. It results in a higher OM/OC ratio with SimRef.

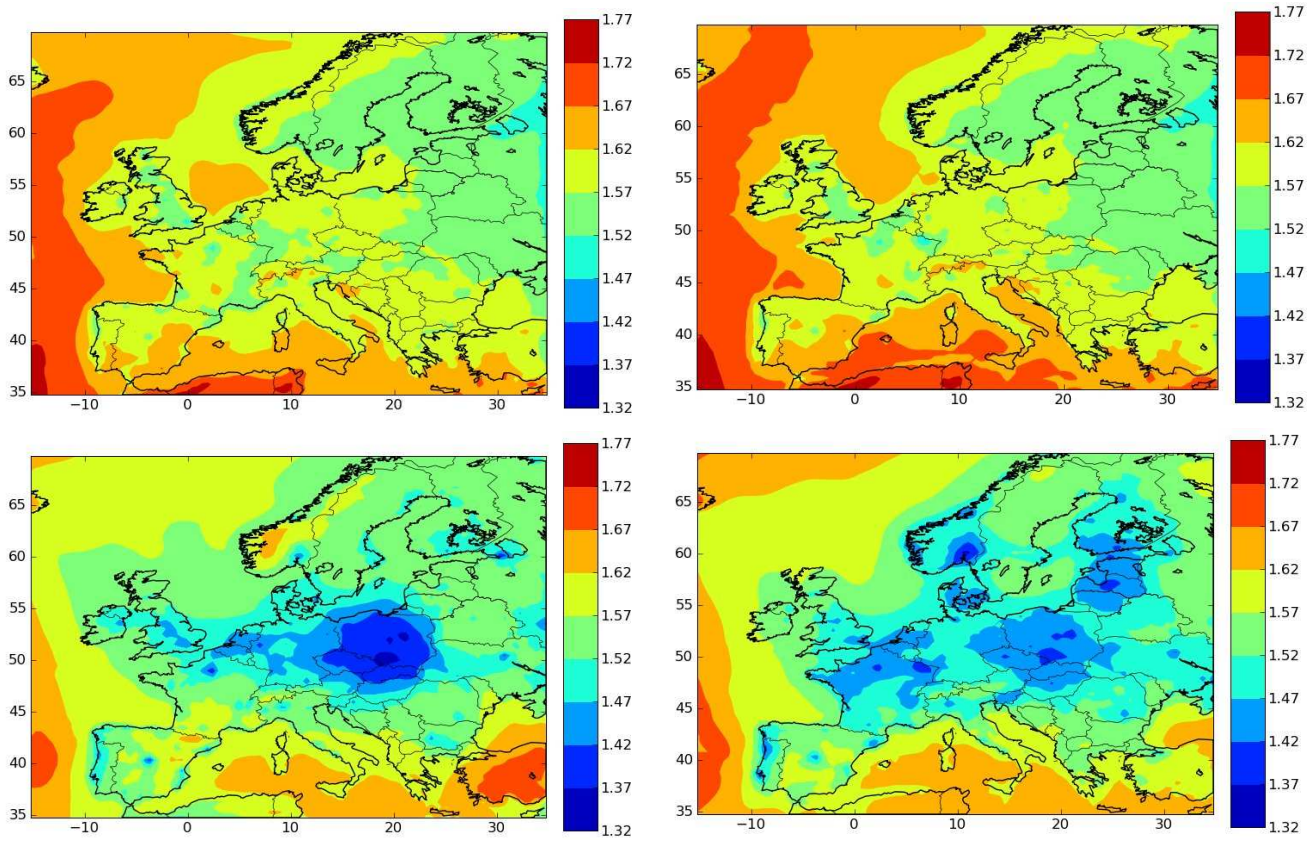

FIGURE 3.7 – OM/OC ratio over Europe calculated with SimRef (left) and SimEMEP (right) for August 2002 (top) and February 2003 (bottom).

3.4 Sensitivity analysis and investigations of organic aerosol formation

3.4.1 Impact of non-ideality on organic aerosol formation

Organic aerosols are assumed to be non-ideal in H^2O and activity coefficients are computed with the UNIFAC model. Ideality (i.e., the state in which activity coefficients are equal to one) is defined according to a reference state. For hydrophobic compounds, the reference state is the pure compound state, whereas for hydrophilic compounds the reference state is infinite dilution in water. Assuming that activity coefficients are equal to one will impact differently the partitioning of hydrophobic compounds and hydrophilic compounds. Organic aerosol concentrations with ideal state assumed were simulated for August 2002 with the SimRef configuration and results are compared with non-ideal organic aerosol concentrations. Fig. 3.8 shows the impact of assuming ideality on hydrophilic compounds, hydrophobic compounds, and OM.

For hydrophilic SOA compounds, assuming ideal conditions decreases the mean hydrophilic SOA concentrations over Europe in August 2002 from 1.32 $\mu g.m^{-3}$ to 1.13 $\mu g.m^{-3}$ on average. This decrease is observed because in an aqueous aerosol, most organic compounds tend to be stabilized by other organic compounds with which they have more affinity than with water. Assuming ideal conditions does not take this effect into account and decreases their concentrations. Over the continent, a decrease of hydrophilic SOA concentrations up to 1 $\mu g.m^{-3}$ is calculated. However, over water, hydrophilic SOA concentrations can in fact slightly increase. This small increase is due to a small increase of particulate concentrations of BiA0D (which is

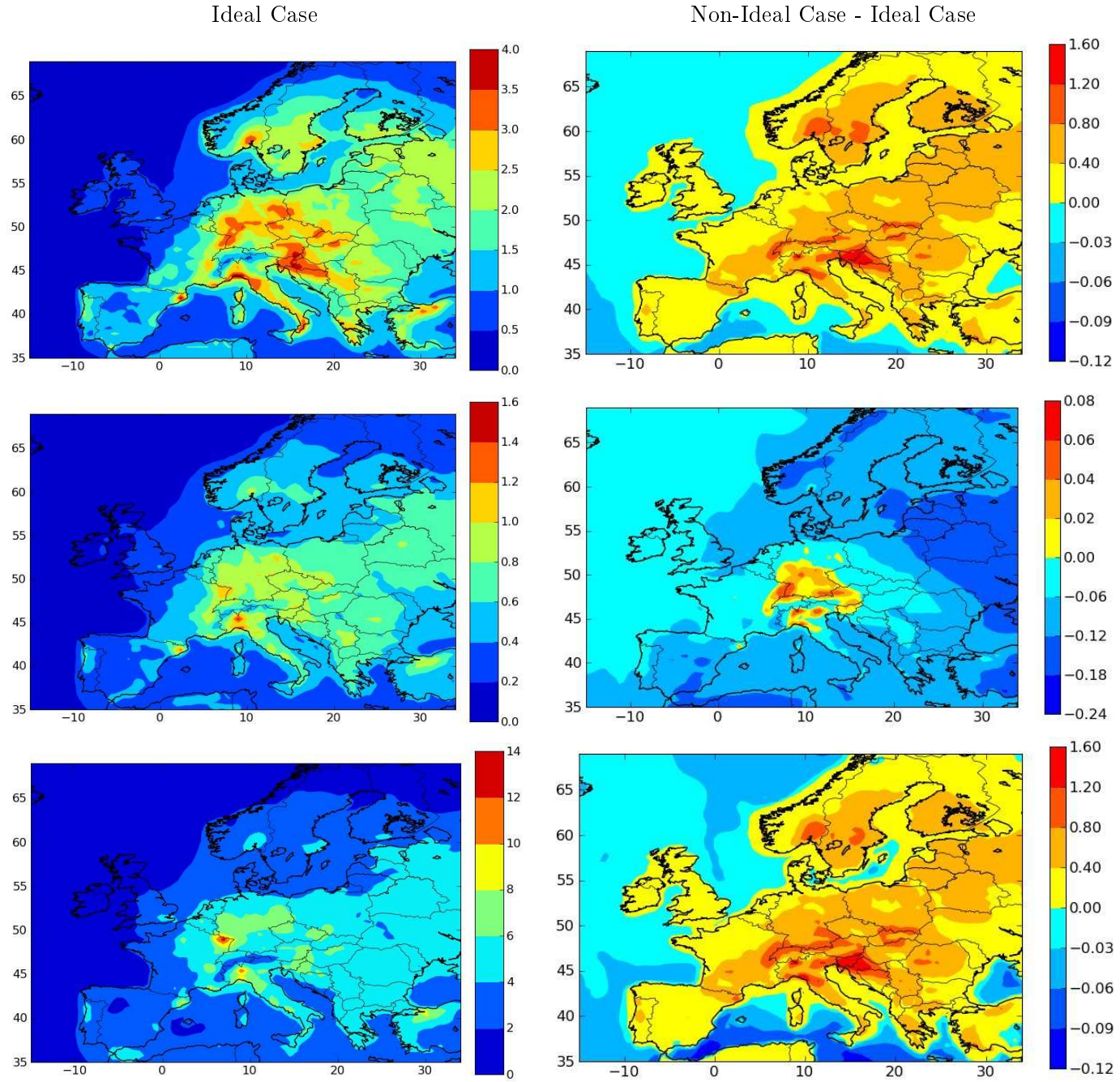

FIGURE 3.8 – Impact of ideality on hydrophilic SOA compounds (top), on hydrophobic SOA compounds (middle) and on OM (bottom). Concentrations (μg.m^{-3}) when ideality is assumed on the left and differences of concentrations (μg.m^{-3}) between ideal and non-ideal SOA solutions on the right.

one of the main contributors of hydrophilic SOA by oligomerization). BiA0D has more affinity with water than other organic compounds and condenses more efficiently when there are only low concentrations of these compounds.

For hydrophobic compounds, assuming ideal conditions increases the mean hydrophobic SOA concentrations over Europe in August 2002 from 0.30 μg.m^{-3} to 0.38 μg.m^{-3} on average. Assuming ideality leads to greater concentrations over most of Europe except over a small area in

the center of Europe. This decrease in the center of Europe is due to the decrease of BiNIT (organonitrate formed by oxidation of monoterpenes with NO_3) concentrations over Europe. When activity coefficients are computed, BiNIT has an activity coefficient lower than one, because the assumed POA structure [*EPRI*, 1999] tends to stabilize it. Therefore, condensation of BiNIT is enhanced and partitions more efficiently. Overall, this decrease in SOA concentrations due to non-ideality is consistent with the results obtained by *Pun* [2008] using a different model.

For total OM, assuming ideal conditions leads to a decrease of the mean OM concentration over Europe in August 2002 from 2.93 μg.m^{-3} to 2.76 μg.m^{-3} on average, because of a greater contribution of hydrophilic SOA than hydrophobic SOA to OM. However, assuming ideality can lead to an increase of the concentrations of some compounds and lead locally to an increase of OM concentrations. This study does not take into account the influence of activity coefficients on primary and aged anthropogenic SVOC. *Pun* [2008] showed that taking into account the activity of POA as well as SOA species may lead to larger effects (lower OM when non-ideality is taken into account). Experimental data on POA molecular composition are needed to better address this potentially important issue.

3.4.2 Comparison of two parameterizations of SOA formation from isoprene oxidation

The parameterization of *Henze and Seinfeld* [2006] (HS hereafter), which is based on a two-product Odum parameterization and yields from *Kroll et al.* [2006], is used currently in most air quality models, including the modeling study of *Zhang et al.* [2007b]. It is compared here for August 2002 with the parameterization of *Couvidat and Seigneur* [2011] (CS hereafter) used in H^{2}O. The main difference between the two parameterizations is that CS take into account the hydrophilic properties of SOA formed from isoprene oxidation whereas HS implicitly assume that the SOA compounds formed are hydrophobic. Moreover, CS take into account the impact of NO_X concentrations on SOA formation.

The CS parameterization leads to higher concentrations of SOA formation from isoprene oxi-

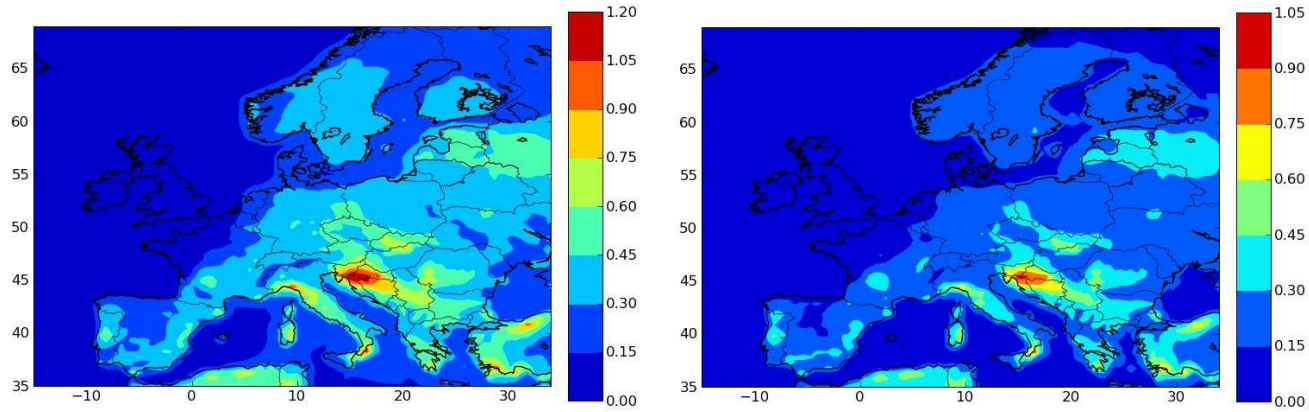

FIGURE 3.9 – Isoprene SOA concentrations (μg.m^{-3}) calculated for August 2002 with the parameterization of *Couvidat and Seigneur* [2011] on the left and difference of isoprene SOA concentrations (μg.m^{-3}) on the right between the parameterizations of *Couvidat and Seigneur* [2011] and *Henze and Seinfeld* [2006].

dation and gives a mean isoprene SOA concentration over Europe in August 2002 of 0.22 μg.m^{-3} against 0.07 μg.m^{-3} for the HS parameterization. Isoprene SOA concentrations calculated with CS are constituted essentially by compounds formed under low-NO_X conditions : BiDER with 0.11 μg.m^{-3} and BiPER with 0.09 μg.m^{-3}. BiPER is a compound formed under a transitional

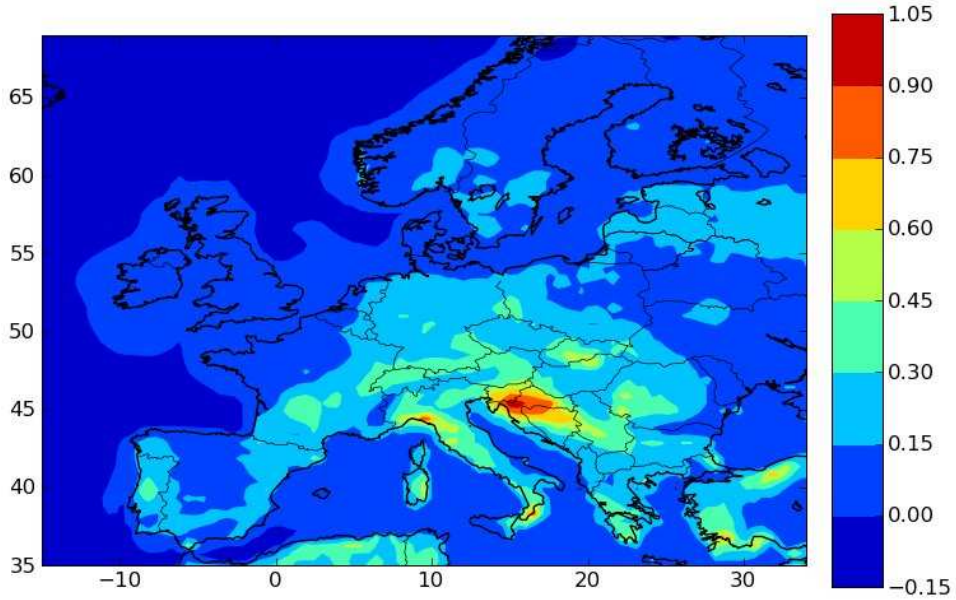

FIGURE 3.10 – Difference in OM concentrations (μg.m^{-3}) for August 2002 between the parameterizations of *Couvidat and Seigneur* [2011] and *Henze and Seinfeld* [2006] for isoprene SOA.

state and is oxidized to form more volatile compounds whereas BiDER represents SOA at the final state. This transitional mass is not taken into account in HS but it represents a significant mass of isoprene SOA in CS. Concentrations of BiDER are higher than the concentrations of SOA obtained with the two-product Odum parameterization. It shows that the hydrophilic properties of SOA can influence greatly SOA concentrations. Fig. 3.9 shows the impact of using the CS parameterization on isoprene SOA concentrations. Isoprene SOA concentrations are greater with CS except over remote areas, especially water far from sources of isoprene where concentrations of isoprene SOA are low. However, marine emissions of isoprene are not taken into account in the model and CS could give greater concentrations of isoprene SOA over marine areas if marine emissions of isoprene were included [*Shaw et al.*, 2010]. Differences in isoprene SOA are very important near source areas. Differences are even larger when OM concentrations are compared (Figure 3.10) ; they can be as high as 1.0 μg.m^{-3} because of the effect of isoprene SOA on the partitioning of other SOA compounds (via activity coefficients and the increase of absorbing medium).

This comparison confirms the conclusions of *Couvidat and Seigneur* [2011] that SOA formation from isoprene oxidation could be underestimated by most current models. Moreover, isoprene could be a major contributor to SOA in areas with very high emissions of isoprene such as the Amazon [*Robinson et al.*, 2011].

3.4.3 Impact of the volatility of primary organic aerosols

As POA are in fact semi-volatile compounds, the contribution of POA should be more important in winter due to lower temperatures, which lead to a decrease of the volatility of SVOC. Therefore, by assuming that POA are non-volatile and using EI-POA emissions, OM can be expected to be underestimated in winter. To verify this hypothesis, OM was simulated during February 2003 by using the non-corrected non-volatile emissions of EMEP (i.e., ignoring the potential gas-phase fraction associated with POA emissions).

By using the non-volatile POA emissions of EMEP, H^{2}O gives a mean concentration over Europe in February 2003 of 0.62 μg.m^{-3} of POA and 0.91 μg.m^{-3} of OM. In that case, POA

constitutes 68% of the organic matter. By using the SimEMEP configuration, H^2O gives much higher concentrations over Europe for the same period : 1.45 $\mu g.m^{-3}$ of POA and 2.97 $\mu g.m^{-3}$ of OM. POA constitutes then only 49% of OM. Using SVOC emissions gives higher concentrations of POA in winter but also a higher fraction of SOA due to the oxidation in the gas phase of primary SVOC. Fig. 3.11 shows the impact of using EI-POA emissions on OM concentrations instead of SVOC emissions. Using non-volatile emissions leads to very low concentrations of OM indicating that for Europe using non-volatile POA emissions of EMEP leads to a large underestimation of OM in winter.

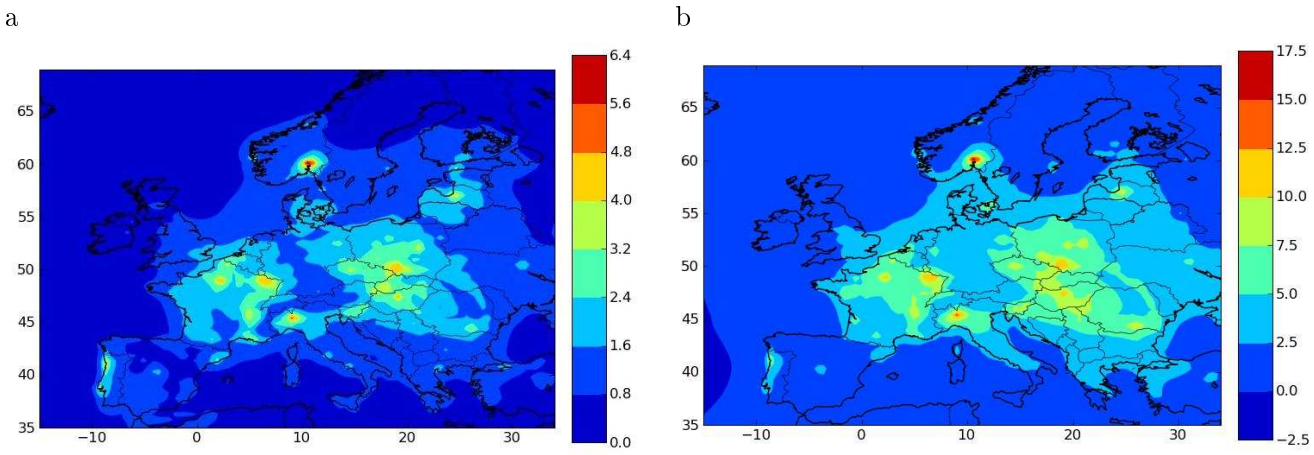

FIGURE 3.11 – Impact of the non-volatility assumption on OM for February 2003. OM concentrations in $\mu g.m^{-3}$ calculated with non-volatile emissions on the left and difference of OM concentrations in $\mu g.m^{-3}$ with and without SVOC emissions on the right. Compare Figure 11a with Figure 4d.

3.4.4 Investigation of the OM/OC ratio

We investigate here the possible reasons for the low OM/OC ratio obtained in the model simulations, focusing on summer. In summer, OM is mainly composed of SOA compounds formed by monoterpene oxidation. As these compounds have low OM/OC ratios (1.40 for BiA0D, 1.57 for BiA1D and 1.72 for BiA2D), the OM/OC ratio obtained by the model is low. However, higher OM/OC ratios could be obtained with second-generation products of monoterpene oxidation. The potential formation of 3-methyl-1,2,3-butanetricarboxylic acid (MBTCA) and organosulfates from pinonaldehyde uptake and their effects on the OM/OC ratio are investigated.

MBTCA has been shown to be formed by oxidation of pinonic acid [*Szmigielski et al.*, 2007; *Zhang et al.*, 2010b]. This product has a low volatility and a high OM/OC ratio of 2.125. Accordingly, the formation of a new surrogate compound BiA3D is added to the model using the molecular structure of the MBTCA. The following reaction is added to the model :

$$\text{BiA1D} + \text{OH} \xrightarrow{k} \text{BiA3D} \tag{3.3}$$

with k = 9.0×10^{-12} $molecule^{-1}.cm^3.s^{-1}$ [*Kamens and Jaoui*, 2001]. BiA3D is supposed to be hydrophilic and non-volatile (i.e., very high Henry's law constant). This reaction is supposed to only produce less volatile compounds, whereas it could produce shorter and more volatile molecules by fragmentation (i.e., the stoichiometric coefficient of BiA3D could be lower than one). Furthermore, pinonaldehyde can be oxidized in the gas phase to form pinonic acid. Accordingly,

the following reaction is added to the model :

$$\text{BiA0D} + \text{OH} \xrightarrow{\text{k}} \text{BiA1D} \tag{3.4}$$

with k = 9.0 $\times$ 10^{-11} molecule^{-1}.cm^3.s^{-1} [*Glasius et al.*, 1997]. Adding these two reactions increases OM concentrations over Europe in August 2002 from 2.93 μg.m^{-3} to 3.22 μg.m^{-3} and OC from 1.84 μg.m^{-3} to 1.97 μg.m^{-3}. However, formation of BiA3D impacts the OM/OC ratio only slightly because monoterpene SOA are still dominated by BiA0D. The ratio remains between 1.6 and 1.7 over most of Europe as shown in Fig. 3.12a.

Lukács et al. [2009] made a first attempt to quantify organosulfate concentrations and found at a monitoring station in Hungary in May-June 2006 between 0.02 and 0.09 μgS.m^{-3} of water soluble organosulfates, which correspond to concentrations between 0.16 and 0.75 μg.m^{-3} if the structure of the organosulfate formed from pinonaldehyde is used. According to *Lukács et al.* [2009], these values are lower bounds as a fraction of the organosulfates may not be water soluble. Organosulfates could then represent a large fraction of aerosols and could strongly impact the OM/OC ratio.

BiA0D (using the structure of pinonaldehyde) was assumed to undergo oligomerization and the effective partitioning is computed according to the parameterization of *Pun and Seigneur* [2007]. However, this parameterization was derived from the effective partitioning in an acidic particle (using H_2SO_4, NH_4HSO_4, $(NH_4)_2SO_4$) observed by *Jang et al.* [2005] and could in fact include organosulfate formation. Significant formation of organosulfates from uptake of pinonaldehyde on acidic sulfate aerosols has indeed been observed by *Liggio and Li* [2006]. To study the potential effect of organosulfate formation from pinonaldehyde, BiA0D was assumed to condense as an organosulfate having a molecular weight of 248 g.mol^{-1}. Concentrations of OC for BiA0D were then calculated by using an OM/OC ratio of 2.1 instead of 1.4. The new OM/OC ratio is shown for August 2002 in Fig. 3.12b. The ratio increases significantly and reaches a value between 1.74 and 1.92 over most of Europe against a ratio between 1.55 and 1.65 in SimEMEP. The effective OM/OC ratio of condensed BiA0D may in reality be somewhere between 1.4 and 2.1.

To study the impact of the OM/OC ratio of anthropogenic aged SVOC, we increased the OM/OC ratio of aged anthropogenic SVOC (PSOAlP, PSOAmP, PSOAhP) from 1.8 to 2.1 as in *Pye and Seinfeld* [2010]. The new OM/OC ratio over Europe is shown in Fig. 3.12c. Most of Europe has then an OM/OC ratio between 1.56 and 1.74 as all primary SVOC are not oxidized.

Finally, the OM/OC ratio was computed by assuming both BiA3D and organosulfate formation, and an increase of the OM/OC ratio of aged anthropogenic SVOC (PSOAlP, PSOAmP, PSOAhP) from 1.8 to 2.1. The computed OM/OC ratio is shown in Fig. 3.12d. The model calculates then an OM/OC ratio between 1.86 and 1.98 over most of Europe.

One other aspect, which was not studied here, is that the reaction of monoterpenes with OH used the SOA yield for high-NO_X conditions instead of that of low-NO_X conditions, which would be more relevant for SOA simulation at the continental scale. However, only few experiments of oxidation of monoterpenes were performed under low-NO_X conditions [*Ng et al.*, 2007a] and data are insufficient to derive a two-product parameterization. However, results from *Ng et al.* [2007a] indicate a higher yield of SOA formation under low-NO_X conditions, which could lead to significantly greater atmospheric SOA levels [*Kim et al.*, 2009]. *Valorso et al.* [2011] developed a theoretical model and calculated under low-NO_X conditions a high contribution of hydroperoxide compounds with a high OM/OC ratio (around 2.0). The incorporation of a representation of monoterpene SOA for low-NO_X conditions could increase the overall calculated OM/OC ratios and change significantly the calculated OM/OC ratio.

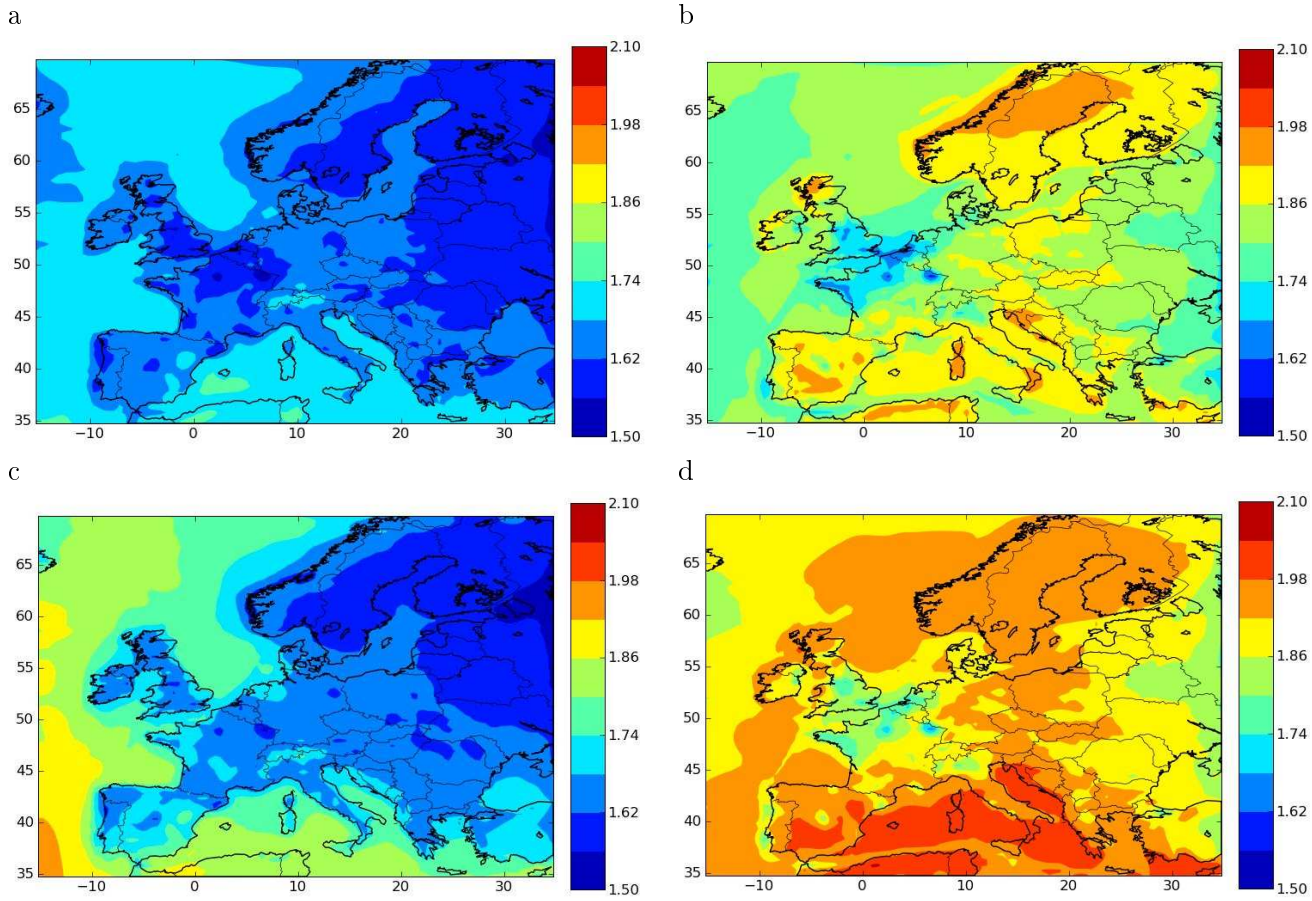

FIGURE 3.12 – OM/OC ratio over Europe for August 2002 calculated by assuming BiA3D formation (top left), by assuming organosulfate formation (top right), with increased OM/OC ratio for aged anthropogenic to 2.1 (bottom left) and with all the previous hypothesis (bottom right).

3.5 Conclusion

A model for SOA formation, H^2O, that uses the molecular approach, has been developed and compared to OC measurements at 12 stations of the EMEP network over Europe for the period of July 2002 to July 2003. This comparison indicates an underestimation of the model for OC especially during winter, which seems to be due to missing sources in anthropogenic inventory emissions. Moreover, the model gives an OM/OC ratio between 1.55 and 1.65, which seems low for non-urban sites. However, by taking into account the gas-phase fraction of SVOC emissions, instead of assuming that POA emissions are non-volatile, the model is able to reproduce higher OC concentrations during winter with good annual correlations (e.g., 0.6 with anthropogenic emissions from EMEP).

The impact of the ideality of organic PM, of the choice of the parameterization for isoprene SOA formation, and of using non-volatile POA emissions has been studied. Non-ideality has a complex effect on SOA formation because SOA may either increase (for hydrophilic SOA mostly) or decrease (for hydrophobic SOA mostly) depending on the compound. Overall, it was estimated that assuming ideality in H^2O leads to a small decrease in OM. The parameterization of *Couvidat and Seigneur* [2011] for SOA formation from isoprene oxidation leads to a significant increase in isoprene SOA compared to that of *Henze and Seinfeld* [2006] and suggests that most models

may currently underestimate SOA formation from isoprene. Finally, assuming non-volatile POA and using an inventory with missing SVOC emissions may lead to an underestimation of OM in winter because of missing SVOC that could condense due to the decrease of temperature and the associated decrease of volatility.

To improve model results, emission inventories that take into account the gas-phase fraction of semi-volatile POA should be developed. More studies are needed to investigate the formation of SOA from different sources of primary SVOC. Moreover, the molecular composition of primary and aged anthropogenic SVOC should be investigated to include the molecular structures of POA in models and take into account their associated effect of non-ideality on OM. Efforts should be made to characterize and possibly improve the representation of the OM/OC ratio in the model, which currently simulates low ratios in summer probably due to the low ratio of first-generation oxidation products of monoterpenes. Second-generation products for monoterpenes and oxidation of monoterpenes by OH under low-NO_X conditions should be investigated.

Chapitre 4

Modélisation des aérosols organiques en zone urbaine : application à l'Île-de-France

Résumé

Après avoir développé le modèle de formation d'aérosols organiques secondaires H^2O et évalué ce modèle en comparant les résultats du modèle aux mesures de carbone organique réalisées sur les stations de fond rural du programme européen EMEP, nous nous proposons d'étudier la formation d'aérosols organiques en zone urbaine. L'objectif est d'estimer les performances du modèle en zone urbaine et d'identifier les processus qui peuvent influencer de manière importante la formation locale d'aérosols organiques secondaires.

Le modèle H^2O couplé au modèle de qualité de l'air Polair3D/Polyphemus est utilisé pour simuler la formation d'aérosols organiques secondaires sur l'Île-de-France au mois de juillet 2009. Des simulations sur l'Europe et la France sont réalisées pour calculer les conditions aux limites de la simulation francilienne et déterminer la contribution régionale des aérosols. Les inventaires d'émissions d'Airparif et d'EMEP sont utilisés, respectivement, pour calculer les émissions anthropogéniques sur et en dehors de l'Île-de-France. La météorologie est calculée avec le modèle WRF, en utilisant un modèle de canopée urbaine pour prendre en compte l'influence d'une zone urbaine sur certains paramètres météorologiques comme la température, la vitesse du vent ou la hauteur de la couche limite atmosphérique.

Deux types de mécanismes pour le traitement des composés organiques semi-volatils primaires sont étudiés : H^2O-Ref et H^2O-Mech. H^2O-Ref utilise le même traitement que celui de l'étude de comparaison sur l'Europe (voir Chapitre 3) : les composés suppléants des composés semi-volatils primaires du modèle n'ont pas de structures chimiques spécifiques (qui sont nécessaires pour calculer les coefficients d'activité via le modèle thermodynamique UNIFAC) ; les données relatives à la condensation de ces espèces et à leur vieillissement sont donc basées sur des données expérimentales. H^2O-Mech consiste en une première tentative pour attribuer des structures moléculaires aux composés semi-volatils primaires et pour utiliser un mécanisme théorique pour l'oxydation de ces composés. H^2O-Mech se limite cependant à une seule étape d'oxydation et suppose que l'oxydation d'un composé primaire ne peut conduire qu'à un composé moins volatil (alors qu'il pourrait se séparer en plusieurs composés plus volatils et de plus petites tailles). Plus d'études devraient porter sur le développement d'un mécanisme complet avec plusieurs étapes d'oxydation. Néanmoins, H^2O-Mech permet de fournir certains éléments sur la condensation des composés semi-volatils primaires.

Les résultats du modèle sont comparés aux résultats de la campagne d'été du programme

MEGAPOLI (Megacities : Emissions, urban, regional and Global Atmospheric POLlution and climate effects, and Integrated tools for assessment and mitigation). Durant cette campagne, des mesures de carbone organique et de carbone élémentaire dans la fraction inférieure à 2.5 μm ont été réalisées sur deux sites : le SIRTA (Site Instrumental de Recherche par Télédétection Atmosphérique) situé en banlieue parisienne au sud-ouest de Paris et le site du LHVP (Laboratoire d'Hygiène de la Ville de Paris) dans le 13$^{\text{ème}}$ arrondissement de Paris. Le carbone organique et le carbone élémentaire ont été mesurés pour des périodes moyennes de 12 heures sur filtres aux deux stations et mesurés chaque heure au LHVP avec un "Sunset field instrument". Les mesures du Sunset ont un "offset" constant de 1,0 μg.m^{-3}. Cet offset est dû la condensation de composés semi-volatils et il est donc difficile de savoir s'il faut ou non le prendre en compte.

Le modèle donne des résultats satisfaisants pour les concentrations de carbone élémentaire. Il surestime légèrement les concentrations de carbone élémentaire au SIRTA (0,50 μg.m^{-3} d'après le modèle contre 0,38 μg.m^{-3} d'après les mesures sur filtres) et donne de bons résultats au LHVP jusqu'au 26 juillet (1,08 μg.m^{-3} d'après le modèle contre 1,03 μg.m^{-3} d'après les mesures sur filtres). Les concentrations de carbone organique sur au SIRTA sont légèrement surestimées (2,64 μg.m^{-3} d'après le modèle contre 2,27 μg.m^{-3} d'après les mesures sur filtres). Au LHVP, les concentrations de carbone organique données par le modèle sont généralement inférieures aux mesures sur filtres, mais généralement comprises entre les valeurs des mesures du Sunset avec ou sans "offset". Il est donc difficile de déterminer si le modèle surestime ou sousestime les concentrations de carbone organique dans Paris. Néanmoins, le modèle est capable de reproduire les fortes concentrations de carbone organique observées le 1$^{\text{er}}$ juillet 2009.

En utilisant les données horaires du Sunset, il est possible d'évaluer le profil temporel des concentrations données par le modèle. Pour les concentrations de carbone élémentaire, le modèle donne initialement deux pics, le matin et le soir, correspondant aux pics d'émissions du trafic routier lors des heures de pointe alors que seul le pic du matin est observé dans les mesures. Cependant, en utilisant un profil temporel des émissions du trafic routier plus adapté à la ville de Paris, ce deuxième pic disparaît ce qui montre l'importance de la temporalisation des émissions sur les résultats du modèle. Pour le carbone organique, les mesures du Sunset montrent un profil temporel relativement constant, excepté le soir à 23 h où un pic de concentrations apparaît probablement dû aux émissions dues à la cuisson des aliments. Ce pic n'est pas reproduit par le modèle, mais cela n'est guère étonnant puisque les émissions dues à la cuisson ne sont pas prises en compte dans l'inventaire d'Airparif.

Le modèle donne, en revanche, un pic de concentration le matin dû à la formation d'aérosols organiques primaires émis par le trafic. L'absence de ce pic dans les mesures du Sunset pourrait être due à l'absence d'aérosols organiques primaires dus au trafic ; le profil des mesures est d'ailleurs fortement similaire au profil des concentrations des aérosols organiques secondaires donné par le modèle (excepté le pic du soir probablement dû aux émissions dues à la cuisson). Il est donc possible que les composés semi-volatils primaires émis par le trafic routier ne se condensent pas.

La présence du pic matinal dans les concentrations de carbone organique données par le modèle peut être donc due à la sous-estimation de la volatilité des composés organiques primaires semi-volatils. En effet, étant donné que la volatilité des composés organiques primaires semi-volatils est obtenu par extrapolation de données obtenues à fortes masses d'aérosols organiques (généralement supérieures à 100 μg.m^{-3}) aux conditions ambiantes (avec des concentrations d'aérosols organiques généralement inférieures à 30 μg.m^{-3}), il est tout à fait possible que la volatilité des composés organiques primaires semi-volatils soit sous-estimée. De plus, le mécanisme H^{2}O-Mech semble indiquer qu'en prenant en compte l'influence des coefficients d'activité des composés organiques primaires, leur condensation diminue et qu'ils sont susceptibles de mal se condenser sur un aérosol organique majoritairement secondaire et très oxydé.

D'après les résultats de cette étude, sur Paris au mois de juillet 2009, les concentrations d'aérosols organiques sont comprises entre 4,0 et 5,0 $\mu g.m^{-3}$. L'aérosol organique est majoritairement d'origine régionale avec 30 à 40 % de l'aérosol organique d'origine locale (provenant d'émissions originaires de l'Île-de-France). L'aérosol organique parisien est, d'après le modèle, constitué de 24% de composés organiques primaires (fraction assez incertaine, car les émissions dues à la cuisson ne sont pas prises en compte et le modèle semble surestimer les concentrations de composés primaires dues aux émissions du trafic routier), 23% d'aérosols organiques secondaires formés par l'oxydation de précurseurs biogéniques, 1% d'aérosols organiques secondaires formés par l'oxydation de précurseurs aromatiques anthropogéniques et 52% venant de l'oxydation des composés organiques primaires.

La formation d'aérosols organiques a aussi été étudiée sur Beyrouth, Liban dans l'étude présentée en Annexe 3 : "Modeling air pollution in Lebanon : evaluation at a suburban site in Beirut" [*Waked et al.*, 2012a]. Le modèle y donne des résultats satisfaisants.

Ce chapitre est constitué de :
Couvidat, F., Kim, Y., Sartelet, K., Seigneur, C., Marchand, N. et Sciare, J. **Modeling secondary organic aerosol in an urban area : Application to Paris, France**, Accepté dans à Atmos. Chem. Phys..

Sommaire

Abstract

A secondary organic aerosol (SOA) model, H^2O (Hydrophilic/Hydrophobic Organic), is evaluated over the Paris area. This model treats the formation of SOA with two kinds of surrogate species : hydrophilic species (which condense preferentially on an aqueous phase) and hydrophobic species (which condense only on an organic phase). These surrogates species are formed from the oxidation in the atmosphere of volatile organic compounds (VOC) by radicals (HO and NO_3) and ozone. These VOC are either biogenic (isoprene, monoterpenes and sesquiterpenes) or anthropogenic (mainly aromatic compounds). This model includes the formation of aerosols from different precursors (biogenic precursors, aromatics), and semi-volatile organic compounds (SVOC) from traffic. The H^2O aerosol model was incorporated into the Polyphemus air quality modeling platform and applied to the Paris area and evaluated by comparison to measurements performed during the Megapoli campaign in July 2009.

The comparison to measurements in the suburbs and in the city center of Paris shows that the model gives satisfactory results for both elemental carbon (EC) and organic carbon (OC). However, the model gives a peak of OC concentrations in the morning due to high emissions from traffic, which does not appear in measurements. Uncertainties in the modeled temperature, which can affect the gas-particle partitioning, in the partitioning of primary SVOC or underestimation of primary organic aerosol (POA) evaporation by the model could explain the differences between model and measurements. Moreover, using a theoretical mechanism for the oxidation of primary SVOC and intermediate volatility organic compounds (IVOC), POA concentrations were found to be likely overestimated by models due to the use of simple partitioning constants (which do not take into account the affinity of a compound with the liquid aerosol solution) or due to the assumption that the organic aerosol solution is a one-phase ideal solution. The organic aerosol in the city center of Paris was found to be originating mostly from distant sources with only 30 to 38% due to local sources.

4.1 Introduction

Fine particulate matter (PM) with an aerodynamic diameter inferior to 2.5 μm ($PM_{2.5}$) is regulated because of its impact on human health, in particular, in urban areas with a high traffic density. Furthermore, $PM_{2.5}$ degrades atmospheric visibility and influences climate change. Organic aerosol concentrations are difficult to represent in three-dimensional (3D) air quality models, which estimate $PM_{2.5}$ formation, due to the complexity of phenomena involved (gas and particle phase chemistry, oligomerization, hygroscopicity, non-ideality of particles) and to the large number of organic species involved originating from diverse sources (anthropogenic and biogenic). A large fraction of PM emissions from traffic is organic and, therefore, could contribute significantly to organic $PM_{2.5}$ in urban areas. As 19 of the 20 largest European cities exceed the World Health Organization Air Quality Guideline (10 $\mu g.m^{-3}$ annual mean), efforts have to be made to understand organic aerosol formation in urban areas and to represent organic matter (OM) as accurately as possible in air quality models that are used for the design of emission control strategies. Organic PM is either primary (directly emitted as particles) or secondary (formed in the atmosphere by the nucleation or condensation of the low-volatility oxidation products of gaseous species). Both primary organic aerosols (POA) and secondary organic aerosols (SOA) are currently poorly understood [*Kanakidou et al.*, 2005; *Hallquist et al.*, 2009; *Jimenez et al.*, 2009].

Organic aerosol formation in an urban area has been studied in numerous studies over U.S. cities (e.g., *Griffin et al.* [2002]; *Russell and Allen* [2005]; *Vutukuru et al.* [2006]; *Murphy and Pandis* [2009]) and over Mexico City during the MILAGRO project (e.g., *Dzepina et al.* [2011];

Hodzic et al. [2010]; *Tsimpidi et al.* [2011]; *Shrivastava et al.* [2011]). However, the modeling of organic aerosols in a European urban megacity has not been extensively studied yet, although some comparisons of model simulations to measurements have been reported [*Sciare et al.*, 2010a].

In this work, a model based on the molecular approach is used to simulate organic aerosols in the Paris area : the Hydrophilic/Hydrophobic Organic (H^2O) model [*Couvidat et al.*, 2012a]. The molecular approach [*Pun et al.*, 2002a, 2006] consists in associating experimental data with several molecular structures, which are surrogates of a large number of SOA species, to extrapolate SOA formation from smog chambers to the atmosphere. In the molecular approach, several properties, which are typically not taken into account in empirical approaches, can be readily estimated (e.g., condensation on an aqueous phase, oligomerization, hygroscopicity, non-ideality) and treated explicitly in the model. This model includes primary semi-volatile organic compounds (SVOC), oxidation of several precursors (aromatics, isoprene, monoterpenes, sesquiterpenes) under various conditions (oxidation by HO under high-NO_x and low-NO_x conditions, oxidation by O_3 and by NO_3) and processes (condensation on an organic phase or an aqueous phase, oligomerization, hygroscopicity, and non-ideality).

The H^2O organic model has already been implemented in the Polyphemus air quality platform [*Mallet et al.*, 2007] and evaluated over Europe from June 2002 to July 2003 [*Couvidat et al.*, 2012a]. This evaluation showed that, even if H^2O tends to underestimate organic carbon (OC) concentrations, it gives satisfactory results as the model performance criteria proposed by *Boylan and Russell* [2006] are met for OC concentrations and as it almost achieves the model goal criteria. However, the model has not been evaluated at the scale of a city and the performance of the model over on urban area with fresh emissions from traffic is unknown. Therefore, we present here a model performance evaluation over a megacity : organic aerosols are simulated over the Paris area during July 2009 and are compared to the results of the Megapoli (Megacities : Emissions, urban, regional and Global Atmospheric POLlution and climate effects, and Integrated tools for assessment and mitigation) campaign. The origins of organic aerosols in Paris and the effect of a detailed treatment of primary organic aerosols on modeled concentrations are also investigated.

4.2 Model presentation

The Polair3D air quality model [*Sartelet et al.*, 2007] of the Polyphemus air quality platform [*Mallet et al.*, 2007] is used to simulate air quality over the Paris area. It is used with the Carbon Bond 05 model (CB05) [*Sarwar et al.*, 2008] for the gas phase chemistry, ISORROPIA [*Nenes et al.*, 1998] for the formation of inorganic aerosol, the SIze REsolved Aerosol Model (SIREAM) [*Debry et al.*, 2007a] for simulating the dynamics of the aerosol size distribution, and the H^2O model for SOA formation [*Couvidat et al.*, 2012a]. RACM is modified to take into account the reactions described by *Couvidat et al.* [2012a].

H^2O is based on the AER/EPRI/Caltech (AEC) [*Pun et al.*, 2002a, 2003, 2006; *Kim et al.*, 2011a], which has already been used by *Royer et al.* [2011] to simulate particle concentrations. It distinguishes two kinds of surrogate SOA species : hydrophilic species (which condense mainly on an aqueous phase) and hydrophobic species (which condense only on an organic phase due to their low affinity with water). Hydrophilic species may also condense on an organic phase in the absence of aqueous particles, i.e., at very low relative humidities. Distinction between hydrophobic and hydrophilic compounds is based on their octanol/water coefficient [*Pun et al.*, 2006] or their partitioning between the organic and aqueous phases [*Couvidat and Seigneur*, 2011].

Two approaches are used in this study to treat primary SVOC and their oxidation products.

The first approach called "H^2O-Ref" uses the parameterization of *Couvidat et al.* [2012a] for primary and aged organic species. In this parameterization, POA are treated as SVOC. Their concentrations in the particle phase depend on the amount of OM on which SVOC will condense and on temperature (which influences the volatility of compounds). SVOC emissions are estimated from POA emissions by using a SVOC/POA factor of 5 [*Couvidat et al.*, 2012a]. Then, SVOC are distributed among three compounds : POAlP, POAmP and POAhP representing respectively 25%, 32% and 43% of SVOC, with partitioning constants of 1.1 $m^3.\mu g^{-1}$, 0.0116 $m^3.\mu g^{-1}$ and 0.00031 $m^3.\mu g^{-1}$, respectively. Moreover, SVOC in the gas phase can be oxidized and form less volatile compounds. The aging of primary SVOC is taken into account with the following three reactions :

$$\text{POAlP} + \text{HO} \xrightarrow{k} \text{SOAlP} \quad \text{(R 4.1)}$$

$$\text{POAmP} + \text{HO} \xrightarrow{k} \text{SOAmP} \quad \text{(R 4.2)}$$

$$\text{POAhP} + \text{HO} \xrightarrow{k} \text{SOAhP} \quad \text{(R 4.3)}$$

with k the kinetic rate constant equal to 2×10^{-11} $molecule^{-1}.cm^3.s^{-1}$ [*Grieshop et al.*, 2009]. SOAlP, SOAmP and SOAhP are the aged SVOC and have respectively partitioning constants of 110.0 $m^3.\mu g^{-1}$, 1.16 $m^3.\mu g^{-1}$ and 0.031 $m^3.\mu g^{-1}$. POAlP, POAmP, and POAhP are assigned an OM/OC ratio of 1.3 whereas SOAlP, SOAmP, and SOAhP are assigned an OM/OC ratio of 1.82 due to oxygen addition.

The second type of mechanism called "H^2O-Mech" uses a detailed treatment of primary and aged SVOC where a speciation of primary SVOC is used to attribute molecular structures to primary compounds and to estimate the formation of secondary organic aerosol by aging. The main goal of this mechanism is to attribute molecular structure to primary SVOC and their oxidation products to estimate their activity coefficients in the atmosphere with the UNIversal Functional group Activity Coefficient (UNIFAC) thermodynamic model [*Fredenslund et al.*, 1975]. The impact of activity coefficients on the partitioning of primary SVOC and their oxidation products are not taken into account in "H^2O-Ref" whereas it is possible that POA and SOA have low affinities which each other [*Pun*, 2008; *Song et al.*, 2007]. With "H^2O-Mech", the structure of primary SVOC and their oxidation products are known and it is, therefore, possible to estimate the impact of activity coefficients on their partitioning. The speciation is based on the data of *Schauer et al.* [1999] on the identified fraction of SVOC from medium-duty diesel trucks (14% of SVOC). Molecules with similar properties (high, medium or low volatility) and type (acids, alkanes, polycyclic aromatic hydrocarbons (PAH)) are lumped into a single surrogate species. *Isaacman et al.* [2012] found that about 73% of SVOC above 15 carbons are aliphatic and 27% are aromatic. With the speciation used in this study, 70% of SVOC above 15 carbons are aliphatic and 30% are aromatic. The SVOC speciation used here is, therefore, consistent with the results of *Isaacman et al.* [2012]. Saturation vapor pressures and the emission fractions are chosen to respect the same dilution curve than in the previous approach. Table 4.1 describes these primary SVOC and their properties.

The surrogate species are then used to develop an oxidation mechanism of primary SVOC. For the species HC17, the oxidation mechanism is based on the data of *Presto et al.* [2010] by fitting the saturation vapor pressure and mass yields of products. The most volatile product, AnALKF17, was assumed to be a product of first generation (structure of 1,4-hydroxycarbonyls, which has been observed by *Lim and Ziemann* [2009a]), whereas the less volatile product AnALKS17 was assumed to be of second generation (structure of a hydroxy-dinitrate, which has been observed by *Lim and Ziemann* [2009a]). For the other species, oxidation was assumed to produce only less volatile species without fractionation. For the alkane species, HC20 and HC24,

TABLE 4.1 – Properties of the different surrogate primary SVOC species.

Surrogate	Molecular structure	Saturation vapor pressure (torr)	Percentage of emissions
HC24	tetracosane	3.01×10^{-8}	7.38 %
ACD18	octadecanoic acid	4.80×10^{-8}	9.92 %
DIACD18	octadecanedioic acid	3.60×10^{-8}	7.70 %
HC20	eicosane	9.64×10^{-7}	4.60 %
PYR	pyrene	1.94×10^{-6}	27.40 %
HC17	heptadecane	1.19×10^{-4}	33.11 %
FLU	fluorene	9.95×10^{-5}	3.57 %
AROM	methyl-benzoic acid	1.68×10^{-4}	6.33 %

oxidation was assumed to add one hydroxy and one carbonyl group (1,4-hydroxycarbonyls are one of the first generation products formed by oxidation of alkanes [*Lim and Ziemann*, 2009a,b]). The oxidation of the acid species, ACD18 and DIACD18, was assumed to be similar to the oxidation of the alkanes. For the PAH species, PYR and FLU, oxidation was assumed to add two carbonyl groups (1,4-naphthoquinone and 9,10-phenanthrequinone are among the main products of the oxidation of naphthalene and phenanthrene respectively [*Wang et al.*, 2007; *Lee and Lane*, 2009, 2010; *Kautzman et al.*, 2010]). For the aromatics, AROM, oxidation was assumed to add a hydroxy group on the aromatic ring. The effect of a group addition on the saturation vapor pressure was estimated using the method of *Pankow and Asher* [2008]. The kinetics of the oxidation of alkanes are taken from *Calvert et al.* [2008]. The kinetics of the other compounds were fitted to reproduce the results of the first approach with the observed oxidation of *Robinson et al.* [2007] during the first hours of the oxidation at 10 μg.m^{-3} of POA. Reactions leading to SOA formation from primary SVOC oxidation and the properties of the SOA products are presented in Tables 4.2 and 4.3, respectively. This mechanism could be improved because it only takes into account one oxidation step, assumes that oxidation only leads to less volatile compounds and because aromatics oxidation products are mainly unsaturated ring-opened products containing aldehyde groups that should oligomerize and react rapidly leading to further aging. Nevertheless, the effect of a single-step aging on activity coefficients and on the interactions between POA and SOA can be estimated with this mechanism.

Formation of SOA from the oxidation of some intermediate volatility organic compounds (IVOC) were also included in "H^2O-Mech". We used results from *Schauer et al.* [1999] on identified products from diesel exhaust to provide a speciation of IVOC. IVOC are separated into three products : HC15 for long-chain alkanes, acids and aldehydes (pentadecane is used as surrogate), NAPH for naphthalene and MNAPH for alkylnaphthalenes (2-methylnaphtalene is used as surrogate). IVOC from diesel exhaust was assumed to consist roughly of 79% of HC15, 6% of NAPH and 15% of MNAPH. The oxidation of HC15 is chosen to be similar to that of HC17 and is based on fitting to data of *Presto et al.* [2010] for SOA formation from the oxidation of pentadecane. Data from *Chan et al.* [2009] are used to fit two products from the oxidation of NAPH and MNAPH : AnPAHlN (for SOA formed by PAH oxidation under low-NO_x conditions) and AnPAHhN (for SOA formed by PAH oxidation under high-NO_x conditions). The structures for these surrogates, shown in Fig. 4.1, are those of some major compounds detected under low-NO_x and high-NO_x by *Kautzman et al.* [2010]. These two structures seem suitable as surrogate compounds because their OM/OC ratios of 2.06 and 1.90 are similar to the OM/OC ratios for SOA from naphthalene oxidation of 1.96 for low-NO_x conditions and 1.89 for high-NO_x conditions found by *Chhabra et al.* [2010]. The kinetics of oxidation of NAPH and MNAPH with HO are taken from *Calvert et al.* [2002] for the reaction of naphthalene with HO. To determine whether

TABLE 4.2 – Reactions of oxidation of primary SVOC (top panel) and IVOC (bottom panel) species (the oxidant species is listed as both reactant and product to ensure that the gas phase mechanism is not affected by these additional reactions).

Reaction	Kinetic rate parameter ($molecule^{-1}.cm^3.s^{-1}$)
HC24 + HO → AnALKF24 + HO	1.19×10^{-11}
ACD18 + HO → AnACD18 + HO	1.1×10^{-11}
DIACD18 + HO → AnDIACD18 + HO	1.1×10^{-11}
HC20 + HO → AnALKF20 + HO	1.13×10^{-11}
PYR + HO → 1.0 AnPYR + HO	3.0×10^{-11}
HC17 + HO → 0.516 AnALKF17 + 0.0634 AnALKS17 + HO	1.09×10^{-11}
FLU + HO → 1.0 AnFLU + HO	3.0×10^{-11}
AROM + HO → 1.0 AnAROM + HO	3.0×10^{-11}
HC15 + HO → 0.053 AnALKS15 + 0.46 AnALKF15 + HO	1.07×10^{-11}
NAPH + HO → NAPHP + HO	2.44×10^{-11}
NAPHP + HO_2 → 0.44 AnPAHlN + HO_2	$3.75 \times 10^{-13} \times \exp(\frac{980}{T})$
NAPHP + ACO_3 → 0.44 AnPAHlN + ACO_3	$7.40 \times 10^{-13} \times \exp(\frac{765}{T})$
NAPHP + MO_2 → 0.44 AnPAHlN + MO_2	$3.56 \times 10^{-14} \times \exp(\frac{708}{T})$
NAPHP + NO → 0.26 AnPAHhN + NO	$2.70 \times 10^{-11} \times \exp(\frac{360}{T})$
NAPHP + NO_3 → 0.26 AnPAHhN + NO_3	1.2×10^{-12}
MNAPH + HO → MNAPHP + HO	2.44×10^{-11}
MNAPHP + HO_2 → 0.46 AnPAHlN + HO_2	$3.75 \times 10^{-13} \times \exp(\frac{980}{T})$
MNAPHP + ACO_3 → 0.46 AnPAHlN + ACO_3	$7.40 \times 10^{-13} \times \exp(\frac{765}{T})$
MNAPHP + MO_2 → 0.46 AnPAHlN + MO_2	$3.56 \times 10^{-14} \times \exp(\frac{708}{T})$
MNAPHP + NO → 0.37 AnPAHhN + NO	$2.70 \times 10^{-11} \times \exp(\frac{360}{T})$
MNAPHP + NO_3 → 0.37 AnPAHhN + NO_3	1.2×10^{-12}

TABLE 4.3 – Properties of the different surrogate secondary SVOC species formed from primary SVOC oxidation (top panel) and IVOC oxidation (bottom panel).

Surrogate	Molecular weight	Saturation vapor pressure (torr)	OM/OC
AnALKF24	368	2.32×10^{-11}	1.28
AnACD18	314	3.69×10^{-11}	1.45
AnDIACD18	344	2.71×10^{-11}	1.59
AnALKF20	312	7.42×10^{-10}	1.30
AnPYR	234	4.00×10^{-8}	1.22
AnALKF17	270	1.03×10^{-8}	1.32
AnALKS17	378	5.32×10^{-7}	1.85
AnFLU	198	2.49×10^{-6}	1.27
AnAROM	152	1.26×10^{-6}	1.58
AnALKF15	242	7.09×10^{-7}	1.34
AnALKS15	350	1.34×10^{-8}	1.94
AnPAHlN	198	1.0×10^{-12}	2.06
AnPAHhN	182	1.0×10^{-6}	1.90

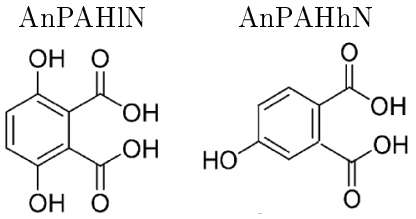

FIGURE 4.1 – Molecular structures of AnPAHlN and AnPAHhN used as surrogates for SOA formation from naphthalene and alkylnaphthalene oxidation under low-NO_x and high-NO_x conditions, respectively.

the radical formed from the oxidation of NAPH or MNAPH (RO_2) will react under low-NO_x conditions (RO_2 reacts with the radical HO_2, the methylperoxy radical MO_2 or the peroxyacetyl radical ACO_3) or high-NO_x conditions (RO_2 reacts with the radical NO_3 or NO), the kinetics of the reactions of the radical formed from toluene oxidation (TOLP) with these radicals used by *Couvidat et al.* [2012a] are used. Reactions leading to SOA formation from IVOC oxidation and the properties of the SOA products are presented in Tables 4.2 and 4.3, respectively.

Fig. 4.2 shows the concentrations of SOA from primary SVOC oxidation computed by a box model with the two mechanisms for 10 $\mu g.m^{-3}$ and 1 $\mu g.m^{-3}$ of POA at 298 K and [HO] = 2.0×10^6 molecules.cm^{-3} (concentrations used to have an OM evolution similar to *Robinson et al.* [2007]). The two mechanisms 'H^2O-Ref" and "H^2O-Mech", give similar concentrations of OM at both low and high organic aerosol loadings whereas these two mechanisms used different approaches. One significant difference between "H^2O-Mech" and "H^2O-Ref" for the formation of SOA from primary SVOC is in the degree of oxidation of SOA. SOA from "H^2O-Ref" has a OM/OC ratio of 1.82, which is rather high for first-generation oxidation products. OM/OC ratios for "H^2O-Mech" are more realistic (ratios between 1.27 and 1.85) because it uses molecular structures of some first-generation oxidation products. "H^2O-Mech" and "H^2O-Ref" should then give similar amounts of SOA from primary SVOC oxidation, when used in a 3D air quality model simulation, but "H^2O-Mech" should give higher concentrations of OC than "H^2O-Ref". Moreover, as the "H^2O-Mech" mechanism only takes into account one oxidation step, it probably underestimates aging of SVOC that would become less volatile and more oxidized. More work should be done to develop a complete and more realistic aging mechanism for SOA formation from primary SVOC with numerous oxidation steps. Nevertheless, the use of "H^2O-Mech" is useful here to obtain insight on the interaction between POA and SOA species, because such information is not available otherwise from mechanisms such as "H^2O-Ref".

4.3 Simulation setup and measurement dataset

OM was simulated over the Paris area during the Megapoli campaign of July 2009. Input data to Polair3D/Polyphemus were prescribed as follows, the simulation domain being the same as in *Royer et al.* [2011]. Boundary conditions for gaseous and particulate species were obtained from nested simulations over Europe and France. These simulations were conducted using the same data as *Couvidat et al.* [2012a], i.e., the EMEP emission inventory [*Vestreng*, 2003] was used for anthropogenic emissions and the MEGAN emission model [*Guenther et al.*, 2006] was used for biogenic VOC emissions. For simulations over the Paris area, anthropogenic emissions of gases and particles were obtained from the Airparif (the Paris air quality agency) inventory for the year 2005. Meteorology was simulated with the Weather Research & Forecasting (WRF) model [*Skamarock et al.*, 2008a] using an urban canopy model and an updated Corine land-use data base [*Kim*, 2011] with the YSU parameterization [*Hong et al.*, 2006] for the planetary boundary

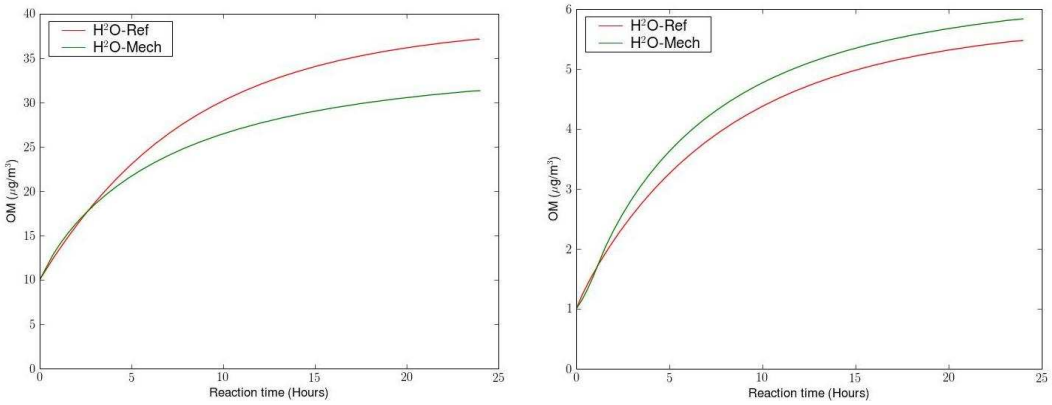

FIGURE 4.2 – Concentrations of SOA from primary SVOC oxidation computed with the two mechanisms for 10 μg.m^{-3} (left) and 1 μg.m^{-3} (right) of POA.

layer (PBL) dynamics.

Emissions of PM from traffic were assumed to consist of 50 % EC, 40 % POA, and 10 % non-volatile non-carbonaceous PM based on measurements conducted in Paris in summer 2010 by *Airparif* [2011]. Emissions of EI-POA (Emissions Inventory POA) are transformed into SVOC emissions using a SVOC/EI-POA ratio of 5 as done and discussed by *Couvidat et al.* [2012a]. To estimate IVOC, we used an IVOC/SVOC factor of 1.70 based on emissions of *Pye and Seinfeld* [2010] for anthropogenic sources, which should be the major source of SVOC in the Paris area.

$PM_{2.5}$ OC was measured at two stations : the SIRTA station (Site Instrumental de Recherche par Télédétection Atmosphérique, *Haeffelin et al.* [2005]), located southwest of Paris in a sub-urban setting, and the LHVP (Laboratoire d´Hygiène de la Ville de Paris) station located in downtown Paris. Two measurement datasets were used to compare model results to measurements. The first dataset uses daily measurements of $PM_{2.5}$ OC and EC with aerosol filters at both stations. $PM_{2.5}$ filter samples (150 mm-diameter quartz fiber filters, Tissuquartz®) were collected on a 12-hour basis, using a high-volume sampler (Digitel, DA-80). A 1 cm^2 filter punch was analyzed for elemental carbon (EC) and organic carbon (OC), using a Sunset Lab analyzer and following the EUSAAR_2 protocol temperature program proposed by *Cavalli et al.* [2010].

The second dataset uses semi-continuous hourly concentrations of EC and OC in $PM_{2.5}$, which were obtained at LHVP from an OCEC Sunset field instrument (Sunset Laboratory, Forest Grove, OR, USA ; *Bae et al.* [2004]) running at 8 L/mn. A denuder provided by the manufacturer was set upstream in order to remove possible adsorption of VOC onto the filter used to collect $PM_{2.5}$ in the instrument. Measurement uncertainty given by the OCEC Sunset field instrument is poorly described in literature, although a 20% uncertainty was etimated by *Peltier et al.* [2007].

Preliminary comparisons of OC and EC obtained by this instrument have been performed in the region of Paris against low-volume VOC denuded manual filter sampling and showed very consistent results [*Sciare et al.*, 2010b, 2011]. During the Megapoli campaign, a comparison was also performed between EC (OCEC Sunset field instrument) and uncorrected Black Carbon provided by the Aethalometer instrument (Magee Scientific, model AE31) leading also to very satisfactory results (r^2=0.96 ; N=620 ; Sciare et al., unpublished data).

During this Megapoli campaign, dynamic filter blanks were performed on a daily basis by placing a total filter upstream of the $PM_{2.5}$ cyclone of the OCEC Sunset field instrument. A systematic offset of 1.0 μg.m^{-3} was found for July 2009. This offset, which depends strongly on the sampled air volume is traditionally considered to be due to VOC absorption [*Bae et al.*, 2004; *Arhami et al.*, 2006; *Polidori et al.*, 2006] and ranges from 0.5 to 2.0 μg.m^{-3} [*Offen-*

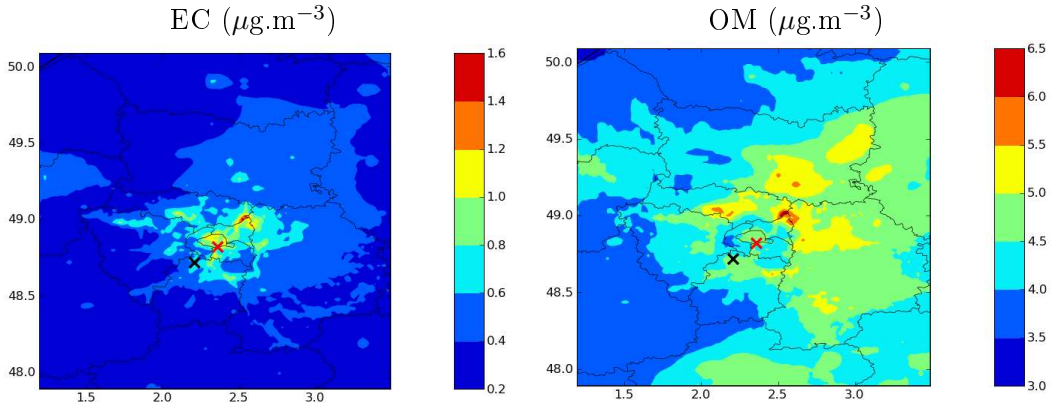

FIGURE 4.3 – Simulated concentrations in μg.m^{-3} of EC (left) and OM (right) for July 2009. The red and black crosses correspond to the LHVP and SIRTA sites, respectively.

berg et al., 2007]. The filters and Sunset instrument measurements are consistent for EC at the LHVP station. However, filter measurements of OC are much higher than the Sunset instrument measurements especially for the second half of July 2009. The differences between the two measurements could be due to condensation of SVOC or adsorption of some VOC on the filter or to the evaporation of some SVOC from the Sunset instrument. However, as OC concentrations during this campaign are very low, it is not surprising that the results from these two measurements are different since the analytical bias (from the sampling and the chemical analysis) are then relatively strong compared to the signal.

Three simulations were conducted : two simulations with the "H^{2}O-Ref" mechanism with and without anthropogenic emissions in the Paris area (all other emissions being the same) to estimate the local contribution of OM and one simulation with the the "H^{2}O-Mech" with all emissions. The simulation with "H^{2}O-Ref" mechanism with anthropogenic emissions reaches the criteria of performance of *Russell and Dennis* [2000] for ozone (mean normalized bias of -4.2% and mean normalized gross error of 15.4%) and the model performance goal of *Boylan and Russell* [2006] for $PM_{2.5}$ (mean fractional bias of -9.0% and mean fractional error of 39%).

4.4 Comparison of the model results with measurements

Concentrations of EC and OC simulated with "H^{2}O-Ref" are shown in Fig. 4.3 at the LHVP and SIRTA stations, and are compared with the 12-h filter measurements at both sites and with hourly Sunset field instrument measurements (with or without the offset of 1 μg.m^{-3}) average over 12-h at the LHVP site. Comparisons with measurements for EC and OC are shown in Figures 4.4 and 4.5, respectively with correlations and root mean square errors (RMSE) between filter measurements and model concentrations.

The model reproduces the high concentrations of OC at the SIRTA and LHVP sites on July 1st, which is a day of high pollution [*Royer et al.*, 2011] and shows satisfactory results at the SIRTA site for EC and OC, although they are both slightly overestimated (0.50 μg.m^{-3} of modeled EC against 0.38 μg.m^{-3} in measurements and 2.64 μg.m^{-3} of modeled OC against 2.27 μg.m^{-3} in measurements). As EC is an inert pollutant (i.e. it does not undergo chemical transformation), it may indicate an overestimation of anthropogenic emissions near the SIRTA site. At the LHVP site, the model shows satisfactory results for EC until July 26th (1.08 μg.m^{-3} of modeled EC against 1.03 μg.m^{-3} in filter measurements) but greatly underestimates EC and OC concentrations between July 26th and July 29th (1.22 μg.m^{-3} of modeled EC on average against

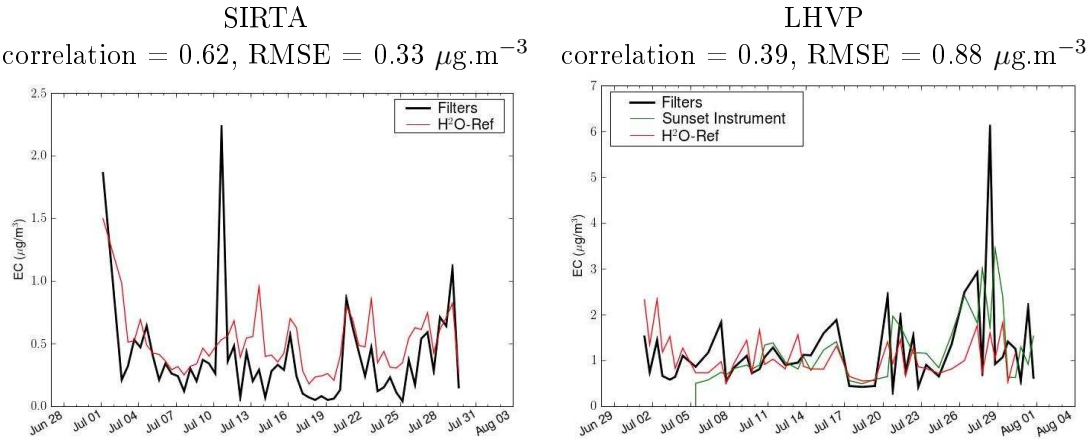

FIGURE 4.4 – 12 h averaged concentrations of EC modeled with "H^2O-Ref" and measured with filters at the SIRTA site (left) and with both filters and Sunset filed instrument at the LHVP (right) site (correlations and RMSE are between the model and the filter measurements).

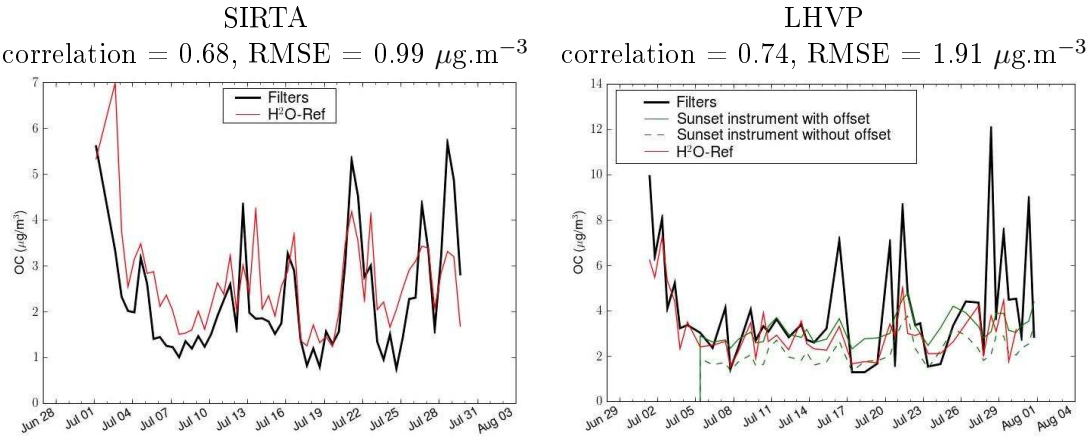

FIGURE 4.5 – 12 h averaged concentrations of OC modeled with "H^2O-Ref" and measured with filters at the SIRTA (left) and with both filters and Sunset field instrument at the LHVP (right) site (correlations and RMSE are between the model and the filter measurements).

2.11 $\mu g.m^{-3}$ in filter measurements). This underestimation could be explained by difficulties in modeling urban meteorology and/or underestimation of emissions due to missing sources : high traffic emissions due to holiday departures, meteorology potentially favorable to PM resuspension, missing emissions of particles from cooking from the Airparif inventory, whereas cooking was found by *Prevot et al.* [2011] to be one of the main sources of organic aerosols in the Paris city center.

The modeled OC concentrations generally fall between the Sunset instrument measurements with and without offset, but are much lower than the filter measurements (on average, 2.87 $\mu g.m^{-3}$ of modeled OC, 3.15 $\mu g.m^{-3}$ of measured OC with the Sunset instrument with the offset and 3.73 $\mu g.m^{-3}$ of measured OC with filter measurements). The modeled concentration peaks of OC are generally observed by the filter measurements but are not observed by the Sunset field instrument (for example, the peaks of July 20^{th}, 28^{th} and 29^{th}). Thus, the correlation coefficient (r) between the model and the filter measurements (r = 0.75) is much higher than the correlation coefficient between the model and the Sunset field instrument measurements (r = 0.49). Due to the differences between measurements performed with filters and the Sunset

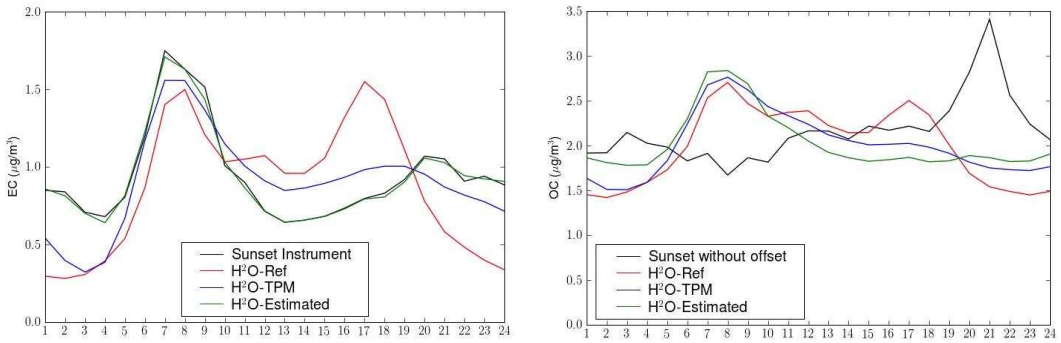

FIGURE 4.6 – Measured and modeled daily temporal profiles for EC (left) and OC (right) at the LHVP site from July 5th to July 25th, 2009. H^2O-TPM stands for the results of "H^2O-Ref" with the temporal profile of *Menut et al.* [2012] for traffic emissions ; H^2O-Estimated corresponds to the use of an estimated emission temporal profile that matches the observed temporal profile of EC.

instrument, it is difficult to conclude if the model underestimates or overestimates OC concentrations.

Since the Sunset instrument measurements are hourly, they provide insight into the temporal profiles of EC and OC at the LHVP station. Fig. 4.6 shows the measured and modeled daily temporal profiles for EC and OC at the LHVP station from July 5th to July 25th (i.e., the period during which the Sunset instrument, the filters and the model give similar EC concentrations). As shown in this figure, "H^2O-Ref" shows two peaks corresponding to high EC emissions from traffic during rush hours. The first peak reproduces well the Sunset instrument measurements. However, the model also shows high EC concentrations between 10 am and 8 pm with a peak at 4-5 pm and low concentrations after 8 pm whereas the measurements show low concentrations between 8 am and 8 pm and an increase in concentrations after 8 pm. This could be due to an incorrect temporal profile for traffic emissions in the Airparif inventory. *Menut et al.* [2012] studied the impact of hourly emission profiles and provided more realistic temporal profiles of traffic emissions for some cities (including Paris). Fig. 4.7 shows the temporal profiles of traffic emissions of the Airparif inventory and *Menut et al.* [2012]. The emission profile of the Airparif inventory gives very high emissions at the end of the afternoon whereas emissions from the temporal profile of *Menut et al.* [2012] (noted TPM hereafter) are much lower in the afternoon and higher at the end and beginning of the day. Using TPM gives better results with lower EC concentrations during the afternoon and higher EC concentrations at night, but the second peak of concentrations given by the model still occurs too early and night concentrations are still too low (see Fig. 4.6). Underestimation of EC concentrations at night could be due to the overestimation of the nighttime PBL height by WRF using the YSU parameterization. It is also possible that TPM does not reproduce exactly the temporal profile of summer traffic emissions, because TPM is estimated by averaging "near traffic" concentrations values measured on Mondays during a whole year. This temporal profile is, therefore, an average temporal profile and is not specific to July, when holidays may strongly affect the emission profile. To address this potential source of uncertainty, a temporal profile of traffic emissions was estimated by matching the temporal profile of EC concentrations. This estimated temporal profile of traffic emissions is shown in Fig. 4.7 and the corresponding modeled EC concentration profile is shown in Fig. 4.6.

For OC concentrations, except for a peak at 10 pm, the measured temporal profile (shown Fig. 4.6) is almost constant with concentrations around 2.0 $\mu g.m^{-3}$ without the offset. *Allan et al.* [2010] found high concentrations of organic aerosols due to cooking between 8 and 10 pm

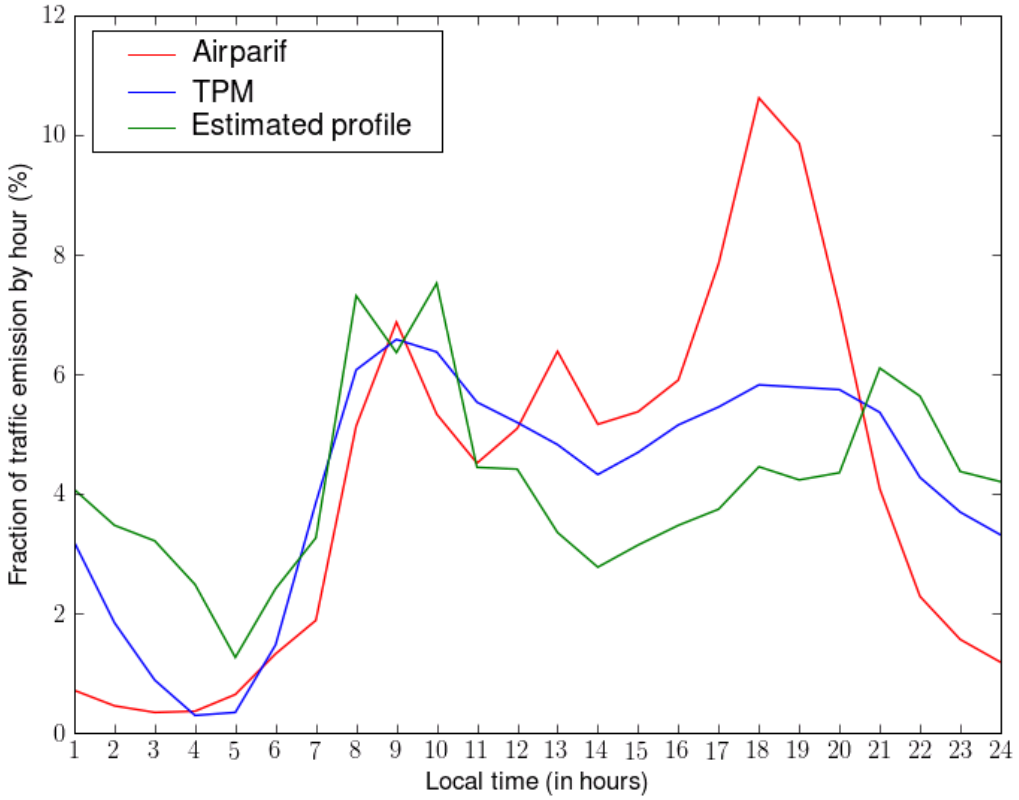

FIGURE 4.7 – Temporal profiles of traffic emissions from the Airparif inventory, from *Menut et al.* [2012] (TPM) and from matching EC observations at the LHVP station (Estimated profile).

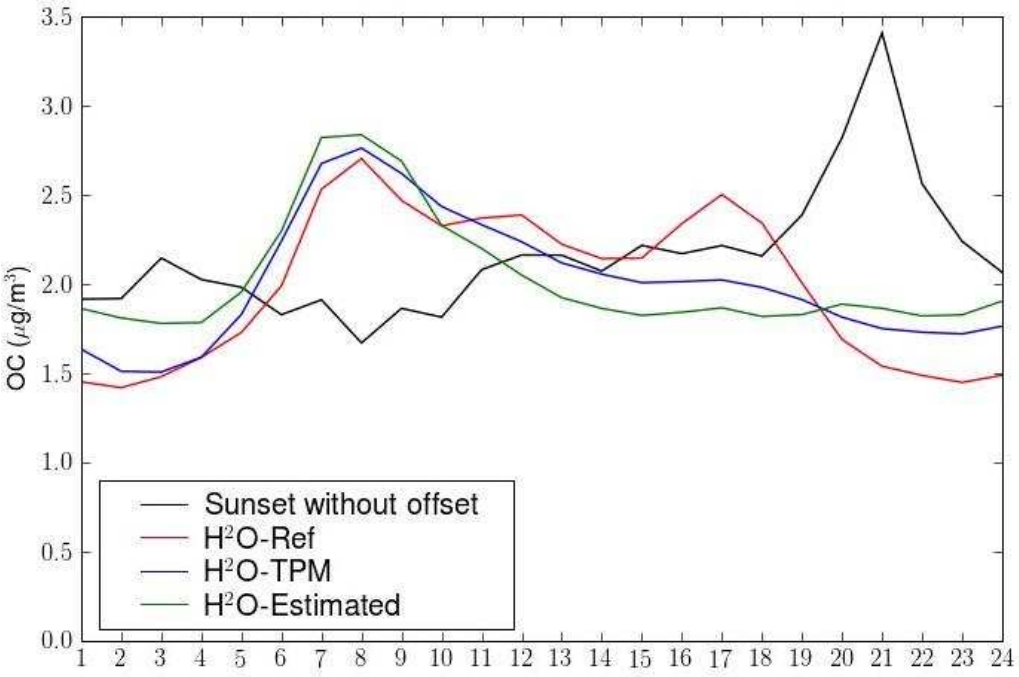

FIGURE 4.8 – Simulation of the daily temporal profiles of secondary OC compared with the daily temporal profile of measured OC (See Figure 4.7 for simulation descriptions).

in London and Manchester. The 10 pm peak observed in Paris could then be due to cooking activities. In that case, since cooking emissions are missing from the inventory, the model should not be able to reproduce this peak. The peaks of EC corresponding to rush-hour high emissions do not appear in the observed temporal profile of OC. "H^2O-Ref" gives two peaks corresponding to high emissions from traffic given by the Airparif inventory, which do not appear in the measurements. However, the second OC peak disappears when TPM (which gives lower emissions in the afternoon and higher emissions at night) is used but the first peak is unchanged. Using the estimated temporal profile of traffic emissions confirms the disappearance of the second peak but could not explain the absence of the first peak which clearly appears in the temporal profile of EC.

One possible explanation is that evaporation of POA is underestimated by the model. This is possible since evaporation of POA is based on results of *Robinson et al.* [2007], which are based on measurements for organic loading higher than 20 μg m^{-3}. Partitioning of primary SVOC is then highly uncertain at the conditions of the simulation with OC concentrations around 2 μg m^{-3}. Primary SVOC may not condense and organic aerosols could then be secondary. It is also possible that the gas-particle partitioning of primary SVOC is affected by temperature and that an underestimation of temperature during the morning rush hours could lead to a slight overestimation of POA. However, no measurements of temperature are available during the campaign at the LHVP site and therefore comparisons can not be made to verify if the temperature at this site is underestimated. Fig. 4.8 shows the secondary OC (SOC) concentrations. This profile is relatively constant around 1.7 μg m^{-3} with a small increase to 2.1 μg m^{-3} and, except for the evening peak, this profile is very similar to the profile of OC measured by the Sunset instrument. It may indicate that primary SVOC from traffic did not condense in Paris in July 2009 or that POA from traffic were not captured by the Sunset field instrument, which could then explain the differences between the Sunset field instruments and the filter measurements.

4.5 Comparison of two mechanisms for primary SVOC aging

A comparison of OC, SOC and primary organic carbon (POC) concentrations between "H^2O-Ref" and "H^2O-Mech" is shown in Fig. 4.9 and the OM/OC ratios for July 2009 computed with the two mechanisms are shown in Fig. 4.10. The OM/OC ratios computed with "H^2O-Ref" are higher than the OM/OC ratios computed with "H^2O-Mech". This difference is due to the lower OM/OC ratios of oxidized SVOC formed from the oxidation of primary SVOC in "H^2O-Mech" (between 1.27 and 1.85) than in "H^2O-Ref" (equal to 1.82). However, only one oxidation step is taken into account in "H^2O-Mech" and, in reality, oxidized SVOC should be more oxidized as numerous oxidation steps could occur. "H^2O-Ref" gives an OM/OC ratio around 1.6 in Paris area ; these results are consistent with the results of *Turpin and Lim* [2001] for urban areas. Concentrations of POC are lower with "H^2O-Mech" than with "H^2O-Ref". As the organic aerosol loading into which SVOC can be absorbed is the same in the two mechanisms, the lower concentrations of POC with "H^2O-Mech" is due to the impact of activity coefficients on the partitioning of primary SVOC (which is not taken into account in "H^2O-Ref"). It indicates that primary SVOC condense less readily on an oxidized aerosol. This point could be very important for SVOC partitioning in the atmosphere and, since "H^2O-Mech" only takes into account one oxidation step whereas numerous oxidation steps are likely to occur in the atmosphere, this effect could be even greater than simulated here. The secondary aerosol should be more oxidized in reality than in the model and primary SVOC are possibly unable to condense on an oxidized aerosol. Those results are confirmed by experimental studies : POA and SOA were shown to possibly not mix [*Song et al.*, 2007] or to mix but with interactions between compounds influen-

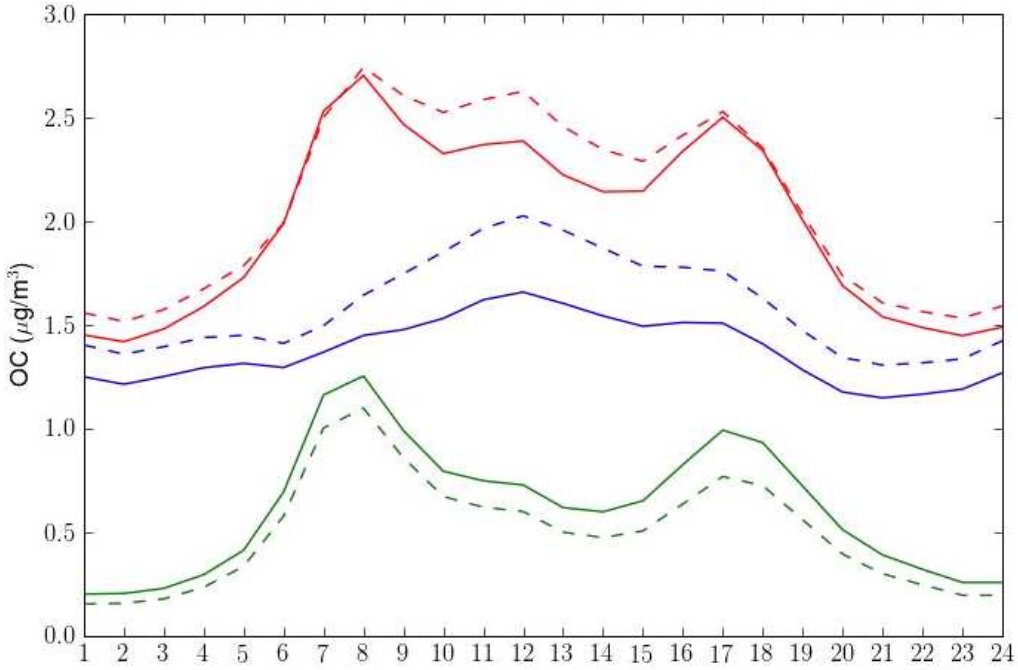

FIGURE 4.9 – Comparison of modeled temporal profiles of OC (in red), SOC (in blue) and POC (in green) between "H^2O-Ref" (solid lines) and of "H^2O-Mech" (dashed lines)

cing the partitioning of SVOC [*Asa-Awuku et al.*, 2009].

In contrast, SOC formation is higher in "H^2O-Mech" than in "H^2O-Ref" but SOA concentrations are similar (as shown in Fig. 4.11). Fig. 4.11 shows that biogenic SOA are similar with the two mechanisms. However, the concentrations of biogenic hydrophobic compounds (BiNIT, BiNIT3, BiNGA, BiBlP, BiBmP, AnBlP, AnBmP), which are absorbed into the organic phase, concentrations are increased by 10%. The higher concentration of biogenic hydrophobic SOA compounds with "H^2O-Mech" is due to lower activity coefficients. "H^2O-Ref" uses for the computation of activity coefficients the same molecular structure as primary SVOC (POAlP, POAmP, POAhP) for SOA formed from the oxidation of primary SVOC (SOAlP, SOAmP, SOAhP) and, therefore, it does not take into account the fact that these SOA compounds are more oxidized than the primary compounds ; this phenomenon is taken into account in "H^2O-Mech". As the organic aerosol should be more oxidized in reality than they are in "H^2O-Mech" (because the model takes into account only one oxidation step), the condensation of some hydrophobic com-

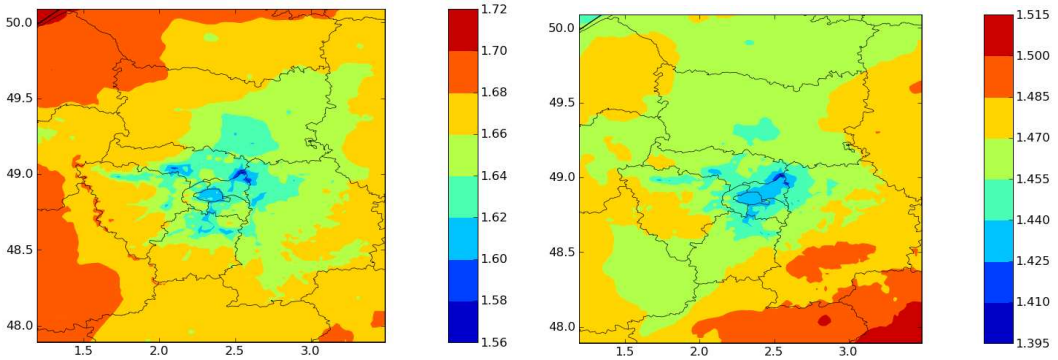

FIGURE 4.10 – Modeled OM/OC ratios with "H^2O-Ref" (left) and "H^2O-Mech" (right).

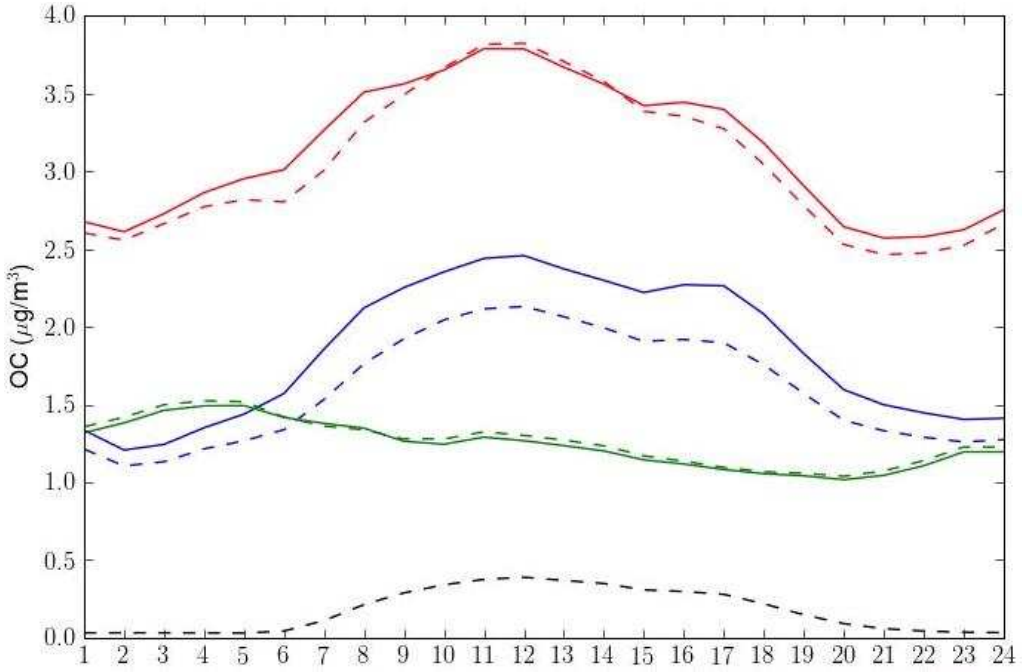

FIGURE 4.11 – Modeled temporal profiles of total SOA (in red), of SOA from primary SVOC oxidation (in blue), of biogenic SOA (in green), and of SOA from IVOC oxidation -in black) for "H^2O-Ref" (solid lines) and for "H^2O-Mech" (dashed lines)

pounds leading to more SOA formation may be underestimated. Concentrations of SOA formed from IVOC oxidation are not insignificant (the average concentration at noon is 0.4 μg.m^{-3}) but are low compared to SOA formation from SVOC oxidation.

4.6 Origins of particulate organic matter in the Paris area

The fraction of carbonaceous aerosol originating from the Paris area (i.e., from local sources) is estimated with "H^2O-Ref" by subtracting the results of a simulation without the anthropogenic emissions in the Paris area from the results of the base simulation, i.e., with those anthropogenic emissions. Fig. 4.12 shows concentrations of EC and OM and the local contribution of anthropogenic sources for July 2009. Whereas EC is found to be almost entirely of local origin, OM inside Paris is found to have both local and regional contributions. About 30 to 38 % of OM in the city center of Paris (30% at the LVHP site) can be attributed to local sources during July 2009. This result is commensurate with those obtained by *Airparif* [2011] using a receptor-based approach : they estimated that at a background urban site, 27% of OM was of local origin. Fig. 4.13 shows the composition of OM given by "H^2O-Ref" at the LHVP and SIRTA sites. OM has a similar composition at the two sites, but there are more primary SVOC that have been oxidized at the suburban SIRTA site. At the LHVP site, OM consists of aerosols from the boundary conditions of the European simulation (28 %), POA (23%), SOA formed from primary SVOC oxidation (19 %), SOA formed by oxidation of biogenic precursors (29%), and SOA formed by oxidation of aromatic precursors (1%).

We defined the amount of local aerosol by the difference between two simulations with or without anthropogenic emissions. However, the system is not linear. For example, the concentrations of some surrogates are higher over Paris with anthropogenic emissions due to the increase

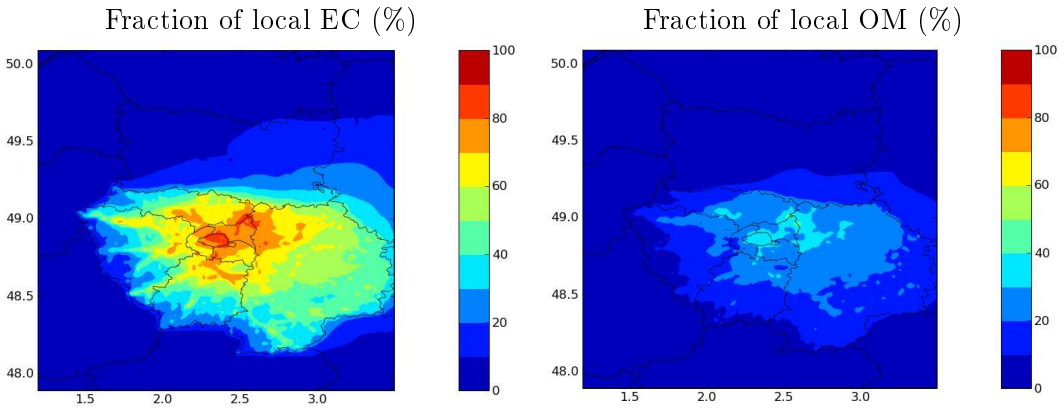

FIGURE 4.12 – Fraction of local aerosol in % (bottom) for EC (left) and OM (right) for July 2009.

of the absorbing media even they come from distant sources. 16% of SOA formed from sesquiterpene oxidation is then found to be local. On the contrary, SOA concentrations from isoprene oxidation increase by 28% when anthropogenic emissions over Paris are removed. This is due to lower NO_x concentrations : instead of being oxidized under high-NO_x conditions, isoprene is oxidized under low-NO_x conditions and forms SOA with higher yields. As the effect of NO_x concentrations is not taken into account for monoterpenes and sesquiterpenes, it is possible that more SOA could be formed from these precursors without anthropogenic emissions over the Paris area.

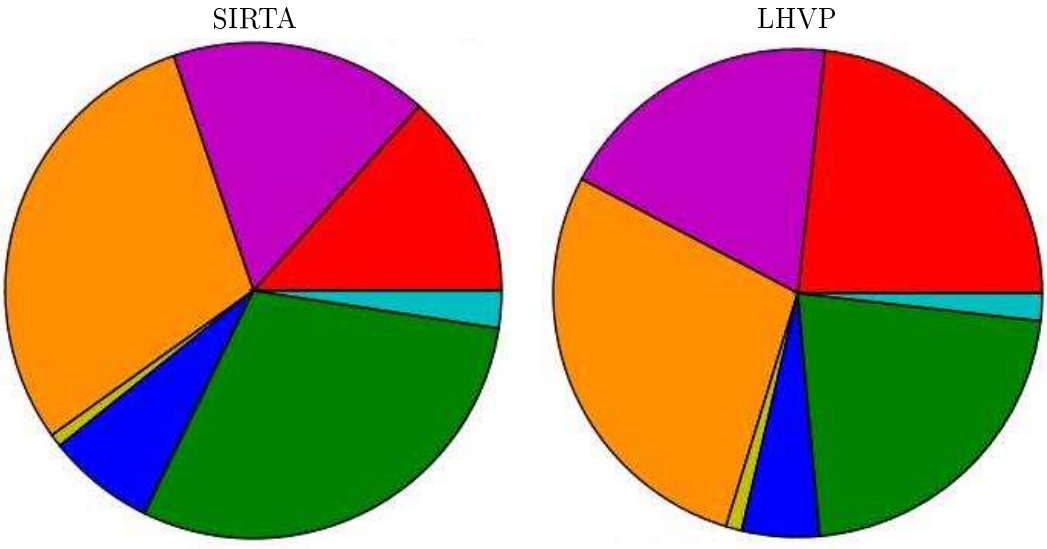

FIGURE 4.13 – Averaged composition of OM at the SIRTA (left) and LHVP (right) sites modeled with "H^2O-Ref". Red : POA, purple : SOA formed form oxidation of primary SVOC, orange : OM from boundary conditions used for the European simulation (long-range transport of OM), yellow : SOA formed from aromatics oxidation, blue : SOA formed from monoterpenes oxidation, green : SOA formed from sesquiterpenes oxidation, aqua : SOA formed from isoprene oxidation

4.7 Conclusions

Organic aerosol formation was simulated over the Paris area during July 2009. Results of the model simulations were compared to measurements conducted during the Megapoli campaign. The model simulated a morning peak of concentrations due to rush-hour traffic for both EC and OC ; however, this peak appears in the EC measurements, but does not appear in the OC measurements. This discrepancy between the model and the measurements could be due to the underestimation of POA evaporation at low organic loading by the model, to uncertainties in the modeled temperature, which can affect the gas-particle partitioning or to POA from traffic, which would not be captured by the Sunset field instrument. Using a mechanism for oxidation of primary SVOC that takes into account the molecular structure of SOA and, therefore, includes explicitly the effect of activity coefficients on SVOC gas/particle partitioning, it was found that oxidized organic aerosols have low affinity with POA and that POA and SOA do not mix well together. POA formation is likely to be overestimated by a model that does not fully account for the non-ideality of the organic condensed phase, whereas SOA is likely to be underestimated. Moreover, treating the organic aerosol solution as a one-phase ideal solution or using simple partitioning constants (which do not take into account the affinity of a compound with the liquid aerosol solutions) probably overestimates the condensation of primary SVOC.

Organic aerosols in Paris were found to be mainly anthropogenic with 30 to 40% of OM due to local sources. According to the model, most of the OM results from the condensation of primary SVOC and their oxidation products. Biogenic VOC form only a small quantity of SOA (29% of OM) and are minor precursors in this simulation. Comparisons of modeled biogenic SOA concentrations with molecular SOA tracer measurements are needed to confirm this result and evaluate the biogenic emission inventory for Europe.

Chapitre 5

Impact de la chimie en phase aqueuse et du dépôt humide sur la formation d'aérosols organiques

Résumé

Le dernier point abordé dans le cadre de cette thèse concerne la formation des aérosols organiques en phase aqueuse. La phase aqueuse des nuages ou des particules constitue un milieu où les composés organiques peuvent subir certaines réactions et former certains composés peu volatils (par exemple des réactions de conversion des aldéhydes en acides). L'oxydation du glyoxal et du méthylglyoxal (qui sont des produits d'oxydation de l'isoprène et des composés aromatiques) dans la phase aqueuse des nuages a été très étudiée et peut former des aérosols organiques via notamment la formation des acides oxaliques, pyruviques et glyoxyliques. La méthacroléine et la méthyl-vinyl-cétone (produits d'oxydation de l'isoprène en régime haut-NO_x) peuvent aussi former des quantités importantes d'aérosols via oxydation dans la phase aqueuse des nuages [*El Haddad et al.*, 2009; *Liu et al.*, 2012]. Certaines réactions peuvent aussi avoir lieu dans la phase aqueuse des particules. Par exemple, l'oxydation de l'isoprène en régime bas-NO_x conduit à la formation d'un époxydiol (noté IEPOX) qui peut être hydrolysé ou réagir avec les anions dans la phase aqueuse des particules. Les méthyltetrols, les C_5-alcènes-triols et certains organosulfates sont des exemples de composés formés par ces réactions.

De nombreuses études expérimentales montrent donc que la phase aqueuse des nuages et des particules peuvent former des quantités importantes d'aérosols. Cependant, la plupart des modèles de qualité de l'air ne prennent pas en compte l'influence de la chimie aqueuse des nuages ou alors prennent seulement en compte la formation des acides oxaliques, pyruviques et glyoxyliques supposés non-volatils ou le vieillissement des aérosols organiques en phase aqueuse. L'objectif de cette étude est d'étudier plus en détail l'impact de la chimie aqueuse sur la formation d'aérosols en ajoutant à la formation des acides oxaliques, pyruviques et glyoxyliques, les dernières informations disponibles : la formation d'aérosols à partir de l'oxydation dans la phase aqueuse des nuages de la méthacroléine et de la méthyl-vinyl-cétone et la formation d'aérosols à partir des réactions de IEPOX dans la phase aqueuse des particules. Le vieillissement des aérosols dans la phase aqueuse des nuages est aussi étudié avec un mécanisme simple.

L'impact des dépôts humides sur la formation d'aérosols organiques est aussi étudié pour déterminer l'impact total des nuages (c'est-à-dire transformations chimiques et lessivage par précipitation). Le dépôt des composés organiques semi-volatiles gazeux absorbés par les gouttes d'eau des nuages qui n'est pas traité par la plupart des modèles est ajouté au modèle.

Les nouvelles espèces sont ajoutées au modèle H^2O pour prendre en compte leur partage entre la phase gazeuse et la phase particulaire. Le module de chimie gazeuse RACM2 est utilisé pour la chimie de la phase gazeuse et un module simple de chimie aqueuse des nuages est ici utilisé. Ce module prend en compte la formation de sulfate dans les nuages via l'oxydation du dioxyde de soufre et suppose que les concentrations des composés dans les nuages sont à l'équilibre avec la phase gazeuse. Le module est modifié pour prendre en compte des réactions suplémentaires menant à la formation d'aérosols organiques. Le pH de la phase aqueuse des nuages est calculé par électroneutralité. La quantité d'aérosols aqueux et le pH des aérosols sont calculés avec le modèle ISORROPIA [*Nenes et al.*, 1998]. Les concentrations d'aérosols sont simulées du 15 juillet 2002 au 14 août 2002. Une période estivale a été choisie car les émissions d'isoprène (précurseur du glyoxal, du méthylglyoxal, de la méthacroléine et de la méthyl-vinyl-cétone) y sont plus importantes.

La formation des acides oxalique, pyruvique et glyoxylique à partir du glyoxal et du méthylglyoxal et d'autres composés organiques volatils est représentée via un mécanisme existant [*Chen et al.*, 2007]. L'absorption de ces acides avec dissociation dans la phase aqueuse des particules est calculée en se basant sur leurs constantes de Henry et leurs constantes d'acidité. Dans ce cas, d'après le modèle, les acides pyruviques et glyoxyliques ne sont pas absorbés dans la phase aqueuse des particules. De plus, moins de 64% de l'acide oxalique est présent dans la particule (avec même certaines régions où l'acide oxalique n'est pas présent dans la particule) alors que certaines études montrent au contraire que l'acide oxalique est majoritairement absorbé dans la particule [*Limbeck et al.*, 2001].

La formation d'aérosols par l'oxydation dans les nuages de la méthacroléine et de la méthyl-vinyl-cétone est ajoutée au modèle en se basant sur les résultats de différentes études [*Liu et al.*, 2009b, 2012]. En supposant les concentrations de la méthacroléine et de la méthyl-vinyl-cétone dans le nuage à l'équilibre avec la phase gazeuse, le modèle donne des concentrations très faibles d'aérosols puisque les concentrations totales (gaz + particule) sont inférieures à 1 $ng.m^{-3}$. Cela est due aux faibles constantes de Henry de ces deux composés. Cependant, d'après certaines études [*van Pinxteren et al.*, 2005], les concentrations de la méthacroléine et de la méthyl-vinyl-cétone dans le nuage pourraient être bien supérieurs aux concentrations à l'équilibre. En multipliant par 200 la constante de Henry de la méthacroléine et par 100 celle de la méthyl-vinyl-cétone, le modèle donne des concentrations moyennes au sol comprises entre 0,8 et 6,4 $ng.m^{-3}$ et des concentrations journalières pouvant atteindre 64 $ng.m^{-3}$. Le partage de la méthacroléine de la méthyl-vinyl-cétone entre la phase aqueuse des nuages et la phase gazeuse devraient être donc étudié plus en détail pour déterminer si ces deux precurseurs peuvent former des quantités significatives d'aérosols par oxydation dans les nuages.

Un mécanisme de formation d'aérosols à partir de IEPOX est développé. Deux composés suppléants sont ajoutés au modèle : le composé suppléant BiMT permet de prendre en compte la formation d'aérosols par hydrolyse (dont la cinétique dépend du pH de la particule) ou réaction de IEPOX avec les ions nitrates (l'organonitrate formé s'hydrolysant très rapidement pour former des méthyltétrols), le composé suppléant BiSULF permet de prendre en compte la formation d'organosulfate via réaction de IEPOX avec les ions sulfate et bisulfate. En utilisant une constante de Henry de 2.0×10^7 $M.atm^{-1}$, le modèle donne des résultats en accord avec les concentrations de traceurs mesurées. Les concentrations d'aérosols formées à partir de IEPOX peuvent atteindre des concentrations importantes (supérieures à 1 $\mu g.m^{-3}$) dans certaines régions et à certaines périodes où la phase aqueuse des aérosols est très acide.

Le mécanisme de vieillissement développé dans cette étude permet d'estimer l'impact des nuages sur la volatilité des aérosols. D'après le modèle une fraction très significative de l'aérosol organique au niveau du sol (10 à 30%) pourrait avoir été vieillie par un nuage. Cela correspond à une augmentation des concentrations moyennés sur la période pouvant atteindre 1 $\mu g.m^{-3}$.

Bien que ce mécanisme soit simple (il suppose une seule étape d'oxydation et fait l'hypothèse que seulement des composés moins volatils soit formés), cela montre que les nuages peuvent contribuer au vieillissement de manière significative et qu'il est par conséquent important de développer des mécanismes pour le vieillissement des aérosols.

Par ailleurs, les résultats des simulations montrent que 20 à 60% de l'aérosol organique formé durant la période de simulation est déposé via des dépôts humides sur l'Europe. Les dépôts humides influencent grandement les concentrations organiques et les modèles doivent donc traiter correctement ce processus. Par exemple, le lessivage des composés organiques semi-volatils gazeux qui n'est traditionnellement pas pris en compte dans les modèles conduit à une diminution des concentrations pouvant atteindre 0.7 μg.m^{-3} et ne pas prendre en compte ce processus mène à une surestimation des concentrations de 3 to 17%.

Ce chapitre est constitué de :
Couvidat, F., Sartelet, K. et Seigneur, C. (2013). **Investigating the impact of aqueous-phase chemistry and wet deposition on organic aerosol formation using a molecular surrogate modeling approach**. *Environ. Sci. Tech.*, 42 : 914-922.

Sommaire

Abstract

A molecular surrogate representation of secondary organic aerosol (SOA) formation is used to investigate the effect of aqueous-phase (in clouds and particles) chemical processing and wet deposition on SOA atmospheric concentrations. To that end, the hydrophilic/hydrophobic organic (H^2O) model was augmented to account for several gas/aqueous-phase equilibria and aqueous-phase processes, including the formation of oxalic, glyoxilic and pyruvic acids, the oxidation of methyl vinyl ketone (MVK) and methacrolein (MACR), the formation of tetrols and organosulfates from epoxydiols (IEPOX), and further oxidation of water-soluble SOA (aging). Among those processes, SOA chemical aging and IEPOX reactions led to the most significant increases (up to 1 μg m^{-3} in some areas) in SOA concentrations in a one-month summer simulation over Europe. However, large uncertainties remain in the gas/aqueous-phase partitioning of oxalic acid, MVK and MACR. Below-cloud scavenging of SOA precursor gases and of gas-phase SVOC was found to affect SOA concentrations by up to 20%, which suggests that it should be taken into account in air quality models.

5.1 Introduction

Fine particulate matter (PM) with an aerodynamic diameter less than 2.5 μm ($PM_{2.5}$) is regulated because of its impact on human health. Furthermore, $PM_{2.5}$ degrades atmospheric visibility and influences climate change. Organic aerosol concentrations, which constitute a significant fraction of $PM_{2.5}$, are difficult to represent in three-dimensional (3D) air quality models due to the complexity of the phenomena involved (gas and particle phase chemistry, oligomerization, hygroscopicity, non-ideality of particles) and the large number of organic species originating from diverse sources (anthropogenic and biogenic). Organic PM is either primary (directly emitted as particles) or secondary (formed in the atmosphere as the result of chemical production of low-volatility compounds). Secondary organic aerosols (SOA) can be formed by the oxidation of gaseous species or by the oxidation of species absorbed by the aqueous phase of clouds, fog or particles.

Aqueous-phase SOA formation has been studied in reactors and could form significant amount of SOA [*Ervens et al.*, 2011]. Glyoxal and methylglyoxal have been the most studied volatile organic compounds (VOC) leading to in-cloud SOA formation. They have been shown to produce in-cloud SOA via formation of oxalic acid [*Carlton et al.*, 2007; *Ervens et al.*, 2008], oligomer formation [*Gao et al.*, 2004; *Jang et al.*, 2005], nighttime cloud processing [*Yasmeen et al.*, 2010], reaction with amines [*De Haan et al.*, 2009a] and amino acids [*De Haan et al.*, 2009b]. Moreover, glyoxal was shown to form oligomers in the aqueous phase of particles and to partition efficiently in ammonium sulfate solution [*Ervens and Volkamer*, 2010]. The formation of SOA from the aqueous-phase oxidation of methacrolein (MACR) and methyl-vinyl-ketone (MVK), which are compounds formed by the oxidation of isoprene under high-NO_x conditions, were also recently studied and were shown to lead to significant amounts of SOA [*El Haddad et al.*, 2009; *Liu et al.*, 2012]. Isoprene was also found to form under low-NO_x conditions compounds that could lead to SOA formation after aqueous-phase reaction. Tetrols, which were first identified during field studies in Amazonia [*Claeys et al.*, 2004], are mostly formed via the particle aqueous-phase hydrolysis of an isoprene derived epoxidiol formed under low-NO_x conditions [*Surratt et al.*, 2010]. Organosulfates can also be formed by aqueous-phase reactions via nucleophilic addition or substitution [*Darer et al.*, 2011] or by radical-radical reactions [*Perri et al.*, 2010].

Only a few air quality models take into account the formation of low-volatility compounds via aqueous-phase reactions and generally only take into account the formation of oxalic acid

[*Carlton et al.*, 2008] and the theoretical aqueous-phase aging of some semi-volatile organic compounds [*Chen et al.*, 2007]. *Carlton et al.* [2008] found that, by including formation of oxalic acid, concentrations of organic aerosols are increased in altitude and *Chen et al.* [2007] found that ground-level SOA concentrations are increased by 9% when aqueous-phase reactions, including aging, are added to the model.

However, even if clouds can be a source of SOA, they can also be a sink for organic aerosols and their precursors via the wet deposition of water-soluble organic compounds (WSOC). To our knowledge, the gaseous WSOC wet deposition issue has not been adressed so far. The deposition of organic vapors could be a large source of uncertainty in SOA formation [*Hallquist et al.*, 2009]. Only the issue of their dry deposition has been adressed to date[*Bessagnet et al.*, 2010].

The aim of this study is to investigate the impact of clouds on SOA concentrations considering both sources and sinks, i.e., increased SOA formation via aqueous-phase reactions and increased removal of SOA and WSOC. To that end, available information on in-cloud SOA formation processes is added to the cloud chemical scheme and additional organic aerosol species, which are involved in aqueous-phase reactions, are added to the hydrophilic/hydrophobic organic (H^2O) aerosol model [*Couvidat et al.*, 2012a] to compute organic aerosol concentrations. Wet deposition of gaseous precursors and SVOC is added to the 3D air quality model, which hosts H^2O. A modeling study is then conducted to provide a first estimate of the impact of clouds on organic aerosol formation over Europe in summer.

5.2 Methods

5.2.1 Model presentation

The Polair3D air quality model [*Sartelet et al.*, 2007] of the Polyphemus air quality platform [*Mallet et al.*, 2007] is used to simulate air quality over Europe. It is used with the Regional Atmospheric Chemistry Mechanism 2 (RACM2) [*Goliff and Stockwell*, 2008; *Kim et al.*, 2009] for the gas-phase chemistry, the SIze REsolved Aerosol Model (SIREAM) [*Debry et al.*, 2007a] for simulating the dynamics of the aerosol size distribution, ISORROPIA [*Nenes et al.*, 1998] for the formation of inorganic aerosols and the H^2O model for SOA formation [*Couvidat et al.*, 2012a]. RACM2 is modified to take into account the reactions described by *Couvidat et al.* [2012a].

H^2O distinguishes two kinds of surrogate SOA species : hydrophilic species (which condense mainly on an aqueous phase) and hydrophobic species (which condense only on an organic phase due to their low affinity with water). Hydrophilic species may also condense on an organic phase in the absence of aqueous particles, i.e., at very low relative humidities. Distinction between hydrophobic and hydrophilic compounds is based on their octanol/water coefficient [*Pun et al.*, 2006] or their partitioning between the organic and aqueous phases [*Couvidat and Seigneur*, 2011]. H^2O has been evaluated over Europe [*Couvidat et al.*, 2012a] and the Paris area [*Couvidat et al.*, 2012b].

A simple aqueous-phase chemistry module is used here to represent inorganic cloud chemistry. Although detailed chemical kinetic mechanisms have been developped [*Jacob*, 1986; *Deguillaume et al.*, 2009], model performance evaluations have shown that simple mechanisms give satisfactory results for the concentrations of major inorganic species and that cloud and precipitation fields are larger sources of uncertainty [*Middleton et al.*, 1988; *Vijayaraghavan et al.*, 2007; *Appel et al.*, 2011]. Therefore, since we focus here on organic aqueous-phase processes, the simple module used by *Roustan et al.* [2010] is used here. It treats sulfate production in clouds via the aqueous-phase oxidation of sulfur dioxide (SO_2) by hydrogen peroxide (H_2O_2), ozone (O_3) and oxygen (O_2) catalyzed by trace metals. Nitrate formation in the presence of clouds is treated via heterogeneous reactions of dinitrogen pentaoxide (N_2O_5) and nitrate radicals (NO_3). This

module is modified here to take into account the absorption of several organic species and their oxidation in the aqueous phase. The concentration of the hydroxyl radical (HO) in the cloud is assumed to be half the concentration of HO at equilibrium following *Seigneur et al.* [2001], *Jaeglé et al.* [2001] and *Jacob* [2000] to account for aqueous-phase consumption of HO based on the measurements by *Mauldin III et al.* [1997]. The added reactions are presented in the following sections.

The pH of the cloud droplet is calculated assuming electroneutrality of the solution and accounting for the gas/droplet partitioning of several water-soluble inorganic species such as nitric acid (HNO_3) and ammonia (NH_3). The pH of particles is calculated with the ISORROPIA model for the inorganic species, i.e., the weak organic acids do not affect the pH notably, and therefore, are not included in the pH computation. The pH is used to compute some aqueous-phase reactions and the partitioning of organic acids between the gas phase and the aqueous phase of particles by taking into account their acid dissociation.

Two types of aqueous-phase reactions are studied : photochemical reactions which take place in the aqueous phase of cloud droplets like the aqueous-phase oxidation of glyoxal, methylglyoxal, MACR and MVK and non-photochemical reactions, which can take place in both the aqueous phase of clouds and the water of delisquescent aerosol (noted aqueous-phase of particles hereafter) like the aqueous-phase hydrolysis of an isoprene-derived epoxidiol.

5.2.2 In-cloud formation of SOA

The formation of oxalic, pyruvic and glyoxylic acids from the in-cloud oxidation of glyoxal, methylglyoxal and some other VOC (ethanol, acetaldehyde, acetic acid) is added based on the mechanism described by *Chen et al.* [2007]. These three acids are often assumed to be non-volatile because they remain in the particle phase after cloud evaporation [*Carlton et al.*, 2006]. However, measurements done in a rural background site in the South African savanna show that oxalic acid is semi-volatile with 90% present in the particle phase [*Limbeck et al.*, 2001]. Moreover, according to *Clegg et al.* [1996], oxalic acid condenses almost entirely on an aqueous aerosol except when the aerosol is very acid. Therefore, in this study, the formation of aerosols from these three compounds is done following two assumptions. Either these three acids are assumed non-volatile (they are entirely in the particle phase) or their partitioning is obtained by assuming equilibrium between the gas phase and an aqueous phase where acids can dissociate based on their acid dissociation constants. Henry's law constants for oxalic, pyruvic and glyoxylic acids and their acid dissociation constants are taken from *Chen et al.* [2007]. It is, however, possible that these compounds could form complexes in the particle phase [*Furukawa and Takahashi*, 2011], which could affect the partitioning of these acids. However, due to lack of data, this phenomenon is not taken into account.

SOA formed from in-cloud oxidation of MACR and MVK is added to the model based on the results of several experimental studies. *Liu et al.* [2012] showed that a significant amount of oligomers is formed from the aqueous-phase oxidation of MVK and MACR. The same phenomenon was observed by *Surratt et al.* [2006] for SOA formed from the gas-phase oxidation of MACR. Moreover, *Liu et al.* [2009b] detected the formation of the 2,2-dihydroxymethacrylic acid, which is also formed from the gas-phase oxidation of MACR. Therefore, in the absence of other information on molecular oxidation products, one assumes that the organic aerosols formed from the aqueous-phase oxidation of MACR and MVK are similar to the organic aerosols formed from the gas-phase oxidation of MACR. For this reason, the surrogate compound BiMGA, which is used as a surrogate compound for SOA from the gas-phase oxidation of MACR [*Couvidat and Seigneur*, 2011; *Couvidat et al.*, 2012a], is also used as a surrogate compound for the aqueous-phase oxidation of MACR and MVK. By fitting an Odum curve to the results of *El Haddad et al.* [2009], the maximal aerosol mass yield from the aqueous-phase oxidation was found to be

around 25%, which gives a stoichiometric coefficient for BiMGA of 0.15 (the molecular weight of BiMGA being 120 g.mol^{-1}). As the in-cloud oxidation of MVK has a similar yield, the following two reactions are added to the model :

$$\mathrm{MACR + HO \Rightarrow 0.15BiMGA} \quad \text{(R 5.1)}$$

$$\mathrm{MVK + HO \Rightarrow 0.15BiMGA} \quad \text{(R 5.2)}$$

A kinetic rate of 5.8 $\times$ 10^9 M^{-1}.s^{-1} is used for reaction R5.1 [*Liu et al.*, 2009b] and 7.0 $\times$ 10^9 M^{-1}.s^{-1} is used for reaction R5.2 [*Szeremeta et al.*, 2009]. Henry's law constants for MACR (6.5 M.atm^{-1}) and MVK (41.0 M.atm^{-1}) are taken from *Iraci et al.* [1999].

5.2.3 SOA formation from IEPOX in the aqueous phases of clouds and particles

An isoprene-derived epoxidiol (IEPOX) has been shown to form methyltetrols and C_5-alkene triols in the aqueous phase of particles and droplets by hydrolysis, organosulfates by reaction with sulfate or bisulfate ions and oligomers [*Surratt et al.*, 2010]. An hydroxyhydroperoxide (ISHP) is formed from the oxidation of isoprene under low-NO_x conditions, which can lead after further reaction to IEPOX. According to *Surratt et al.* [2010], IEPOX is formed with molar yields between 52% and 87% [*Paulot et al.*, 2010]. The following reaction is added to RACM2 with a IEPOX yield that is in the range reported above :

$$\mathrm{ISHP + HO \Rightarrow 0.69\ IEPOX + 0.28\ BiPER + 0.03\ BiDER} \quad \text{(R 5.3)}$$

BiDER and BiPER are two surrogate compounds used by *Couvidat and Seigneur* [2011] to account for SOA formation under dry conditions. Methyltetrol formation is taken into account via the following reaction, which may occur in cloud droplets and in the aqueous phase of particles :

$$\mathrm{IEPOX_p + H^+ \Rightarrow BiMT} \quad \text{(R 5.4)}$$

BiMT is a surrogate compound for methyltetrols and other compounds formed from the hydrolysis of IEPOX (such as C_5-alkene triols) and $IEPOX_p$ is IEPOX present in the particle. The kinetic rate of the hydrolysis of 3-methyl-3,4-epoxy-1,2-butanediol (one of the possible isomers of IEPOX) is used for reaction R5.4 and is equal to 0.05 M^{-1}.s^{-1} [*Eddingsaas et al.*, 2010]. However, this reaction can be much lower in the case of the hydrolysis of 2-methyl-3,4-epoxy-1,2-butanediol (0.002 M^{-1}.s^{-1} [*Eddingsaas et al.*, 2010]).

IEPOX can also react with sulfate ions (SO_4^{2-}) and bisulfate ions (HSO_4^-) to form sulfate esters [*Darer et al.*, 2011; *Eddingsaas et al.*, 2010]. Accordingly, the following reactions are added to take into account organosulfate formation :

$$\mathrm{IEPOX_p + SO_4^{2-} \Rightarrow BiSULF} \quad \text{(R 5.5)}$$

$$\mathrm{IEPOX_p + HSO_4^- \Rightarrow BiSULF} \quad \text{(R 5.6)}$$

BiSULF is the surrogate compound for sulfate ester formation (which is assumed non-volatile). Kinetic rates for reactions R5.5 and R5.6 are respectively 2.0$\times$10^{-4} and 7.3$\times$10^{-4} M^{-1}.s^{-1} [*Eddingsaas et al.*, 2010].

Finally, IEPOX can also react with nitrate ions NO_3^- to form organonitrates. However,

according to *Darer et al.* [2011], the organonitrate formed from the reaction of 3-methyl-3,4-epoxy-1,2-butanediol with NO_3^- leads to the formation of a ternary organonitrate, which will be quickly hydrolyzed (lifetime around 0.67 hr in the aqueous phase) to form methyltetrols. We assume that, when NO_3^- reacts with IEPOX, the organonitrate formed is quickly hydrolyzed and forms immediately methyltetrols :

$$\mathrm{IEPOX_p} + \mathrm{NO_3^-} \Rightarrow \mathrm{BiMT} + \mathrm{HNO_3} \qquad (\mathrm{R}\,5.7)$$

The kinetic rate for reaction R5.7 is taken to be 2.0×10^{-4} $\mathrm{M^{-1}.s^{-1}}$ [*Eddingsaas et al.*, 2010]. However, the Henry's law constant of IEPOX is unknown. *Eddingsaas et al.* [2010] estimated with the EPA's HENRYWIN program [*Meylan and Howard*, 2000] two very different values of the Henry's law constant of IEPOX (2.7×10^6 $\mathrm{M.atm^{-1}}$ with the bond contribution method and 2.9×10^{10} $\mathrm{M.atm^{-1}}$ with the group contribution method). Because of the high uncertainty in the value of the Henry's law constant of IEPOX, we studied the formation of methyltetrols and organosulfates for two different values of the Henry's law constant of IEPOX : 2.0×10^6 $\mathrm{M.atm^{-1}}$ (approximately the lower estimated value by *Eddingsaas et al.* [2010], the second value being very high it would lead to a very high unrealistic value of SOA) and 2.0×10^7 $\mathrm{M.atm^{-1}}$ (an increased value to take into account the high uncertainty in this parameter and to test the sensitivity to this parameter).

5.2.4 In-cloud aging of semi-volatile organic compounds

To evaluate the in-cloud aging of semi-volatile organic compounds (SVOC), a simple mechanism is developped with a single oxidation step, based on typical aqueous-phase reactions. Reactions leading to the formation of aged species and their properties are presented in the supplementary information.

Organonitrates are assumed to be hydrolyzed quickly and nitrate groups are replaced by hydroxyl groups and the formed compounds can then react with HO. SVOC are oxidized by HO with an assumed kinetic rate parameter of 2.0×10^9 $\mathrm{M^{-1}.s^{-1}}$ (which is the order of magnitude of the kinetics of oxidation of SVOC by HO based on the method of *Monod and Doussin* [2008]). If an aldehyde group is present, this group is transformed into a carboxylic acid [*Tilgner and Herrmann*, 2010]. If there is no aldehyde group, H abstraction on an alkyl group or on a hydroxyl group is assumed. Using the structure-activity relationships of *Monod and Doussin* [2008], we determined for each surrogate if H abstraction is more probable on an alkyl group or on a hydroxyl group. If H abstraction happens on a hydroxyl group, the group is replaced by a carbonyl group. If H abstraction happens on an alkyl group, the group is replaced by a hydroperoxyl group (as in the gas-phase oxidation of alkanes under low-$\mathrm{NO_x}$ conditions).

To compute the partitioning of aged species, the saturation vapor pressure or the Henry's law constant must be known. The effect of the addition or substitution of a group on the saturation vapor pressure is estimated with the method of *Pankow and Asher* [2008]. Following *Couvidat and Seigneur* [2011], the Henry's law constant is estimated from the saturation vapor pressure by computing the activity coefficient at infinite dilution with the thermodynamic model UNIFAC (UNIversal Functional group Activity Coefficient [*Fredenslund et al.*, 1975]). We used this method because the effect of some groups (like the nitrate group) on Henry's law are not available in most structure activity relationships. Moreover, the saturation vapor pressure of surrogate compounds are fitted to reproduce experiments. The saturation vapor pressure is not the one of the molecule from which we used the structure as surrogate. By using the activity coefficients at infinite dilution, it is then possible to estimate the Henry's law constants of the surrogate rather than estimating the Henry's law constant of the real molecule. If an aldehyde is

formed by H abstraction from a hydroxyl group, the effective partitioning constant of *Pun and Seigneur* [2007] for aldehydes is used to take into account possible oligomerization at low pH.

For example, in the case of the aging of the H^2O species BiNIT3 and BiMT (organitrates formed respectively from the oxidation of monoterpenes and isoprene), these two compounds will produce the same compound named AqMT. The nitrate groups of BiNIT3 are replaced by hydroxyl groups (which will give a methyl-tetrol BiMT) and, after reaction with HO, one of the hydroxyl group is transformed into an aldehyde to form AqMT with the trihydroxy-3-methylbutanal. Based on its structure, AqMT should be very hydrophylic and non-volatile if oligomerization is assumed.

5.2.5 Wet deposition of water-soluble organic compounds

All simulations include the in-cloud scavenging (necessary to compute concentrations of absorbed species in the aqueous phase of clouds and evaluate kinetic rates of reactions) of gaseous precursors (glyoxal, methylglyoxal, ethanol, acetic acid, MACR and MVK) and SVOC. For SVOC, only below-cloud scavenging of aerosols is taken into account in the air quality model and gas-phase SVOC are not deposited. In a sensitivity simulation, below-cloud savenging of gases (including the scavenging of SVOC) is added to investigate the impact of wet deposition on organic aerosol formation.

Based on Henry's law constants estimated from the chemical structure of SOA surrogate species, most surrogate species have a Henry's law constant greater than 1.0×10^5 M.atm^{-1} and can be scavenged efficiently. Even though some of these compounds are considered to be hydrophobic and can not be absorbed into the aqueous phase of particles, they can at least be partially absorbed by the aqueous phase of clouds (because the liquid water content of cloud is much greater). Primary SVOC compounds were assumed to have insufficient affinity for water to be absorbed like an alkane (the Henry's law constant of nonadecane is equal to 0.34 M/atm[*Yaws and Yang*, 1992]). However, primary SVOC compounds in the gas phase can be oxidized and should form compounds with a higher affinity for water. A Henry's law constant of 3000 M.atm^{-1} is used for these compounds to take into account the fact that they may be absorbed by an aqueous phase. Henry's law constants of surrogate compounds are presented in the supplementary information.

5.3 Results

A summer period was studied to favor the formation of large amounts of glyoxal, methylglyoxal, MACR, MVK and IEPOX, which are oxidation products of isoprene. SOA formation is simulated from July 15$^{\text{th}}$ to August 14$^{\text{th}}$, 2002 over Europe (i.e., period simulated by *Couvidat et al.* [2012a]). Input data to Polair3D/Polyphemus and the simulation domain (horizontal resolution of 0.5 degree with 9 vertical levels extending from the surface to 12000 m altitude) are the same as in *Couvidat et al.* [2012a]. Meteorology was obtained from the European Centre for Medium-Range Weather Forecasts (ECMWF) model, which gives an average precipitation rate over the simulated period of 0.082 mm/h against 0.090 mm/h for the one-year period simulated by *Couvidat et al.* [2012a]. The simulated period is therefore characterized by typical wet deposition rates. A map of the pH of the aqueous phase of particles and the vertical profiles of studied SOA concentrations are available in the supplementary information.

5.3.1 Formation of oxalic, glyoxylic and pyruvic acids

When pyruvic, glyoxylic and oxalic acids are assumed to be semi-volatile, pyruvic and glyoxylic acids do not form significant concentrations of SOA and only a small fraction of oxalic acid

condenses on the particle phase. The fraction of oxalic acid in the particle phase is shown in 5.1. Even if the fraction of oxalic acid is significant in some regions (15% to 64% of the oxalic acid in the particle phase), there is almost no oxalic acid in the particle phase over most of Europe because the pH of the aqueous phase is too low (areas with mean pH lower than 2.5). The fraction of oxalic acid in the particle phase modeled here is significantly lower than the value of 90 % found by *Limbeck et al.* [2001] over the South African savanna ; no data were found over Europe. The low fraction of oxalic acid modeled may be due to an underestimation of the pH or to the missing formation of oxalate complexes. Simulated surface concentrations of oxalic acid over Europe are shown in 5.2 along with concentrations of oxalic acid when it is assumed to be non-volatile and the sum of concentrations of pyruvic, glyoxylic and oxalic acids when assumed to be non-volatile. When those acids are assumed to be non-volatile, mean surface concentrations over most of Europe range from 10 to 50 ng.m^{-3} with maximum daily concentrations which can be locally greater than 100 ng.m^{-3} (190 ng.m^{-3} at most). Therefore, the contribution of those three acids to organic aerosol surface concentrations are at most a few percent. However, concentrations between 800 and 1500 m altitude of the non-volatile acids increase by 14% (mean concentrations of 33 ng.m^{-3} against 24 ng.m^{-3} at the surface), thereby reflecting greater concentrations near clouds.

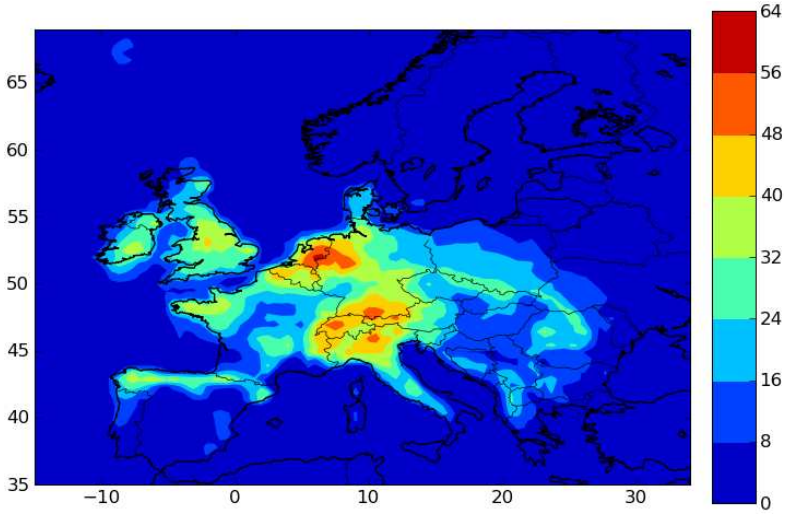

FIGURE 5.1 – Fraction of oxalic acid in the particle phase (in %) at ground level over Europe when absorption by an aqueous phase with dissociation of acids is assumed.

5.3.2 Formation of SOA via in-cloud oxidation of MACR and MVK

Very low concentrations of aerosols formed from the aqueous-phase oxidation of MACR and MVK are simulated, since the total (gas + particle) concentrations of semi-volatile products are less than 1 ng.m^{-3}. This is due to the low Henry's law constants of these two compounds. However, according to *van Pinxteren et al.* [2005], concentrations in clouds can be higher than predicted by the Henry's law by a factor 200 for MACR and 100 for MVK. Similar discrepancies have been observed for acetaldehyde partitioning in cloud droplets with deviations from Henry's law equilibrium by factors of 10 to 500[*Seigneur and Wegrecki*, 1990]. Simulations conducted with Henry's law constants multiplied by 200 and 100 for MACR and MVK, respectively, lead to temporal mean surface concentrations of organic aerosols formed via aqueous oxidation of MACR

Concentrations of semi-volatile oxalic acid in particles (only dissociation in the aqueous phase is treated)

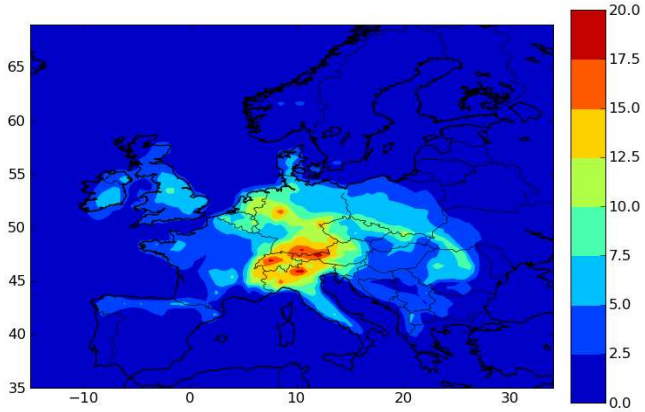

Concentrations of non-volatile oxalic acid

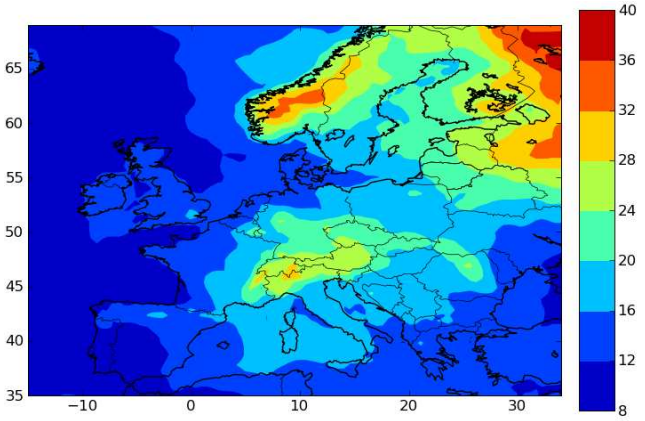

Sum of concentrations of non-volatile pyruvic, glyoxylic and oxalic acids

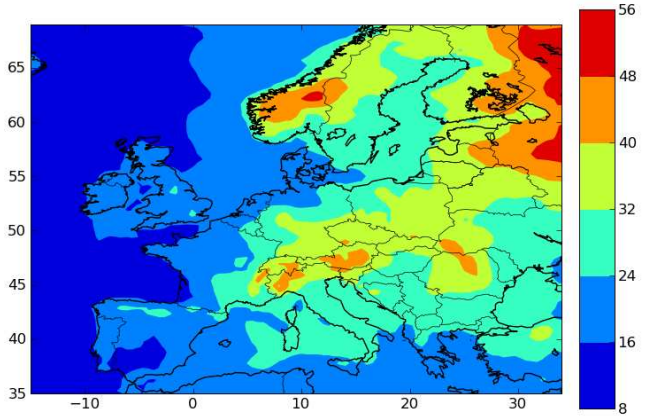

FIGURE 5.2 – Simulated surface concentrations of acids in the particle phase (in ng.m^{-3}) produced from in-cloud glyoxal and methyl glyoxal oxydation averaged from July 15 to August 14, 2002.

and MVK between 0.8 and 6.4 ng.m^{-3} with daily concentrations up to 64 ng.m^{-3}. However, total (gas + particle) daily concentrations are up to 280 ng.m^{-3} in northern Europe, due to high concentrations of SVOC from aqueous oxidation of MACR and MVK. These SVOC remain in the gas phase in this region because of low concentrations of particles on which SVOC can condense. On average, modeled concentrations in the particles between 800 and 1500 m altitude are twice higher than surface concentrations. Therefore, it could be possible that MACR and MVK could form significant amount of SOA in some regions of the world, where concentrations of MACR and MVK are important and cloudy meteorological conditions occur. Concentrations and the partitioning of MACR and MVK in clouds should be investigated further to determine why concentrations of these compounds are higher than predicted by equilibrium and to assess whether these compounds can form significant amount of SOA via oxidation in the aqueous phase.

5.3.3 Aqueous-phase chemistry of IEPOX

Concentrations of the surrogate species BiMT and BiSULF are shown in 5.3 for the two values of the Henry's law constant of IEPOX. Changing the Henry's law constant of IEPOX does not affect the geographic repartition of BiMT and BiSULF but affects significantly the amount of aerosol formed. Increasing the Henry's law constant of IEPOX by a factor of 10 leads to concentrations of BiMT and BiSULF that are 5 times higher. With a Henry's law constant of 2×10^6 M.atm^{-1}, temporal mean concentrations range from 2 to 200 ng.m^{-3} for BiMT and from 0.1 to 20 ng.m^{-3} for BiSULF. With a Henry's law constant of 2×10^7 M.atm^{-1}, temporal mean concentrations range from 10 to 900 ng.m^{-3} for BiMT and from 1 to 100 ng.m^{-3} for BiSULF. Therefore, BiMT and BiSULF display strong spatial variations.

Modeled concentrations of BiMT are compared to several measurements reported over Europe in summer to determine whether the modeling results are consistent with reported measurements. Concentrations of modeled BiMT and reported measurements of methyltetrols and alkene-triols are presented in 5.1. BiMT is the surrogate for all SOA formed by the hydrolysis of IEPOX, therefore, it should be compared with the sum of alkene-triols and methyltetrols. The median concentrations of BiMT (interpolated at the locations of the measurements) with a Henry's law constant of 2×10^7 M.atm^{-1} are commensurate with the measurements. The model shows some very high maximal daily concentrations (up to 1700 ng.m^{-3} at K-puszta, Hungary), whereas the maximal measurement obtained at K-puszta is 119 ng.m^{-3}. However, the maximal concentration of BiMT at K-puszta (see temporal profile in supplementary information) corresponds to a very strong one-day peak, whereas most of the values are within the range of the measurements. The modeled concentrations can be very high in some areas such as North Africa and southeastern Europe (see 5.3) where the pH of the aqueous phase (lower than 2) is very low and where the sulfate aerosol is not fully neutralized by ammonium. This result is consistent with the results of *Froyd et al.* [2010] who found very high contentrations of SOA formed from IEPOX in Atlanta, USA (910 ng.m^{-3}), due to a very acidic aerosol. Temporal mean concentrations of modeled BiSULF were found to represent 12 to 28 % of total SOA formed from IEPOX, which is consistent with the range of 17 to 37 % reported for the southeastern United States[*Chan et al.*, 2010b].

5.3.4 In-cloud aging of semi-volatile compounds

In-cloud aging was found to significantly increase OM concentrations by transforming SVOC into less volatile compounds. The temporal mean increase shown in 5.4 ranges from 0.15 μg.m^{-3} to 1.0 μg.m^{-3}, suggesting that clouds could contribute significantly to the aging of SOA. However, the modeled increase in organic matter (OM) due to in-cloud aging could be overestimated

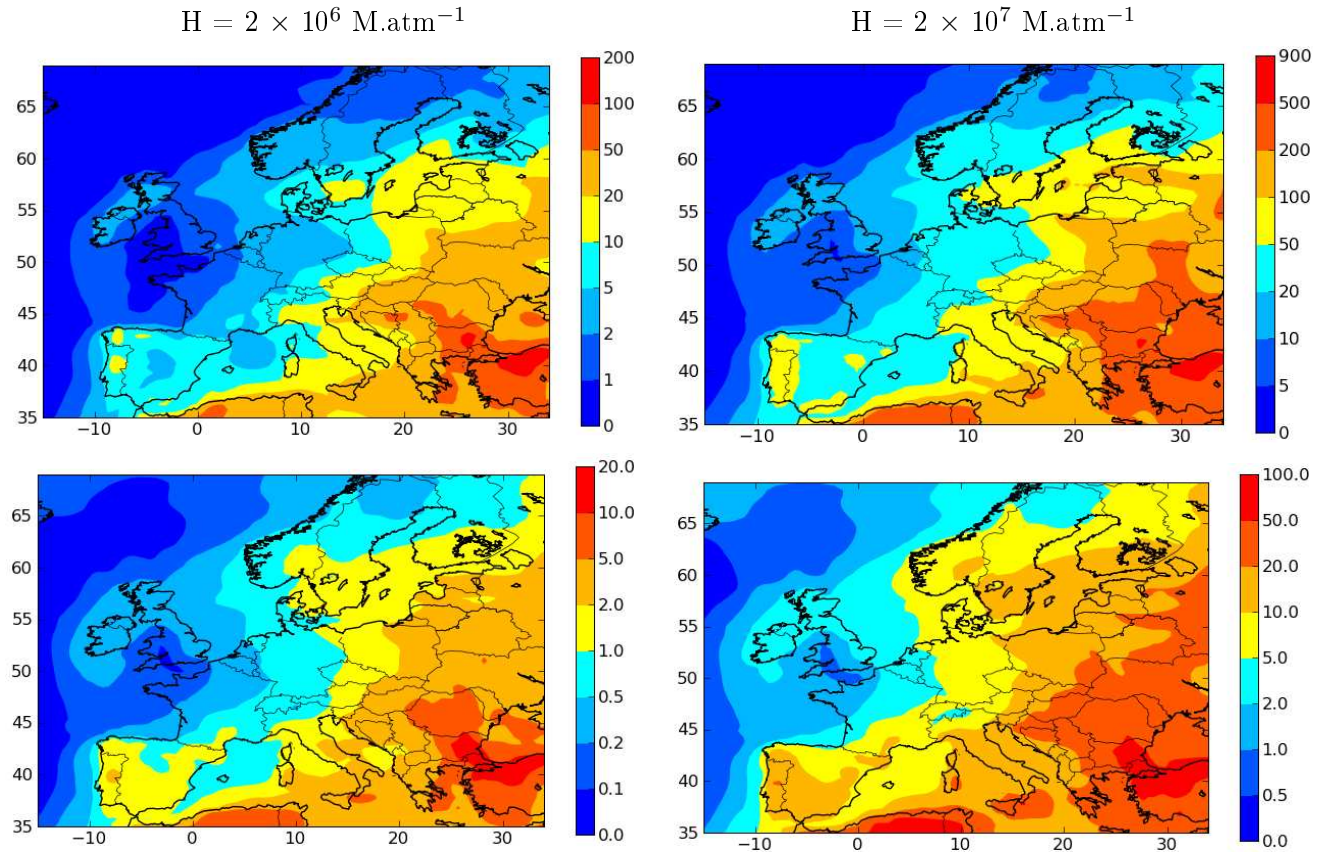

FIGURE 5.3 – Simulated surface concentrations of BiMT (top) and BiSULF (bottom) in ng.m^{-3} from July 15 to August 14, 2002 for two values of the Henry's law constant of IEPOX : H = 2 × 10^6 M.atm^{-1} (left) and H = 2 × 10^7 M.atm^{-1} (right).

TABLE 5.1 – Surface concentrations (in ng.m^{-3}) of modeled BiMT with the Henry's law of IEPOX values of 2× 10^6 M.atm^{-1} and 2× 10^7 M.atm^{-1} compared to surface measurements of the sum of methyltetrols and alkene triols.

	Measurements (methyltetrols + alkene triols)		Model with H = 2× 10^6 M.atm^{-1}		Model w 2× 10^7 M
Location	Median	Range	Median	Range	Median
Jülich, Germany 16-22 Jul. 2003 *Kourtchev et al.* [2008a]	18.2	6.2-28.2	1.6	0.1-17	14
K-puszta, Hungary* 4 Jun.-10 Jul. 2003 *Ion et al.* [2005]	>29	>1.8-119	6.5	0.5-414	49
Hyytiälä, Finland 24 Jul. -6 Aug. 2004 *Kourtchev et al.* [2008b]	17.2	0.46-33.3	2.1	0.1-156	18

(*) C5-alkene-triols were not measured, therefore, the measurements represent only a fraction of the amount of SOA from IEPOX.

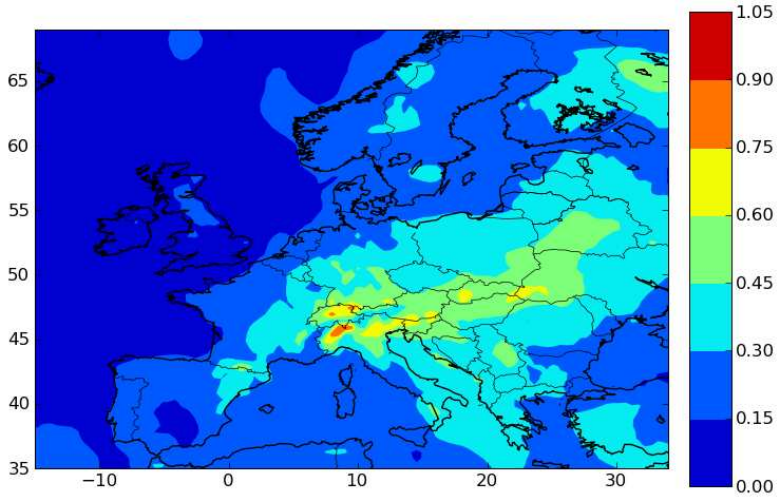

FIGURE 5.4 – Increase in OM concentrations (in μg.m^{-3}) from July 15 to August 14, 2002 due to in-cloud aging of SVOC.

because in-cloud aging was assumed to only produce less volatile compounds. Nevertheless, the model predicts that a significant fraction of OM at the surface (10% to 30% over most of Europe) and aloft (20% to 40% between 800 and 1500 m altitude over most of Europe) has been aged in clouds. Thus, clouds may strongly impact SOA by changing the volatility of the compounds and its chemical composition. Aging of SVOC in clouds should be studied more extensively to confirm these results. However, the model does not include a complete aging mechanism in the gas phase. With a complete gas-phase aging mechanism, SOA would be less volatile and, therefore, adding an aqueous-phase mechanism would have a lesser impact (because SOA would already be less volatile). In that case, the increase in OM due to the decrease of volatility by aqueous-phase aging would be less important.

5.3.5 Impact of wet deposition on organic aerosol concentrations

To study the impact of wet deposition (in-cloud and below-cloud scavenging) on organic aerosol concentrations, the results of three simulations are compared : (1) without wet deposition, (2) with wet deposition but without below-cloud scavenging of gaseous precursors of SOA and of the gas-phase fraction of SVOC, which is typically not taken into account in models, and (3) with all the wet deposition processes. As shown in 5.5, organic aerosol concentrations from July 15 to August 14, 2002 are decreased by 20% to 60% due to wet deposition. Below-cloud scavenging of gases alone accounts for a decrease from 3 to 15% (a decrease up to 0.7 μg.m^{-3}). *Bessagnet et al.* [2010] have suggested that organic aerosol concentrations could be overestimated by as much as 50% over Europe because dry deposition of SVOC is typically not treated in models. According to our results, monthly organic aerosol concentrations could be overestimated by a factor of 2 if wet deposition of organic aerosols is not taken into account and by up to 18% if only the below-cloud scavenging of gaseous precursors and SVOC is not included. Therefore, both wet and dry deposition could have a significant effect on OM concentrations.

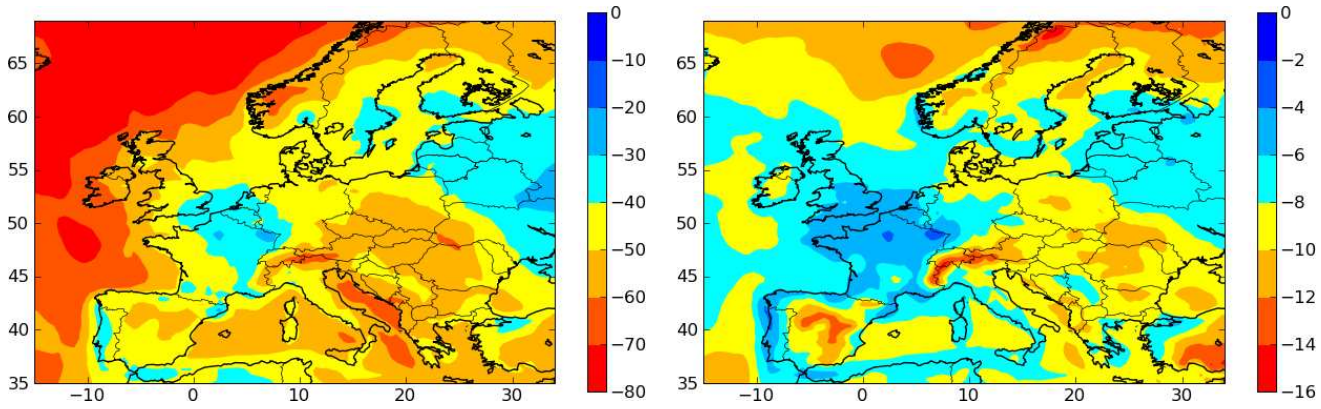

FIGURE 5.5 – Decrease of organic aerosol concentrations (in %) from July 15 to August 14, 2002 due to wet deposition (left) and due to the below-cloud scavenging of gases including the gas-phase fraction of SVOC (right).

5.4 Discussion

Modeling cloud processing of organic compounds suggests that some aqueous-phase processes may lead to significant SOA formation and should, therefore, be included in air quality models for PM. Among the processes considered here, chemical aging of SOA in cloud droplets was the largest contributor to additional SOA formation with increases in the range of 0.15 to 1 μg.m^{-3} and a significant fraction of the organic aerosol has been aged. This result is similar to the results of *Chen et al.* [2007] who found on average an increase of 9% with an in-cloud aging mechanism over eastern united states over a few days. Next, the aqueous-phase chemistry of IEPOX was found to lead to increases of 10 to 50 ng.m^{-3} SOA on average, but could lead to increases in excess of 1 μg.m^{-3} in areas with acidic sulfate aerosols. The in-cloud formation of glyoxylic, pyruvic and oxalic acids could lead to SOA increases in the range of 16 to 56 ng.m^{-3}, but only if their partitioning is strongly displaced toward the particulate phase. The aqueous chemistry of MACR and MVK did not lead to large increases in SOA concentrations, but there is still large uncertainty concerning their gas/droplet partitioning.

Major areas of uncertainties that should be investigated via experiments include the atmospheric partitioning of IEPOX, MACR and MVK and the particle chemistry of oxalic acid. Also, the processes leading to SOA aging in droplets should be studied in the laboratory so that more realistic in-cloud aging mechanisms of key SOA compounds can be developped. Comparisons between models and measurements of some key components should be done to evaluate models of aqueous-phase chemistry and to give insights on SOA formation form aqueous-phase reactions.

Wet deposition (including in-cloud and below cloud scavenging of gas-phase and particle-phase SVOC and of major gaseous precursors) influences greatly OM concentrations. Over Europe, from July 15 to August 15 2002, not taking into account wet deposition leads to OM concentrations and should be treated in air quality models.

Introducing all theses processes in the model leads to an increase in computation time of a factor 2-3, which is mainly due to the significant increase in the number of organic aerosol species (from 21 to 36) that are treated in H^{2}O.

5.5 Supplementary materials

5.5.1 SOA species of H^2O

TABLE 5.2 – Name and structure of the different surrogate SOA species of the H^2O model as used in previous studies.

Species	Precursor	Type[a]	Molecular structure
BiMT	Isoprene	Hydrophilic	methyl tetrol
BiPER		Hydrophilic	methyl dihydroxy dihydroperoxide
BiDER		Hydrophilic	methyl tetrol
BiMGA		Hydrophilic	methyl glyceric acid (MGA)
BiNGA		Hydrophobic	nitrate derivative of MGA
BiNIT3		Hydrophobic	methyl hydroxy trinitrate butane
BiA0D	Monoterpenes	Hydrophilic	pinonaldehyde
BiA1D		Hydrophilic	norpinic acid
BiA2D		Hydrophilic	pinic acid
BiNIT		Hydrophobic	Nitrooxy-limonene-1-ol
BiBlP	Sesquiterpenes	Hydrophobic	C15 hydroxy nitrate aldehyde
BiBmP		Hydrophobic	C15 oxo aldehyde
AnBlP	Aromatics	Hydrophobic	methyl nitro benzoic acid
AnBmP		Hydrophobic	methyl hydroxy benzoic acid
AnClP		Hydrophobic	No structure

5.5.2 Reactions for in-cloud SOA aging

$$\text{BiA0D} + \text{HO} \Rightarrow \text{BiA1D} \quad \text{(R 5.8)}$$

$$\text{BiA1D} + \text{HO} \Rightarrow \text{AqA1D} \quad \text{(R 5.9)}$$

$$\text{BiA2D} + \text{HO} \Rightarrow \text{AqA2D} \quad \text{(R 5.10)}$$

$$\text{BiNIT} + \text{HO} \Rightarrow \text{AqNIT} \quad \text{(R 5.11)}$$

$$\text{BiPER} + \text{HO} \Rightarrow \text{AqPER} \quad \text{(R 5.12)}$$

$$\text{BiDER} + \text{HO} \Rightarrow \text{AqMT} \quad \text{(R 5.13)}$$

$$\text{BiMT} + \text{HO} \Rightarrow \text{AqMT} \quad \text{(R 5.14)}$$

$$\text{BiNIT3} + \text{HO} \Rightarrow \text{AqMT} \quad \text{(R 5.15)}$$

$$\text{BiMGA} + \text{HO} \Rightarrow \text{AqMGA} \quad \text{(R 5.16)}$$

$$\text{BiNGA} + \text{HO} \Rightarrow \text{AqNGA} \quad \text{(R 5.17)}$$

$$\text{BiBlP} + \text{HO} \Rightarrow \text{AqBlP} \quad \text{(R 5.18)}$$

$$\text{BiBmP} + \text{HO} \Rightarrow \text{AqBmP} \quad \text{(R 5.19)}$$

$$\text{SOAlP} + \text{HO} \Rightarrow \text{AqlP} \quad \text{(R 5.20)}$$

$$\text{SOAmP} + \text{HO} \Rightarrow \text{AqmP} \quad \text{(R 5.21)}$$

$$\text{SOAhP} + \text{HO} \Rightarrow \text{AqhP} \quad \text{(R 5.22)}$$

5.5.3 Parameters for partitioning of aged species and for wet deposition

TABLE 5.3 – Parameters of aged species used to compute their partitioning.

Surrogate	Type[a]	M[b]	Psat[c]	H[d]	Comments
AqA2D	A	218	4.97×10^{-10}	1.00×10^{11}	Diacid (pK_{a1} = 3.4, pK_{a2} = 5.1)
AqA1D	A	202	7.50×10^{-10}	5.46×10^{10}	Monoacid (pK_a = 3.2)
AqNIT	A	208	8.70×10^{-9}	2.56×10^{7}	-
AqPER	A	167	2.17×10^{-5}	3.26×10^{7}	Oligomerization[e]
AqMT	A	135	1.08×10^{-5}	1.04×10^{10}	Oligomerization[e]
AqMGA	A	119	1.04×10^{-4}	1.25×10^{8}	Oligomerization[e]
AqBlP	B	315	3.72×10^{-12}	4.12×10^{10}	-
AqBmP	B	253	1.86×10^{-9}	8.54×10^{7}	-
AqlP	C	424	-	8.4×10^{5}	Non-volatile
AqmP	C	424	-	8.4×10^{5}	Non-volatile
AqhP	C	424	-	8.4×10^{5}	Non-volatile

a) Type A : hydrophilic species, type B : hydrophobic species, type C : hydrophobic non-volatile species, which is not used to compute activity coefficients
b) Molecular weight [$g.mol^{-1}$]
c) Henry's law constant [M/atm] at 298K
d) Saturation vapor pressure [torr] at 298K
e) Oligomerization follows Pun and Seigneur (2007)

TABLE 5.4 – Effective Henry's law constants of RACM2 and H^2O species for in-cloud and below-cloud scavenging for a pH of 5.6.

Surrogate	H[a]
GLY	8.45×10^5
MGLY	3710
ORA2	4.39×10^4
ACD	11.4
EOH	190
IEPOX	2.0×10^7
OXACD	1.82×10^{12}
GLACD	2.37×10^6
PYACD	5.0×10^8
BiMT	3.3×10^{10}
BiPER	8.09×10^9
BiDER	8.91×10^{10}
BiMGA	2.15×10^{10}
BiNGA	2.71×10^9
BiNIT3	4.75×10^6
BiA0D	3.12×10^6
BiA1D	1.76×10^{10}
BiA2D	2.7×10^{11}
BiNIT	7.66×10^4
BiBlP	1.47×10^8
BiBmP	3.05×10^5
SOAlP	3000
SOAmP	3000
SOAhP	3000
AqA2D	1.00×10^{11}
AqA1D	5.46×10^{10}
AqNIT	2.56×10^7
AqPER	3.26×10^7
AqMT	1.04×10^{10}
AqMGA	1.04×10^{-4}
AqBlP	4.12×10^{10}
AqBmP	8.54×10^7
AqlP	8.4×10^5
AqmP	8.4×10^5
AqhP	8.4×10^5

a) Henry's law constant [M/atm] at 298K

5.6 Map of the pH

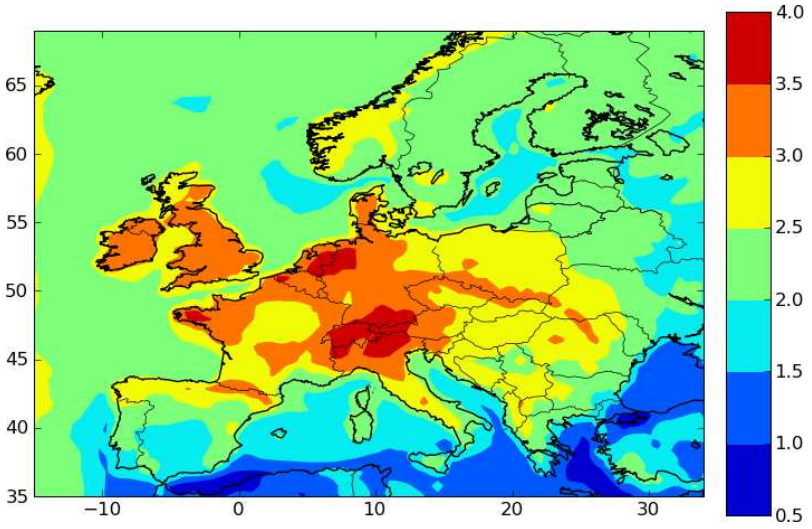

FIGURE 5.6 – Mean pH in the aqueous-phase of particles computed with ISORROPIA.

5.7 Vertical profiles

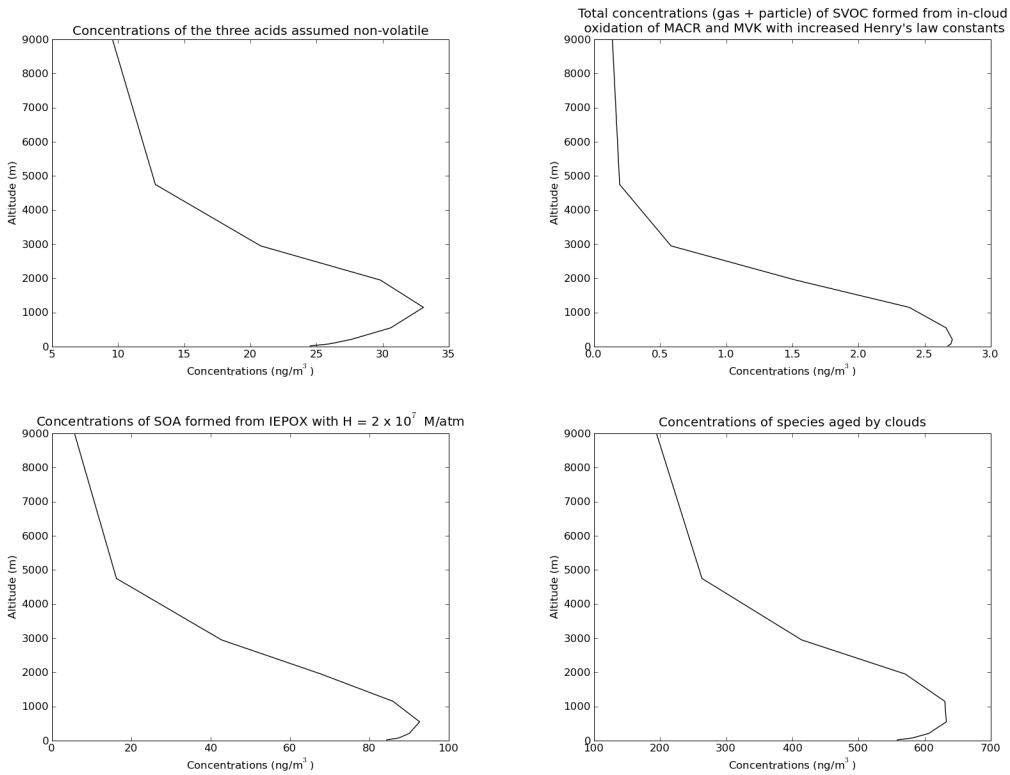

FIGURE 5.7 – Vertical profiles of simulated SOA from aqueous-phase reactions.

5.8 Temporal profile of BiMT

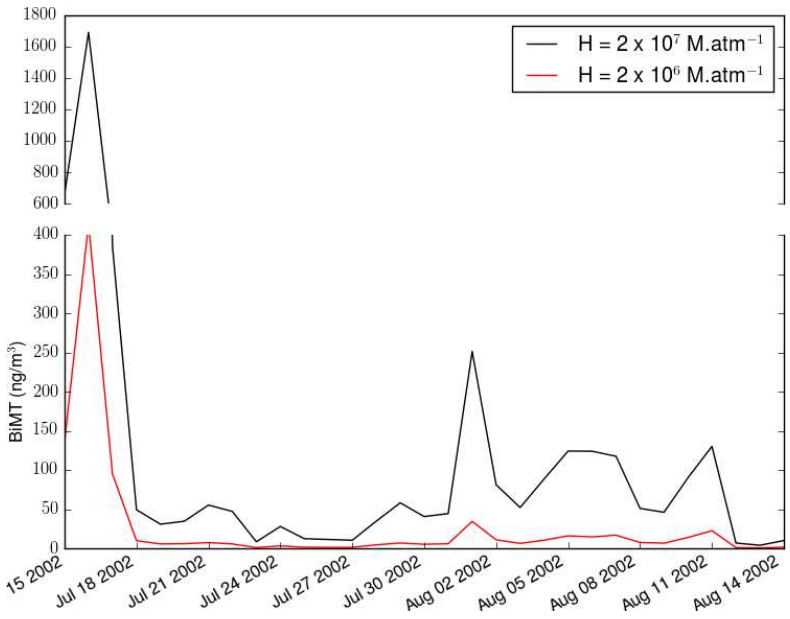

FIGURE 5.8 – Simulated surface concentration of BiMT (in ng.m^{-3}) at K-puszta, Hungary, from July 15 to August 14, 2002 for two values of the Henry's law constant of IEPOX.

Chapitre 6

Conclusions et perspectives

6.1 Conclusions

Le but de cette thèse était d'affiner la modélisation des aérosols organiques dans l'atmosphère afin d'améliorer la simulation des particules dans les modèles de qualité de l'air. Dans cette étude, quatre points principaux ont été abordés : la modélisation de la formation des aérosols obtenus par oxydation de l'isoprène, la modélisation des aérosols organiques par un modèle de qualité de l'air dans l'atmosphère à l'échelle continentale, puis à l'échelle régionale en simulant les aérosols sur une zone urbaine (Paris en juillet 2009 durant la campagne été de MEGAPOLI) pour étudier la formation locale d'aérosols et enfin la modélisation des aérosols formés dans la phase aqueuse des nuages et des particules.

Dans un premier temps, un modèle de formation d'aérosols organiques par oxydation de l'isoprène a été développé en tenant compte des différents régimes d'oxydation possibles (oxydation par les radicaux nitrates, oxydation par les radicaux hydroxyles en régime bas-NO_x et en régime haut-NO_x). Une approche utilisant des composés suppléants a été utilisée. À ces composés suppléants sont attachés une structure moléculaire qui permet par exemple d'estimer les propriétés hydrophiles des aérosols. En extrapolant ainsi la formation d'aérosols organiques en conditions sèches aux conditions humides, on a trouvé que les aérosols organiques venant de l'oxydation de l'isoprène pouvait être très hydrophiles en régime bas-NO_x et que les composés formés pouvait être absorbés par la phase aqueuse des particules plutôt que par la phase organique.

Ensuite, cette paramétrisation a été ajoutée au modèle de qualité de l'air Polyphemus. D'autres changements ont aussi été effectués au modèle d'éarosols organiques afin de refléter l'état de la science. Les aérosols organiques ont été simulés sur l'Europe de juillet 2002 à juin 2003 et les résultats du modèle ont été comparés aux mesures effectuées à douze stations EMEP. On a considéré que des émissions de composés organiques semi-volatils (COSV) présents dans la phase gazeuse sont manquantes des inventaires d'émissions et que les aérosols organiques primaires ne sont pas non-volatils. Dans ce cas, il faut corriger les émissions de composés supposés non-volatils données par les inventaires, en émissions de plusieurs composés organiques avec différentes volatilités (ces composés formeront plus ou moins d'aérosols selon les quantités d'aérosols organiques sur lesquelles ces composés peuvent se condenser). Les émissions de COSV ont été estimées à partir des émissions d'inventaire d'aérosols organiques primaires (EI-AOP) en utilisant un facteur COSV/EI-AOP. Avec un facteur égal à 5, les performances du modèle sont grandement améliorées en hiver (où il y avait une très forte sous-estimation des concentrations d'aérosols organiques) mais aussi en été. Ces COSV peuvent en effet se condenser sur la particule organique si la température est faible (les composés deviennent moins volatils quand la température diminue), d'où l'augmentation des concentrations en hiver, et peuvent aussi former des composés moins volatils après oxydation. En hiver, d'après le modèle, l'aérosol organique est

majoritairement constitué de COSV primaires et de leurs produits d'oxydation. En été, l'aérosol organique est majoritairement constitué des produits d'oxydation des COSV primaires (ce qui montre l'importance du vieillissement pour la formation d'aérosols) et des aérosols formés par oxydation des monoterpènes.

Les aérosols organiques ont ensuite été simulés sur l'Île-de-France en juillet 2009 (période où s'est déroulée la campagne de mesures MEGAPOLI) pour étudier la formation d'aérosols organiques en zone urbaine. Les résultats ont été comparés aux mesures effectuées à deux stations : le SIRTA en banlieue de Paris et le LHVP à l'intérieur de Paris. Le modèle donne de très bons résultats au SIRTA et est capable de bien estimer la contribution régionale en aérosols organiques. D'après le modèle entre 30 et 40% de l'aérosol organique provient de la région Île-de-France, environ 30 % de l'aérosol organique provient de sources à l'extérieur du domaine de simulation (c'est à dire en dehors de l'Europe) et le reste (30 à 40%) provient du domaine de simulation hors Île-de-France. Le modèle donne aussi d'assez bons résultats au LHVP bien que deux problèmes soient identifiés. Tout d'abord, les mesures prédisent un pic le soir provenant des émissions dues à la cuisson des aliments, ce pic n'est pas prédit par le modèle car les émissions dues à la cuisson sont absentes de l'inventaire d'émissions utilisé. Il est donc nécessaire d'ajouter les émissions dues à la cuisson dans les futurs inventaires. Ensuite, le modèle simule un pic de concentrations d'aérosols dû aux émissions du trafic routier le matin durant les heures de pointe. Ce pic n'apparaît cependant pas dans les mesures. La présence de ce pic peut être due au fait que la volatilité des SVOC primaires est sous-estimée par le modèle, cela est possible vu que la volatilité des SVOC primaires émis par les moteurs diesel est estimée à partir de mesures réalisées à fortes concentrations d'aérosols organiques (supérieures à 30 μg.m^{-3}) alors que les concentrations sur Paris sont de l'ordre de quelques μg.m^{-3}. De plus, les interactions des aérosols organiques primaires avec les aérosols organiques secondaires ne sont pas prises en compte dans le calcul du partage des SVOC primaires (les coefficients d'activité ne sont pas calculés pour les SVOC primaires). En utilisant une spéciation pour les SVOC primaires avec un mécanisme simplifié d'oxydation de ces composés, une première tentative pour prendre en compte l'effet des coefficients d'activité a été réalisée. D'après cette étude, il semble que les SVOC primaires peu oxydés aient peu d'affinités avec des SVOC secondaires très oxydés. Dans ce cas, les SVOC primaires qui d'après le modèle se condensent sur la phase organique, pourraient en réalité ne pas se condenser dû aux faibles affinités des SVOC primaires peu oxydés avec une phase organique plus oxydée.

Enfin, l'impact de la chimie de la phase aqueuse et des dépôts humides sur la formation d'aérosols a été étudié. Il apparaît que la faible volatilité de l'acide oxalique, formé via réaction chimique dans la phase aqueuse des nuages, ne peut pas être expliquée simplement par l'absorption du composé dans la phase aqueuse des particules avec dissociation de l'acide. Le pH des particules est trop faible pour cela. La faible volatilité de l'acide oxalique peut cependant être expliquée par la formation de complexes dans la particule. Pour la formation d'aérosols organiques secondaires via l'oxydation de la méthacrolèine et de la méthyl-vinyl-cétone dans la phase aqueuse des nuages, le modèle ne donne pas de concentrations significatives d'aérosols à cause des faibles constantes de Henry de ces deux composés. Cependant, d'après des mesures réalisées dans les nuages, les concentrations de méthacrolèine et de méthyl-vinyl-cétone dépassent les concentrations calculées avec la loi de Henry de plusieurs ordres de grandeur. En augmentant les constantes de Henry de ces deux composés, les concentrations d'aérosols formés atteignent quelques ng.m^{-3}. Le partage de la méthacrolèine et de la méthyl-vinyl-cétone entre la phase gazeuse et la phase aqueuse des nuages doit être étudié plus en détails pour déterminer dans quelles mesures ces composés peuvent former des aérosols via oxydation dans le nuage. La formation d'aérosols via réaction dans la phase aqueuse des particules d'un époxydiol formé par oxydation de l'isoprène a été modélisée. Ce précurseur peut donner des concentrations très

importantes d'aérosols (supérieures à 1 $\mu g.m^{-3}$) dans certaines régions et pour certaines périodes correspondant à des situations où la phase aqueuse des aérosols est très acide et les concentrations de sulfate significative. La chimie aqueuse des époxydes pourrait donc former des concentrations importantes d'aérosols. Le vieillissement des COSV dans la phase aqueuse des nuages a été pris en compte avec un mécanisme simple. Une fraction importante des aérosols organiques au niveau du sol a été vieillie par un nuage (de 10 à 30%) et les nuages peuvent contribuer de manière significative aux concentrations d'aérosols. Enfin, l'influence des dépôts humides sur les concentrations d'aérosols organiques a été étudiée. De 20 à 60% de l'aérosol organique formé durant la période de simulation est déposé via les dépôts humides sur l'Europe. Les dépôts humides influencent grandement les concentrations organiques et les modèles doivent donc traiter correctement ce processus. Par exemple, ne pas prendre en compte le lessivage des composés organiques semi-volatils gazeux (qui n'est traditionnellement pas pris en compte dans les modèles) mène à une surestimation des concentrations de 3 to 17%.

Le modèle donne donc des résultats satisfaisants sur l'ensemble des études réalisées dans le cadre de cette thèse. L'importance des émissions manquantes de composés organiques semi-volatils anthropiques a été mise en évidence. Ces composés sont la principale source d'aérosols organiques en hiver et une source importante de composés secondaires en été. Cependant, il est possible que les concentrations de composés organiques primaires soient surestimées par le modèle du fait d'une possible sous-estimation de la volatilité des composés organiques primaires ou de l'importance des interactions entre composés primaires et secondaires. Le vieillissement de ce type de composés est aussi très important et il est probable que des erreurs soient liées au mécanisme de vieillissement relativement simple utilisé dans cette étude. Les composés biogéniques peuvent être une source importante d'aérosols en été (même en zone urbaine où une fraction significative de l'aérosol est d'origines régionale et biogénique) et peuvent former via des réactions en phase gazeuse ou en phase aqueuse des composés très hydrophiles comme dans le cas de l'isoprène dont la prise en compte des propriétés hydrophiles peut mener à de fortes augmentations des concentrations d'aérosols. La non-idéalité de l'aérosol est un phénoméne très complexe. L'absorption de certains composés peut être favorisée par la non-idéalité de l'aérosol tandis que l'absorption d'autres composés sera défavorisée. De manière générale, dans le modèle, prendre en compte la non-idéalité favorise la formation d'aérosols pour les composés hydrophiles mais pas pour les composés hydrophobes. Cependant, toute la complexité de l'aérosol organique n'est pas prise en compte comme la saturation des phases pouvant mener à de nouvelles phases, l'absorption des composés organiques entre plusieurs phases (et non absorption sur soit la phase organique soit la phase aqueuse), l'interaction entre composés organiques et composés inorganiques et la viscosité de la phase organique qui peut limiter le transfert des composés gazeux vers la particule ou, au contraire, la volatilisation de certains composés. Ces phénomènes pourraient en effet modifier nos connaissances des particules organiques.

6.2 Perspectives

Les perspectives de cette thèse peuvent être divisées en plusieurs axes de recherches pour améliorer la modélisation des aérosols organiques secondaires ; Chacun de ces axes de recherche est rattaché à un processus : les inventaires d'émissions, les mécanismes chimiques de formation d'aérosols organiques, le partage des composés entre phase gazeuse et phase particulaire, les dépôts, les conditions aux limites des simulations européennes.

6.2.1 Améliorer les inventaires d'émissions

La quantité d'aérosols formée est très sensible aux émissions utilisées, il est donc nécessaire de développer des inventaires détaillés et précis aussi bien pour les émissions anthropiques que pour les émissions naturelles.

Les émissions anthropiques :

Les inventaires d'émissions anthropiques supposent traditionnellement que les aérosols organiques primaires sont non-volatils. Dans cette thèse, les émissions de COSV ont été estimées en supposant que toutes les sources d'émissions avaient la même courbe de dilution (fraction de COSV dans la phase particulaire en fonction de la masse d'aérosol organique) et que le rapport COSV/EI-AOP est le même pour toutes les sources. Cependant, il est nécessaire de développer une méthodologie plus détaillée et des inventaires d'émissions de COSV plus précis pour bien représenter la formation d'aérosols organiques secondaires.

Il est nécessaire pour bien modéliser les aérosols organiques primaires de bien connaître le profil de dilution pour chacune des sources. Pour cela, il faut établir le profil de dilution pour chacune des principales sources d'émissions (trafic routier, maritime et aérien, feux de biomasse, cuisson des aliments). *Robinson et al.* [2007] ont estimé le profil de dilution pour les moteurs diesel, mais ce profil se base principalement sur des mesures à fortes concentrations d'aérosols organiques (supérieures à 30 μg.m^{-3}) alors qu'il est nécessaire d'avoir des données en conditions ambiantes (concentrations d'aérosols organiques représentatives de l'atmosphère, inférieures à 30 μg.m^{-3}) pour pouvoir bien estimer les concentrations d'aérosols organiques primaires dans l'atmosphère. Il est donc nécessaire d'établir des profils de dilution aussi bien à fortes concentrations qu'à faibles concentrations d'aérosols organiques, mais aussi à différentes températures pour bien représenter la formation d'aérosols organiques primaires sous différentes conditions.

Un rapport COSV/EI-AOP de 5 a été utilisé dans cette thèse pour l'Europe. Ce rapport correspond approximativement à des conditions ambiantes. Il peut être adapté pour les émissions de particules par le trafic routier en France qui sont dominées par les émissions des véhicules particuliers roulant au diesel et qui sont mesurées à des concentrations de masse d'organique correspondant à des conditions ambiantes. Ce rapport peut ne pas être adapté pour les facteurs d'émissions du trafic routier pour d'autres pays. Par exemple aux États-Unis, les émissions de particules sont dominées par les camions roulant au diesel (alors que les voitures roulent à l'essence). En utilisant un facteur de dilution de 100 pour mesurer les émissions, d'après *Robinson et al.* [2007], environ 60 % des particules devraient être dans la phase particulaire. Dans ce cas, le rapport COSV/EI-AOP pour les émissions du trafic devrait être d'environ 1,67. Comme les facteurs d'émissions d'une source correspondent à des conditions spécifiques (conditions ambiantes ou fortes concentrations d'aérosols organiques), la masse d'aérosols organiques associée au facteur d'émissions devraient être également fournie afin de pouvoir corriger le facteur d'émissions et estimer le facteur d'émissions de COSV en connaissant le profil de dilution de la source.

Les émissions naturelles :

Les émissions biogéniques sont aussi une grande source d'incertitude. Les émissions de sesquiterpènes sont souvent sous-estimées du fait de la forte réactivité de ces composés. Ils peuvent réagir en grande quantité et former d'autres composés en dessous de la canopé. Ils peuvent d'ailleurs réduire fortement les concentrations d'ozone et ainsi protéger les plantes [*Jardine et al.*, 2011]. Développer des modèles de canopé pour déterminer de façon plus explicites les émissions de sesquiterpenes et la formation d'aérosols à l'intérieur de la canopé est donc nécessaire pour simuler correctement la formation d'aérosols organiques secondaires. De plus, certains composés

biogéniques comme le méthyl chavicol ou le linalool sont absents du modèle d'émissions biogéniques alors qu'ils pourraient contribuer à la formation d'aérosols.

Une partie des émissions naturelles pourraient également provenir des micro-organismes marins. Certains composés organiques volatils peuvent donc être émis au-dessus de zones maritimes. De plus, une fraction des sels marins pourrait également être organique. Certaines paramétrisations [*Gantt et al.*, 2009, 2011] ont été développées pour déterminer les émissions marines d'isoprène et la fraction d'aérosols organiques dans les sels marins. Ces paramètrisations devraient être implémentées dans les modèles de qualité de l'air pour estimer la contribution des émissions marines aux concentrations d'aérosols organiques.

6.2.2 Améliorer les mécanismes chimiques de formation d'aérosols organiques

Les principales améliorations à faire dans les mécanismes chimiques concernent la chimie des monoterpènes et le vieillissement des aérosols organiques.

Pour l'instant, le modèle utilise uniquement des rendements en régime haut-NO_x pour l'oxydation des monoterpènes alors que ces composés étant d'origine biogénique devraient être principalement oxydés en régime bas-NO_x. La formation d'aérosols organiques pour l'oxydation de l'α-pinène a été récemment étudié [*Eddingsaas et al.*, 2012]. Les résultats de cette étude pourraient être utilisés pour développer des paramétrisations pour l'oxydation de l'α-pinène en régime bas-NO_x.

D'après les résultats de cette thèse, la formation d'aérosols est très sensible au vieillissement. Des paramétrisations plus détaillées devraient donc être développées pour prendre en compte le vieillissement des aérosols. Ces paramétrisations doivent être capable de bien reproduire l'évolution de la volatilité et de l'oxydation des composés formés avec chaque étape d'oxydation. Pour développer ces paramétrisations de vieillissement, il faut étudier expérimentalement le vieillissement des aérosols ou utiliser les résultats de mécanismes théoriques d'oxydation de composés organiques. Peu d'informations expérimentales sont disponibles sur le vieillissement des aérosols du fait de la difficulté d'étudier la formation d'aérosols sur de longues périodes à l'intérieur des chambres de simulation (les composés se déposent aux parois au bout de quelques heures). Les mécanismes théoriques peuvent donc être un outil intéressant pour étudier le vieillissement. Ces mécanismes utilisant beaucoup de composés sont généralement trop compliqués pour être implémentés dans un modèle 3D de qualité de l'air, mais les résultats de ces mécanismes pourraient être utilisés pour développer des paramétrisations avec un nombre réduit d'espèces. Les paramétrisations développées pourraient être ensuite évaluées avec les données expérimentales disponibles.

6.2.3 Améliorer le calcul du partage

Le partage des composés entre la phase gazeuse et la phase particulaire nécessite encore d'effectuer des recherches. Le modèle H^2O suppose que les composés sont uniquement hydrophiles ou hydrophobes. Cependant, des tests effectués avec le modèle montrent que certains composés (par exemple, ceux formés par l'oxydation des monoterpènes) pourraient se condenser à la fois sur la phase aqueuse et sur la phase organiques. Il faudrait donc modifier le modèle pour prendre en compte le partage des composés sur toutes les phases. De plus, certains processus influençant la formation d'aérosols ont été peu étudiés. Par exemple, l'aérosol organique pourrait être constitué de différentes phases organiques où chaque phase est constitué de composés ayant beaucoup d'affinités entre eux et non d'une seule phase organique. Introduire un calcul de saturation et de séparation de phases pourrait dans ce cas s'avérer utile. Il faudrait également, comme le montre les résultats de l'étude de modélisation sur Paris, attribuer une structure chimique aux COSV primaires et à leurs composés d'oxydation (ce qui peut être plus facile en utilisant un méca-

nisme d'oxydation détaillé) pour prendre en compte l'influence des coefficients d'activité sur ces composés. Des valeurs de coefficients d'activité élevés pourraient dans certains cas, empêcher la condensation de ces COSV. Un autre point concerne l'hypothèse que la phase particulaire est à l'équilibre avec la phase organique. Des études récentes montrent que la phase organique pourrait être très visqueuse et que la vitesse de transfert des composés entre la phase gazeuse et la phase particulaire pourrait être limitée dans certains cas par la diffusion des composés dans la phase organique [*Shiraiwa et al.*, 2011]. Le modèle pourrait être modifié pour étudier dans quelle mesure la viscosité de la phase organique pourrait influencer la formation d'aérosols. Le dernier point consiste à développer des paramètrisations théoriques pour étudier l'influence de l'oligomérisation, par exemple via estérification. Une partie de certains acides et alcools supposés volatils pourraient en effet se condenser sur la phase particulaire et réagir pour former des oligomères. L'estérification est en plus fortement influencée par la teneur en eau de la phase organique. Elle peut être efficace pour de faibles teneurs en eau et donc à faibles humidités. La formation d'aérosols via oxydation de l'isoprène en régime haut-NO_x est sujette à la formation d'oligomères via estérification et se révélerait donc être un bon sujet d'étude.

6.2.4 Améliorer le calcul des dépôts

Les dépôts constituent un puits important d'aérosols organiques. Le calcul des dépôts secs de composés hydrophiles selon la méthode proposée par *Bessagnet et al.* [2010] pourrait réduire de manière significative les concentrations d'aérosols. De même, ajouter le dépôt humide des COSV dans la phase gazeuse peut donner une dimunition importante des concentrations comme le montre les résultats du Chapitre 5. Comme ces calculs de dépôts n'étaient pas pris en compte lors de la comparaison sur l'Europe, le modèle pourrait encore sous-estimer la formation d'aérosols organiques de façon importante.

6.2.5 Améliorer les conditions aux limites des simulations européennes et étudier la formation d'aérosols à l'échelle du globe

Les concentrations d'aérosols organiques simulées sur l'Europe sont très sensibles aux conditions aux limites utilisées (28 % de l'aérosol organique sur Paris en juillet 2009 provient des conditions aux limites). Ces conditions aux limites proviennent de résultats de modèle globaux qui généralement ne traitent pas la formation d'aérosols organiques de manière détaillée. Les résultats du modèle pourraient être améliorés de manière significative en améliorant les conditions aux limites sur l'Europe. Pour cela, les concentrations d'aérosols organiques pourraient être simulées à l'échelle du globe pour évaluer le transport à longues-distances de matières organiques. De plus, certaines régions du monde peuvent être des zones d'études intéressantes, par exemple, l'Amazonie qui est une zone avec de fortes émissions biogéniques. D'autres zones du monde pourraient être fortement influencées par les aérosols organiques secondaires formés par oxydation des composés aromatiques. Cependant, simuler correctement les aérosols organiques à l'échelle du globe exige au préalable de développer un inventaire d'émissions mondial de COSV.

Annexe A

Comparison of different gas-phase mechanisms and aerosol modules for simulating particulate matter formation

Cet appendice est constitué de

Kim, Y., Couvidat, F., Sartelet, K. et Seigneur, C. (2011). **Comparison of different gas-phase mechanisms and aerosol modules for simulating particulate matter formation**. *J. Air & Waste Manage. Assoc.*, 61 :1-9.

Sommaire

Abstract

The effects of two gas-phase chemical kinetic mechanisms, Regional Atmospheric Chemistry Mechanism version 2 (RACM2) and Carbon-Bond 05 (CB05), and two secondary organic aerosol (SOA) modules, the Secondary Organic Aerosoi Model (SORGAM) and AER/EPRI/Caltech model (AEC), on fine (aerodynamic diameter ≤ 2.5 μm) particulate matter (PM2.5) formation is studied. The major sources of uncertainty in the chemistry of SOA formation are investigated. The use of all major SOA precursors and the treatment of SOA oligomerization are found to be the most important factors for SOA formation, leading to 66% and 60% more SOA, respectively. The explicit representation of high-NOx and low-NOx gas-phase chemical regimes is also important with increases in SOA of 30–120% depending on the approach used to implement the distinct SOA yields within the gas-phase chemical kinetic mechanism; further work is needed to develop gas-phase mechanisms that are fully compatible with SOA formation algorithms. The treatment of isoprene SOA as hydrophobic or hydrophilic leads to a significant difference, with more SOA being formed in the latter case. The activity coefficients may also be a major source of uncertainty, as they may differ significantly between atmospheric particles, which contain a myriad of SOA, primary organic aerosol (POA), and inorganic aerosol species, and particles formed in a smog chamber from a single precursor under dry conditions. Significant interactions exist between the uncertainties of the gas-phase chemistry and those of the SOA module.

A.1 Introduction

Modeling air quality requires a complex system, which includes algorithms to simulate transport processes, a chemical kinetic mechanism, and an aerosol module. Various gas-phase mechanisms are currently available to simulate ozone formation and several aerosol modules are also available to simulate the evolution of particulate matter (PM) chemical composition and size distribution. A few studies have been conducted to investigate the effect of the gasphase chemical kinetic mechanism [*Luecken*, 2008; *Sarwar et al.*, 2008] or the effect of the aerosol module [*Pun et al.*, 2003; *Morris et al.*, 2006; *Bailey et al.*, 2007] on secondary PM formation. The objective of this work is to evaluate the differences in fine (aerodynamic diameter $\leq 2.5\mu$m) PM ($PM_{2.5}$) concentrations that result from the use of two different chemical mechanisms and $PM_{2.5}$ modules, with a special emphasis on identifying the major sources of uncertainties for secondary organic aerosol (SOA) formation. First, the models used in this study are briefly described and model performance evaluation against observations from routine monitoring networks is summarized. Then, $PM_{2.5}$ concentrations simulated using two different gas-phase chemical mechanisms and two secondary organic aerosol modules are compared. In particular, we investigate whether the uncertainties associated with those two distinct types of modules (gas-phase chemistry and secondary aerosol formation) are additive or whether their combination is nonlinear.

A.2 Description of the models

The air quality model used in this work is the threedimensional (3D) Eulerian chemical-transport model POLAIR3D of the Polyphemus modeling platform [*Sartelet et al.*, 2007; *Mallet et al.*, 2007].

Two recent gas-phase mechanisms are used in the following simulations: the Carbon-Bond 05 mechanism (CB05) [*Sarwar et al.*, 2008] and the Regional Atmospheric Chemistry Mechanism version 2 (RACM2) [*Goliff and Stockwell*, 2008]. The former is based on the carbon-bond formulation to represent organic chemistry, whereas the latter uses a surrogate molecule representation. Some differences also exist in the selection and kinetics of some inorganic reactions,

Table A.1: Major characteristics of the SORGAM and AEC SOA modules.

Characteristics	SORGAM	AEC
Precursors	Aromatics, long-chain alkanes, long-chain alkenes, monoterpenes	Aromatics, long-chain alkanes, long-chain alkenes, isoprene, monoterpenes, sesquiterpenes
SOA species	Two surrogates per precursor and oxidation pathway	Surrogate molecular species selected according to physicochemical properties
Gas/particle partitioning	Absorption into an hydrophobic organic phase	Absorption of hydrophobic SOA into an organic phase and absorption of hydrophilic SOA into an aqueous phase
Non-ideality of the particulate phase	Assumed constant and identical to that implicitly assumed in the gas/particle partitioning from the smog chamber experiments	Calculated via activity coefficients
Gas-phase chemistry	SOA yields for the first oxidation step with high-NO_x conditions	SOA yields from various oxidation steps with both high-NO_x and low-NO_x pathways
Particulate-phase chemistry	None	Oligomerization as a function of pH

as discussed by *Kim et al.* [2009]. For $PM_{2.5}$ formation, the ISORROPIA module [*Nenes et al.*, 1999], version 1.7, is used for inorganic species. For SOA formation, two distinct modules are used: the SORGAM module [*Schell et al.*, 2001], which uses the two-compound Odum approach [*Odum et al.*, 1996b], and the AEC module [*Pun et al.*, 2006; *Debry et al.*, 2007b], which simulates both hydrophilic and hydrophobic organic aerosols. The two-compound Odum approach consists in using two surrogate SOA compounds to represent SOA formation from a given precursor and the first step of oxidation (e.g., oxidation by the hydroxyl radical, ozone, or the nitrate radical). The stoichiometric coefficient and gas/particle partitioning coefficient of each surrogate SOA compound are estimated by fitting this empirical model to smog chamber data [*Odum et al.*, 1996b]. The treatment of gas/particle partitioning assumes that the SOA compounds absorb into a hydrophobic organic particle. This two-compound Odum approach is currently used in many air quality models such as the Community Multiscale Air Quality (CMAQ) model [*Carlton et al.*, 2010a], the Comprehensive Air quality Model with extensions (CAMx) [*Gaydos et al.*, 2007], the Weather Research & Forecast model with Chemistry (WRF/Chem) [*Zhang et al.*, 2010a], the European Monitoring and Evaluation Programme (EMEP) model [*Simpson et al.*, 2007], the European Air pollution and Dispersion (EURAD) model [*Schell et al.*, 2001], and POLAIR3D/Polyphemus [*Sartelet et al.*, 2007]. The AEC hydrophobic/hydrophilic SOA approach is used in several models such as CMAQ [*Zhang et al.*, 2004], WRF/Chem [*Zhang et al.*, 2010a], POLAIR3D/Polyphemus [*Debry et al.*, 2007b], and CHIMERE [*Bessagnet et al.*, 2008]. Thus, as for the gas-phase chemistry, two operational formulations for SOA formation are considered. SORGAM represents a standard SOA formulation with hydrophobic absorption of SOA into organic particles, whereas AEC includes a more complete set of physicochemical processes for SOA formation. In particular, AEC treats hydrophilic SOA in addition to hydrophobic SOA and it accounts for the variable nonideality of particles via the calculation of activity coefficients; in addition, the AEC version used here distinguishes between high-NO_x and low-NO_x regimes for SOA yields, it includes more SOA precursors (isoprene and sesquiterpenes) than SORGAM, and it treats pH-dependent oligomerization processes. Table A.1 summarizes the main characteristics of these two SOA modules.

Kim et al. [2009] presented a detailed discussion of the results of an application of the air

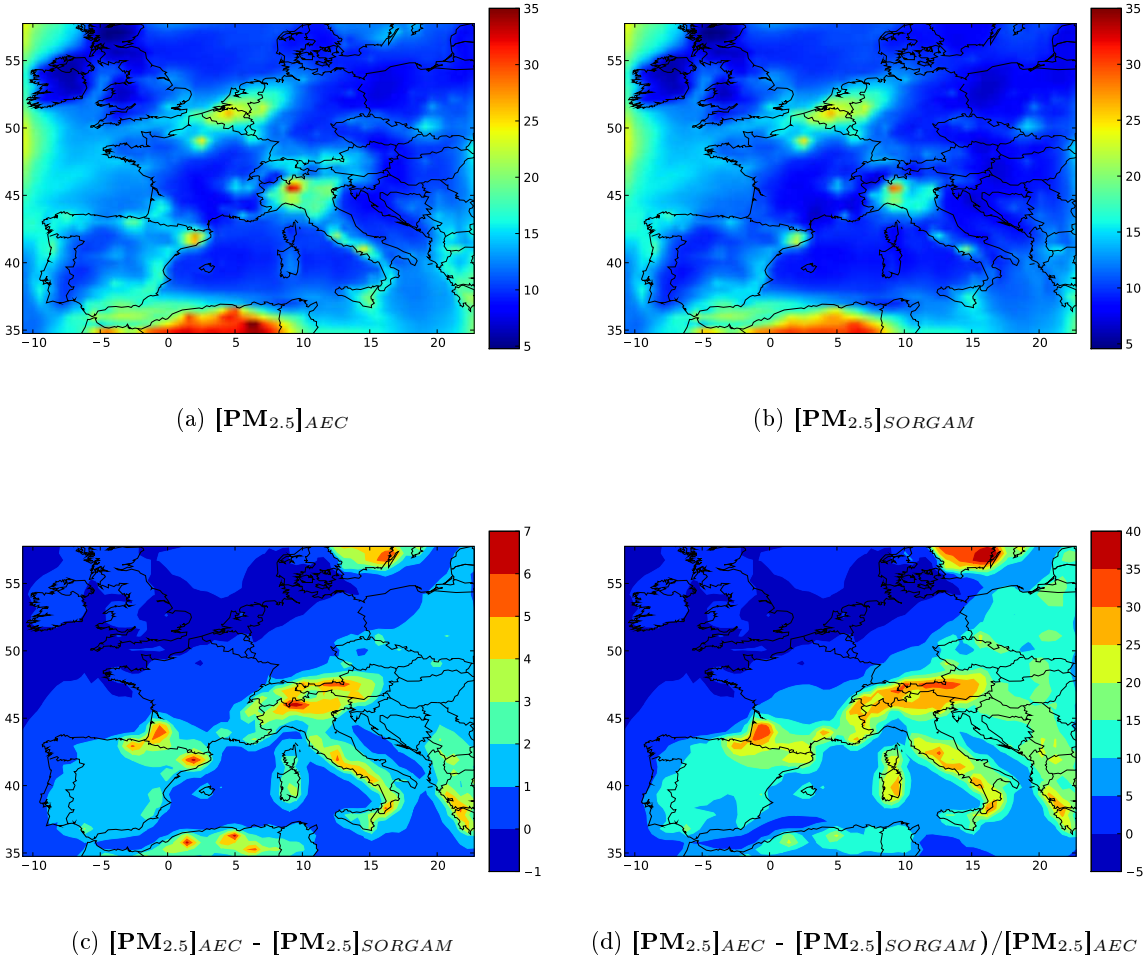

(a) $\mathbf{[PM_{2.5}]}_{AEC}$ (b) $\mathbf{[PM_{2.5}]}_{SORGAM}$

(c) $\mathbf{[PM_{2.5}]}_{AEC}$ - $\mathbf{[PM_{2.5}]}_{SORGAM}$ (d) $\mathbf{[PM_{2.5}]}_{AEC}$ - $\mathbf{[PM_{2.5}]}_{SORGAM}$)/$\mathbf{[PM_{2.5}]}_{AEC}$

Figure A.1: $PM_{2.5}$ concentrations ($\mu g/m^3$) over Europe simulated with AEC and SORGAM for SOA formation and RACM2 for gas-phase chemistry. Results are averaged over the 1-month simulation of 15 July to 15 August 2001: (a) $[PM_{2.5}]_{AEC}$ (top left); (b) $[PM_{2.5}]_{SORGAM}$ (top right); (c) $[PM_{2.5}]_{AEC}$ - $[PM_{2.5}]_{SORGAM}$ (bottom left); (d) ($[PM_{2.5}]_{AEC}$ - $[PM_{2.5}]_{SORGAM}$)/$[PM_{2.5}]_{AEC}$ (bottom right)

quality model with CB05 and RACM2 to Europe for the period 15 July to 15 August 2001. Model performance evaluation for hourly ozone (O_3) concentrations shows mean normalized error and bias of 23% and 9% for RACM2 and 21% and 4% for CB05, normalized mean error and bias of 43% and 30% for RACM2 and 39% and 25% for CB05, and mean fractional error and bias of 22% and 5% for RACM2 and 21% and 0% for CB05 (a threshold of 60 ppb was used for the observed hourly O_3 concentrations). This model performance is satisfactory compared to guidelines of mean normalized error and bias less than or equal to 35% and 15%, respectively [*Russell and Dennis*, 2000]. Average differences in O_3 concentrations between CB05 and RACM2 are on the order of 3 ppb, that is, about 5%. Maximum differences are 6 ppb (9%). It was concluded that both inorganic and organic chemistry contributed to differences between the mechanisms. Formation of inorganic PM is identical in those two simulations and differences are due solely to the SOA formation modules. When using RACM2, the $PM_{2.5}$ mean fractional error and bias are

41% and -4% with AEC and 45% and -16% for SORGAM, respectively; the normalized mean error and bias are 38% and 2% with AEC and 40% and -8% for SORGAM, respectively. When using CB05, the $PM_{2.5}$ mean fractional error and bias are 37% and -4% with AEC and 47% and -22% for SORGAM, respectively; the normalized mean error and bias are 36% and 1% with AEC and 44% and -15% for SORGAM, respectively. These values are within the performance goals recommended by *Boylan and Russell* [2006]. Model performance is comparable for the inorganic components and the differences in model performance are due to the particulate organic fraction (no particulate organic carbon measurements are available from the EMEP monitoring network for the period considered here). Therefore, model performance is satisfactory for $PM_{2.5}$ with both gas-phase chemical mechanisms and both SOA modules and commensurate with those of other models for atmospheric PM [*Russell*, 2008].

A.3 Sensitivity of PM concentrations to the aerosol module

The sensitivity of PM concentrations is first investigated with respect to the aerosol module. The molecule-based formulation of RACM2 is more conducive to detailed interactions between gas-phase chemistry and SOA formation than the carbon-bond formulation of CB05; therefore, RACM2 is used here for the gas-phase chemistry.

Figure A.1 presents the $PM_{2.5}$ concentrations simulated with AEC and SORGAM over Europe, as well as the differences between the two model simulations. Overall, more $PM_{2.5}$ is formed with AEC than with SORGAM. This result is due to the fact that more SOA formation processes are included in AEC (see Table A.1). Differences are significant; they reach 6-7 $\mu g/m^3$ in parts of northern Italy, southwestern France, northern Spain, and North Africa and are in the range of 3-6 $\mu g/m^3$ in southern Sweden (the European regulation is 20 $\mu g/m^3$ for annual concentrations). Relative differences follow a similar spatial pattern with differences up to 40% (with respect to the AEC simulation) in southern Sweden, southwestern France, and Austria. These results highlight that uncertainties in PM formation greatly exceed those in ozone gas-phase chemistry, which is consistent with earlier findings [*Pun et al.*, 2003; *Bailey et al.*, 2007].

Table A.2: Characteristics of SOA modules used in the sensitivity simulations.

SOA module	Precursors	NO_x regime	Hydrophobic and hydrophilic absorption	Activity coefficients	Oligomerization	Enthapies of vaporization
SORGAM	Anthropogenics, monoterpenes	High-NO_x only	Hydrophobic only	Implicit and constant	None	156 kJ/mol [*Schell et al.*, 2001]
SORGAM-ΔH	Anthropogenics, monoterpenes	High-NO_x only	Hydrophobic only	Implicit and constant	None	88 kJ/mol [*Pun et al.*, 2006]
SORGAM-NO_x	Anthropogenics, monoterpenes	High- and low-NO_x	Hydrophobic only	Implicit and constant	None	88 kJ/mol [*Pun et al.*, 2006]
SORGAM-bio	Anthropogenics, all terpenes	High- and low-NO_x	Hydrophobic only	Implicit and constant	None	42-175 kJ/mol[a]
Super-SORGAM	Anthropogenics, all terpenes	High- and low-NO_x	Hydrophobic, parametrization for hydrophilic isoprene SOA	Implicit and constant	None	42-175 kJ/mol[a]
Mini-AEC	Anthropogenics, all terpenes	High- and low-NO_x	Hydrophobic and hydrophilic	Constant (unity)	None	25-175 kJ/mol[b]
AEC-no-oligo	Anthropogenics, all terpenes	High- and low-NO_x	Hydrophobic and hydrophilic	Calculated and variable	None	25-175 kJ/mol[b]
AEC	Anthropogenics, all terpenes	High- and low-NO_x	Hydrophobic and hydrophilic	Calculated and variable	Parametrization for aldehyde SOA	25-175 kJ/mol[b]

Notes: [a]42 kJ/mol for isoprene SOA [*Zhang et al.*, 2007b], 88 kJ/mol for anthropogenic and monoterpene SOA [*Pun et al.*, 2006], 175 kJ/mol for sesquiterpene SOA [*Pun et al.*, 2006].
[b]25 kJ/mol for glyoxal [*Debry et al.*, 2007b], 38 kJ/mol for methylglyoxal [*Debry et al.*, 2007b], 42 kJ/mol for isoprene SOA [*Zhang et al.*, 2007b], 88 kJ/mol for biogenic hydrophilic aldehyde and monocarboxylic SOA and for anthropogenic SOA [*Pun et al.*, 2006], 109 kJ/mol for biogenic dicarboxylic acids [*Pun et al.*, 2006], 175 kJ/mol for biogenic hydrophobic SOA [*Pun et al.*, 2006].

Because SORGAM and AEC represent two ends of a spectrum of SOA models, it is of particular interest to investigate which of the structural differences that distinguish SORGAM from AEC contribute the most to the differences in simulated SOA concentrations: number of SOA precursors, treatment of high- versus low-NO_x regimes, treatment of hydrophilic SOA, treatment of the variability of activity coefficients, or treatment of oligomerization. To that end, we conducted a series of simulations with SORGAM and AEC that involve modifications to the SOA modules to represent these various structural modifications. In addition to these structural changes, the influence of the enthalpies of vaporization on SOA concentrations was also investigated. Table A.2 presents the characteristics of the SOA modules used in those sensitivity simulations.

Figures A.2 and A.3 present the SOA concentrations averaged over the 1-month simulation period for each of the eight simulations. Differences between a model simulation and the simulation of the nearest model in terms of formulation are also presented. Overall, SOA concentrations increase as the SOA module evolves from SORGAM (the simplest mechanistic representation of SOA formation) to AEC (the most complete representation of SOA formation processes). The results are discussed in detail below.

The values of the enthalpies of vaporization for the equilibrium calculations of SOA have been shown to have some effects on average SOA concentrations [*Zhang et al.*, 2007b] as well as on their diurnal patterns [*Pun and Seigneur*, 2008]. Accordingly, we replaced the original enthalpies of vaporization of SORGAM (156 kJ/mol for all SOA) by a value of 88 kJ/mol, which better reflects the more recent values used in AEC, as shown in Table A.2 (SORGAM-ΔH). The difference in SOA concentrations averaged over the entire domain is low (0.01 $\mu g/m^3$) because there are both positive and negative differences in various parts of the domain depending on temperature. In areas with the lower temperatures (the Alps, the Pyrenean Mountains, and Sweden), the decrease in the enthalpies of vaporization leads to a decrease in SOA concentrations by as much as 0.5 $\mu g/m^3$ because the experimental data used in the SOA model were obtained at greater temperatures than those modeled in those areas and the temperature correction, which leads to greater SOA concentrations as the temperature decreases, is less for a smaller value of the enthalpy of vaporization. For the other areas where the temperatures are higher, the opposite effect is obtained. The lower enthalpy of vaporization used in SORGAM-ΔH leads to less displacement of the gas/particle equilibrium toward the gas phase and the SOA concentrations are consequently greater than in SORGAM by up to 0.2 $\mu g/m^3$.

Adding some representation of the NO_x regime for SOA formation (SORGAM-NO_x) has some effects because SOA formation is more important for aromatics and monoterpenes (which are major SOA precursors in SORGAM) under low-NO_x conditions than under high-NO_x conditions according to the smog chamber results of *Ng et al.* [2007a,b]. Here the stoichiometric coefficients and partitioning coefficients of *Ng et al.* [2007a,b] were used for the low-NO_x regime. Because most SOA formation at the regional scale occurs under low-NO_x conditions, SOA yields increase when one allows the mechanism to treat both high- and low-NO_x regimes. The effect depends, however, on how the low-NO_x versus high-NO_x regimes are implemented in the gas-phase chemical kinetic mechanism. On one hand, if one simply uses the low-NO_x regime SOA yields in the first oxidation step of the precursor species (for both aromatics and monoterpenes), thereby neglecting the occurrence of the high-NO_x regime for SOA formation, the differences in SOA concentrations are significant: they reach 2 $\mu g/m^3$ in northern Italy and are about 0.35 $\mu g/m^3$ on average over the entire domain (not shown). On the other hand, if one implements the high-NO_x and low-NO_x SOA yields in later oxidation steps corresponding to reactions of precursor oxidation products with nitrogenous species and peroxyl radicals, respectively, but for aromatics only (because of insufficient information for monoterpenes), the differences are smaller, because the overall SOA yields include a combination of all oxidation routes and the

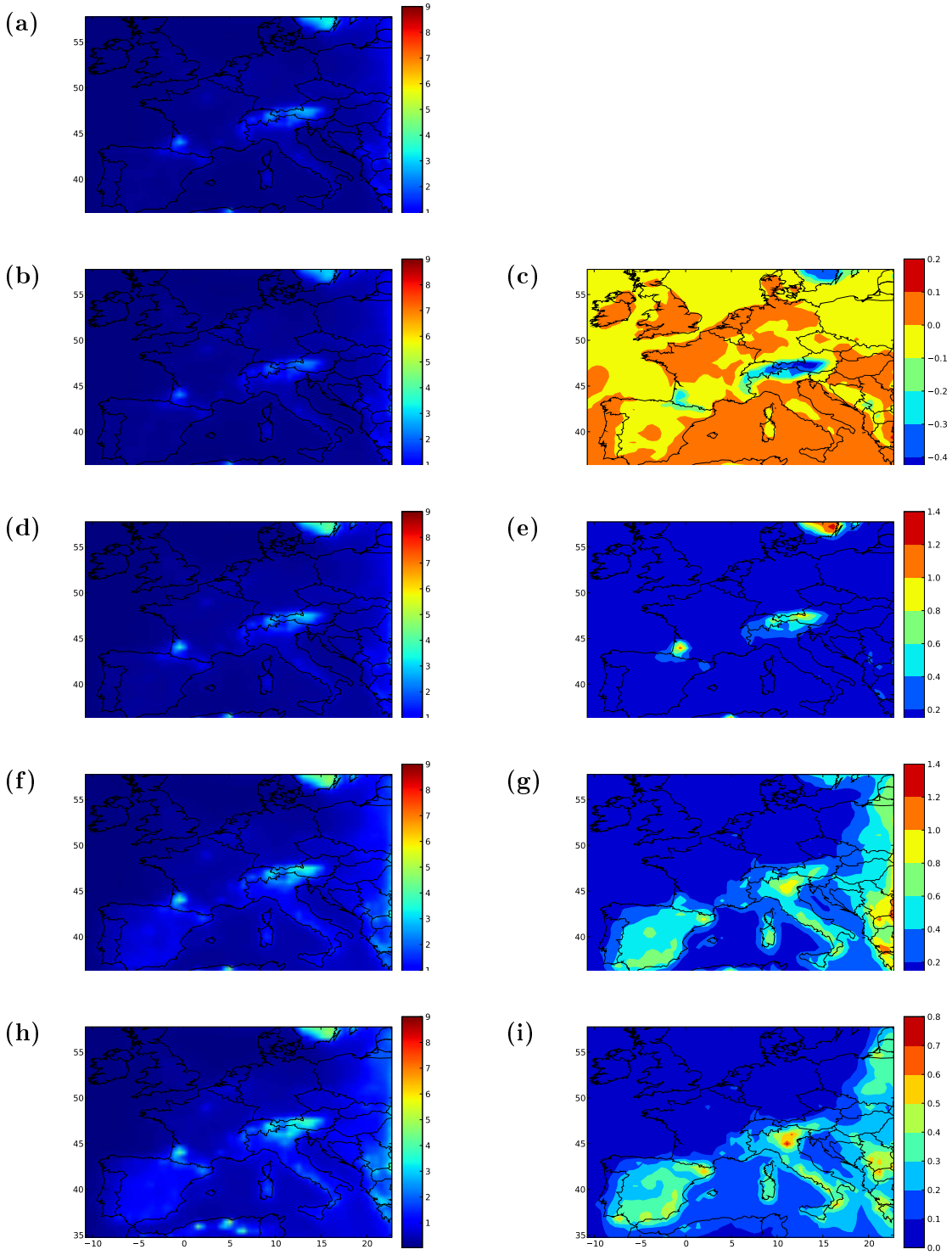

Figure A.2: Simulations of $PM_{2.5}$ SOA ($\mu g/m^3$) over Europe with RACM2 for gas-phase chemistry and distinct SORGAM modules for SOA formation: (a) SORGAM (first row); (b) SORGAM-ΔH (second row left); (c) [SORGAM-Δ - SORGAM] (second row right); (d) SORGAM-NO_x (third row left); (e) [SORGAM-NO_x - SORGAM-ΔH] (third row right); (f) SORGAM-bio (fourth row left); (g) [SORGAM-bio - SORGAM-NO_x] (fourth row right); (h) Super-SORGAM (fifth row left); (i) [Super-SORGAM - SORGAM-bio] (fifth row right).

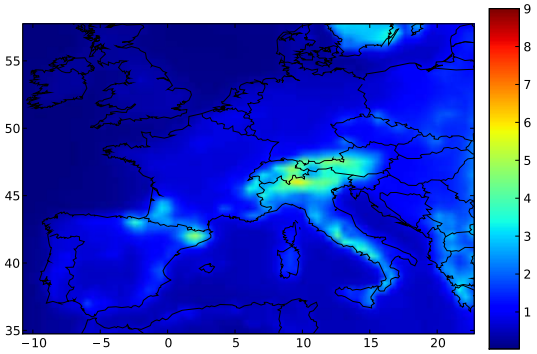

(a) **Mini-AEC**

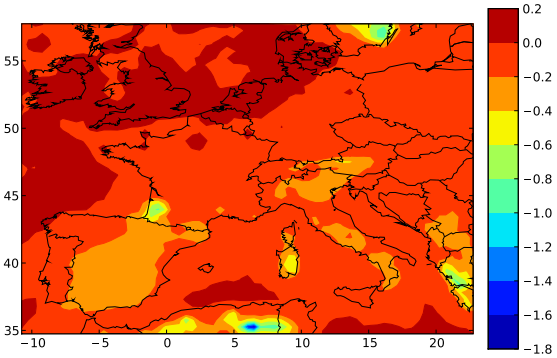

(b) **Mini-AEC - AEC-no-oligo**

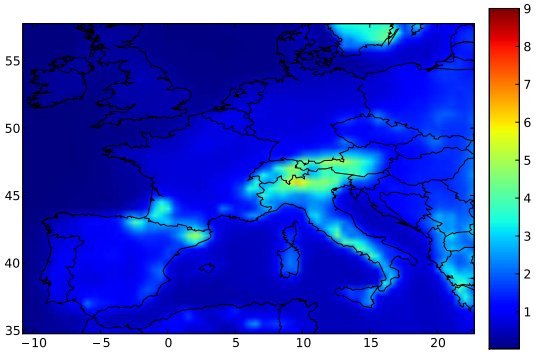

(c) **AEC-no-oligo**

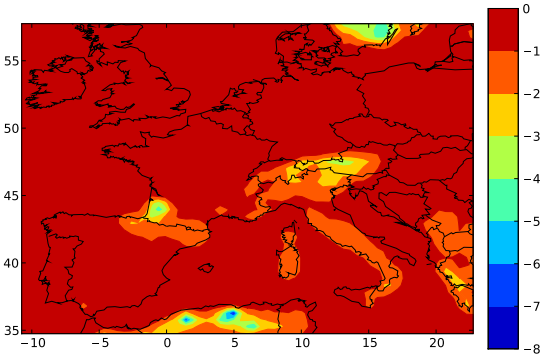

(d) **AEC-no-oligo - AEC**

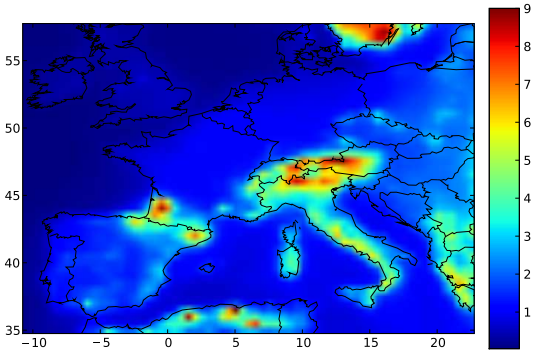

(e) **AEC**

Figure A.3: Simulations of $PM_{2.5}$ SOA ($\mu g/m^3$) over Europe with RACM2 for gas-phase chemistry and distinct AEC modules for SOA formation: (a) Mini-AEC (first row left); (b) [Mini-AEC - AEC-no-oligo] (first row right); (c) AEC-no-oligo (second row left); (d) [AEC-no-oligo - AEC] (second row right); and (e) AEC (third row).

low-NO_x regime is not treated for monoterpenes. Then, as shown in Figure A.2, the differences in SOA concentrations reach 1.4 $\mu g/m^3$ in Sweden, southwestern France, and North Africa and approach 1 $\mu g/m^3$ in northern Italy; they are, however, only 0.08 $\mu g/m^3$ on average. These two results underscore the importance of treating the effect of the NO_x regime with sufficient detail in the gas-phase mechanism and further work is needed to develop gas-phase chemical kinetic mechanisms that can better integrate the dependency of SOA yields on NO_x regimes.

Adding isoprene and sesquiterpenes as precursors of SOA also increases the SOA concentrations (SORGAM-bio). The effect of NO_x regimes is also included in this simulation. However, SOA formation from sesquiterpenes is assumed to be lower under low-NO_x conditions than under high-NO_x conditions following *Ng et al.* [2007a]. For isoprene, no NO_x dependency is considered here, following *Zhang et al.* [2007b]. The enthalpy of vaporization used by *Zhang et al.* [2007b] was used for isoprene SOA; this value is in good agreement with the more recent experimental values of *Kleindienst et al.* [2009]. The enthalpy of vaporization used by *Pun et al.* [2006] was used for sesquiterpene SOA. Most of the increase in SOA concentrations is due to isoprene oxidation rather than sesquiterpene oxidation [*Debry et al.*, 2007b]. The largest increases occur in the lower latitudes where temperature and solar radiation are greater and, therefore, where isoprene emissions are higher. The SOA concentration increase reaches 1.4 $\mu g/m^3$ in the eastern part of the domain and is 0.25 $\mu g/m^3$ on average over the entire domain.

SOA formed from isoprene oxidation are believed to be hydrophilic and, therefore, may absorb into aqueous particles rather than into hydrophobic organic particles [*Pun*, 2008]. The affinity of those SOA compounds for aqueous particles is significantly larger than for organic particles, which could lead to greater SOA formation under humid conditions; for example, *Pun* [2008] calculated that SOA concentrations due to isoprene oxidation could be up to 5 times greater under humid conditions than under dry conditions. To account for this process, a simple parameterization is incorporated in the version of SORGAM, which already includes NO_x regimes and all terpene precursors. This parameterization accounts for a linear increase in isoprene SOA formation as a function of relative humidity (RH) (Super-SORGAM): $K_i(\mathrm{RH}) = K_i(\mathrm{RH} = 0)\ (1 + 4\ \mathrm{RH})$, where K_i, $i = 1, 2$, are the partitioning constants of the two isoprene SOA species and RH is expressed as a fraction (i.e., RH = 1 at 100% relative humidity). This parameterization leads to about 5 times more isoprene formation at 100% relative humidity than at 0% relative humidity, following the simulation results of *Pun* [2008]. The result shows an increase in SOA concentrations in regions where SOA formation from isoprene is significant, that is, mostly near the Mediterranean Sea. They reach 0.5-0.8 $\mu g/m^3$ in northern Italy and northern Spain, where SOA concentrations are in the 2-3 $\mu g/m^3$ range. They are less than 0.1 $\mu g/m^3$ in northern Europe, where SORGAM-NO_x SOA concentrations are mostly less than 2 $\mu g/m^3$.

AEC was simplified to obtain a version that closely resembles the formulation of Super-SORGAM, hereafter referred to as Mini-AEC. In that version, the activity coefficients are set to one (i.e., assuming ideal solutions) and oligomerization of SOA in the particulate phase is not simulated. The effect of activity coefficients set to one (ideal organic and aqueous solutions) for particulate SOA leads to a decrease in SOA concentrations of about 10% on average (0.08 $\mu g/m^3$). This relatively small effect, for example, compared to the difference reported by *Pun* [2008] is due in part to compensating effects for hydrophobic particles and aqueous particles. In some areas, the effect can be significant with the largest differences (> 0.5 $\mu g/m^3$) occurring in southern Sweden, southwestern France, Corsica, and North Africa.

The two other versions of AEC used here include one where only oligomerization [*Pun and Seigneur*, 2007] is not taken into account but the activity coefficients are calculated (referred to as AEC-no-oligo), and the base AEC configuration where all processes are simulated (see Table A.1).

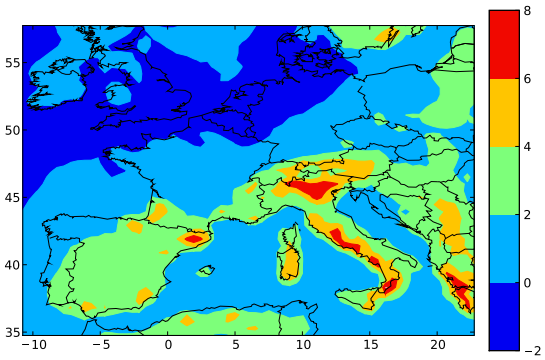

(a) $[\mathbf{PM}_{2.5}]_{CB05,AEC}$ - $[\mathbf{PM}_{2.5}]_{CB05,SORGAM}$

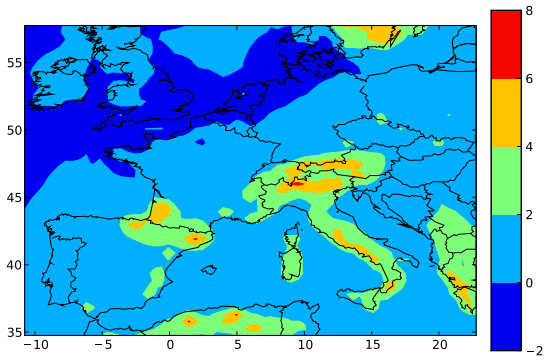

(b) $[\mathbf{PM}_{2.5}]_{RACM2,AEC}$ - $[\mathbf{PM}_{2.5}]_{RACM2,SORGAM}$

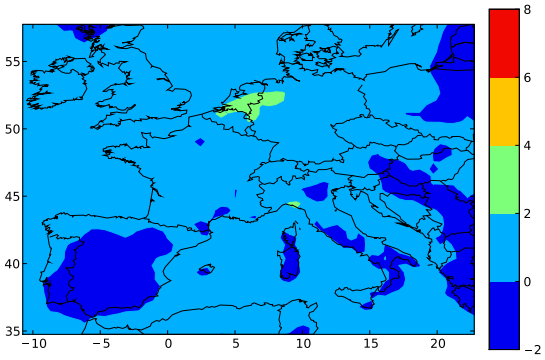

(c) $[\mathbf{PM}_{2.5}]_{RACM2,AEC}$ - $[\mathbf{PM}_{2.5}]_{CB05,AEC}$

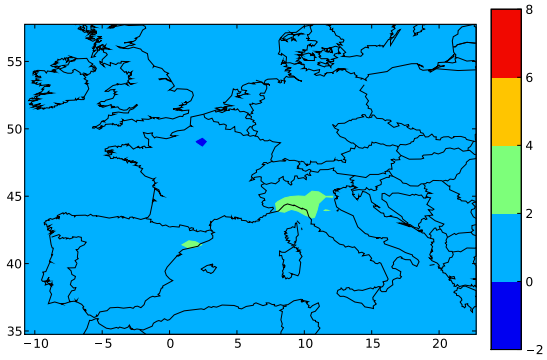

(d) $[\mathbf{PM}_{2.5}]_{RACM2,SORGAM}$ - $[\mathbf{PM}_{2.5}]_{CB05,SORGAM}$

Figure A.4: Differences in $PM_{2.5}$ concentrations ($\mu g/m^3$) over Europe simulated with RACM2 and CB05 for gas-phase chemistry and with AEC and SORGAM for SOA formation. Results are averaged over the one-month simulation of 15 July to 15 August 2001: (a) $[PM_{2.5}]_{CB05,AEC}$ - $[PM_{2.5}]_{CB05,SORGAM}$ (top left); (b) $[PM_{2.5}]_{RACM2,AEC}$ - $[PM_{2.5}]_{RACM2,SORGAM}$ (top right); (c) $[PM_{2.5}]_{RACM2,AEC}$ - $[PM_{2.5}]_{CB05,AEC}$ (bottom left); (d) $[PM_{2.5}]_{RACM2,SORGAM}$ - $[PM_{2.5}]_{CB05,SORGAM}$ (bottom right).

Neglecting oligomerization has a significant effect with an average decrease of 0.57 $\mu g/m^3$ in SOA concentrations over the entire domain. The largest decrease occurs in North Africa (up to 8 $\mu g/m^3$). Decreases in southwestern France and Austria are up to 5 $\mu g/m^3$. Significant increases are also obtained over southern Sweden. These regions have significant emissions of monoterpenes, which are precursors of the aldehyde SOA surrogate species that is subject to oligomerization in AEC.

A.4 Joint sensitivity of PM concentrations to the gas-phase chemistry and aerosol module

The joint sensitivity of PM concentrations to different treatments of both gas-phase chemistry and SOA formation is investigated. In particular, we evaluate whether the effects of gas-phase chemistry and SOA formation are simply additive or whether synergistic or antagonistic effects are significant. Figure A.4 presents the differences in $PM_{2.5}$ concentrations averaged over the 1-month simulation obtained with the four possible combinations of gasphase chemistry (RACM2 and CB05) and SOA modules (SORGAM and AEC).

The effect of the gas-phase chemical mechanism differs depending on which aerosol module is used. With both aerosol modules, the average $PM_{2.5}$ concentration is greater with RACM2 than with CB05: when SORGAM is used, the difference in $PM_{2.5}$ concentrations is 6% on average; it is 3% on average when AEC is used. These differences are commensurate with the 5% difference obtained for ozone concentrations between CB05 and RACM2 [*Kim et al.*, 2009]; however, the $PM_{2.5}$ differences result from compensating differences in inorganic and organic $PM_{2.5}$ concentrations. Secondary inorganic aerosol concentrations are greater on average with RACM2 than with CB05 by about 14%. On the other hand, SOA concentrations are greater with CB05 than with RACM2. The difference is only 3% with SORGAM, but it is 20% on average with AEC. This larger difference obtained with AEC is due in part to the fact that AEC takes into account the influence of the NO_x regime on SOA formation explicitly. At low NO_x concentrations, the formation of organic peroxide SOA is favored, whereas at high NO_x concentrations, the formation of other condensable products such as organic nitrates is favored. Because the SOA yields differ for those distinct SOA species, the gas-phase chemical mechanism has a strong influence on the SOA formation rate, particularly in the transition regime between high-NO_x and low-NO_x regimes (i.e., as the air mass is transported, for example, from an urban area to a remote location). CB05 switches more rapidly from a high-NO_x regime to a low-NO_x regime than RACM2, as documented by a map of HO_2/NO concentration ratios (not shown), which are greater with CB05 than with RACM2. As a result, CB05 is more conducive to SOA formation than RACM2.

This result demonstrates that the formation of SOA is very closely tied to the gas-phase chemical kinetic mechanism because the types of SOA formed and, therefore, the SOA yields differ in low-NO_x versus high-NO_x regimes. Consequently, uncertainties in the gas-phase chemistry and the aerosol module should not be treated separately but jointly.

A.5 Conclusion

The gas-phase chemical mechanism and aerosol module used in air quality models are shown to influence the simulated ozone and PM concentrations. Differences in SOA formation resulting from the use of different modules are more significant than those due to gas-phase chemistry and can be up to about 65%. The major sources of those differences include the following: the list of VOC included as VOC precursors (+66%, particularly isoprene, +44%), the explicit treatment of high-NO_x and low-NO_x regimes in the gas-phase chemistry leading to SOA (+32% to +122% depending on the implementation within the gas-phase chemical mechanism), and the treatment of oligomerization (+60%). Further work is needed to develop gas-phase chemical kinetic mechanisms that can explicitly account for different SOA yields depending on the oxidation pathways for high-NO_x (e.g., organonitrate formation) and low-NO_x (e.g., peroxide formation) regimes.

The enthalpies of vaporization have a small effect on average (4%) but may have an important effect locally with lower values leading to less SOA in regions with low temperature and more SOA in regions with high temperature.

The treatment of activity coefficients in the particulate phase has a small effect on average (+9%); however, the effect can be significant in some areas. Furthermore, the values of the activity coefficients may differ significantly between their implicit value in SORGAM and their calculated values in AEC because the activity coefficients of an SOA compound may differ significantly between their values in a smog chamber experiment with only one precursor and ammonium sulfate seed particles under dry conditions and the atmosphere where a myriad of SOA and POA species interact with inorganic salts and water.

The treatment of isoprene SOA (hydrophobic in SORGAM and hydrophilic in AEC) has a significant effect on SOA concentrations: 0.15 $\mu g/m^3$ of isoprene SOA is formed with SORGAM, whereas 0.34 $\mu g/m^3$ is formed with AEC. This result is consistent with that obtained by *Pun* [2008], who found a large increase in SOA concentration when hydrophilic SOA condensed in an aqueous phase. However, the two models differ because AEC includes interactions among SOA and inorganic salts in the aqueous phase, whereas the model of *Pun* [2008] only considered SOA in the aqueous phase. Further investigations appear warranted to better characterize the effect of an atmospheric aqueous particulate phase on isoprene SOA. Aqueous-phase formation of SOA species was not considered here; it could be a significant factor [*Pun et al.*, 2000; *Lim et al.*, 2005; *Carlton et al.*, 2008; *Ervens et al.*, 2008; *El Haddad et al.*, 2009; *Deguillaume et al.*, 2009] and should be investigated in future work.

The uncertainties due to the gas-phase chemistry and to the aerosol module are not additive and some strong nonlinearities occur for PM concentrations. In this study, one gas-phase chemical mechanism led to greater secondary inorganic aerosol formation, but to less secondary organic aerosol formation due to the intricate interactions between the gas-phase mechanism and secondary aerosol formation processes. These results have implications for air quality modeling in general, as they highlight which processes appear to be the most important for SOA modeling and the uncertainties associated with neglecting or parameterizing those processes.

Appendix B

Impact of biogenic emissions on air quality over Europe and North America

Cet appendice est constitué de

Sartelet, K., Couvidat, F., Seigneur, C. et Roustan, Y. (2012). **Impact of biogenic emissions on air quality over Europe and North America**. *Atmos. Environ.*, 53:131-141.

Sommaire

Abstract

This study aims to compare the relative impact of biogenic emissions on ozone (O_3) and particulate matter (PM) concentrations between North America (NA) and Europe. The simulations are conducted with the Polyphemus air quality modeling system over July and August 2006. Prior to the sensitivity study on the impact of biogenic emissions on air quality, the modeling results are compared to observational data, as well as to the concentrations obtained by other modeling teams of the Air Quality Model Evaluation International Initiative (AQMEII) study.

Over Europe, three distinct emission inventories are used. Model performance is satisfactory for O_3, PM_{10} and $PM_{2.5}$ with all inventories with respect to the criteria described in the literature. Furthermore, the rmse and errors are lower than the average rmse and errors of the AQMEII simulations. Over North America, the model performance satisfies the criteria described in the literature for O_3, PM_{10} and $PM_{2.5}$. Polyphemus results are within the range of the AQMEII model results. Although the rmse and errors are higher than the average of the AQMEII simulations for O_3, they are lower for PM_{10} and $PM_{2.5}$.

The impact of biogenic and anthropogenic emissions on O_3 and PM concentrations is studied by removing alternatively biogenic and anthropogenic emissions in distinct simulations. Because biogenic species interact strongly with NO_x, the impact of biogenic emissions on O_3 concentrations varies with variations of the Volatile Organic Compound (VOC)/NO_x ratio. This impact is larger over NA than Europe. O_3 decreases by 10-11% in average over Europe and 20% over NA. Locally, the relative impact is also higher in NA (60% maximum) than in Europe (35% maximum). O_3 decreases near large urban centers where biogenic emissions are large (e.g., Los Angeles, Chicago, Houston in NA, Milan in Europe).

Most of secondary organic aerosols (SOA) formed at the continental scale over Europe and NA are biogenic aerosols. Eliminating biogenic emissions reduces SOA by 72% to 88% over Europe and by 90% over NA. However, biogenic SOA are not only impacted by biogenic but also by anthropogenic emissions: eliminating all anthropogenic emissions affects oxidant levels and the absorbing carbon mass, reducing the formation of SOA by 15 to 16% over Europe and by about 10% over NA; Furthermore, locally, the reduction may be as large as 50%, especially over large urban centers in Europe and NA.

B.1 Introduction

Ozone (O_3) and particulate matter (PM) concentrations are believed to contribute to adverse health effects [*Ostro and Chestnut*, 1998] and climate change [*Yu et al.*, 2006]. Emissions of volatile organic compounds (VOC) and nitrogen oxides (NO_x) affect both O_3 and PM concentrations. Emissions are from different origins: anthropogenic, biogenic, marine, natural and re-suspended dust and biomass burning. Biogenic VOC (BVOC) emissions are highest in summer [e.g. *Guenther et al.*, 1995; *Steinbrecher et al.*, 2009]. During the summer heat wave of 2006, O_3 concentrations frequently exceeded air quality standards over Europe [*Struzewska and Kaminski*, 2008]. The year 2006 was also the second-hottest year in North America (NA) since the mid 1900s. As BVOC emissions depend on light and temperature, their impact on air quality during the summer 2006 may be high. Because precursor emission regulations can only target anthropogenic emissions, high biogenic emissions are not controllable and it is essential to understand how they may increase difficulties in meeting air quality standards via their interactions with anthropogenic species.

Over Europe, *Curci et al.* [2009] showed that for the years 1997, 2000, 2001 and 2003, BVOC emissions increased summer daily O_3 maxima by 5% on average. They also found that the average impact is higher during the hot summer of 2003 than during the other cooler summers.

Over the northeastern United States, *Pun et al.* [2002b] estimated the contribution of biogenic emissions to O_3 and $PM_{2.5}$ for a few days in July 1995. They showed that the contribution to O_3 was lower than 23%. The contribution to $PM_{2.5}$ was low (4 to 13%). *Pun et al.* [2002b] argued that it is because of the long life-time of $PM_{2.5}$, and the relatively short time period and small spatial domain of the simulations. In their simulations, biogenic secondary organic aerosols (SOA) only contributed to a small fraction of $PM_{2.5}$ and isoprene SOA was not modeled. *Mueller and Mallard* [2011] studied the relative contributions of natural to total emissions over the United States. They found that biogenic emissions were the primary source of fine particles in all parts of the country. For the eastern United States, *Hogrefe et al.* [2011] found that the impact of uncertainties in biogenic estimates from two models on O_3 and $PM_{2.5}$ is significant. *Koo et al.* [2011] studied the impact of natural emissions on anthropogenic emission control strategies, and found substantial uncertainties in current representation of natural sources, such as lightning NO emissions, which affect O_3 concentrations in the southeastern US where biogenic VOC emissions are large.

Anthropogenic NO_x concentrations may increase the oxidation of BVOC and the formation of O_3 and PM. *Curci et al.* [2009] and *Pun et al.* [2002b] found that O_3 production is more impacted by BVOC emissions in metropolitan regions than in rural areas. O_3 production depends on the initial amounts of VOC (non-methane VOC)/NO_x ratio (in ppbC/ppb, see the ozone isopleth diagram of *Seinfeld and Pandis* [1998] for example). The variations of this VOC/NO_x ratio is used in this paper to understand the variation of the O_3 production regime. *Hoyle et al.* [2011] detailed the mechanisms through which the anthropogenic emissions enhance the formation of biogenic SOA: anthropogenic emissions impact the concentration of oxidants (O_3, OH, NO_3), which oxidize BVOC to form semi-volatile species, and anthropogenic primary organic aerosols may serve as an absorbing medium favoring their condensation. *Carlton et al.* [2010b] estimated that more than 50% of biogenic SOA in the eastern U.S. can be controlled via the influence of anthropogenic emissions on biogenic SOA.

For the Air Quality Model Evaluation International Initiative (AQMEII) study, several air quality models were compared over North America (NA) and Europe [*Rao et al.*, 2011]. One of these models (Polyphemus) is used here to investigate the effect of biogenic emissions on air quality. The model is described in the first section. Then, its performance is evaluated by comparisons to available observations in the Ensemble system [*Bianconi et al.*, 2004] as well as by comparisons with other models of the AQMEII study. Over Europe, four simulations are conducted with and without biomass burning emissions and with different anthropogenic emission inventories and biogenic emission schemes. Over North America (NA), the simulation is conducted using the default data provided for the AQMEII study. Finally, the relative impacts of biogenic and anthropogenic emissions on air quality over Europe and NA are estimated and compared for the different Polyphemus simulations.

B.2 Model Description

The Polyphemus air-quality modeling platform (http://cerea.enpc.f/polyphemus) is used here with the chemistry transport model Polair3D. Polyphemus/Polair3D has already been used for many applications at the continental scale over Europe and East Asia [e.g. *Sartelet et al.*, 2007; *Kim et al.*, 2009; *Roustan et al.*, 2010; *Kim et al.*, 2011b; *Sartelet et al.*, 2008].

For gas-phase chemistry, the Regional Atmospheric Chemistry Mechanism [RACM, *Stockwell et al.*, 1997] is used over Europe and the Carbon-Bond Mechanism [CB05, *Yarwood et al.*, 2005] over NA. Over NA, photolysis rates are computed online, that is the influence of particles on photolysis rates is taken into account [*Real and Sartelet*, 2011]. The aerosol model used is SIREAM-SuperSorgam [*Debry et al.*, 2007a; *Kim et al.*, 2011a]. It models coagulation and

condensation/evaporation. It uses a standard SOA formulation with hydrophobic absorption of SOA into organic particles. The SOA precursors are aromatics, long-chain alkanes, long-chain alkenes, isoprene, monoterpenes and sesquiterpenes. The biogenic SOA formation varies depending on the NO_x regime.

Simulations are performed from 1 July 2006 to 31 August 2006. In all simulations, 9 vertical levels are considered from the ground to 12 km (40m, 120m, 300m, 800m, 1500m, 2400m, 3500m, 6000m, 12000m). The Global Land Cover Facility (GLCF2000) map with 23 categories is used for land use coverage. Initial and boundary conditions are the default AQMEII conditions provided by ECMWF-GEMS. Sea-salt emissions are parameterized following *Monahan et al.* [1986]. The emitted mass of sea salt is assumed to be made of 30.61% of sodium, 55.025% of chloride and 7.68% of sulfate [*Seinfeld and Pandis*, 1998]. Over Europe, the horizontal domain is (35°N-70°N ; 15°W-35°E) with a resolution of 0.25° x 0.25°. The meteorological data correspond to the default MM5 data provided for the AQMEII inter-comparison with 32 vertical levels [*Vautard et al.*, 2012]. In the first of the four simulations conducted over Europe, and labelled Pol 1, anthropogenic emissions are the default AQMEII emissions data provided by TNO [*Pouliot et al.*, 2012]. They are referred to as the TNO anthropogenic emission inventory. Biogenic emissions are computed as in *Simpson et al.* [1999], and referred to as the Simpson biogenic emission scheme. Biogenic (terpene) emissions are distributed among pinene (62.54%), limonene (37.03%) and sesquiterpene (humulene, 0.43%), following *Johnson et al.* [2006] and *Helmig et al.* [1999a,b]. Biomass burning emissions provided by Finnish Meteorological Institute (FMI) for AQMEII are also used in one simulation. Following Mikhail Sofief (communication on AQMEII web site), 50% is emitted between the surface and 200 m, and the remaining 50% is emitted between 200 m and 1000 m. The fire PM emissions are assumed to consist of 70% of $PM_{2.5}$ and 30% of PM_{10}-$PM_{2.5}$. For gaseous species emissions from biomass burning, the PM emission rate is multiplied by 7.88 and then split amongst CO, HCHO, NO_x, NH_3 and SO_2 according to the following fractions: 0.94, 0.013, 0.029, 0.014 and 0.004, respectively. In the other three simulations conducted over Europe, biomass burning is ignored, because $PM_{2.5}$ are strongly over-estimated over Portugal when biomass burning emissions are used. The second simulation labelled "Pol 2" uses the TNO emission inventory for anthropogenic emissions and Simpson for biogenic emissions, as Pol 1. The third simulation, labelled "Pol 3", uses the European Monitoring and Evaluation Program (EMEP, http://www.emep.int/) expert inventory for 2006 and Simpson for biogenic emissions. The time distribution of EMEP emissions, as well as the speciation are detailed in *Sartelet et al.* [2007]. The fourth simulation, labelled "Pol 4", uses the EMEP emission inventory for anthropogenic emissions and the Model of Emissions of Gases and Aerosols from Nature with the EFv2.1 dataset [MEGAN, *Guenther et al.*, 2006]. Differences between the MEGAN and Simpson emission schemes are discussed elsewhere [*Steinbrecher et al.*, 2009]. The two biogenic emission schemes use different methodologies: MEGAN uses canopy-scale emission factors based on leaf area index obtained from the standard MEGAN LAIv database [MEGAN-L, *Guenther et al.*, 2006] whereas Simpson uses leaf-scale emission factors based on GLC2000 land-use categories. Furthermore, although terpene emissions are distributed amongst pinene, limonene and sesquiterpenes with constant factors, different emission factors are used for several species in MEGAN. Table B.1 compares the domain-mean Simpson and MEGAN biogenic emissions. Except for sesquiterpenes, MEGAN emissions are lower than Simpson emissions, especially over the northeastern part of the domain, such as over Finland. Differences in the spatial distribution are also observed, such as in Poland, Croatia or central France. Table B.2 summarizes the emission inventories used in the four simulations.

Over North America, the horizontal domain is (24°N-53.75°N; 125.5°W-64°W) with a resolution of 0.25° x 0.25°. The meteorological data correspond to the default WRF data provided for the AQMEII inter-comparison [*Vautard et al.*, 2012]. As Polyphemus uses a Lat-Lon projection

	Simpson	MEGAN
Isoprene	0.0799	0.0312
Terpenes	0.0436	0.01792
Sesquiterpenes	0.000188	0.00129
NO	0.00118	0.00108

Table B.1: Domain-mean Simpson and MEGAN biogenic emissions (in μg m^{-2} s^{-1}).

	Pol 1	Pol 2	Pol 3	Pol 4
Anthropogenic emissions	TNO	TNO	TNO	Emep
Biogenic emissions	Simpson	Simpson	Simpson	MEGAN
Biomass burning emissions	Yes	No	No	No

Table B.2: Emission inventories used in the four simulations conducted over Europe with Polyphemus.

versus Lambert for WRF, the meteorological data do not cover the whole computational domain. Therefore, the Polyphemus domain (24°N-53.75°N; 125.5°W-64°W) is slightly smaller than the AQMEII domain (23.5°N-58.5°N; 130°W-59.5°W). For the remaining few grid cells missing in the southwestern and southeastern parts of the domain over the ocean, the same meteorological fields as those along the boundary are used. Anthropogenic, biogenic from BEIS3.14 and biomass burning emissions are those provided by US-EPA for AQMEII [*Pouliot et al.*, 2012].

B.3 Base simulations over Europe and North America

B.3.1 Model performance evaluation

The following statistics are computed for comparing the surface levels from the base case simulation with observations between 7 July 2006 and 31 August 2006: root mean square error (rmse), mean fractional error (mfe), mean fractional bias (mfb), and correlation coefficient (r). For O_3, the mean normalized gross error (mnge) and mean normalized gross bias (mngb) are also computed with a cutoff of 80 μg m^{-3} (i.e. about 40 ppb). *Russell and Dennis* [2000] recommend performance criteria for hourly O_3 to be mngb $\leq \pm$ 15% and mnge $\leq$ 30%. For PM, *Boylan and Russell* [2006] propose that a model performance goal is met when both the mfe is less than or equal to +50% and the mfb is within $\pm$30% respectively, and a model performance criterion is met when both mfe $\leq$ +75% and $-60\% \leq$ mfb $\leq$ 60%. The first week is excluded when computing statistics to allow for model initialization and spin-up. Observational data at rural and suburban stations were obtained from the ensemble system. The results of simulations provided by other modeling teams at these stations were also obtained and compared with the results of this modeling study. Over Europe, the observational data include stations from Airbase (http://air-climate.eionet.europa.eu/databases/airbase) and EMEP (http://tarantula.nilu.no/projects/ccc/emepdata.html) databases. Over NA, these data include stations from Interagency Monitoring of Protected Visual Environments (IMPROVE, http://vista.cira.colostate.edu/improve/), the U.S. Environmental Protection Agency (EPA) Aerometric Information Retrieval System (AIRS, http://www.epa.gov/air/data/index.html), and the Environment Canada National Air Pollution Surveillance network (Cast and Naps) databases. Hourly concentration data are used for gaseous species and daily data are used for particulate matter (PM).

Over Europe

Over Europe, the 4 different Polyphemus simulations are compared to observations for O_3, PM_{10} and $PM_{2.5}$ in Tables B.3, B.4 and B.5 respectively. Comparisons for NO_2 and SO_2, PM_{10} sulfate, PM_{10} nitrate and PM_{10} ammonium are presented in the supplementary electronic materials. The comparison of model results with observations is also conducted for 9 different models that participated to the AQMEII inter-comparisons, not including Polyphemus, in order to compare the performances. The mean of the statistics of the AQMEII models is computed as well as the minimum and maximum values.

For all pollutants, the different simulations using Polyphemus perform well according to the performance criteria detailed above and they are within the range of results obtained by other AQMEII models.

For hourly O_3, the average simulated concentration is close to the average measured concentration, although it is slightly lower (73.0 μg m^{-3} measured against between 67.0 and 69.3 μg m^{-3} simulated with rmse between 28.6 and 29.9 μg m^{-3}). The mngb is slightly higher than the range of the model performance criterion of *Russell and Dennis* [2000] ($\leq \pm$ 15%). However, the mnge is well within the range of the model performance criterion of *Russell and Dennis* [2000] ($\leq$ 30%). The different Polyphemus simulations compare well to other AQMEII simulations: the highest rmse of the Polyphemus simulations is lower than the lowest rmse of the AQMEII simulations, while the correlation of Polyphemus are close to the highest correlation of the AQMEII simulations or higher for Pol 4. Other errors and bias are close to the average of the AQMEII simulations. The differences between the different Polyphemus simulations are much lower than differences between the different AQMEII simulations.

O_3 - Europe	Pol 1	Pol 2	Pol 3	Pol 4	AQMEII models		
					Min	Mean	Max
Number of stations	796	796	796	796	790	795.4	796
Mean obs	73.0	73.0	73.0	73.0	73.0	73.0	73.1
Mean sim	68.7	67.0	69.3	67.5	60.9	72.4	97.0
rmse	29.8	29.9	29.2	28.6	30.0	32.8	38.8
correlation	65.8%	66.4%	67.3%	69.8%	56.6%	62.8%	68.6%
mfb	-24.5%	-27.3%	-23.2%	-25.2%	-39.0%	-21.7%	5.7%
mfe	28.3%	30.0%	27.1%	28.1%	17.1%	29.5%	41.8%
mngb	-19.6%	-22.1%	-18.7%	-20.6%	-29.4%	-15.8%	8.3%
mnge	24.0%	25.1%	23.1%	23.8%	18.3%	24.9%	32.6%

Table B.3: Comparisons to observations for surface O_3 over Europe (concentrations and rmse are in μg m^{-3}).

The average PM_{10} concentration is well simulated, although it is slightly under-estimated for Pol 2, Pol 3 and Pol 4 (23.2 μg m^{-3} measured against between 18.5 and 21.1 μg m^{-3} simulated, and rmse between 28.6 and 29.9 μg m^{-3}). The model performance goal of *Boylan and Russell* [2006] is met for all Polyphemus simulations as the mfb is within $\pm$30%, and the mfe is lower than 50%. The different Polyphemus simulations compare well to other AQMEII simulations: the highest rmse is lower than the lowest rmse of the AQMEII simulations. The correlation of Polyphemus are above the average of the correlations of the AQMEII simulations. As for O_3, the differences between the different Polyphemus simulations are much lower than the differences between the different AQMEII simulations.

The average simulated $PM_{2.5}$ concentration is higher than the average measured $PM_{2.5}$ con-

PM_{10} - Europe	Pol 1	Pol 2	Pol 3	Pol 4	AQMEII models		
					Min	Mean	Max
Number of stations	235	235	235	235	235	235	235
Mean obs	23.2	23.2	23.2	23.2	23.2	23.2	23.2
Mean sim	21.1	19.3	19.9	18.5	6.2	12.9	23.4
rmse	15.9	14.7	14.7	15.1	16.2	23.2	24.6
correlation	18.6%	19.1%	19.6%	18.9%	8.2%	17.3%	25.0%
mfb	-5.2%	-11.4%	-9.0%	-16.3%	-111.0%	-64.3%	3.9%
mfe	46.9%	46.6%	46.3%	48.7%	44.5%	80.8%	112.7%

Table B.4: Comparisons to observations for surface PM_{10} over Europe (concentrations and rmse are in μg m^{-3}).

centration (13.3 μg m^{-3} measured against between 17.4 and 19.2 μg m^{-3} simulated, with rmse between 12.0 and 14.0 μg m^{-3}). The model performance goal of *Boylan and Russell* [2006] is met for the mfb for Pol 4, but it is not met for Pol 1 to Pol 3. The model performance goal is not met for the mfe. However the model performance criteria are met for both the mfb and the mfe for all Polyphemus simulations, as the mfb and mfe are within ±60% and lower than 75% respectively. The different Polyphemus simulations compare well to other AQMEII simulations: the mfe and the rmse are in the low range of the AQMEII models, while correlation is in the high range. As for O_3 and PM_{10}, the differences between the different Polyphemus simulations are lower than differences between the different AQMEII simulations.

$PM_{2.5}$ - Europe	Pol 1	Pol 2	Pol 3	Pol 4	AQMEII models		
					Min	Mean	Max
Number of stations	39	39	39	39	39	39	39
Mean obs	13.3	13.3	13.3	13.3	13.3	13.3	13.3
Mean sim	19.2	17.7	18.6	17.4	5.0	12.3	21.4
rmse	14.0	12.0	12.7	12.2	11.4	24.1	69.2
correlation	14.1%	10.6%	9.2%	9.1%	3.2%	11.8%	21.1%
mfb	36.8%	31.7%	35.7%	28.9%	-85.7%	-30.5%	44.9%
mfe	59.6%	57.0%	59.0%	57.4%	55.1%	72.3%	94.2%

Table B.5: Comparisons to observations for surface $PM_{2.5}$ over Europe (concentrations and rmse are in μg m^{-3}).

Over Portugal, where high-intensity biomass burning occurred, taking biomass burning into account (Pol 1) leads to a large over-estimation of $PM_{2.5}$. The mean measured concentration at the 6 rural Airbase stations over Portugal is equal to 14.3 μg m^{-3}. The simulated concentration is equal to 34.1 μg m^{-3} for Pol 1, 15.2 for Pol 2, 17.1 for Pol 3 and 14.0 μg m^{-3} for Pol 3. One of the reason for this large over-estimation of $PM_{2.5}$ at the ground over Portugal for Pol 1 is related to the emission height of biomass burning. For example, *Hodzic et al.* [2007] relates the emission height to the intensity of fire. They estimate that 95% of emissions of the largest fires over Portugal is emitted above the boundary layer, whereas in Pol 1 all the pollutants are emitted in the boundary layer. Therefore, Pol 1 is not considered in the impact study conducted below.

Over North America

Over NA, only one Polyphemus simulation is performed using the default AQMEII emission inputs. It is compared to observations for O_3, PM_{10} and $PM_{2.5}$ in Tables B.6, B.7 and B.8, respectively. The comparison to observations is also conducted for 6 different models that participated to the AQMEII inter-comparisons. Performance evaluation for NO_2 and SO_2 is presented in the supplementary electronic materials, as well as for elemental carbon of $PM_{2.5}$, organic matter of $PM_{2.5}$, sulfate of $PM_{2.5}$, nitrate of $PM_{2.5}$ and ammonium of $PM_{2.5}$.

For O_3, PM_{10} and $PM_{2.5}$, the Polyphemus simulation performs well according to the performance criteria detailed above and it is within the range of results obtained by other AQMEII models.

Although O_3 is over-estimated by Polyphemus (34.0 ppb measured and 43.6 ppb simulated with a rmse of 20.1 ppb), the Polyphemus simulation satisfies the model performance criterion of *Russell and Dennis* [2000]: the mngb and mnge are within ±15% and lower than 30%. Compared to the other AQMEII models, the rmse of the Polyphemus simulation is slightly higher than the higher rmse of all models, but the mfe and mnge corresponds to the average of all models.

For PM_{10}, the average simulated PM_{10} concentration is under-estimated (28.0 μg m^{-3} measured and 15.1 μg m^{-3} simulated with a rmse of 27.5 μg m^{-3}). The model performance goal of *Boylan and Russell* [2006] is not met, but the model performance criterion of *Boylan and Russell* [2006] is met as the mfb is within ±60% and the mfe is less than 75%. Compared to the other AQMEII models, the rmse and mfe of the Polyphemus simulation are lower than the average of all models.

For $PM_{2.5}$, the average simulated $PM_{2.5}$ concentration is over-estimated (12.9 μg m^{-3} measured and 16.1 simulated with a rmse of 9.3 μg m^{-3}). However, the model performance goal of *Boylan and Russell* [2006] is met as the mfb is within ±30% and the mfe is less than 50%. As for PM_{10}, the correlation is lower than the average of all models, but the rmse and the mfe are also lower.

O_3 - NA	Polyphemus	AQMEII models		
		Min	Mean	Max
Number of stations	634	634	634	634
Mean obs	34.0	34.0	34.0	34.0
Mean sim	43.6	33.8	39.4	44.6
rmse	20.2	15.3	17.5	19.9
correlation	60.4%	61.9%	66.0%	69.5%
mfb	-1.3%	-19.2%	-7.4%	1.7%
mfe	24.7%	18.7%	25.3%	39.9%
mngb	3.8%	-12.3%	-2.2%	5.5%
mnge	25.6%	18.5%	23.7%	34.5%

Table B.6: Comparisons to observations for surface O_3 over NA (concentrations and rmse are in ppb).

B.3.2 Spatial distribution

Over Europe

Over Europe, Figure B.1 shows the O_3 concentrations averaged over July and August for Pol 2. The spatial distribution of O_3 shows similar patterns to previously computed distributions [e.g.

PM_{10} - NA	Polyphemus	AQMEII models		
		Min	Mean	Max
Number of stations	638	638	638	638
Mean obs	28.0	28.0	28.0	28.0
Mean sim	15.1	5.4	13.8	30.7
rmse	27.5	24.5	28.4	32.6
correlation	15.1%	11.4%	20.4%	29.3%
mfb	-49.4%	-122.4%	-65.8%	19.1%
mfe	67.5%	49.7%	81.6%	123.7%

Table B.7: Comparisons to observations for surface PM_{10} over NA (concentrations and rmse are in μg m^{-3}).

$PM_{2.5}$ - NA	Polyphemus	AQMEII models		
		Min	Mean	Max
Number of stations	733	733	733	733
Mean obs	12.9	12.9	12.9	12.9
Mean sim	16.1	6.7	12.6	28.2
rmse	9.3	7.0	9.6	20.0
correlation	50.4%	47.5%	60.3%	67.0%
mfb	23.1%	-59.6%	-11.6%	75.4%
mfe	47.7%	33.1%	52.5%	79.6%

Table B.8: Comparisons to observations for surface $PM_{2.5}$ over NA (concentrations and rmse are in μg m^{-3}).

Curci et al., 2009]. O_3 is high in southern Europe, especially over the Black Sea, the Mediterranean Sea and the Baltic Sea. O_3 is low in northern Europe (Finland and northern Sweden). Over land, the highest concentrations are observed over Greece, Italy, Portugal, southern Spain and central Europe. O_3 concentrations lower than the surrounding values are observed over large cities, such as Paris and Milan, because of NO titration. The NO titration is also observed along the sea traffic lines. Maps of O_3 concentrations for simulations other than Pol 2 are not shown, as they are similar despite local differences. Taking into account biomass burning emissions (Pol 1 rather than Pol 2) only slightly increases O_3 locally where biomass burning occurs, such as over Portugal. Using the EMEP rather than the TNO anthropogenic emission inventory, i.e. Pol 3 rather than Pol 2, leads to lower NO titration along the sea traffic lines and therefore higher O_3. Using the MEGAN biogenic emission scheme rather than Simpson, i.e. Pol 4 rather than Pol 3, leads to higher O_3 over the northeastern part of the domain such as over Finland, where MEGAN biogenic emissions are much lower than Simpson's. This O_3 increase with lower biogenic emissions is explained by the very high VOC/NO_x ratio over this part of the domain (see Figure B.7 and section B.4.1).

Figure B.2 shows PM_{10} concentrations averaged over July and August for Pol 2. The spatial distribution of PM_{10} shows similar patterns to previously computed distributions [e.g. *Sartelet et al.*, 2007] with high concentrations over cities, and areas such as northern Italy, the northeastern Spain, and the Netherlands. Although the map of PM_{10} shows high concentrations around cities, the highest concentrations appear to be generated by maritime traffic and by sea-salt emissions. Maps of PM_{10} concentrations for simulations other than Pol 2 are not shown, as they

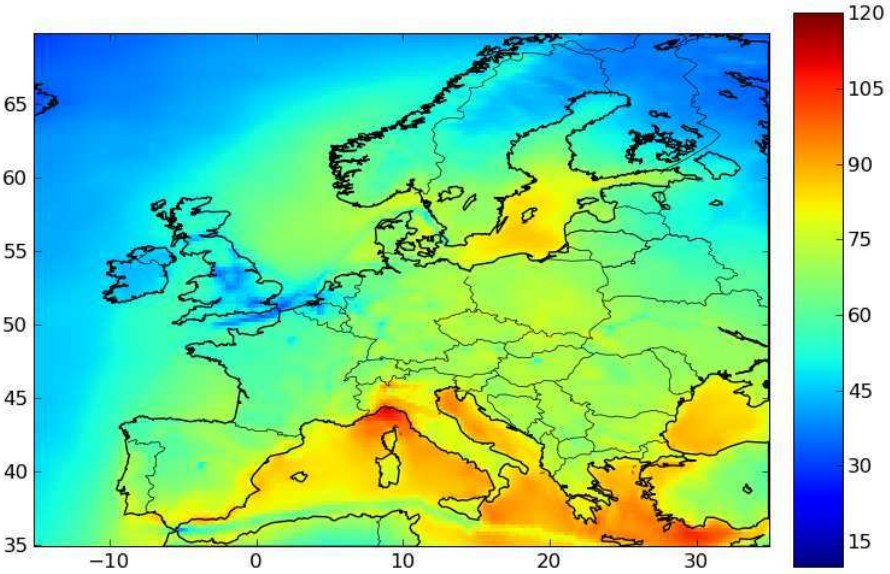

Figure B.1: Surface O_3 concentrations (in μg m^{-3}) over Europe averaged over July and August for Pol 2.

are similar despite local differences. As for O_3, the impact of maritime traffic on the formation of PM_{10} is slightly higher using the TNO rather than the EMEP anthropogenic emission inventory, i.e. Pol 3 rather than Pol 2. Furthermore, the variations of PM_{10} around cities are more sharply defined using TNO than EMEP. Using the MEGAN biogenic emission scheme rather than Simpson, i.e. Pol 4 rather than Pol 3, leads to lower PM_{10} over the northeastern part of the domain such as over Finland (see below).

Figure B.3 shows secondary organic aerosol (SOA) concentrations averaged over July and August using the Simpson (Pol 3, left panel) and MEGAN (Pol 4, right panel) biogenic emission schemes. The spatial distribution is very similar between Pol 2 and Pol 3, i.e. when changing the anthropogenic emission inventory. The overall spatial distribution agrees with previously published distributions [*Kim et al.*, 2011a], and similarities in spatial distributions are found between Pol 3 and Pol 4: high SOA concentrations are observed in Portugal, southwestern France, northeastern Spain, southeastern France, northern Italy, Greece, western Russia, Finland and southern Sweden. However, the spatial distribution locally differs in areas such as in Poland, Croatia and central France. The amplitude of SOA concentrations is very different in Sweden and Finland when using Simpson and MEGAN: the concentrations are locally reduced by a factor 5 when using MEGAN, because of lower biogenic emissions in MEGAN. On average over Europe, the SOA concentrations are reduced by a factor of 2 with MEGAN.

Over North America

O_3 concentrations (see Figure B.4) are higher in the eastern United States than in the western U.S., except in California where high O_3 is simulated. High O_3 concentrations are also simulated along the east coast in the region of New York, as well as near Alabama in the southern U.S., and near the Michigan and Erie Great Lakes. The spatial distribution corresponds well to those simulated by others such as *Luecken et al.* [2008].

The map of $PM_{2.5}$ concentrations averaged over July and August (Figure B.5) shows high concentrations especially around cities. The spatial distribution corresponds well to the ones

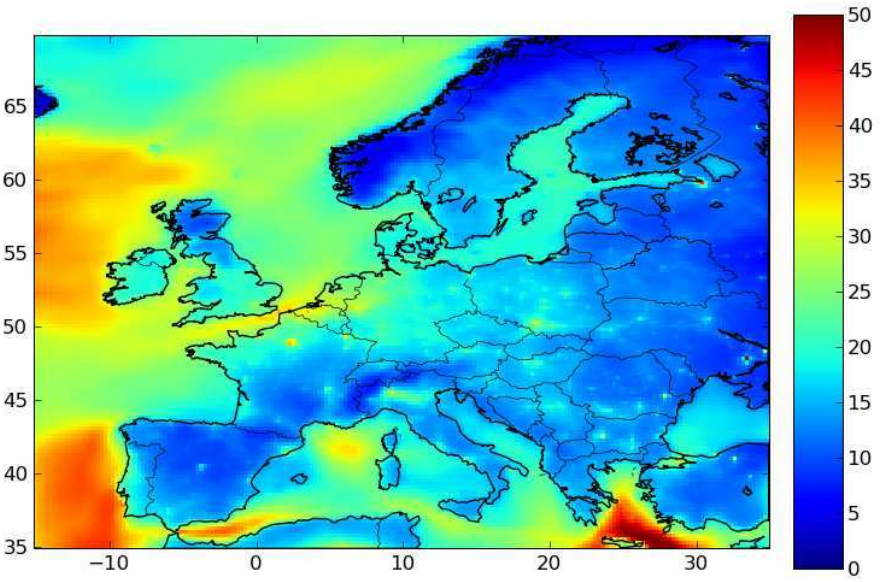

Figure B.2: Surface PM_{10} concentrations (in μg m^{-3}) over Europe averaged over July and August for Pol 2.

simulated in *Bailey et al.* [2007], with high concentrations in California as well as in the eastern U.S. along the coast.

For SOA, the spatial distribution (see Figure B.6) corresponds to that obtained by *Carlton et al.* [2010b]: high concentrations are observed in the southeastern U.S., in California near Los Angeles as well as in the western U.S. However, the concentrations are much higher here with a maximum SOA concentration of 11 μg m^{-3}, against about 1 μg m^{-3} in *Carlton et al.* [2010b] for controllable biogenic SOA. However, the simulated SOA compare relatively well to observations, as shown in the supplementary electronic materials: the average simulated concentration is equal to 3.6 μg m^{-3} against 2.8 μg m^{-3} estimated from measurements, with a mfb of 35.5%. In the southeast where high concentrations are simulated, measurements from the database "AIRS" at the station AIRSUSGA1MCN (-83.65, 32.78) report an average concentration of 7.7 μg m^{-3} over July and August, whereas the simulated concentration is 9.3 μg m^{-3}.

B.4 Impact of biogenic emissions

To estimate the contribution of biogenic emissions to O_3 and PM under current conditions, the methodology of *Pun et al.* [2002b] and *Curci et al.* [2009] is used. The simulation with all emissions is considered as the base case, and a simulation is performed without biogenic emissions (BVOC and NO) to calculate their contribution. As biogenic emissions interact with anthropogenic emissions to form O_3 and secondary PM, a simulation is also performed without anthropogenic emissions to compare the impact.

B.4.1 Over Europe

Over Europe, the sensitivity simulations are performed for the three simulations Pol 2, Pol 3 and Pol 4.

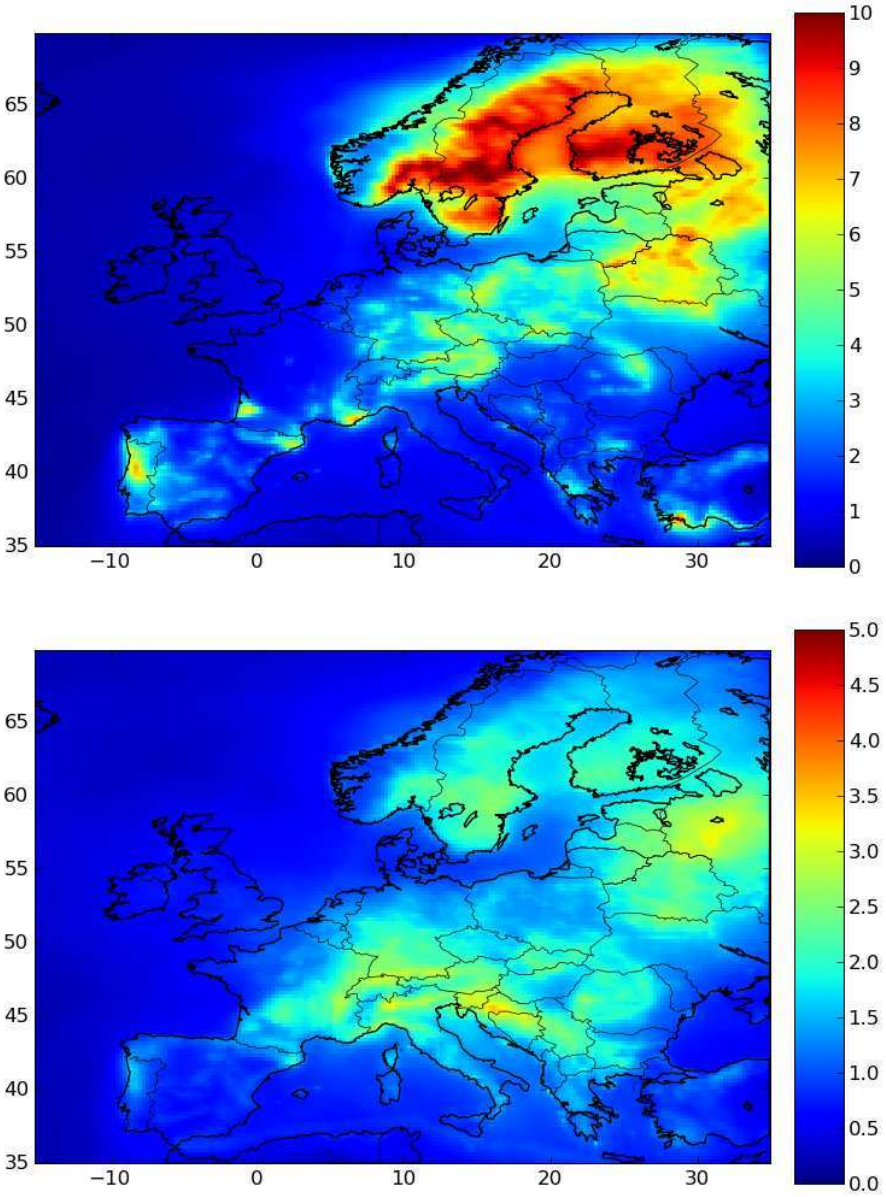

Figure B.3: Surface SOA concentrations (in μg m^{-3}) over Europe averaged over July and August using Simpson (Pol 3, upper panel) and MEGAN (Pol 4, lower panel) biogenic emission schemes.

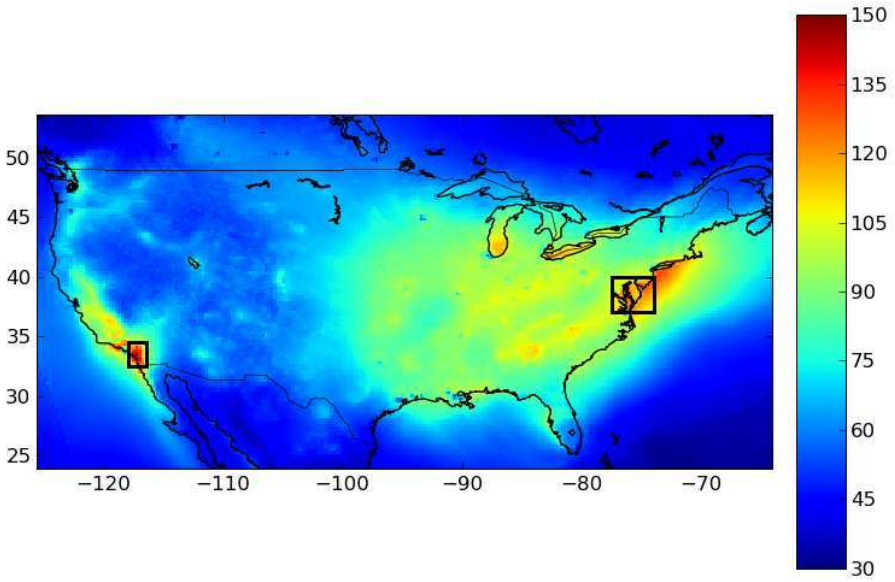

Figure B.4: Surface O_3 concentrations (in μg m^{-3}) over North America averaged over July and August.

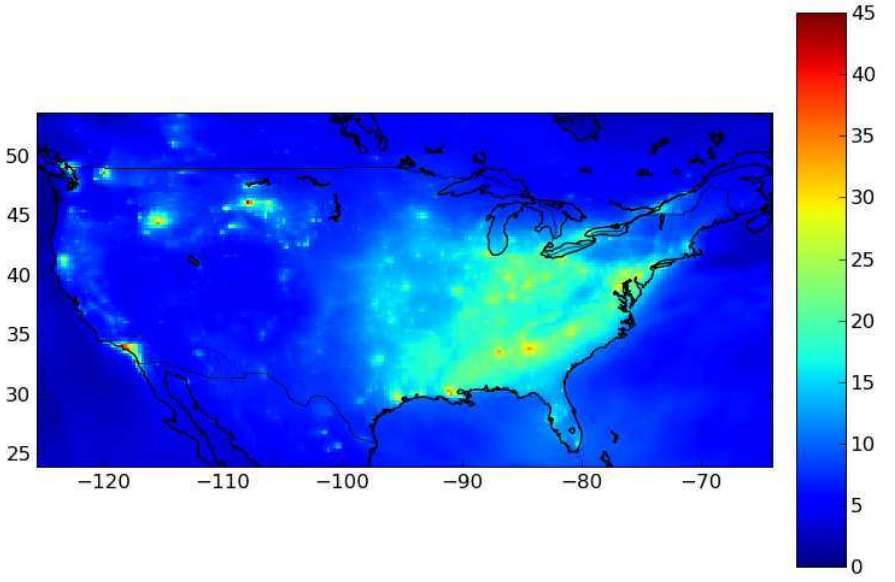

Figure B.5: Surface $PM_{2.5}$ concentrations (in μg m^{-3}) over North America averaged over July and August.

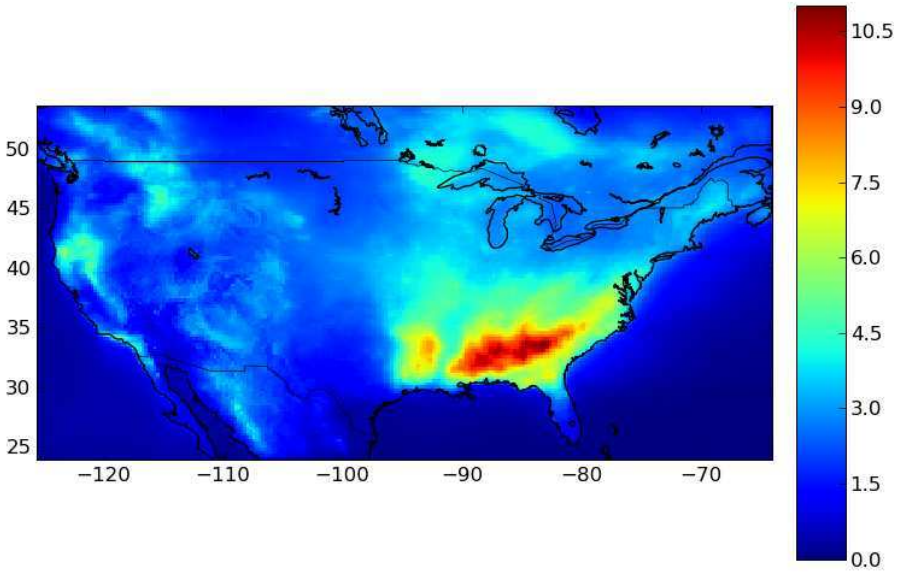

Figure B.6: Surface SOA concentrations (in μg m^{-3}) over North America averaged over July and August.

Table B.9 shows the mean concentrations of O_3, PM_{10} (without Na and Cl), SOA, isoprene SOA and terpene SOA averaged over Europe for July and August.

The impact of biogenic emissions on O_3 concentrations is lower than the impact of anthropogenic emissions. Removing biogenic emissions reduces O_3 concentrations by 10 to 11%, whereas removing anthropogenic emissions reduces O_3 concentration by 38% to 42%. The impact of removing biogenic emissions is lower when MEGAN biogenic emission scheme is used instead of Simpson (10% instead of 11%). This slightly lower impact is a consequence of the lower VOC emissions in MEGAN than in Simpson. Removing anthropogenic emissions also has a lower impact with Pol 4 (-38%) than with Pol 2 or Pol 3 (-41 to -42%), that is when MEGAN biogenic emission scheme is used rather than Simpson. Differences in the impacts of emission computed using the two different anthropogenic emission inventories are small, as EMEP and TNO emissions are commensurate.

To understand the local variations of O_3 concentrations when BVOC emissions are removed, the relative difference in O_3 computed with all emissions and without BVOC emission is shown in Figure B.8 for Pol 2, Pol 3 and Pol 4. Figure B.7 shows the VOC/NO_x concentration ratio for Pol 3 and Pol 4. The regions where the impact of biogenic emissions is high in Figure B.8 are strongly correlated to those where the VOC/NO_x ratio is low compared to surroundings in Figure B.7 (e.g. Milan, northeastern Spain, central Europe). The decrease in O_3 concentration is as high as 30% near cities, which are surrounded by biogenic emissions, such as Milan in Italy, Porto in Portugal or Warsaw in Poland. Around these cities, although BVOC emissions are high, the O_3 regime is probably VOC limited, leading to a strong decrease in O_3 concentrations when BVOC are removed. On the opposite, O_3 increases by as much as 10 to 20% in northern Sweden, Finland and part of Russia, where the VOC/NO_x ratio becomes higher than 200. This increase is removed when using MEGAN. Because BVOC emissions over Sweden and Finland are lower in MEGAN, the VOC/NO_x ratio is lower and O_3 concentrations are not modified by removing BVOC emissions. Although the impact of BVOC emissions on O_3 is almost the same for the two different anthropogenic emission inventories, local differences are important in

central Europe near cities such as in Ukraine and Lithuania. Sea-traffic also has a larger impact using Pol 2 (TNO) than Pol 3 (EMEP).

PM_{10} is much more impacted by anthropogenic than biogenic emissions: the concentration decreases by 8 to 21% on average when biogenic emissions are removed, whereas it decreases by as much as 54 to 62% when anthropogenic emissions are removed. As for O_3, differences in the impacts of emission computed using the two different anthropogenic emission inventories are small. The impact of removing biogenic emissions is lower when using MEGAN rather than the Simpson biogenic emission scheme (8% for MEGAN and 21% for Simpson).

As SOA is mostly formed from isoprene (20% to 23%) and terpenes (62% to 67%) in our simulations, it is strongly impacted by biogenic emissions. SOA is very low when biogenic emissions are ignored: the concentrations are reduced by 87% to 88% on average in Pol 2 and Pol 3 and by 72% in Pol 4 where MEGAN is used. However, removing anthropogenic emissions only reduces SOA by 15 to 16%.

Locally, removing anthropogenic emissions may lead to a large decrease in SOA as shown in Figure B.9. SOA is reduced by as much as 40% to 50% along the maritime traffic lines, as well as around large cities such as Milan or Paris. The map of the relative difference of SOA when all emissions are taken into account and when biogenic emissions are removed is strongly correlated to the map of NO_x emissions, with emphasis where biogenic emissions are high (such as Portugal, southern Spain and Poland). In Figure B.9, the impact of anthropogenic emissions on SOA is shown only for Pol 3 and Pol 4, as the impact is very similar for Pol 2 and Pol 3, as suggested by the average numbers of Table B.9. Differences between Pol 3 and Pol 4 arise mostly in Germany, Poland, Estonia and Belarus, southwestern Spain and southwestern France, which are places where the two biogenic emission schemes lead to different patterns of SOA concentrations, and where significant anthropogenic emissions are present. In contrast, despite large differences in SOA concentrations simulated in Pol 3 and Pol 4 over northern Sweden and northern Finland, the impact of anthropogenic emissions is low over these countries because anthropogenic emissions are low.

Removing biogenic emissions does not only affect the biogenic compounds of SOA, but also the anthropogenic ones. By providing an absorbing organic mass, the biogenic compounds of particles facilitate the condensation of anthropogenic compounds. The absolute impact is low as the concentration of anthropogenic SOA is low compared to biogenic SOA at the continental scale. However, the relative impact of biogenic SOA on anthropogenic SOA may be as high as 40%, as shown in Figure B.10, which shows the relative difference of anthropogenic SOA when all emissions are taken into account and when biogenic emissions are ignored for Pol 3 and Pol 4. The map describing the impact of biogenic SOA on anthropogenic SOA is strongly correlated with the map of biogenic SOA concentrations. The relative impact is higher in Pol 3 than in Pol 4 as biogenic emissions are higher.

B.4.2 Over North America

The contributions of biogenic and anthropogenic emissions to domain-wide averaged concentrations of O_3, PM_{10}, SOA, isoprene SOA and terpene SOA over North America are shown in Table B.10.

Removing biogenic emissions reduces O_3 concentrations by about 20% on average, whereas removing anthropogenic emissions reduces O_3 concentrations by 49%. This result is consistent with the seminal work of *Pun et al.* [2002b] who estimated the contribution of biogenic emissions to O_3 to be less than 23% in Nashville/TN and the northeastern U.S., with a contribution between 22% and 34% in urban areas. The contribution of biogenic emissions to O_3 is also observed to be regionally more important around urban areas, especially in the northeastern U.S. and in California near Los Angeles, as shown in Figure B.12, which depicts the relative

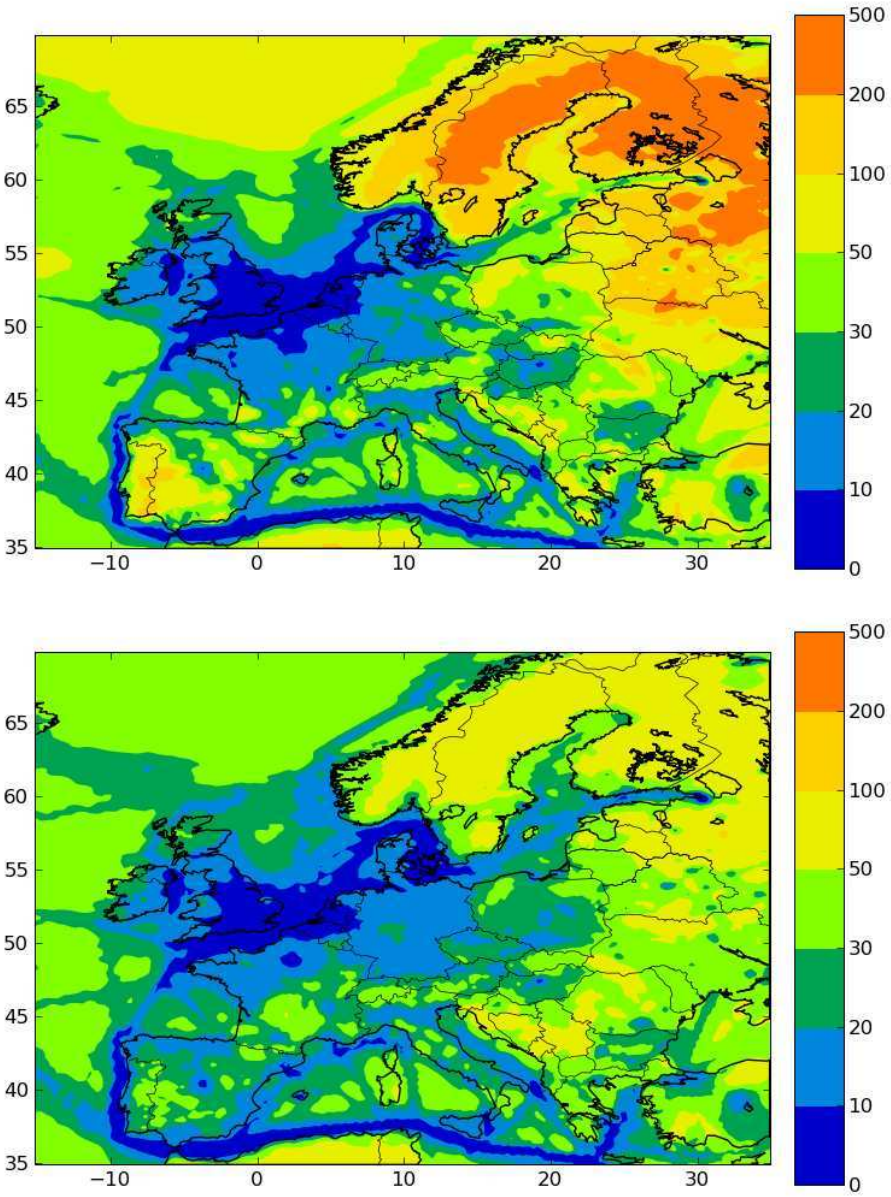

Figure B.7: Ratio of surface VOC over NO_x concentrations averaged over July and August computed using Pol 3 (Simpson biogenic emission scheme, upper panel) and Pol 4 (MEGAN biogenic emission scheme, lower panel).

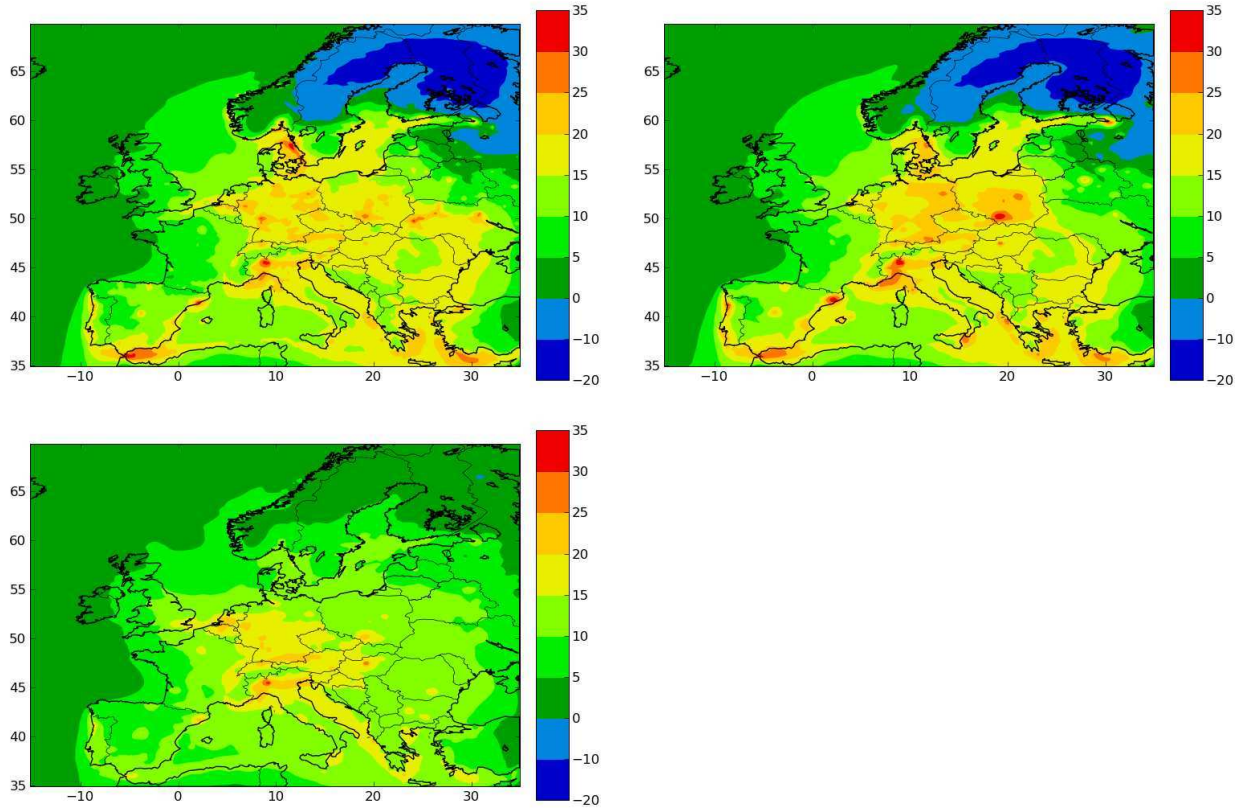

Figure B.8: Relative difference between surface O_3 concentrations (in %) averaged over July and August computed with and without biogenic emissions, using Pol 2 (upper panel), Pol 3 (middle panel) and Pol 4 (lower panel).

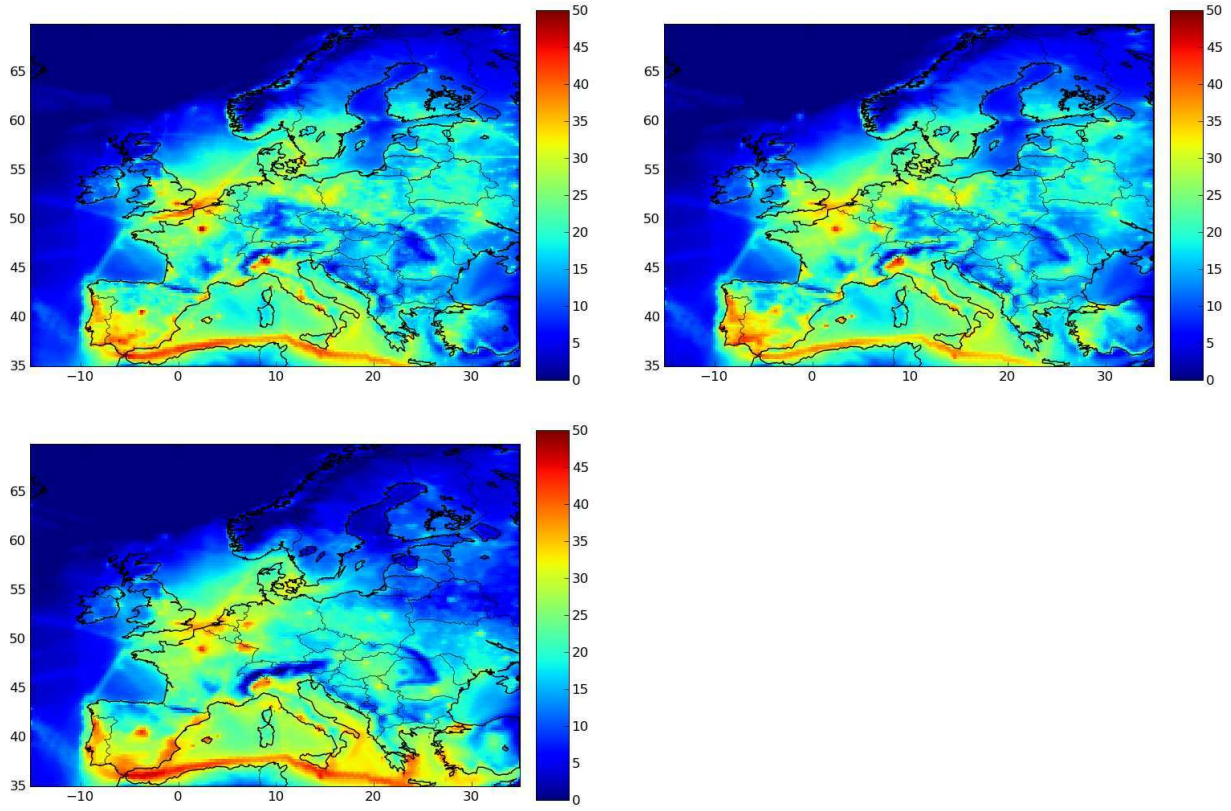

Figure B.9: Relative difference between surface SOA concentrations (in %) averaged over July and August computed with and without anthropogenic emissions, using Pol 2 (upper panel), Pol 3 (middle panel) and Pol 4 (lower panel).

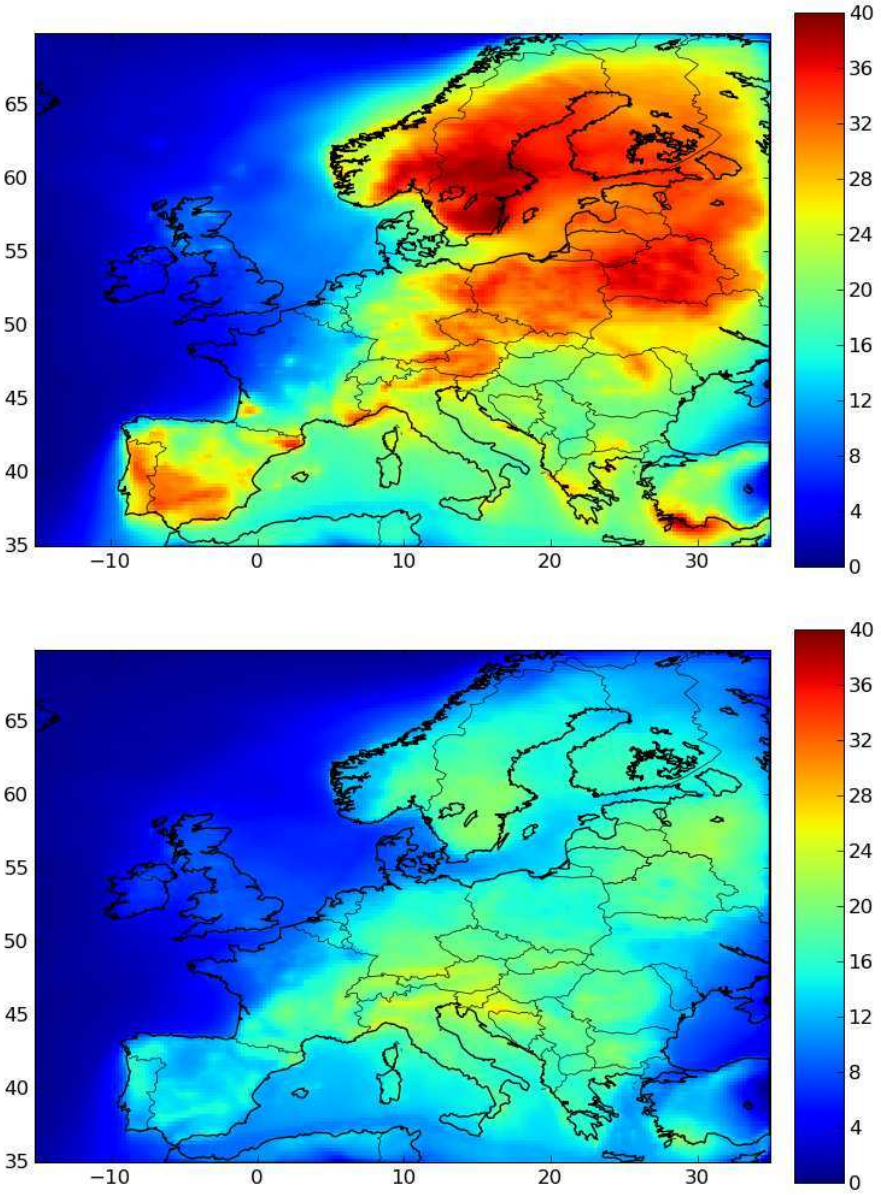

Figure B.10: Relative difference averaged over July and August between surface anthropogenic SOA concentrations (in %) computed with and without biogenic emissions, using Pol 3 (upper panel) and Pol 4 (lower panel).

		Base case	No biogenic emissions	No anthropogenic emissions
O_3	Pol 2	61.9	55.2 (-11%)	36.6 (-41%)
	Pol 3	63.0	56.0 (-11%)	36.6 (-42%)
	Pol 4	61.9	56.0 (-10%)	38.2 (-38%)
PM_{10}	Pol 2	9.4	7.4 (-21%)	4.4 (-54%)
	Pol 3	9.7	7.6 (-21%)	4.4 (-55%)
	Pol 4	8.3	7.6 (-8%)	3.2 (-62%)
SOA	Pol 2	2.6	0.3 (-87%)	2.1 (-16%)
	Pol 3	2.6	0.3 (-88%)	2.1 (-16%)
	Pol 4	1.1	0.3 (-72%)	1.0 (-15%)
Isoprene SOA	Pol 2	0.6	0.0 (-94%)	0.4 (-24%)
	Pol 3	0.6	0.0 (-94%)	0.4 (-24%)
	Pol 4	0.2	0.0 (-84%)	0.2 (-22%)
Terpene SOA	Pol 2	1.7	0.1 (-93%)	1.5 (-10%)
	Pol 3	1.7	0.1 (-93%)	1.5 (-10%)
	Pol 4	0.7	0.1 (-84%)	0.7 (-6%)

Table B.9: Contribution of biogenic emissions to concentration of surface O_3, PM_{10}, SOA, isoprene SOA and terpene SOA averaged over Europe and over July and August (concentrations are in μg m^{-3}). Sea-salt (sodium and chloride) are not included in PM_{10}.

difference of hourly O_3 concentrations averaged over July and August when all emissions are taken into account and when biogenic emissions are removed. O_3 is found to be 26% and 38% lower in the northeastern U.S. (near Washington DC and New Jersey) and California near Los Angeles, respectively (see rectangles in Figure B.12). A high decrease in O_3 concentration is observed over large cities close to high-VOC emission areas when biogenic emissions are removed. As for Europe, the regions where the impact of biogenic emissions is high correspond to those where the VOC/NO_x concentration ratio is low compared to surroundings (large urban centers), as seen by comparing Figures B.11 and B.12.

PM_{10} is not much impacted by biogenic emissions: the concentration decreases by 14% on average when biogenic emissions are removed, whereas it decreases by as much as 50% when anthropogenic emissions are removed. However, biogenic emissions largely contribute to secondary organic aerosols (SOA). If they are not considered, SOA decrease by 90% on average over the domain. In comparison, removing anthropogenic emissions only reduces SOA by 10% on average. SOA are composed mostly of isoprene (23%) and terpene (67%) oxidation products. Isoprene and terpene SOA are reduced by 16% and 7%, respectively, on average over the domain when anthropogenic emissions are removed. However, locally, the reduction may be larger. Large cities, such as Los Angeles, Atlanta, Birmingham, Saint Louis, Washington DC, Chicago and Minneapolis may clearly be identified by looking at the map of the relative difference of SOA concentrations when all emissions are considered and when anthropogenic emissions are removed (Figure B.13). Removing anthropogenic emissions leads to a large decrease of biogenic SOA near these large cities. A decrease as large as 60% is observed locally around cities such as Los Angeles and Houston. A decrease on the order of 60% around cities is consistent with the results of *Carlton et al.* [2010b].

As for the European study, removing biogenic emissions does not only affect the biogenic compounds of SOA, but also the anthropogenic ones. The relative impact of biogenic SOA on anthropogenic SOA may be as high as 60%, as shown in Figure B.14, which shows the relative difference of anthropogenic SOA when all emissions are taken into account and when biogenic

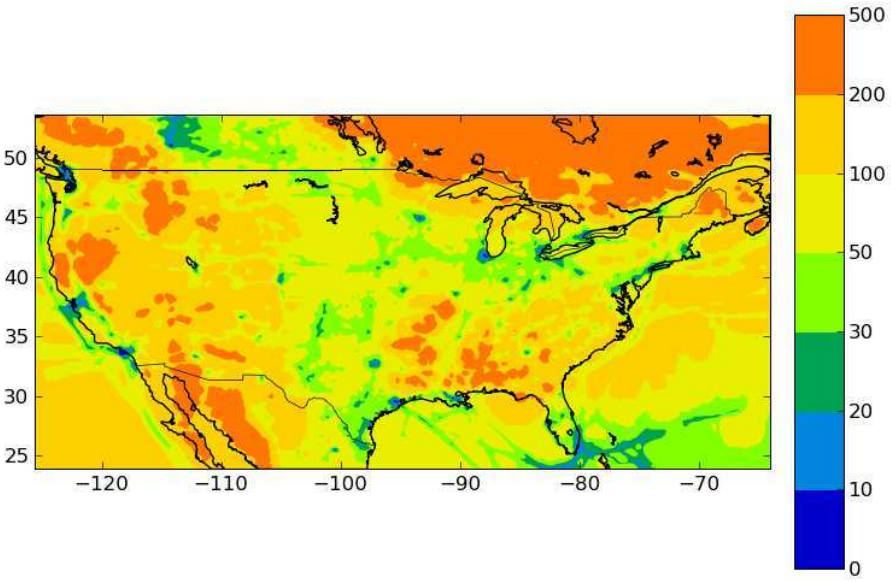

Figure B.11: Ratio of surface VOC over NO_x concentrations averaged over July and August.

emissions are ignored.

	Base case	No biogenic emissions	No anthropogenic emissions
O_3	64.5	51.5 (-20%)	33.2 (-49%)
PM_{10}	9.3	8.1 (-14%)	4.6 (-50%)
SOA	2.3	0.2 (-90%)	2.1 (-10%)
Isoprene SOA	0.5	0.0 (-93%)	0.4 (-16%)
Terpene SOA	1.6	0.1 (-94%)	1.5 (-7%)

Table B.10: Contribution of biogenic emissions to concentration of surface O_3, PM_{10}, SOA, isoprene SOA and terpene SOA averaged over North America and over July and August (concentrations are in μg m^{-3}). Sea-salt (sodium and chloride) are not included in PM_{10}.

B.5 Conclusion

Over both Europe and NA, Polyphemus performances are satisfactory for O_3 and PM with respect to criteria used in the literature, as well as in comparison to other AQMEII models. Over Europe, the simulation with biomass burning emissions over-estimate $PM_{2.5}$ over Portugal, probably because the fire emission height is not accurately modeled.

The impact of biogenic emissions is higher on average over NA than over Europe for O_3, and it is commensurate for SOA. Locally, the impacts of biogenic emissions tends to be higher in NA than in Europe because of the presence in NA of large urban centers surrounded by regions of high biogenic emissions.

Both over Europe and NA, the impact of biogenic emissions on O_3 (-10% to -20%) is lower than the impact of anthropogenic emissions (-38% to -49%). The regions where the impact of biogenic emissions is high correspond to those where the VOC/NO_x ratio is low compared

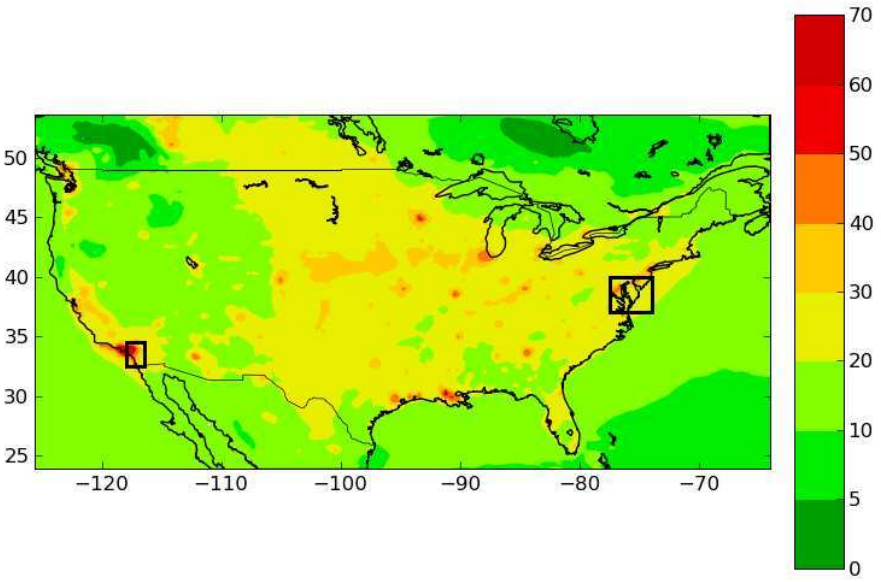

Figure B.12: Relative difference between surface O_3 concentrations (in %) averaged over July and August computed with and without biogenic emissions.

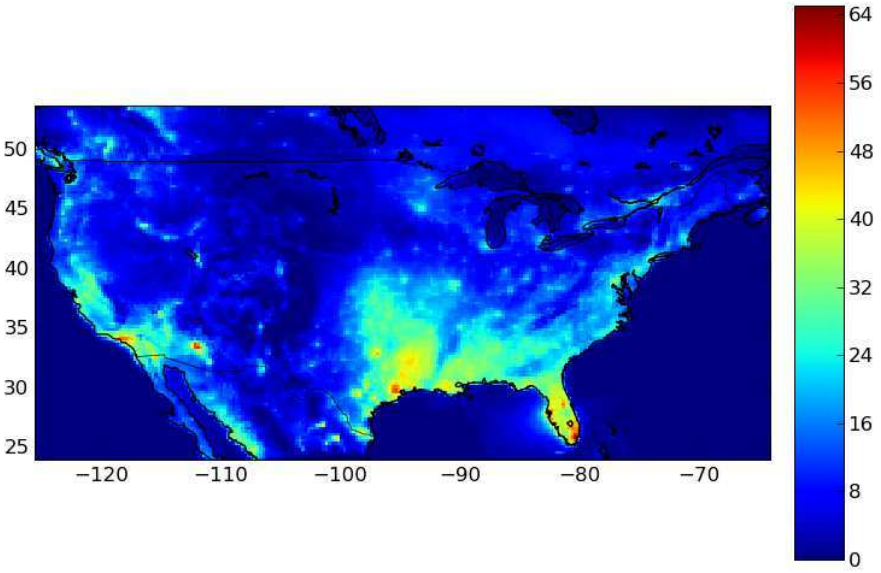

Figure B.13: Relative difference between surface SOA concentrations (in %) averaged over July and August computed with and without anthropogenic emissions.

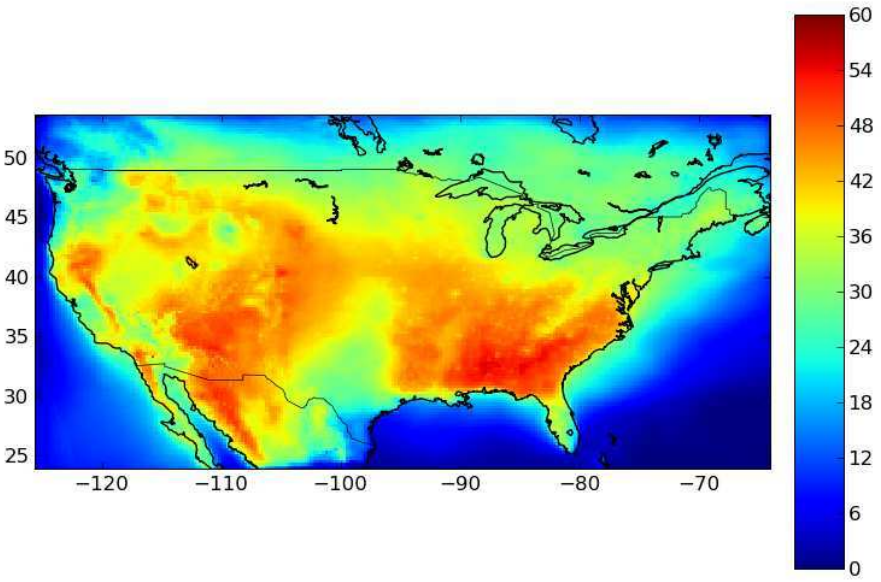

Figure B.14: Relative difference between surface anthropogenic SOA concentrations (in %) averaged over July and August computed with and without biogenic emissions.

to surroundings. For SOA, which are mostly biogenics, the impact of biogenic emissions (72% to 90%) is much greater than the impact of anthropogenic emissions (10% to 16%). However, locally, the impact of anthropogenic emissions may be high (up to 50%, both in NA and Europe), stressing the fact that even biogenic SOA may be controlled for a large part by controlling anthropogenic emissions. The biogenic SOA reduction when all anthropogenic emissions are eliminated varies depending on the chemical precursors: isoprene SOA is more reduced than terpene SOA because of differences in their volatility. Anthropogenic SOA are also impacted by biogenic emissions (absorbing organic mass for SOA), with a relative impact that can be as high as 40% locally. To accurately model SOA, it is, therefore, necessary to accurately model both biogenic and anthropogenic SOA.

Over Europe, for O_3 and SOA, the impact of biogenic emissions is lower in Pol 4 (which uses the MEGAN biogenic emission scheme) than in Pol 2 or Pol 3 (which use the Simpson biogenic emission scheme). The largest differences between the impacts simulated with Pol 4 compared to those simulated with Pol 2 and Pol 3 show that uncertainties in the biogenic emission schemes used here are larger than uncertainties in the two anthropogenic emission inventories.

B.6 Supplementary electronic materials

B.6.1 Model performance evaluation over Europe

The Polyphemus simulations are compared to observations for NO_2, SO_2, sulfate, ammonium and nitrate in Tables B.11, B.12, B.13, B.14 and B.15, respectively. Observational data at rural and suburban stations were extracted from the Ensemble system, except for sulfate, ammonium and nitrate, which are obtained from the EMEP databases.

NO_2 - Europe	Pol 1	Pol 2	Pol 3	Pol 4	AQMEII models		
					Min	Mean	Max
Number of stations	684	684	684	684	681	683.7	684
Mean obs	12.8	12.8	12.8	12.8	12.8	12.8	12.8
Mean sim	8.8	8.3	8.7	8.8	5.6	9.3	15.1
rmse	13.8	13.1	13.2	13.1	12.5	14.1	15.9
correlation	38.0%	41.3%	40.1%	40.4	20.7%	33.2%	42.4%
mfb	-40.9%	-44.3%	-38.4%	-36.2	-66.7%	-32.3%	-2.7%
mfe	77.7%	78.6%	77.1%	76.2%	67.6%	77.8%	90.9%

Table B.11: Comparisons to observations for surface NO_2 over Europe (concentrations and rmse are in μg m^{-3}).

SO_2 - Europe	Pol 1	Pol 2	Pol 3	Pol 4	AQMEII models		
					Min	Mean	Max
Number of stations	501	501	501	501	498	500.7	501
Mean obs	3.7	3.7	3.7	3.7	3.7	3.7	3.8
Mean sim	4.3	4.2	3.5	3.6	1.1	2.5	4.2
rmse	9.5	9.4	9.3	9.3	9.0	9.3	10.2
correlation	14.5%	14.0%	12.9%	12.9%	7.6%	16.0%	20.8%
mfb	19.6%	17.5%	1.7%	2.3%	-110.0%	-46.6%	-0.7%
mfe	79.2%	79.0%	78.5%	78.4%	74.3%	95.0%	127.4%

Table B.12: Comparisons to observations for surface SO_2 over Europe (concentrations and rmse are in μg m^{-3}).

PM_{10} sulfate - Europe	Pol 1	Pol 2	Pol 3	Pol 4
Number of stations	25	25	25	25
Mean obs	2.2	2.2	2.2	2.2
Mean sim	3.1	3.1	3.0	3.0
rmse	1.8	1.8	1.7	1.7
correlation	65.7%	65.4%	69.0%	68.6%
mfb	32.5%	31.6%	31.7%	32.9%
mfe	54.5%	54.3%	53.7%	53.8%

Table B.13: Comparisons to observations for surface $PM_{2.5}NO_3$ sulfate over Europe (concentrations and rmse are in μg m^{-3}).

$PM_{2.5}NO_3$ ammonium - Europe	Pol 1	Pol 2	Pol 3	Pol 4
Number of stations	7	7	7	7
Mean obs	0.8	0.8	0.8	0.8
Mean sim	1.7	1.7	1.9	1.9
rmse	1.4	1.3	1.6	1.6
correlation	42.7%	39.9%	40.1%	39.2%
mfb	79.1%	75.7%	83.7%	86.3%
mfe	92.9%	91.2%	97.9%	99.5%

Table B.14: Comparisons to observations for surface $PM_{2.5}NO_3$ ammonium over Europe (concentrations and rmse are in μg m^{-3}).

$PM_{2.5}NO_3$ nitrate - Europe	Pol 1	Pol 2	Pol 3	Pol 4
Number of stations	11	11	11	11
Mean obs	1.3	1.3	1.3	1.3
Mean sim	1.9	1.7	2.3	2.4
rmse	2.6	2.5	3.1	3.2
correlation	14.3%	13.9%	14.2%	12.6%
mfb	-13.1%	-25.2%	-3.0%	2.2%
mfe	108.2%	112.7%	113.2%	112.7%

Table B.15: Comparisons to observations for surface $PM_{2.5}NO_3$ nitrate over Europe (concentrations and rmse are in μg m^{-3}).

B.6.2 Model performance evaluation over NA

The Polyphemus simulation is compared to observations for NO_2, SO_2, elemental carbon of $PM_{2.5}$, organic mass of $PM_{2.5}$, sulfate of $PM_{2.5}$, ammonium of $PM_{2.5}$ and nitrate of $PM_{2.5}$ in Tables B.16, B.17, B.18, B.19, B.20, B.21 and B.22, respectively. Observational data at rural and suburban stations were extracted from the Ensemble system.

NO_2 - NA	Polyphemus	AQMEII models		
		Min	Mean	Max
Number of stations	315	315	315	315
Mean obs	8.2	8.2	8.2	8.2
Mean sim	8.4	3.0	9.7	17.8
rmse	10.0	8.3	11.6	19.0
correlation	43.1%	41.5%	46.9%	53.5%
mfb	-16.6%	-79.7%	-11.2%	53.2%
mfe	74.4%	67.7%	78.2%	93.4%

Table B.16: Comparisons to observations for surface NO_2 over NA (concentrations and rmse are in ppb). Six models are included in the AQMEII models used for the comparison.

SO_2 - NA	Polyphemus	AQMEII models		
		Min	Mean	Max
Number of stations	379	379	379	379
Mean obs	2.7	2.7	2.7	2.7
Mean sim	3.8	0.7	4.0	8.1
rmse	6.8	6.7	8.0	10.7
correlation	21.0%	12.5%	16.8%	22.3%
mfb	26.6%	-108.8%	0.2%	71.0%
mfe	81.9%	86.6%	94.1%	119.3%

Table B.17: Comparisons to observations for surface SO_2 over NA (concentrations and rmse are in ppb). Six models are included in the AQMEII models used for the comparison.

$PM_{2.5}$EC - NA	Polyphemus	AQMEII models		
		Min	Mean	Max
Number of stations	262	262	262	262
Mean obs	0.4	0.4	0.4	0.4
Mean sim	0.5	0.2	0.5	1.1
rmse	0.5	0.5	0.7	1.3
correlation	51.5%	39.5%	46.5%	56.3%
mfb	23.6%	-70.5%	1.5%	80.6%
mfe	56.5%	50.4%	70.7%	90.4%

Table B.18: Comparisons to observations for surface $PM_{2.5}$ elemental carbon ($PM_{2.5}$EC) over NA (concentrations and rmse are in μg m^{-3}). Five models are included in the AQMEII models used for the comparison.

$PM_{2.5}$OM - NA	Polyphemus	AQMEII models		
		Min	Mean	Max
Number of stations	265	265	265	265
Mean obs	2.6	2.6	2.6	2.6
Mean sim	3.5	0.4	4.7	11.5
rmse	3.1	2.4	5.6	12.7
correlation	24.6%	19.7%	37.1%	50.0%
mfb	41.5%	-132.4%	15.7%	120.3%
mfe	72.1%	56.2%	97.2%	136.7%

Table B.19: Comparisons to observations for surface $PM_{2.5}$ organic mass ($PM_{2.5}$OM) over NA (concentrations and rmse are in μg m^{-3}). Four models are included in the AQMEII models used for the comparison.

$PM_{2.5}SO_4$ - NA	Polyphemus	AQMEII models		
		Min	Mean	Max
Number of stations	113	113	113	113
Mean obs	4.2	4.2	4.2	4.2
Mean sim	4.0	3.4	4.1	4.8
rmse	3.2	1.9	2.5	2.9
correlation	55.7%	63.9%	75.3%	85.8%
mfb	-8.1%	-28.9%	-2.5%	14.6%
mfe	54.8%	32.7%	43.8%	53.0%

Table B.20: Comparisons to observations for surface $PM_{2.5}$ sulfate ($PM_{2.5}SO_4$) over NA (concentrations and rmse are in $\mu g\ m^{-3}$). Four models are included in the AQMEII models used for the comparison.

$PM_{2.5}NH_4$ - NA	Polyphemus	AQMEII models		
		Min	Mean	Max
Number of stations	112	112	112	112
Mean obs	1.4	1.4	1.4	1.4
Mean sim	1.9	1.2	1.4	1.5
rmse	1.4	0.8	1.0	1.2
correlation	50.4%	27.3%	61.5%	78.5%
mfb	28.8%	-4.9%	8.1%	16.7%
mfe	62.9%	41.0%	54.3%	77.7%

Table B.21: Comparisons to observations for surface $PM_{2.5}$ ammonium ($PM_{2.5}NH_4$) over NA (concentrations and rmse are in $\mu g\ m^{-3}$). Four models are included in the AQMEII models used for the comparison.

$PM_{2.5}NO_3$ - NA	Polyphemus	AQMEII models		
		Min	Mean	Max
Number of stations	264	264	264	264
Mean obs	0.4	0.4	0.4	0.4
Mean sim	0.9	0.3	0.4	0.7
rmse	1.8	0.7	0.8	0.8
correlation	35.3%	36.0%	38.0%	40.0%
mfb	-32.6%	-96.7%	-50.3%	60.9%
mfe	129.3%	90.5%	115.7%	129.9%

Table B.22: Comparisons to observations for surface $PM_{2.5}$ nitrate ($PM_{2.5}NO_3$) over NA (concentrations and rmse are in $\mu g\ m^{-3}$). Four models are included in the AQMEII models used for the comparison.

Appendix C

Modeling air pollution in Lebanon: evaluation at a suburban site in Beirut.

Cet appendice est constitué de

Waked, A., Seigneur, C., Couvidat, F., Kim, Y., Sartelet, K., Afif, C., Borbon, A., Formenti, P. and Sauvage, S. (2012). **Modeling air pollution in Lebanon : evaluation at a suburban site in Beirut.**. Soumis à *Atmos. Chem. Phys.*.

Sommaire

Abstract

Beirut, the capital city of Lebanon, which is located on the eastern shore of the Mediterranean basin, experiences high air pollution episodes. Annual average concentrations of coarse and fine particulate matter ($PM_{2.5}$) as well as nitrogen oxides (NO_x) often exceed the World Health Organization (WHO) guidelines. Therefore, improving air quality in this region is essential. The Polyphemus/Polair3D modeling system is used here to investigate air pollution episodes in Beirut during 2-18 July 2011. The modeling domain covers two nested grids of 1 and 5 km horizontal resolution over the greater Beirut and Lebanon, respectively. The anthropogenic emission inventory was developed earlier [*Waked et al.*, 2012b]. The Weather and Research Forecasting (WRF) model is used to generate the meteorological fields and the Model of Emissions of Gases and Aerosols from Nature (MEGAN) is used for biogenic emissions. The results of the study are compared to measurements from a field campaign conducted in the suburb of Beirut during 2-18 July 2011. The model reproduces satisfactorily the concentrations of most gaseous pollutants, the total mass of PM2.5 as well as PM2.5 elemental carbon (EC), organic carbon (OC), and sulfate.

C.1 Introduction

The Middle East region is characterized by a diverse landscape including elevated terrain, semi-arid and Saharan deserts, sea shores and vast plains. Covering fourteen Arab countries as well as Turkey and Iran, the region stretches from Egypt in the West to Iran in the East, Turkey in the North and the Arabian Peninsula in the South. Being an enclosed region, it experiences high pollution episodes, elevated particulate matter (PM) concentrations and major acid deposition problems [*Saliba et al.*, 2006]. Moreover, anthropogenic emissions are increasing rapidly over this region due to large industrialized areas, the absence of any efficient public transport system, dense traffic areas and high population densities [*ESCWA*, 2010; *Lelieveld et al.*, 2009]. In addition, steady winds originating from eastern Europe as well as intense solar radiation contribute to the formation of high levels of secondary pollutants and other reactive species [*Lelieveld et al.*, 2002; *Kouvarakis et al.*, 2000]. To date, few studies have been conducted to investigate air pollution in this region. *Lelieveld et al.* [2002, 2009]; *Smoydzin et al.* [2012] investigated ozone (O_3) pollution over the Middle East region and the Arabian Peninsula. The results showed that in the Arabian Peninsula, high levels of O_3 concentrations were observed especially in summer [*Liu et al.*, 2009a] due to the highly favorable weather conditions and high local air pollutant emissions [*Lelieveld et al.*, 2009]. In particular, nitrogen oxides (NO_x) concentrations in this area are exceptionally high [*Stavrakou et al.*, 2008]. As a result, air pollution in this region needs to be investigated, monitored, and reduced. Lebanon, a small developing country in the Middle East region, located on the eastern shore of the Mediterranean Sea, experiences high pollution episodes due to local emissions because of a growing population, especially in urban areas, the absence of any public transport system [*MoE*, 2005], steady winds from eastern Europe and Saharan dust storms from the desert [*Saliba et al.*, 2007]. Therefore, the country represents a good case study for investigating air pollution in the region. The few measurements conducted in Beirut, the capital city of Lebanon, revealed high levels of nitrogen dioxide (NO_2) with an annual average concentration of 66 $\mu g/m^3$ [*Afif et al.*, 2009] and high levels of particulate matter, PM_{10} and $PM_{2.5}$, with annual concentrations of 64 and 20 mug/m^3, respectively [*Massoud et al.*, 2011]. The levels exceed World Health Organization (WHO) guideline values of 40 mug/m^3 for NO_2 and 20 and 10 mug/m^3 for PM_{10} and $PM_{2.5}$, respectively. Although these measurements provide valuable information on air pollution, they are scarce and limited to a few areas. Therefore, the use of chemical-transport models (CTM) is essential for understanding

the spatio-temporal distribution of gaseous and particulate pollutants in the region. Previous studies have focused on simulating the distribution of O_3 over this region using regional CTM. The EMAC chemistry general circulation model [*Roeckner et al.*, 2006] was used to investigate O_3 levels in the Persian gulf region [*Lelieveld et al.*, 2009] and a fully coupled on-line model (WRF-Chem version 3.3.1) [*Grell et al.*, 2005] was used for the Arabian Peninsula [*Smoydzin et al.*, 2012]. However, no modeling study has yet been conducted for Lebanon or its capital city Beirut. In this study, the WRF-ARW version 3.3 meteorological model [*Skamarock et al.*, 2008b] is used with the Polyphemus/Polair3D CTM [*Mallet et al.*, 2007; *Sartelet et al.*, 2007] to investigate air pollution in Beirut as well as in Lebanon from July 2 till July 18, 2011. WRF has been evaluated against observations in many regions [*Borge et al.*, 2008; *Carvalho et al.*, 2012; *Molders*, 2008] but, to our knowledge, has never been applied to Lebanon. The Polyphemus/Polair3D CTM has been evaluated over Europe [*Sartelet et al.*, 2007, 2012; *Couvidat et al.*, 2012a], Asia [*Sartelet et al.*, 2008], and North America [*Sartelet et al.*, 2012], but not in the Middle East region. This study aims to investigate air pollution in Beirut in July 2011 via meteorological and air quality modeling. The evaluation of WRF and Polyphemus/Polair3D in this region is essential prior to the use of such models for future air quality studies.

The methodology and the model configurations for WRF and Polyphemus/Polair3D are described in Section C.2. The evaluation results for the meteorological and chemical simulations against observations are presented and discussed in Sections C.3 and C.4, respectively. Conclusions are provided in Section C.5.

C.2 Method

C.2.1 Modeling domains

For meteorological modeling, three modeling domains were set on a latitude-longitude projection. A mother domain (D3) with 25 km horizontal resolution covering the Middle East region, as well as some parts of eastern Europe, northern Africa and the Mediterranean Sea, and two nested domains with 5 km resolution for Lebanon (D2) and 1 km resolution for Beirut and its suburbs (D1) were adopted. The two nested domains D1 and D2 are used for the air quality model simulations. A map of the modelind domain is shown in Figure C.1.

C.2.2 Episode selection and observational data set

The modeling study was conducted from July 2 till July 18, 2011. During this period, meteorological and air quality measurements were conducted at the Faculty of Sciences of the Saint Joseph University campus (USJ site) in the region of Mansourieh (33.86 N ; 35.56 E) distant by 6 km from the center of Beirut. Meteorological measurements included wind speed (anemometer), wind direction (weather vane), surface temperature (thermometer), relative humidity (hygrometer) and atmospheric pressure (barometer). Average temperatures in Beirut exceeded 28 °C and clear skies were dominant. No precipitation was recorded during this period. These weather conditions, as well as westerly and easterly winds coming from eastern Europe and Asia, respectively, favored oxidant and secondary organic aerosol (SOA) formation. Trace gases including carbon monoxide (CO), NO_x and O_3 were measured on-line on a 1-min basis using trace gas analyzers [*Michoud et al.*, 2012] while VOC were measured on a 1-hour basis using an on-line Thermal Desorption Gas Chromatography with a Flame Ionization Detector (TD-GC-FID) and on a 5-min basis using a Proton Transfer Reaction Mass Spectrometry (PTRMS). However only, the results obtained from the TD-GC-FID are used for the evaluation of modeled VOC. $PM_{2.5}$ samples were collected using a high-volume sampler (30 m3/h) on a 12-h basis. They were analyzed for OC and EC using the EUSAAR2 protocol [*Cavalli et al.*, 2010], for organic aerosols

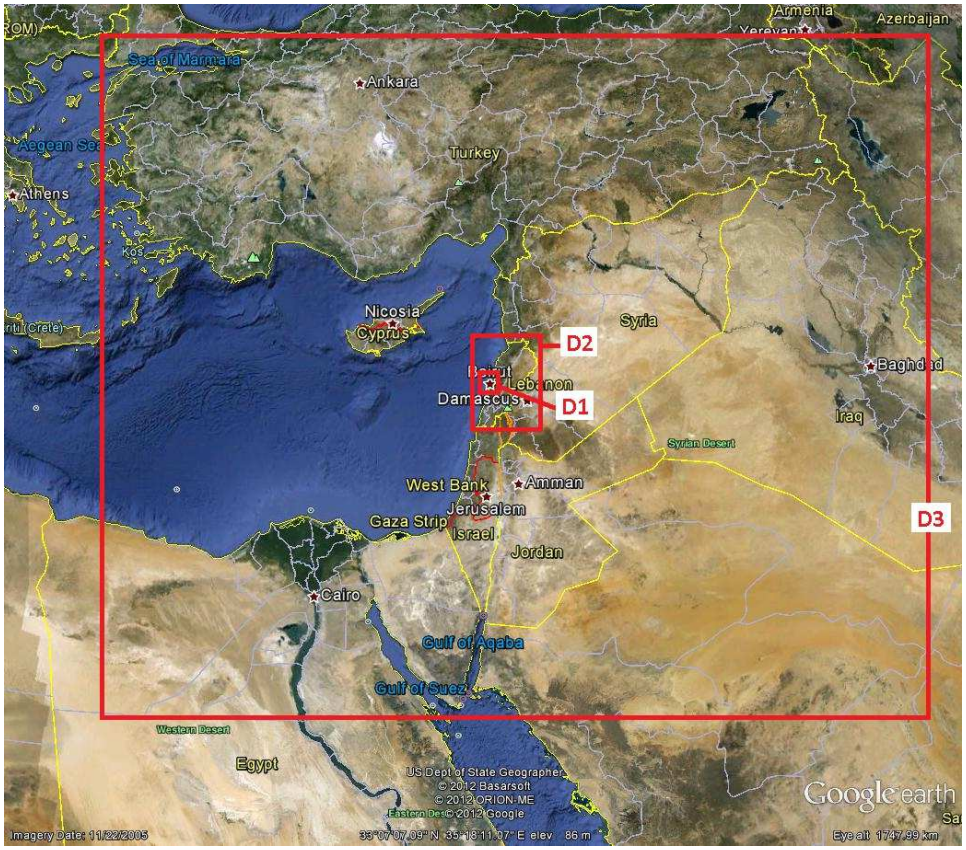

Figure C.1: The modeling domains D1, D2 and D3 used in this study.

using a gas chromatography coupled to a mass spectrometry (GC/MS) technique and for inorganic aerosols using an ion chromatography (IC) technique. The model simulation results are compared with those measurements to evaluate the ability of the model to reproduce major chemical components of photochemical air pollution in Beirut.

C.2.3 Meteorological modeling

WRF-ARW was used to generate the meteorological fields using a two-way nesting approach with a vertical structure of 24 layers covering the whole troposphere. Initial and boundary conditions were driven by the National Centers for Environmental Prediction (NCEP) global tropospheric analyses with 1°x 1°spatial resolution and 6 h temporal resolution. Topography and land use were interpolated from the United States Geological Survey (USGS) global land covers with the appropriate spatial resolution for each domain.

Physical parameterizations used in the model include the Kessler microphysics scheme [*Kessler*, 1969], the RRTM long-wave radiation scheme [*Mlawer et al.*, 1997], the Goddard NASA short-wave scheme [*Chou and Suarez*, 1994], the Grell-Devenyi ensemble cumulus parameterization scheme [*Grell and Devenyi*, 2002] and the Noah land surface model [*Chen et al.*, 2001]. Several physical options such as planetary boundary layer (PBL) dynamics, land surface model as well as several numerical options are available in WRF. A series of model experiments changing one option at a time was conducted to identify the simulation which provides the lowest biases and errors when compared to the observations. Because meteorological models tend to diverge after some integration time (typically two or three days), segmented simulations were also performed. Thus, several two-day restarted simulations were performed to complete an 18

day long simulation. For each simulation, the first 12-hour period was considered as a spin-up period for the model. Because the PBL has an important impact on the near surface wind field, two PBL schemes were tested: the Yunsai University (YSU) PBL scheme [*Hong et al.*, 2006], which is a non-local closure scheme [*Stull*, 1988] and the Mellor-Yamada-Nakanishi and Niino (MYNN) level 2.5 scheme [*Nakanishi and Niino*, 2004], which is a local TKE-based scheme. The MYNN scheme was developed to improve performance of its original Mellor-Yamada model [*Mellor and Yamada*, 1974]. Major differences between the two schemes (MYNN and MY) are the formulations of the mixing length scale and the method to determine unknown parameters. In addition, because the inner domain (D1) includes large urban areas, an urban surface model was used. WRF includes three urban surface models: the urban canopy model (UCM) [*Kusaka et al.*, 2001], which is a single layer model, and two multi-layer models, the Building Environmental Parameterization (BEP) [*Martilli et al.*, 2002] and the Building Energy Model (BEM) [*Salamanca et al.*, 2010]. In this study, UCM was used because it includes the anthropogenic heat release, which is not included in the multi-layer models [*Kim*, 2011]. Using UCM, several influential parameters such as the anthropogenic heat flux, road width, and building width and height values typical for Beirut were chosen, whereas for other parameters (urban ratio for a grid, surface albedo of roof, road and wall, thermal conductivity of roof, road and wall, etc.), the values provided by the WRF configuration file were adopted because of a lack of data. Therefore, a reference building width of 11 m [*CBDE*, 2004] and a road width of 8.5 m were adopted [*Chélala*, 2008]. A building height of 17.9 m was chosen [*Chélala*, 2008] while the mean annual anthropogenic heat flux for Beirut was estimated to be 17 W/m^2 [*IIASA*, 2012].

C.2.4 Air quality modeling

The Polyphemus/Polair3D CTM was used. Aerosol modeling was performed using SIREAM (Size Resolved Aerosol Model) [*Debry et al.*, 2007a] coupled to the Hydrophilic/Hydrophobic Organic (H^2O) model for SOA formation [*Couvidat et al.*, 2012a], ISORROPIA [*Nenes et al.*, 1998] for inorganic aerosols thermodynamics, and the CB05 chemical kinetic mechanism for gas-phase chemistry [*Yarwood et al.*, 2005; *Kim et al.*, 2009, 2011a]. SIREAM segregates the particle size distribution into sections and solves the general dynamic equation by splitting coagulation and condensation/evaporation-nucleation [*Debry et al.*, 2007a]. In H^2O, two anthropogenic and five biogenic SOA precursors species are used as surrogate precursors. In order to account for the fact that primary organic aerosols (POA) are semi-volatile organic compounds (SVOC), an SVOC/EI-POA (Emissions Inventory based POA) value of 5 was adopted following *Couvidat et al.* [2012a] to estimate SVOC emissions.

The USGS land cover was used. Initial and boundary conditions for the outer domain (D2) were extracted from the output of the Model for Ozone And Related chemical Tracers version 4 (MOZART-4; http://www.acd.ucar.edu/wrf-chem/mozart.shtml), which is an off-line global tropospheric CTM [*Emmons et al.*, 2010]. It is driven by NCEP/NCAR reanalysis meteorology and uses emissions based on a database of surface emissions of ozone precursors (POET), Regional Emission Inventory in Asia (REAS) and Global Fire Emissions Database (GEFD2). The results are at 2.8°x 2.8°horizontal resolution for 28 vertical levels. It should be noted that a pre-simulation was performed for the D1 (June 24 till July 2) and D2 (June 15 till July 2) domains to eliminate the effect of initial conditions. Outputs from the meteorological model (WRF-ARW) were used to compute vertical diffusion with the *Troen and Mahrt* [1986] and *Louis* [1979] parameterizations within the PBL. For horizontal diffusion, the CMAQ parameterization was used [*Byun and Schere*, 2009]. Gas and particle deposition as well as sea-salt emissions were pre-processed using relevant meteorological variables. Biogenic emissions were calculated using the Model of Emissions of Gases and Aerosols from Nature [*Guenther et al.*, 2006]. This model, which is designed for global and regional emission modeling, has a global

Table C.1: Numerical options and physical parameterizations considered.

Options	M1	M2	M3	M4	M5
UCM	no	yes	yes	no	no
PBL	YSU	YSU	MYNN	MYNN	YSU
Continuous simulations	yes	yes	yes	yes	no*

*Restarts every two days.

coverage with a 1 km x 1 km resolution.

For anthropogenic emissions, a spatially-resolved and temporally-allocated emission inventory was developed for Lebanon as well as for Beirut and its suburbs in a previous study [*Waked et al.*, 2012b]. This emission inventory is used here. Emissions were spatially allocated using a resolution of 5 km over Lebanon and a resolution of 1 km over Beirut. The inventory includes the emissions of CO, NO_x, sulfur dioxide (SO_2), VOC, ammonia (NH_3), PM_{10}, and $PM_{2.5}$. A wide variety of emission sources including road transport, maritime shipping, aviation, energy production, residential and commercial activities, industrial processes, agriculture, and solvent use are included in this inventory. A bottom-up methodology was used for the major contributing sources such as road transport, cement industries and power plant energy production. For other sources, a top-down approach was adopted. Spatial allocation was performed using population density maps, land cover and road network as well as traffic count data and surveys in many regions [*Waked and Afif*, 2012]. Temporal profiles were allocated with monthly, daily, and diurnal resolutions for all sources. The inventory was developed for a base year of 2010.

C.3 Meteorological simulations

C.3.1 Model simulation configurations

The results obtained from WRF were evaluated with meteorological data collected at the USJ site. Reliable meteorological data at other locations were not available within the D1 and D2 domains, thereby preventing a more complete model performance evaluation. Different simulations from M1 to M5 (Table C.1) were performed in order to select the meteorological simulation which has the lowest biases and errors when compared to observations.

For physical parameterizations, the YSU PBL scheme (simulation M2) and the MYNN scheme (simulation M3) were tested with the use of UCM. In addition, two simulations (M1 and M4) with the YSU and MYNN schemes, respectively, were performed without the use of UCM. To test numerical options, a simulation (M5) was performed using segmented simulations with two-day restarts to assess whether the model tends to diverge significantly after 2 days of simulation.

C.3.2 Results

To evaluate a model, several approaches can be used [*Gilliam et al.*, 2006]. Here, we compare model simulation results to measurements at one site using model performance statistical indicators that include the root mean square error (RMSE), mean fractional bias (MFB), mean fractional error (MFE), normalized mean bias (NMB), normalized mean error (NME), and the correlation coefficient (see Appendix C.6). The results of the statistical evaluation for wind speed and wind direction at 10 m above ground level (agl), surface temperature, relative humidity, and

pressure at 2 m agl are presented in Table C.2 for the five simulations tested. Overall, the model is able to reproduce local wind speed, surface air temperature, and pressure with correlations greater than 0.74 (simulation M1). For wind direction and relative humidity, lower correlations (0.2 - 0.4) are obtained. Wind speed and wind direction have values of MFB and NMB in the range of 20 to 60 %. For surface temperature, relative humidity, and pressure, the statistical biases indicate a low over-prediction of 1 to 10 %. Accordingly, RMSE reported values for surface temperature (1.54 °C) and wind speed (1.34 m/s) are low, those of relative humidity (13 %) and pressure (14 hPa) are moderate, and that of wind direction is high (92°, simulation M1). Thus, model predictions of wind direction are the worst among the five variables. Other studies have shown RMSE values for surface temperature of 2.8 °C in Alaska [*Molders*, 2008], 3.46 °C in the southern U.S. [*Zhang et al.*, 2006], and 2.82 °C in Paris [*Kim*, 2011]. For wind speed, these values were 3 m/s in Portugal [*Carvalho et al.*, 2012], 1.62 m/s in the southern U.S. [*Zhang et al.*, 2006], and 1.93 m/s in Paris [*Kim*, 2011]. For wind direction, RMSE values of 92°are comparable to the value obtained in the southern U.S. (97°, *Zhang et al.* [2006]), but greater than the value obtained in Portugal (52°, *Carvalho et al.* [2012]). Therefore, this meteorological simulation shows satisfactory performance when compared to other similar studies.

C.3.3 Numerical options

The evaluation of segmented simulations is reported in this section because grid nudging of the NCEP initial and boundary conditions was used in all simulations. Comparison between simulation M5 (segmented simulations with two-day restarts) and the other simulations (M1-M4) showed better correlations for all the variables for the long simulations without segmentation, especially for wind components where M5 gives correlations of 0.55 and 0.23 for wind speed and wind direction respectively, compared to values of 0.74 and 0.38 obtained from a long simulation without segmentation such as M1. For other variables, differences between simulations are not significant. RMSE and other statistical indicator values are comparable between M5 and the continuous simulations. This leads to the conclusion that the model does not diverge significantly after some integration time, which results in part from the small size of the D1 domain and its two-way nesting to greater domains. On the other hand, there is considerable uncertainty in the initial conditions, which are generated every two days in the non-continuous simulations because these initial conditions are provided with a spatial resolution of 100 km to be used in a simulation for Beirut with a spatial resolution of 1 km, thereby leading to biases and errors that are higher than those of a continuous simulation.

C.3.4 Physical parameterizations

The MYNN PBL scheme used with UCM (simulation M3) was found to produce the best statistical results for all the variables. Accordingly, this physical option influences wind speed, surface temperature, relative humidity, and pressure. Using this option leads to the best correlations among all the simulations for all variables except for wind speed. The correlations are 0.63, 0.39, 0.91, 0.31, and 0.97 for wind speed, wind direction, surface temperature, relative humidity, and pressure. For MFB, MFE, NMB and NME, no significant differences are observed among these simulations (M1-M4). In summary, M1 with the YSU scheme gives the best results for wind speed and M3 with the MYNN scheme and UCM gives the best results for wind direction and relative humidity.

C.3.5 Best configuration

Temporal variations for wind speed, wind direction, surface temperature, and relative humidity of the two best selected simulations (M1 and M3) are shown from July 2 0h00 till July 17 0h00, 2011 in Figure C.2 because after July 17 0h00, no observations were recorded. The model reproduces wind direction better from July 6 till July 10 in both simulations while from July 2 till July 6 and from July 12 till July 16, the model is not able to reproduce winds originating from the East. The model reproduces satisfactorily relative humidity for the selected period in simulations except on July 4, 5, 15 and 16 when the model over-predicts relative humidity. Surface temperature is better reproduced in simulation M3 than in simulation M1 which over-predicts surface temperature. Lastly, a comparable pattern is observed with lower values for wind speed in simulation M3 due to the use of UCM, which has an effect of decreasing wind speeds due to urbanization. In summary, the model performs better from July 6 till July 10 for all the variables.

Clearly, the PBL scheme influences wind speed, wind direction, and surface temperature [*Borge et al.*, 2008]. Temperature is best modeled with the MYNN scheme using UCM. This result agrees with that obtained by *Kim* [2011] in a simulation over Paris, France. Outside the center of the city, the effect of UCM on temperature is not significant and is compensated by the effect of the PBL scheme. For wind speed and wind direction, no significant variation is observed between M1 and M3. For relative humidity, a better correlation is obtained using the MYNN PBL scheme, and a lower non-significant correlation is obtained for wind speed. Overall, simulation M3 performs slightly better for most variables than simulation M1 particularly for temperature and humidity and we may consider that the correlation of 0.63 obtained for wind speed in simulation M3 is close to the correlation of 0.74 (systematic error of 18 %) obtained in simulation M1 while the correlation for relative humidity of 0.31 obtained in simulation M3 is significantly different from the value of 0.2 (systematic error of 43 %) obtained in simulation M1. In addition, surface air temperature and wind direction were slightly better modeled in simulation M3 in terms of temporal variation (Figure C.2) and NMB (Table C.2). Based on these considerations, the results obtained from simulation M3 are used for air quality modeling.

C.4 Air quality simulations

The results obtained from Polyphemus/Polair3D were evaluated against measurements of gaseous species (O_3, NO_2, VOC and CO) and $PM_{2.5}$ (total mass and major components) collected at the USJ site. Statistical indicators used for model evaluation include MFB, MFE, mean normalized bias (MNB), and mean normalized error (MNE) (see Appendix C.6).

C.4.1 Gaseous species

The base simulation conducted with the MOZART-4 boundary conditions (A1) led to O_3 concentrations within the D1 domain that were too high compared to the observations by nearly a factor of two (see Table C.3). Sensitivity simulations were conducted where emissions of NO_x (A2) and VOC (A3) were reduced by a factor of two; these simulations did not lead to satisfactory O_3 concentrations, in part because of the strong influence of the boundary conditions. A decrease of NO_x emissions leads to an increase in O_3 concentrations (A2) because the study area is saturated in NO_x. Moreover, NO_x concentrations are well reproduced by the model in the base simulation A1. VOC reductions are effective in reducing O_3 concentrations (A3) due to the fact that the area of the study is considered to be VOC-limited, having a VOC to NO_x ratio in the range of 3 to 5. However, the decrease in O_3 concentrations is insufficient to

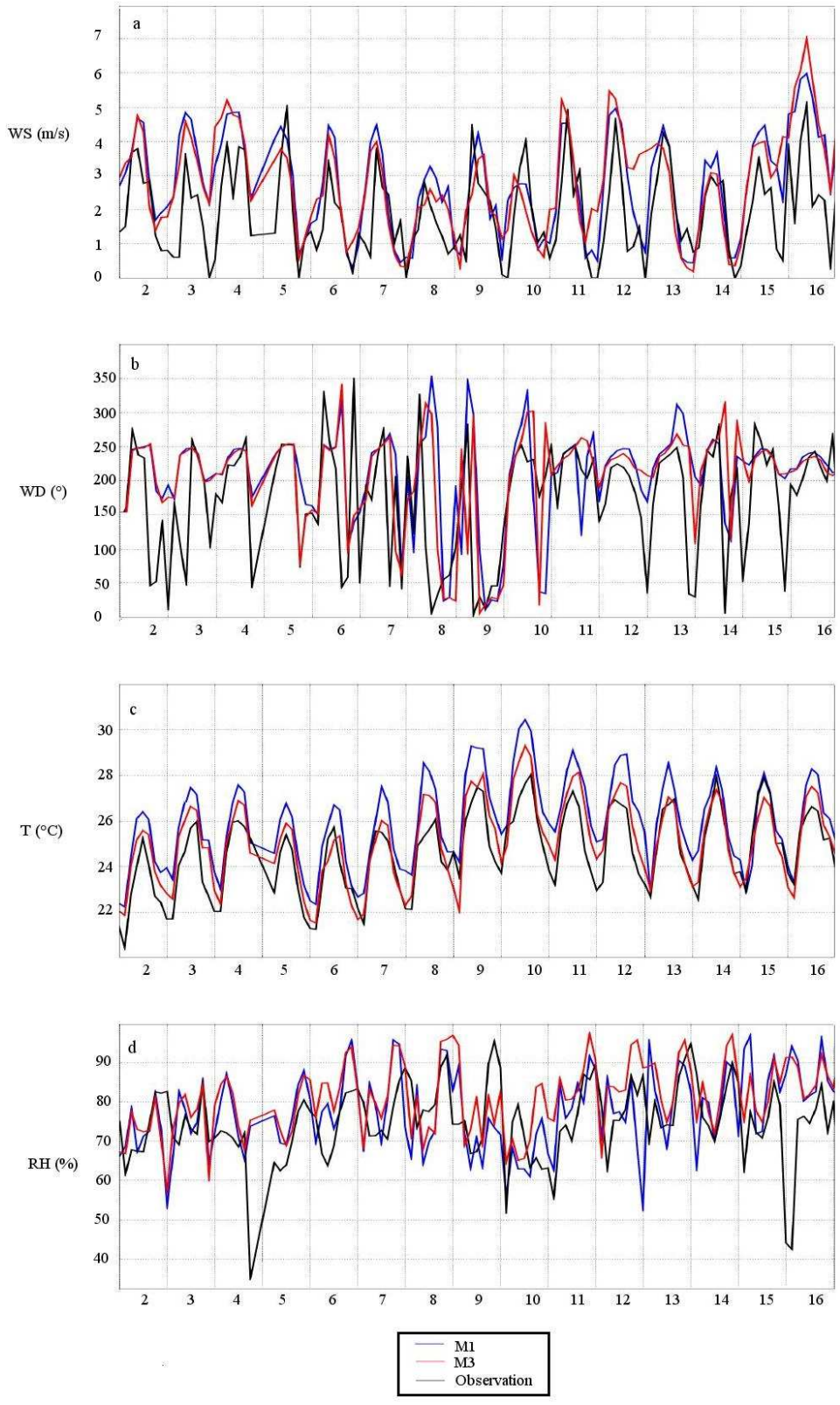

Figure C.2: Temporal variation of meteorological variables (observations and model simulations M1 and M3) from July 2 till July 17, 2011; (a) : wind speed (m/s); (b) : wind direction (°); (c) : air temperature (°C); (d) : relative humidity (%)).

Table C.2: Statistical performance evaluation of the meteorological variables for the WRF simulations.

Wind speed:

Simulation	RMSE (m/s)	MFB (%)	MFE (%)	NMB (%)	NME (%)	Correlation
M1	1.34	34	50	43	55	0.74
M2	1.63	39	55	56	66	0.72
M3	1.54	32	56	45	62	0.63
M4	1.33	26	50	33	53	0.63
M5	1.43	35	54	45	60	0.55

Wind direction:

Simulation	RMSE (°)	MFB (%)	MFE (%)	NMB (%)	NME (%)	Correlation
M1	92.06	23	41	21	35	0.38
M2	93.5	24	41	21	35	0.36
M3	94.23	20	41	19	34	0.39
M4	94.6	20	42	20	35	0.35
M5	132.48	35	62	44	61	0.23

Surface air temperature:

Simulation	RMSE (°C)	MFB (%)	MFE (%)	NMB (%)	NME (%)	Correlation
M1	1.54	5	5	5	5	0.9
M2	1.19	4	4	4	4	0.91
M3	0.88	2	3	2	3	0.91
M4	1.18	4	4	4	4	0.91
M5	1.47	3	5	3	5	0.84

Relative humidity:

Simulation	RMSE (%)	MFB (%)	MFE (%)	NMB (%)	NME (%)	Correlation
M1	12.78	4	12	4	12	0.20
M2	13.46	5	13	5	13	0.14
M3	12.65	8	13	8	13	0.31
M4	12.17	7	12	7	12	0.33
M5	11.62	5	11	5	11	0.21

Atmospheric pressure:

Simulation	RMSE (hPa)	MFB (%)	MFE (%)	NMB (%)	NME (%)	Correlation
M1	13.83	1	1	1	1	0.98
M2	13.85	1	1	1	1	0.98
M3	14.01	1	1	1	1	0.97
M4	14	1	1	1	1	0.97
M5	13.96	1	1	1	1	0.88

Table C.3: Results from simulations A1 to A4 from July 2 to July 18, 2011 at USJ..

	O_3 Mean concentration ($\mu g/m^3$)	CO Mean concentration ($\mu g/m^3$)	NO_x Mean concentration ($\mu g/m^3$)	$PM_{2.5}$ Mean concentration ($\mu g/m^3$)
Obs*	51	519	65	22
A1	95	703	69	21
A2	136	702	31	23
A3	82	702	72	20
A4	50	703	68	21

*Observations at USJ.

match the observed concentrations and VOC concentrations are already underestimated by the model in A1 by a factor of 2 to 3 (Table C.4). An increase of NO_x emissions and a decrease of VOC emissions could lead to satisfactory O_3 concentrations, but would lead to non-satisfactory results for VOC and NO_x modeled concentrations. Therefore, a sensitivity simulation was also conducted with the boundary O_3 concentrations halved (A4). That simulation led to reasonable agreement with the observations for all gaseous species. A comparison between simulation A1 and simulation A4 shows that modifying the O_3 boundary concentrations has negligible effect on CO, NO_x and $PM_{2.5}$ modeled concentrations. Although a recent evaluation of MOZART-4 with ozone study led to satisfactory results [*Emmons et al.*, 2010], a detailed evaluation with PBL O_3 data in the Middle East region has not been conducted because of a lack of data. Better characterization of PBL air pollution concentrations in that region is needed to obtain realistic O_3 boundary concentrations.

This strong influence of boundary conditions which leads to a significant overestimation of O_3 concentrations may be due to the fact that the MOZART-4 data used during this study have a horizontal resolution of 280 km and are used as boundary conditions for a domain D2 with a horizontal resolution of 5 km. It is possible that the use of an intermediate domain of 25 or 50 km horizontal resolution may decrease the uncertainties generated by the MOZART-4 data. However, an emission inventory for the Middle East region is not currently available and the use of an intermediate domain D3 for air quality simulation is therefore not feasible. In addition, we compared the results of this simulation to O_3 concentrations measured in the summer of 2004 in Beirut at an urban site [*Saliba et al.*, 2006] in order to assess the accuracy of the simulation at a different location than the one where the measurements are performed. Such comparisons are not true evaluations of the model because the years of the simulation and observations differ. Nevertheless, such comparisons may point to some possible biases in the air quality simulation if the differences cannot be justified. The results show a modeled value of 1585 $\mu g/m^3$ for CO in both simulations A1 and A4 compared to a measured value of 1213 $\mu g/m^3$. For PM_{10}, a value of 47 $\mu g/m^3$ was modeled in both simulations compared to a measured value of 44 $\mu g/m^3$. The modeled O_3 concentrations are 54 $\mu g/m^3$ in simulation A1 and 32 $\mu g/m^3$ in simulation A4, compared to a measured value of 34 $\mu g/m^3$. Clearly, the results obtained from this evaluation show that simulation A4 with modified O_3 boundary conditions leads to better results for O_3 concentrations and has negligible effect on other pollutants. Therefore, simulation A4 is used below.

Average modeled surface concentrations (over both land and sea) of O_3, NO_2, and CO from July 2 to 18 are 50, 49 and 700 $\mu g/m^3$ in the inner domain (D1) and 72, 10 and 240 $\mu g/m^3$ in the outer domain (D2), respectively. The modeled surface spatial distributions of O_3 and

Table C.4: Statistical performance evaluation for O_3, NO_2, NO_x, CO and some VOC at USJ..

Species	Obs[a]	Mod[b]	MFB	MFE	MNB	MNE
O_3 [c]	51	50	-17 %	33 %	-9 %	33 %
NO_x	65	69	27 %	118 %	74 %	108 %
NO_2	54	54	16 %	105 %	42 %	76 %
CO	519	703	20 %	41 %	55 %	73 %
TOL	19[d]	7[e]	-96 %	97 %	-61 %	62 %
XYL	17[f]	8[g]	-87 %	89 %	-55 %	58 %
α-Pinene	0.05	0.1[h]	37 %	97 %	261 %	301 %
Isoprene	0.62	0.4	-94 %	122 %	-14 %	109 %

a) Observed mean concentrations ($\mu g/m^3$).
b) Modeled mean concentrations ($\mu g/m^3$).
c) A threshold value of 80 $\mu g/m^3$ was used for observations.
d) The "TOL" measured species include toluene, ethylbenzene, butylbenzene, isopropylbenzene and propylbenzene.
e) The "TOL" modeled species includes also other minor monosubstituted aromatics.
f) The "XYL" measured species includes xylene, trimethylbenzenze and ethyltoluene.
g) The "XYL" modeled species includes also other minor polysubstituted aromatics.
h) The "α-pinene" modeled species includes α-pinene and sabinene.

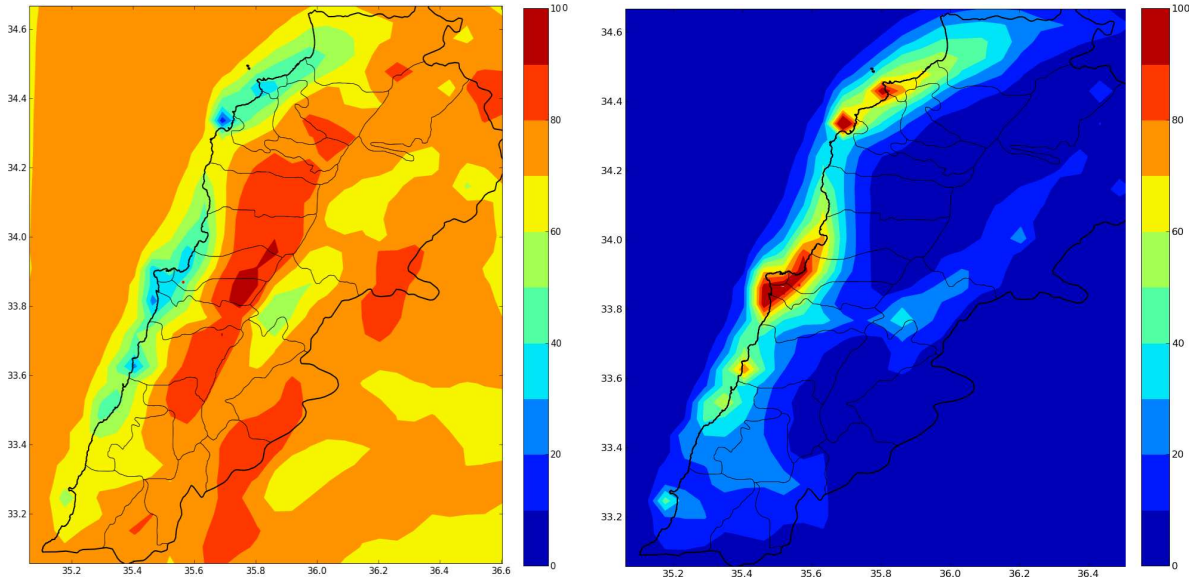

Figure C.3: Modeled average O_3 concentrations (left) and NO_2 concentrations (right) in $\mu g/m^3$ for the outer domain D2 (T = Tripoli ; C = Chekka ; B = Beirut ; J = Jieh).

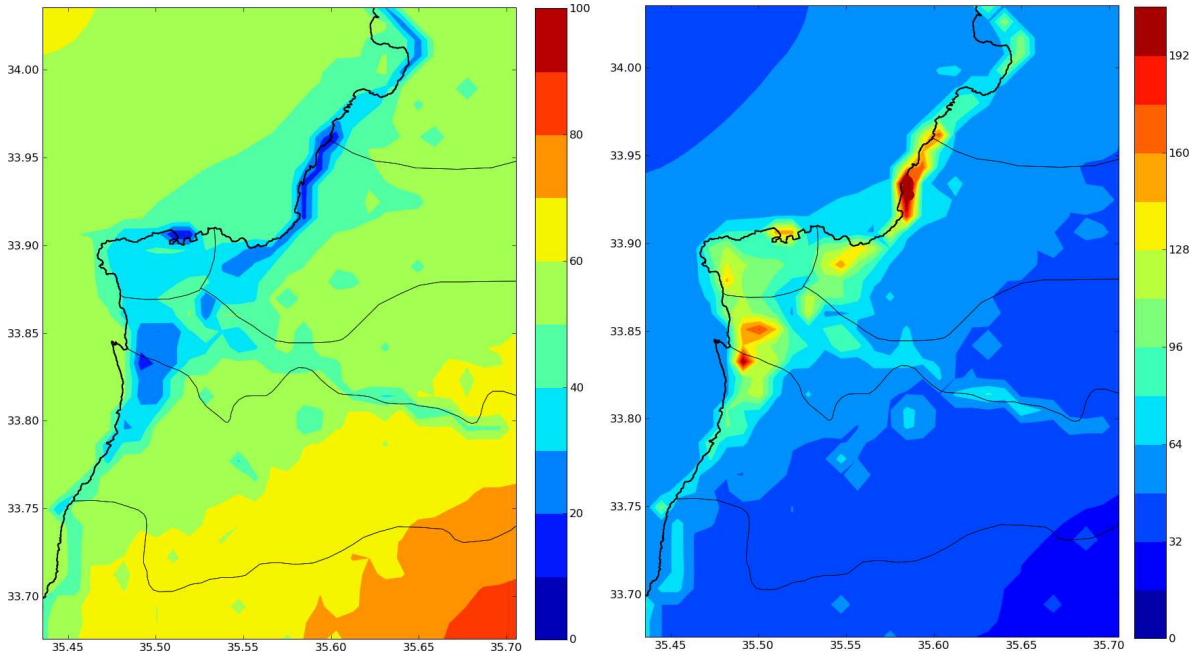

Figure C.4: Modeled average O_3 concentrations (left) and NO_2 concentrations (right) in $\mu g/m^3$ for the inner domain D1.

NO_2 concentrations for D2 and D1 (Figures C.3 and C.4) show lower O_3 concentrations where most NO_x emissions from industries, harbors and road traffic occur and higher values in the mountains. Accordingly, higher concentrations of NO_2 are modeled near the coast in Beirut and its suburbs, in the cities of Tripoli and Chekka in the north and Jieh in the south. Major sources in those areas include dense traffic in urban areas and on highways along the coast, in particular in Beirut and Tripoli, the Zouk power plant located on the coast north of Beirut, the Jieh power plant and the cement plants located in the city of Chekka. Other emissions are generated from the harbors in Beirut and Tripoli and from the international airport located on the coast south of Beirut. Higher O_3 concentrations modeled in the mountains (east of the domain) might be related to a higher VOC/NO_x ratio (Figure C.5), which is more favorable to O_3 formation.

To evaluate the model concentration results at the USJ site, different statistical metrics were calculated for the July 2-18 period, as shown in Table C.4. The model reproduces satisfactorily O_3 concentrations (bias in the range of 9 to 17 %). MNB and MNE values for O_3 of -9 % and 33 %, respectively, are within suggested performance criteria [*Russell and Dennis*, 2000] of 5-15 % for MNB and 30-35 % for MNE. The mean NO_2 concentration is well reproduced by the model but the hourly concentrations show a positive bias. For NO_2, the MNB of 42 % is comparable to the reported value of 35 % obtained during a simulation in the North Sea coastal region in Europe in July 2001 [*Matthias et al.*, 2008] and to the day-time and nigh-time values of -19 % and 31 % reported in Mexico City during the MCMA-2006/MILAGRO field campaign [*Zhang et al.*, 2009]. In addition, a MNB of 74 % for NO_x calculated during this study is in better agreement with observations than the reported value of 101 % for a simulation over Nashville, U.S.A, in July 1999 using the CMAQ model [*Bailey et al.*, 2007]. CO concentrations show an over-prediction by the model on the order of 30 % on average. These results are comparable to those of other studies conducted in Europe, Mexico and the U.S.A [*Matthias et al.*, 2008; *Zhang et al.*, 2009; *Bailey et al.*, 2007]. Biogenic VOC concentrations are small (< 1 $\mu g/m^3$) for both observations and simulations; they show an over-prediction of α-pinene by the model by a factor of two and an under-prediction of isoprene on the order of 30 % on average. However, the α-

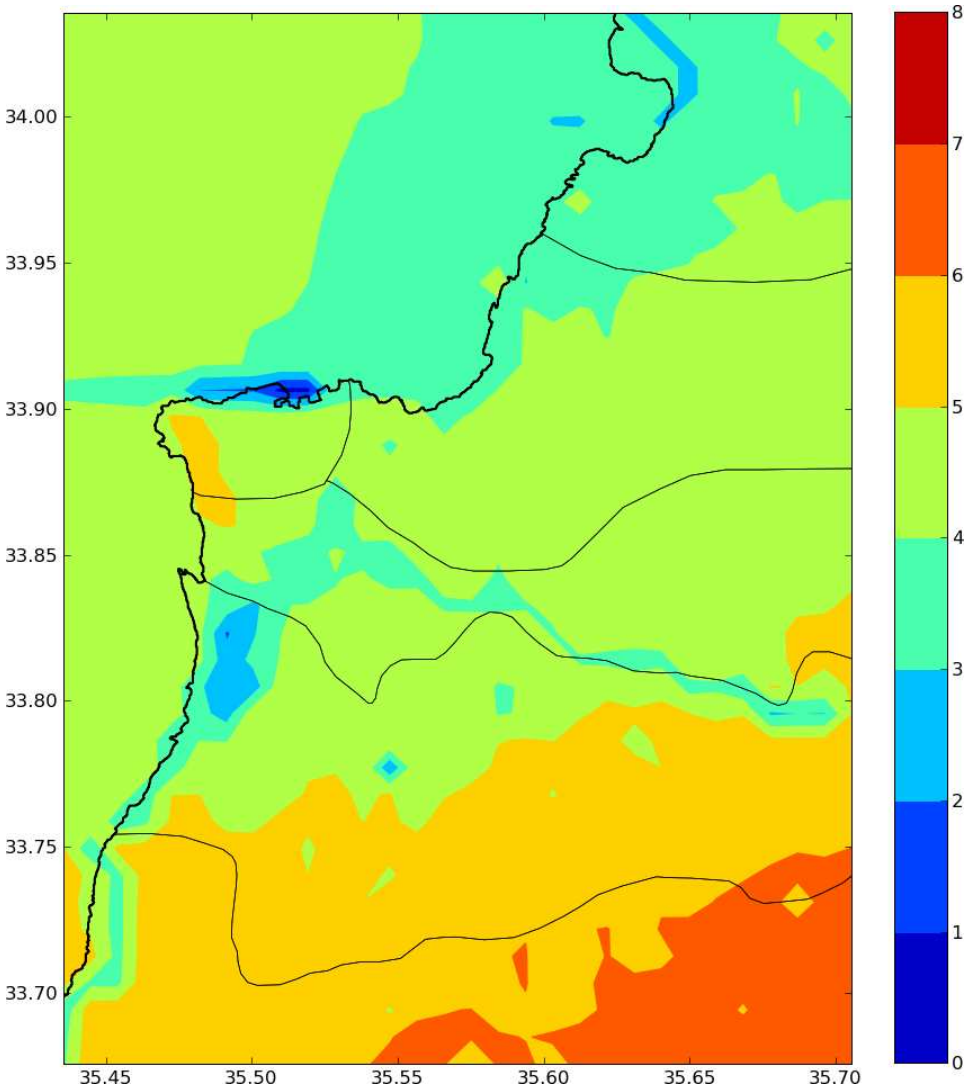

Figure C.5: Modeled average VOC/NO_x ratio for the inner domain D1.

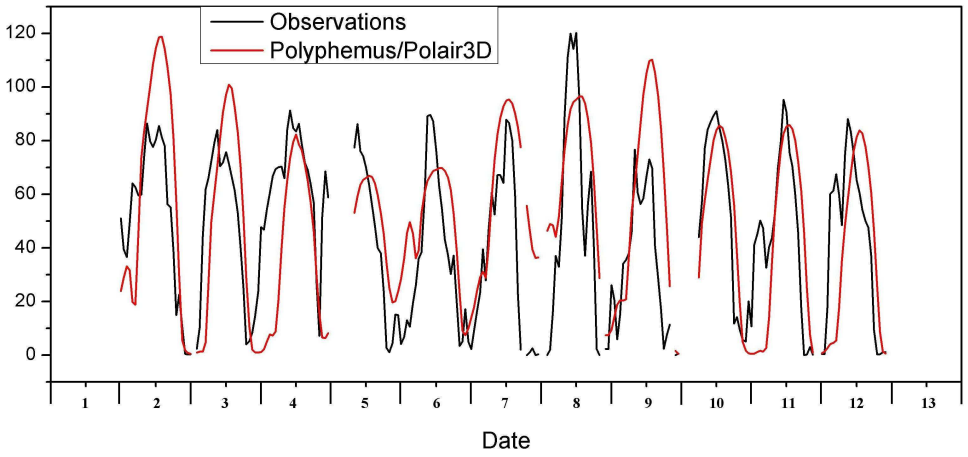

Figure C.6: Temporal variation of observed and modeled O_3 concentrations in $\mu g/m^3$ from July 2 till July 13, 2011.

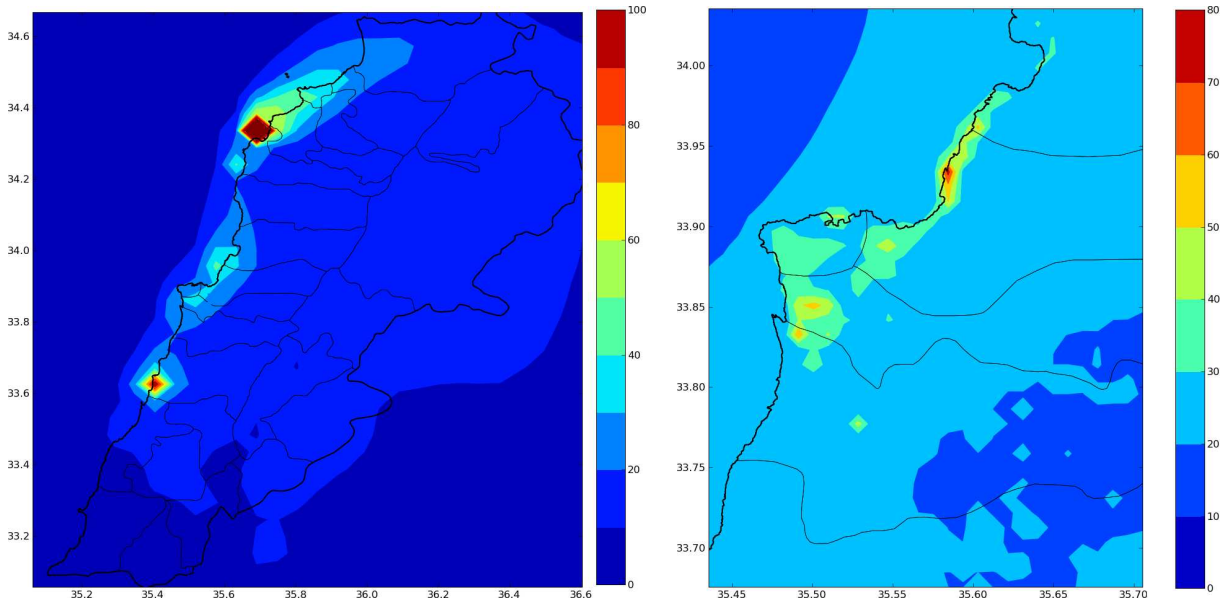

Figure C.7: Modeled average PM2.5 concentrations in $\mu g/m^3$ in Lebanon and in the city of Beirut (T = Tripoli ; C = Chekka ; B = Beirut ; S = Sibline).

pinene model species is a surrogate species that includes α-pinene and sabinene. The MNB value of -14 % reported for isoprene is comparable to the reported values of 14 % and -17 % during a simulation in July 2004 using the MOZART-4 CTM [*Horowitz et al.*, 2007]. Anthropogenic VOC such as toluene and xylene are under-estimated by the model by a factor of 2 to 3. Nevertheless, the results obtained are satisfactory because speciated VOC emissions are associated with large uncertainties and modeled VOC concentrations, which are typically not evaluated, are subject to significant bias. Indeed, monoterpene concentrations are underestimated by almost a factor of two in a simulation over the eastern U.S. using the MOZART-4 CTM [*Horowitz et al.*, 2007] due to a significant underestimation in terpene emissions while isoprene emission estimates can differ by more than a factor of 3 for specific times and locations when different driving variables are used in the emissions calculations [*Guenther et al.*, 2006]. Temporal variations for O_3 are shown in Figure C.6 from July 2 till July 13, 2011 (no measurements were recorded after July 13). The model reproduces satisfactorily the diurnal variation of O_3, with a peak O_3 concentration occurring between 12 pm and 1 pm for both observed and modeled values on most days. However, on some days (2, 3, and 9 July), a second O_3 peak is observed between 9 am and 10 am. This second peak is not reproduced by the model.

C.4.2 Particulate pollutants

Modeled $PM_{2.5}$ average surface concentrations (over both land and sea) from July 2 to 18, 2011 are 10 $\mu g/m^3$ for Lebanon (D2) and 19 $\mu g/m^3$ for Beirut and its suburbs (D1). The spatial distribution of $PM_{2.5}$ concentrations (Figure C.7) shows higher concentrations ($>$ 40 $\mu g/m^3$) in the city of Beirut and its northern suburb, Chekka in the north and Sibline in the south. Dense on-road traffic, industrial sources (Zouk plant north of Beirut and the cement plants near the coast of Chekka and Sibline) and Beirut international airport located south of Beirut lead to significant air pollutant emissions [*Waked et al.*, 2012b]. Lower $PM_{2.5}$ concentrations in the eastern part of the domains ($<$ 20 $\mu g/m^3$), are related to the fact that anthropogenic sources in these areas are less significant. This suggests that $PM_{2.5}$ concentrations are dominated by anthropogenic sources. Indeed, biogenic modeled SOA account for only 4 % of total $PM_{2.5}$

Table C.5: Statistical performance evaluation for $PM_{2.5}$, OC, EC and particulate sulfate, nitrate and ammonium at USJ

Species	Obs[a]	Mod[b]	RMSE($\mu g/m^3$)	MFB	MFE
$PM_{2.5}$	21.9	20.8	9.75	-6 %	37 %
OC	5.6	3.57	2.93	-49 %	54 %
EC	1.8	1.17	1.05	-33 %	56 %
Sulfate	6.06	7.35	5.35	25 %	61 %
Nitrate	0.32	0.0049	0.39	-189 %	189 %
Ammonium	1.87	0.32	1.9	-114%	128%

a) Observed mean concentrations ($\mu g/m^3$).
b) Modeled mean concentrations ($\mu g/m^3$).

modeled concentrations in the inner domain D1 and 8 % in the outer domain D2. Compared to the WHO annual guideline of 10 $\mu g/m^3$ and 24-hour average guideline of 25 $\mu g/m^3$, $PM_{2.5}$ concentrations exceed these values in large urban agglomerations such as Beirut and Tripoli and in the regions of Chekka and Sibline where several cement plants are located and modeled $PM_{2.5}$ are above 100 $\mu g/m^3$.

Statistical model performance at the USJ site is presented in Table C.5. The observed value for $PM_{2.5}$ is a reconstructed mass concentration based on the IMPROVE method (IMPROVE, 2011). Overall, the model reproduces satisfactorily $PM_{2.5}$, OC, EC, and sulfate (SO42-) average concentrations. MFB values in the range of -6 to 49 % and MFE values in the range of 37 to 61 % obtained during this study indicate that the model meets the performance criteria (-60 % $\leqslant$ MFB $\leqslant$ + 60 % and MFE $\leqslant$ 75 %) suggested by Boylan and Russel (2006). For nitrate and ammonium, there is a large underestimation of the model. This high underestimation could be related to uncertainties in NH_3 emissions. The MFB and MFE reported values of -49 % and 54 % obtained for OC during this study are in agreement with the values of -37 % and 50 % reported for Europe in another simulation conducted using Polyphemus/Polair3D [*Couvidat et al.*, 2012a]. In a simulation conducted with the CMAQ model over the eastern U.S., MFB values for $PM_{2.5}$, OC and EC were -3 %, 37 % and 14 %, respectively [*Bailey et al.*, 2007]. Those are lower than the values reported here (Table C.4). However, for sulfate a MFB of 25 % reported here is lower in absolute value than the value of -35 % reported by *Bailey et al.* [2007].

C.5 Conclusion

A modeling study of meteorology and air pollution in Beirut was conducted for the period of July 2-18, 2011 using WRF and Polyphemus/Polair3D. WRF reproduces satisfactorily the diurnal variations for temperature, wind speed, relative humidity and atmospheric pressure and agrees relatively well with observation of wind direction especially from July 6 to July 10, 2011. The WRF results show acceptable performance compared to values reported in other studies in Europe and the United States, however, measurements were available for model performance evaluation only at one site. The air quality modeling results in Beirut, show higher NO_2 concentrations near the coast in the city of Beirut and its northern suburb and lower O_3 concentrations within the city limits. Highest values for $PM_{2.5}$, OC, and EC are modeled within the city limits suggesting that the major sources which lead to the formation of $PM_{2.5}$ are anthropogenic sources. The CTM performance evaluation results show that Polyphemus/Polair3D reproduces

satisfactorily O_3, $PM_{2.5}$, OC, EC, and sulfate concentrations. Statistical indicators obtained for the major pollutants are in the range of other studies conducted in Europe and the U.S.A. Furthermore, the O_3 diurnal variation is well reproduced by the model. This modeling study is the first one conducted for Beirut. It provides an overview of the pollutant concentrations in the summer of 2011. Future work should focus on the improvement of the input data such as the emission inventory and the meteorology in order to reduce bias and errors between modeled and observed concentrations. Moreover, observational data from more than one site are needed in order to better evaluate the model. A measurement campaign will be conducted in 2013 in a road tunnel in Beirut in order to obtain specific road transport emission factors representative of the Lebanese fleet.

C.6 Supplementary materials

Table C.6: Definitions of the statistical indicators.

Indicators	Definitions
Root mean square error (RMSE)	$\sqrt{\frac{1}{n}\sum_{i=1}^{n}(c_i - o_i)^2}$
Mean fractional bias (MFB) and mean fractional error (MFE)	$\frac{1}{n}\sum_{i=1}^{n}\frac{c_i - o_i}{(c_i + o_i)/2}$ and $\frac{1}{n}\sum_{i=1}^{n}\frac{\mid c_i - o_i \mid}{(c_i + o_i)/2}$
Normalized mean bias (NMB) and normalized mean error (NME)	$\frac{\sum_{i=1}^{n}(c_i - o_i)}{\sum_{i=1}^{n} o_i}$ and $\frac{\sum_{i=1}^{n}(\mid c_i - o_i \mid)}{\sum_{i=1}^{n} o_i}$
Mean normalized bias (MNB) and mean normalized gross error (MNGE)	$\frac{1}{n}\sum_{i=1}^{n}\frac{c_i - o_i}{o_i}$ and $\frac{1}{n}\sum_{i=1}^{n}\frac{\mid c_i - o_i \mid}{o_i}$
Correlation coefficient	$\frac{\sum_{i=1}^{n}(c_i - \overline{c})(o_i - \overline{o})}{\sqrt{\sum_{i=1}^{n}(c_i - \overline{c})2}\sqrt{\sum_{i=1}^{n}(o_i - \overline{o})2}}$ with $\overline{o} = \frac{1}{n}\sum_{i=1}^{n} o_i$ and $\overline{c} = \frac{1}{n}\sum_{i=1}^{n} c_i$

c_i: modeled values, o_i: observed values, n: number of data.

Bibliography

Afif, C., A. Dutot, C. Jambert, M. Abboud, J. Adjizian-Gérard, W. Farah, P. Perros, and T. Rizk (2009), Statistical approach for the characterization of NO_2 concentrations in Beirut, *Air Qual. Atmos. Health*, *2*, 57-67, 10.1007/s11869-009-0034-2.

Airparif (2011), Source apportionment of airborne particles in Ile-de-France - final report, *Tech. Rep.*, Airparif, Paris, France.

Allan, J. D., P. I. Williams, W. T. Morgan, C. L. Martin, M. J. Flynn, J. Lee, E. Nemitz, G. J. Phillips, M. W. Gallagher, and H. Coe (2010), Contributions from transport, solid fuel burning and cooking to primary organic aerosols in two UK cities, *Atmos. Chem. Phys.*, *10*, 647-668, 10.5194/acp-10-647-2010.

Altieri, K., S. P. Seitzinger, A. G. Carlton, B. Turpin, G. C. Klein, and A. G. Marshall (2008), Oligomers formed through in-cloud methylglyoxal reactions: chemical composition, properties, and mechanisms investigated by ultra-high resolution FT-ICR Mass Spectrometry, *Atmos. Environ.*, *42*, 1476-1490, 10.1016/j.atmosenv.2007.11.015.

Aphekom (2011), Health impact assessment of short and long-term exposure to ozone and PM in 25 european cities, *Tech. Rep.*, Aphekom.

Appel, K. W., K. M. Foley, J. O. Bash, R. W. Pinder, R. L. Dennis, D. J. Allen, and K. Pickering (2011), A multi-resolution assessment of the Community Multiscale Air Quality (CMAQ) model v4.7 wet deposition estimates for 2002-2006, *Geosci. Model Dev.*, *4*, 357-371, 10.5194/gmd-4-357-2011.

Arhami, M., T. Kuhn, P. M. Fine, R. J. Delfino, and C. Sioutas (2006), Effects of sampling artifacts and operating parameters on the performance of a semicontinuous particulate elemental carbon/organic carbon monitor, *Environ. Sci. Tech.*, *40*, 945–954, 10.1021/es0510313.

Asa-Awuku, A., M. A. Miracolo, J. H. Kroll, A. L. Robinson, and N. M. Donahue (2009), Mixing and phase partitioning of primary and secondary organic aerosols, *Geophys. Res. Lett.*, *36*, L15827, 10.1029/2009GL039301.

Bae, M.-S., J. J. Schauer, J. T. DeMinter, J. R. Tuner, D. Smith, and R. A. Cary (2004), Validation of a semi-continuous instrument for elemental carbon and organic carbon using a thermal-optical method, *Atmos. Environ.*, *38*, 2885–2893, 10.1016/j.atmosenv.2004.02.027.

Bailey, E. M., L. L. Gautney, J. J. Kelsoe, M. E. Jacobs, Q. Mao, J. W. Condrey, B. Pun, S.-Y. Wu, C. Seigneur, S. Douglas, J. Haney, and N. Kumar (2007), A comparison of the performance of four air quality models for the Southern Oxidants Study episode in July 1999, *J. Geophys. Res.*, *112, D05306*, 10.1029/2007JD008675.

Barley, M. H., and G. McFiggans (2010), The critical assessment of vapour pressure estimation methods for use in modelling the formation of atmospheric organic aerosol, *Atmos. Chem. Phys.*, *10*, 749-767, 10.5194/acp-10-749-2010.

Bessagnet, B., L. Menut, G. Curci, A. Hodzic, B. Guillaume, C. Liousse, S. Moukhtar, B. Pun, C. Seigneur, and M. Schulz (2008), Regional modeling of carbonaceous aerosols over Europe-focus on secondary organic aerosols, *J. Atmos. Chem.*, *61*, 175-202, 10.1007/s10874-009-9129-2.

Bessagnet, B., C. Seigneur, and L. Menut (2010), Impact of dry deposition of semi-volatile organic compounds on secondary organic aerosols, *Atmos. Environ.*, *44*, 1781-1787, 10.1016/j.amtosenv.2010.01.027.

Bianconi, R., S. Galmarini, and R. Bellasio (2004), Web-based system for decision support in case of emergency: ensemble modelling of long-range atmospheric dispersion of radionuclides, *Environmental Modelling and Software*, *19*, 401-411, 10.1016/S1364-8152(03)00139-7.

Borge, R., V. Alexandrov, J. José del Vas, J. Lumbreras, and E. Rodriguez (2008), A comprehensive sensitivity analysis of the WRF model for air quality applications over the iberian peninsula, *Atmos. Environ.*, *42*, 8560-8574, 10.1016/j.atmosenv.2008.08.032.

Boylan, J. W., and A. G. Russell (2006), PM and light extinction model performance metrics, goals, and criteria for three-dimensional air quality models, *Atmos. Environ.*, *40*, 4946-4959, 10.1016/j.atmosenv.2005.09.087.

Byun, D., and K. L. Schere (2009), Review of the governing equations, computational algorithms and other components of the models-3 community multi scale air quality (CMAQ) modeling system, *Appl. Mech. Rev.*, *59*, 51.

Calvert, J. G., R. Atkinson, K. H. Becker, R. M. Kamens, J. H. Seinfeld, T. J. Wallington, and G. Yarwood (2002), *The mechanisms of atmospheric oxidation of the aromatic hydrocarbons*, Oxford University Press.

Calvert, J. G., R. G. Derwent, J. J. Orlando, G. S. Tyndall, and T. J. Wallington (2008), *Mechanisms of atmospheric oxidation of the alkanes*, Oxford University Press.

Carlton, A. G., B. J. Turpin, H.-J. L. Lim, K. E. Altieri, and S. Seitzinger (2006), Link between isoprene and secondary organic aerosol (SOA): Pyruvic acid oxidation yields low volatility organic acids in clouds, *Geophys. Res. Lett.*, *33*, L06822, 10.1029/2005GL025374.

Carlton, A. G., B. J. Turpin, K. E. Altieri, S. Seitzinger, A. Reff, H. J. Lim, and B. Ervens (2007), Atmospheric oxalic acid and SOA production from glyoxal: Results of aqueous photooxidation experiments, *Atmos. Environ.*, *41*, 7588-7602, 10.1016/j.atmosenv.2007.05.035.

Carlton, A. G., B. J. Turpin, K. E. Altieri, S. P. Seitzinger, R. Mathur, S. J. Roselle, and R. J. Weber (2008), CMAQ model performance enhanced when in-cloud secondary organic aerosol is included: comparisons of organic carbon predictions with measurements, *Environ. Sci. Technol.*, *42*, 8798-8802, 10.1021/es801192n.

Carlton, A. G., C. Wiedinmyer, and J. H. Kroll (2009), A review of secondary organic aerosol (SOA) formation from isoprene, *Atmos. Chem. Phys.*, *9*(14), 4987-5005, 10.5194/acp-9-4987-2009.

Carlton, A. G., P. V. Bhave, S. L. Napelenok, E. O. Edney, G. Sarwar, R. W. Pinder, G. A. Pouliot, and M. Houyoux (2010a), Model representation of secondary organic aerosol in CMAQv4.7, *Environ. Sci. Tech.*, *44*(22), 8553-8560, 10.1021/es100636q.

Carlton, A. G., R. W. Pinder, P. V. Bhave, and G. A. Pouliot (2010b), To what extent can biogenic SOA be controlled?, *Environ. Sci. Technol.*, *44*, 3376-3380, 10.1021/es903506b.

Carter, W. P. L., D. R. Cocker III, D. R. Fitz, I. L. Malkina, K. Bumiller, C. G. Sauer, J. T. Pisano, C. Bufalino, and C. Song (2005), A new environmental chamber for evaluation of gas-phase chemical mechanisms and secondary aerosol formation, *Atmos. Environ.*, *39*, 7768-7788, 10.1016/j.atmosenv.2005.08.040.

Carvalho, D., A. Rocha, M. Gomez-Gesteira, and C. Santos (2012), A sensitivity study of WRF model in wind simulation for an area of high wind energy, *Environ. Modell. Softw.*, *33*, 23-34, 10.1016/j.envsoft.2012.01.019.

Cavalli, F., M. Viana, K. E. Yttri, J. Genberg, and J. P. Putaud (2010), Toward a standardised thermal-optical protocol for measuring atmospheric organic and elemental carbon: the EUSAAR protocol, *Atmos. Meas. Tech.*, *3*, 79-89, 10.5194/amt-3-79-2010.

CBDE (2004), Consensus of buildings and establishments report, *Tech. Rep.*, Central Administrate of Statistics, Beirut, Lebanon.

Chan, A. W. H., K. E. Kautzman, P. S. Chhabra, J. D. Surratt, M. N. Chan, J. D. Crounse, A. Kürten, P. O. Wennberg, R. C. Flagan, and J. H. Seinfeld (2009), Secondary organic aerosol formation from photooxidation of naphthalene and alkylnaphthalenes: implications for oxidation of intermediate volatility organic compounds (IVOCs), *Atmos. Chem. Phys.*, *9*, 3049-3060, 10.5194/acp-9-3049-2009.

Chan, A. W. H., M. N. Chan, J. D. Surratt, P. S. Chhabra, C. L. Loza, J. D. Crounsoe, L. D. Yee, R. C. Flagan, P. O. Wennberg, and J. H. Seinfeld (2010a), Role of aldehyde chemistry and NO_X concentrations in secondary organic aerosol formation, *Atmos. Chem. Phys. Discuss.*, *10*, 10219-10269, 10.5194/acpd-10-10219-2010.

Chan, M. N., J. D. Surratt, M. Claeys, E. S. Edgerton, R. L. Tanner, S. L. Shaw, M. Zheng, E. M. Knipping, N. C. Eddingsaas, P. O. Wennberg, and J. H. Seinfeld (2010b), Characterization and quantification of isoprene-derived epoxydiols in ambient aerosol in the southeastern United States, *Environ. Sci. Technol.*, *44*, 4590-4596, 10.1021/es100596b.

Chang, W. L., R. J. Griffin, and D. Dabdub (2010), Partitiong phase preferences for secondary organic aerosol via an urban atmosphere, *Proc. National Academy Sci.*, *107*, 6705-6710, 10.1073/pnas.0911244107.

Chélala, C. (2008), Transport routier et pollution de l'air en NO_2, Ph.D. thesis, Université Saint Joseph, Lebanon.

Chen, J., R. J. Griffin, A. Grini, and P. Tulet (2007), Modeling secondary organic aerosol formation through cloud processing of organic compounds, *Atmos. Chem. Phys.*, *7*, 5343-5355, 10.5194/acp-7-5343-2007.

Chen, W., H. Kuze, A. Uchiyama, Y. Suzuki, and N. Takeuchi (2001), One-year observation of urban mixed layer characteristics at Tsukuba, Japan using a micro pulse lidar, *Atmos. Environ.*, *35*, 4273-4280, 10.1016/S1352-2310(01)00181-9.

Chhabra, P. S., R. C. Flagan, and J. H. Seinfeld (2010), Elemental analysis of chamber organic aerosol using an aerodyne high-resolution aerosol mass spectrometer, *Atmos. Chem. Phys.*, *10*, 4111-4131, 10.5194/acp-10-4111-2010.

Chirico, R., A. S. H. Prevot, P. F. DeCarlo, M. F. Heringa, R. Richter, E. Weingartner, and U. Baltensperger (2011), Aerosol and trace gas vehicle emission factors measured in a tunnel using an aerosol mass spectrometer and other on-line instrumentation, *Atmos. Environ.*, *45*, 2182-2192, 10.1016/j.atmosenv.2011.01.069.

Chou, M.-D., and M. J. Suarez (1994), An efficient thermal infrared radiation parameterization for use in general circulation models.

Claeys, M., B. Graham, G. Vas, W. Wang, R. Vermeylen, V. Pashynska, J. Cafmeyer, P. Guyon, M. O. Andreae, P. Araxo, and W. Maenhaut (2004), Formation of secondary organic aerosols through photooxidation of isoprene, *Science*, *303*, 1173-1176, 10.1126/science.1092805.

Clegg, S. L., P. Beimblecombe, and I. Khan (1996), The Henry's law constant of oxalic acid and its partitioning into the atmospheric aerosol, *Idöjár ás*, *100*, 51-68.

Cocker III, D. R., R. C. Flagan, and J. H. Seinfeld (2001), State-of-the-art chamber facility for studying atmospheric aerosol chemistry, *Environ. Sci. Technol.*, *35*, 2594-2601, 10.1021/es0019169.

Compernolle, S., K. Ceulemans, and J.-F. Müller (2009), Influence of non-ideality on condensation to aerosol, *Atmos. Chem. Phys.*, *9*, 1325-1338, 10.5194/acp-9-1325-2009.

Cooke, W. F., C. Liousse, H. Cachier, and J. Feichter (1999), Construction of a 1°x 1° fossil fuel emission data set for carbonaceous aerosol and implementation and radiative impact in the ECHAM4 model, *J. Geophys. Res.*, *104*, 22137–22162, 10.1029/1999JD900187.

Couvidat, F., and C. Seigneur (2011), Modeling secondary organic aerosol formation from isoprene oxidation under dry and humid conditions, *Atmos. Chem. Phys.*, *11*(2), 893–909, 10.5194/acp-11-893-2011.

Couvidat, F., É. Debry, K. Sartelet, and C. Seigneur (2012a), A Hydrophilic/Hydrophobic Organic (H^2O) model: Model development, evaluation and sensitivity analysis, *J. Geophys. Res.*, *117*, D10304, 10.1029/2011JD017214.

Couvidat, F., Y. Kim, K. Sartelet, C. Seigneur, N. Marchand, and J. Sciare (2012b), Modeling secondary organic aerosol in an urban area: Application to Paris, France, *Submitted to Atmos. Chem. Phys.*

Curci, G., M. Beekmann, R. Vautard, G. Smiatek, R. Steinbrecher, J. Theloke, and R. Friedrich (2009), Modelling study of the impact of isoprene and terpene biogenic emissions on European ozone levels, *Atmos. Environ.*, *43*, 1444-1455, 10.1016/j.atmosenv.2008.02.070.

Darer, I. A., N. C. Cole-Filipiak, A. E. O´Connor, and M. J. Elrod (2011), Formation and stability of atmospheric relevant isoprene-derived organosulfates and organonitrates, *Environ. Sci. Technol.*, *45*, 1895-1902, 10.1021/es103797z.

De Haan, D. O., M. A. Tolbert, and J. L. Jimenez (2009a), Atmospheric condensed-phase reactions of glyoxal with methylamine, *Geophys. Res. Lett.*, *36*, L11819, 10.1029/2009GL037441.

De Haan, D. O., A. L. Corrigan, K. W. Smith, D. R. Stroik, J. J. Turley, F. E. Lee, M. A. Tolbert, J. L. Jimenez, K. E. Cordova, and G. R. Ferrell (2009b), Secondary organic aerosol-forming reactions of glyoxal with amino acids, *Environ. Sci. Technol.*, *43*, 2818–2824, 10.1021/es803534f.

Debry, E., K. Fahey, K. Sartelet, B. Sportisse, and M. Tombette (2007a), Technical note: A new SIze REsolved Aerosol Model (SIREAM), *Atmos. Chem. Phys.*, *7*(6), 1537-1547, 10.5194/acp-7-1537-2007.

Debry, E., C. Seigneur, and K. Sartelet (2007b), Organic aerosols in the air quality platform polyphemus: oxidation pathways, hydrophilic/hydrophobic partitioning and oligomerization, International Aerosol Modeling Algorithms, Davis, USA, 5-7 december 2007.

Deguillaume, L., A. Tilgner, R. Schrödner, R. Wolke, N. Chaumerliac, and H. Herrmann (2009), Towards an operational aqueous phase chemistry mechanism for regional chemistry-transport models: CAPRAM-RED and its application to the COSMO-MUSCAT model, *J. Atmos. Chem.*, *64*, 1-35, 10.1007/s10874-010-9168-8.

Donahue, N. (2011), Implementing the 2d vbs, International Aerosol Modeling Algorithms, Davis, USA, 30 november - 2 december 2011.

Donahue, N. M., A. L. Robinson, C. O. Stanier, and S. N. Pandis (2006), Coupled partitioning, dilution, and chemical aging of semivolatile organics, *Environ. Sci. Technol.*, *40*, 2635–2643, 10.1021/es052297c.

Donahue, N. M., S. A. Epstein, S. N. Pandis, and A. L. Robinson (2011), A two-dimensional volatility basis set: 1. Organic-aerosol mixing thermodynamics, *Atmos. Chem. Phys.*, *11*, 3303-3318, doi:10.5194/acp-11-3303-2011.

Dzepina, K., C. D. Cappa, R. M. Volkamer, S. Madronich, P. F. DeCarlo, R. A. Zaveri, and J. L. Jimenez (2011), Modeling the multiday evolution and aging of secondary organic aerosol during MILAGRO 2006, *Environ. Sci. Technol.*, *45*, 3496–3503, 10.1021/es103186f.

Eddingsaas, N. C., D. G. VanderVelde, and P. O. Wennberg (2010), Kinetics and products of the acid-catalyzed ring-opening of atmospherically relevant butyl epoxy alcohols, *J. Phys. Chem. A*, *114*, 8106-8113, 10.1021/jp103907.

Eddingsaas, N. C., C. L. Loza, L. D. Yee, M. Chan, K. A. Schilling, P. S. Chhabra, J. H. Seinfeld, and P. O. Wennberg (2012), α-pinene photooxidation under controlled chemical conditions – part 2: Soa yield and composition in low- and high-no_x environments, *Atmos. Chem. Phys.*, *12*, 7413-7427, 10.5194/acp-12-7413-2012.

Edney, E. O., T. E. Kleindienst, M. Jaoui, M. Lewabdowski, J. H. Offenberg, W. Wang, and M. Claeys (2005), Formation of 2-methyltetrols and 2-methylglyceric acid in secondary organic aerosol from laboratory irradiated isoprene/NO_X/SO_2/air mixtures and their detection in ambient $PM_{2.5}$ samples collected in the eastern United States, *Atmos. Environ.*, *39*, 5281-5289, 10.1016/j.atmosenv.2005.05.031.

El Haddad, I., Y. Liu, L. Nieto-Gligorovski, V. Michaud, B. Temime-Roussel, E. Quivet, N. Marchand, K. Sellegri, and A. Monod (2009), In-cloud processes of methacrolein under simulated conditions - Part 2: formation of secondary organic aerosol, *Atmos. Chem. Phys.*, *9*, 5107-5117, 10.5194/acp-9-5107-2009.

Emmons, L. K., S. Walters, P. G. Hess, J. F. Lamarque, G. G. Pfister, D. Fillmore, C. Granier, A. Guenther, D. Kinnison, T. Laepple, J. Orlando, X. Tie, G. Tyndall, C. Wiedinmyer, S. L. Baughcum, and S. Kloster (2010), Description and evaluation of the Model for Ozone and Related chemical Tracers, version 4 (MOZART-4), *Geosci. Model Dev.*, *3*, 43-67, 10.5194/gmd-3-43-2010, 2010.

EPRI (1999), Organic aerosol partition module documentation, EPRI, Palo Alto, CA, USA, *Technical Report*.

Ervens, B., and R. Volkamer (2010), Glyoxal processing by aerosol multiphase chemistry: towards a kinetic modeling framework of secondary organic aerosol formation in aqueous particles, *Atmos. Chem. Phys.*, *10*, 8219-8244, 10.5194/acp-10-8219-2010.

Ervens, B., A. G. Carlton, B. J. Turpin, K. E. Altieri, S. M. Kreidenweis, and G. Feingold (2008), Secondary organic aerosol yields from cloud-processing of isoprene oxidation products, *Geophys. Res. Lett.*, *35*, L02816, 10.1029/2007GL031828.

Ervens, B., B. J. Turpin, and R. J. Weber (2011), Secondary organic aerosol formation in cloud droplets and aqueous particles (aqSOA): a review of laboratory, field and model studies, *Atmos. Chem. Phys.*, *11*, 11069-11102, 10.5194/acp-11-11069-2011.

ESCWA (2010), Transport for sustainable development for the arab region: Measures, progress achieved, challenge and policy framework report, *Tech. Rep.*

Fredenslund, A., R. L. Jones, and J. M. Prausnitz (1975), Group-contribution estimation of activity-coefficients in nonideal liquid-mixtures, *AIChE J.*, *21*, 1086-1099.

Froyd, K. D., S. M. Murphy, D. M. Murphy, J. A. de Gouw, N. C. Eddingsaas, and P. O. Wennberg (2010), Contribution of isoprene-derived organosulfates to free tropospheric aerosol mass, *Proc. Natl. Acad. Sci.*, *107*, 21360-21365, 10.1073/pnas.1012561107.

Furukawa, T., and Y. Takahashi (2011), Oxalate metal complexes in aerosol particles: implications for the hygroscopicity of oxalate-containing particles, *Atmos. Chem. Phys.*, *11*, 4289-4301, 10.5194/acp-11-4289-2011.

Gantt, B., N. Meskhidze, and D. Kamykowski (2009), A new physically-based quantification of marine isoprene and primary organic aerosol emissions, *Atmos. Chem. Phys.*, *9*, 4915-4927, 10.5194/acp-9-4915-2009.

Gantt, B., N. Meskhidze, M. C. Facchini, M. Rinaldi, D. Ceburnis, and C. D. O'Dowd (2011), A new physically-based quantification of marine isoprene and primary organic aerosol emissions, *Atmos. Chem. Phys.*, *11*, 8777-8790, 10.5194/acp-11-8777-2011.

Gao, S., N. L. Ng, M. Keywood, V. Varutbangkul, R. Bahreini, A. Nenes, J. He, K. Y. Yoo, J. L. Beauchamp, R. P. Hodyss, R. C. Flagan, and J. H. Seinfeld (2004), Particle phase acidity and oligomer formation in secondary organic aerosol, *Environ. Sci. Technol.*, *38*, 6582-6589, 10.1021/es049125k.

Gaydos, T. M., R. Pinder, B. Koo, K. M. Fahey, G. Yarwood, and S. N. Pandis (2007), Development and application of a three-dimensional aerosol chemical transport model, PMCAMx, *Atmos. Environ.*, *41*(12), 2594-2611, 10.1016/j.atmosenv.2006.11.034.

Gilliam, R. C., C. Hogrefe, and S. Rao (2006), New methods for evaluating meteorological models used in air quality applications, *Atmos. Environ.*, *40*, 5073-5086, 10.1016/j.atmosenv.2006.01.023.

Glasius, M., A. Calogirou, N. R. Jensen, J. Hjorth, and C. J. Nielsen (1997), Kinetic study of gas-phase reactions of pinonaldehyde and structurally related compounds, *Int. J. Chem. Kinet.*, *29*, 527-533, 10.1002/(SICI)1097-4601(1997)29:7<527::AID-KIN7>3.0.CO;2-W.

Goliff, W. S., and W. R. Stockwell (2008), The regional atmospheric chemistry mechanism, version 2, an update, international conference on atmospheric chemical mechanisms, University of California, Davis, CA, USA, available at http://airquality.ucdavis.edu/pages/events/2008/acm/goliff.pdf, last access: 10 august 2010.

Grell, G. A., and D. Devenyi (2002), A generalized approach to parameterizing convection combining ensemble and data assimilation techniques, *Geophys. Res. Lett.*, *29*, 1693, doi:10.1029/2002GL015311.

Grell, G. A., S. E. Peckham, R. Schmitz, S. A. McKeen, G. Frost, W. C. Skamarock, , and B. Eder (2005), Fully coupled online chemistry within the WRF model, *Atmos. Environ.*, *39*, 6957-6975, 10.1016/j.atmosenv.2005.04.027.

Grieshop, A. P., J. M. Logue, N. M. Donahue, and A. L. Robinson (2009), Laboratory investigation of photochemical oxidation if organic aerosol from wood fires. 1: measurement and simulation of organic aerosol evolution, *Atmos. Chem. Phys.*, *9*, 1263-1277, 10.5194/acp-9-1263-2009.

Griffin, R. J., D. Dabdub, M. J. Kleeman, P. Fraser, M., G. R. Cass, and J. H. Seinfeld (2002), Secondary organic aerosol, 3, Urban/regional scale model of size- and composition-resolved aerosols, *J. Geophys. Res.*, *107*, 4334, 10.1029/2001JD000544.

Griffin, R. J., K. Nguyen, D. Dabdub, and J. H. Seinfeld (2003), A coupled hydrophobic-gydrophilic model for predicting secondary organic aerosol formation, *J. Atmos. Chem.*, *44*, 171-190, 10.1023/A:1022436813699.

Guenther, A., N. C. Hewitt, D. Erickson, R. Fall, C. Geron, T. Graedel, P. Harley, L. Klinger, M. Lerdau, W. A. McKay, T. Pierce, B. Scholes, R. Steinbrecher, R. Tallamraju, J. Taylor, and P. A. Zimmerman (1995), A global model of natural volatile organic compounds emissions, *J. Geophys. Res.*, *100*, 8873-8892, 10.1029/94JD02950.

Guenther, A., T. Karl, P. Harley, C. Wiedinmyer, P. I. Palmer, and C. Geron (2006), Estimates of global terrestrial isoprene emissions using MEGAN (Model of Emissions of Gases and Aerosols from Nature), *Atmos. Chem. Phys.*, *6*, 3181-3210, 10.5194/acp-6-3181-2006.

Haeffelin, M., L. Barthès, O. Bock, C. Boitel, S. Bony, D. Bouniol, H. Chepfer, M. Chiriaco, J. Cuesta, J. Delanö, P. Drobinski, J.-L. Dufresne, C. Flamant, M. Grall, A. Hodzic, F. Hourdin, F. Lapouge, Y. Lemaître, A. Mathieu, Y. Morille, C. Naud, V. Noël, W. O´Hirok, J. Pelon, C. Pietras, A. Protat, B. Romand, G. Scialom, and R. Vautard (2005), SIRTA, a ground-based atmospheric observatory for cloud and aerosol research, *Ann. Geophysic.*, *23*, 253-275, 10.5194/angeo-23-253-2005.

Hallquist, M., I. Wängberg, E. Ljungström, I. Barnes, and K.-H. Becher (1999), Aerosol and product yield from NO_3 radical-initiated oxidation of selected monoterpenes, *Environ. Sci. Technol.*, *33*, 553-559, 10.1021/es980292s.

Hallquist, M., J. C. Wenger, U. Baltensperger, Y. Rudich, D. Simpson, M. Claeys, J. Dommen, N. M. Donahue, C. George, A. H. Goldstein, J. F. Hamilton, H. Herrmann, T. Hoffmann,

Y. Iinuma, M. Jang, M. E. Jenkin, J. L. Jimenez, A. Kiendler-Scharr, W. Maenhaut, G. McFiggans, T. F. Mentel, A. Monod, A. S. H. Prévôt, J. H. Seinfeld, J. D. Surratt, R. Szmigielski, and J. Wildt (2009), The formation, properties and impact of secondary organic aerosol: current and emerging issues, *Atmos. Chem. Phys.*, *9*, 5155-5236, 10.5194/acp-9-5155-2009.

Helmig, D., A. Klinger, L. Vierling, P. Zimmerman, and C. Geron (1999a), Biogenic volatile organic compound emissions (BVOCs) I. Identifications from three continental sites in the U.S., *Chemosphere*, *38*, 2163-2187, 10.1016/S0045-6535(98)00425-1.

Helmig, D., A. Klinger, L. Vierling, P. Zimmerman, and C. Geron (1999b), Biogenic volatile organic compound emissions (BVOCs) II. Landscape fluxes potentials from three continental sites in the U.S., *Chemosphere*, *38*, 2189-2204, 10.1016/S0045-6535(98)00424-X.

Henze, D. K., and J. H. Seinfeld (2006), Global secondary organic aerosol from isoprene oxidation, *Geophys. Res. Lett.*, *33*, L09812, 10.1029/2006GL025976.

Henze, D. K., J. H. Seinfeld, N. L. Ng, J. H. Kroll, T.-M. Fu, D. J. Jacob, and C. L. Heald (2008), Global modeling of secondary organic aerosol formation from aromatic hydrocarbons: high- vs. low-yield pathways, *Atmos. Chem. Phys.*, *8*, 2405-2420, 10.5194/acp-8-2405-2008.

Hilal, S. H., S. N. Ayyampalayam, and L. A. Carreira (2008), Air-liquid partition coefficient for a diverse set of organic compounds: Henry's law constant in water and hexadecane, *Environ. Sci. Technol.*, *42*, 9231-9236, 10.1021/es8005783.

Hodzic, A., S. Madronich, B. Bohn, S. Massie, L. Menut, and C. Wiedinmyer (2007), Wildfire particulate matter in Europe during summer 2003: meso-scale modeling of smoke emissions, transport and radiative effects, *Atmos. Chem. Phys.*, *7*, 4043–4064, 10.5194/acp-7-4043-2007.

Hodzic, A., J. L. Jimenez, S. Madronich, M. R. Canagaratna, P. F. DeCarlo, L. Kleinman, and J. Fast (2010), Modeling organic aerosols in a megacity: potential contribution of semi-volatile and intermediate volatility primary organic compounds to secondary organic aerosol formation, *Atmos. Chem. Phys.*, *10*, 5491-5514, 10.5194/acp-10-5491-2010.

Hogrefe, C., S. Isukapalli, X. Tang, P. Georgopoulos, S. He, E. Zalewsky, W. Hao, J. Ku, T. Key, and G. Sistla (2011), Impact of biogenic emission uncertainties on the simulated response of ozone and fine Particulate Matter to anthropogenic emission reductions, *J. Air Waste Manag. Assoc.*, *61*, 92-108, 10.3155/1047-3289.61.1.92.

Hong, S.-Y., Y. Noh, and J. Dudhia (2006), A new vertical diffusion package with an explicit treatment of entrainment processes, *Mon. Wea. Rev.*, *134*, 2318–2341, 10.1175/MWR3199.1.

Horowitz, L. W., S. Walters, D. L. Mauzerall, L. K. Emmons, P. J. Rasch, C. Granier, X. Tie, J. F. Lamarque, M. G. Schultz, G. S. Tyndall, J. J. Orlando, and G. P. Brasseur (2003), A global simulation of tropospheric ozone and related tracers: description and evaluation of MOZART, version 2, *J. Geophys. Res.*, *108*, D24, 4784, 10.1029/2002JD002853.

Horowitz, L. W., A. M. Fiore, G. P. Milly, R. C. Cohen, A. Perring, P. J. Wooldridge, P. G. Hess, L. K. Emmons, and J. F. Lamarque (2007), Observational constraints on the chemistry of isoprene nitrates over the eastern United States, *J. geophys. Res.*, *112*, D12S08, 10.1029/2006JD007747.

Hoyle, C. R., M. Boy, N. M. Donahue, J. L. Fry, M. Glasius, A. Guenther, A. G. Hallar, K. Huff Hartz, M. D. Petters, T. Petäjä, T. Rosenoern, and A. P. Sullivan (2011), A review of the anthropogenic influence on biogenic secondary organic aerosol, *Atmos. Chem. Phys.*, *11*, 321-343, 10.5194/acp-11-321-2011.

IIASA (2012), Average annual anthropogenic heat flux for major capital cities in the world, *Tech. Rep.*

Ion, A. C., R. Vermeylen, I. Kourtchev, J. Cafmeyer, X. Chi, A. Gelencsér, W. Maenhaut, and M. Claeys (2005), Polar organic compounds in rural $pm_{2.5}$ aerosols from K-puszta, Hungary, during a 2003 summer field campaign: Sources and diel variations, *Atmos. Chem. Phys.*, *5*, 1805-1814, 10.5194/acp-5-1805-2005.

Iraci, L. T., B. M. Baker, G. S. Tyndall, and J. J. Orlando (1999), Measurements of the Henry's law coefficients of 2-methyl-3-buten-2-ol, methacrolein and methylvinyl ketone, *J. Atmos. Chem.*, *33*, 321-330, 10.1023/A:1006169029230.

Isaacman, G., K. R. Wilson, W. H. Chan, D. R. Worton, J. R. Kimmel, T. Nah, T. Hohaus, M. Gonin, J. H. Kroll, D. R. Worsnop, and A. H. Goldstein (2012), Improved resolution of hydrocarbon structures and constitutional isomers in complex mixtures using gas chromatography-vacuum ultraviolet-mass spectrometry, *Anal. Chem.*, *84*, 2335-2342, 10.1021/ac2030464.

Jacob, D. J. (1986), Chemistry of OH in remote clouds and its role in the production of formic acid and peroxymonosulfate, *J. Geophys. Res.*, *91*, 9807-9826, 10.1029/JD091iD09p09807.

Jacob, D. J. (2000), Heterogeneous chemistry and tropospheric ozone, *Atmos. Environ.*, *34*, 2131-2159, 10.1016/S1352-2310(99)00462-8.

Jaeglé, L., D. J. Jacob, W. H. Brune, and P. O. Wennberg (2001), Chemistry of HO_x radicals in the upper troposphere, *Atmos. Environ.*, *35*, 469-489, 10.1016/S1352-2310(00)00376-9.

Jang, M., N. M. Czoschke, S. Lee, and R. M. Kamens (2002), Heterogeneous atmospheric aerosol production by acid-catalysed particle-phase reactions, *Science*, *298*, 814-817, 10.1126/science.1075798.

Jang, M., N. M. Czoschke, and A. L. Northcross (2005), Semiempirical model for organic aerosol growth by acid-catalyzed heterogeneous reactions of organic carbonyls, *Environ. Sci. Technol.*, *39*, 164-174, 10.1021/es048977h.

Jardine, K., A. Yañez Serrano, A. Arneth, L. Abrell, A. Jardine, J. van Haren, P. Artaxo, L. V. Rizzo, F. Y. Ishida, T. Karl, J. Kesselmeier, S. Saleska, and T. Huxman (2011), Within-canopy sesquiterpene ozonolysis in Amozonia, *J. Geophys. Res.*, *116*, D19301, 10.1029/2011JD016243.

Jimenez, J. L., M. R. Canagaratna, N. M. Donahue, A. S. H. Prevot, Q. Zhang, J. H. Kroll, P. F. DeCarlo, J. D. Allan, H. Coe, N. L. Ng, A. C. Aiken, K. S. Docherty, I. M. Ulbrich, A. P. Grieshop, A. L. Robinson, J. Duplossy, J. D. Smith, K. R. Wilson, V. A. Lanz, C. Hueglin, Y. L. Sun, J. Tian, A. Laaksonen, T. Raatikainen, J. Rautiainen, P. Vaattovaara, M. Ehn, M. Kulmala, J. M. Tomlinson, D. R. Collins, M. J. Cubison, E. J. Dunlea, J. A. Huffman, T. B. Onash, M. R. Alfarra, P. I. Williams, K. Bower, Y. Kondo, J. Schneider, F. Drewnick, S. Borrmann, S. Weimer, K. Demerjian, D. Salcedo, L. Cottrell, R. Griffin, A. Takami, T. Miyoshi, S. Hatakeyama, A. Shimono, J. Y. Sun, Y. M. Zhang, K. Dzepina, J. R. Kimmel, D. Sueper, J. T. Jayne, S. C. Herndon, A. M. Trimborn, L. R. Williams, E. C. Wood, A. M. Middlebrook, C. E. Kolb, U. Baltensperger, and D. R. Worsnop (2009), Evolution of organic aerosols in the atmosphere, *Science*, *326*, 1525-1529, 10.1126/science.1180353.

Johnson, D., S. R. Utembe, M. E. Jenkin, R. G. Derwent, G. D. Hayman, M. R. Alfarra, H. Coe, and G. McFiggans (2006), Simulating regional scale secondary organic aerosol formation during the TORCH 2003 campaign in the southern UK, *Atmos. Chem. Phys.*, *6*, 403-418, 10.5194/acp-6-403-2006.

Junker, C., and C. Liousse (2008), A global emission inventory of carbonaceous aerosol from historic records of fossil fuel and biofuel consumption for the period 1860-1997, *Atmos. Chem. Phys.*, *8*, 1195-1027, 10.5194/acp-8-1195-2008.

Kamens, R. M., and M. Jaoui (2001), Modeling aerosol formation from α-pinene + NOx in the presence of natural sunlight using gas-phase kinetics and gas-particle partitioning theory, *Environ. Sci. Technol.*, *35*, 1394–1405, 10.1021/es001626s.

Kamens, R. M., M. W. Gery, H. E. Jeffries, M. Jacksons, and E. I. Cole (1982), Ozone-isoprene reactions: product formation and aerosol potential, *Int. J. Chem. Kinet.*, *14*, 955-975.

Kanakidou, M., J. H. Seinfeld, S. N. Pandis, I. Barnes, F. J. Dentener, M. C. Facchini, R. Van Dingenen, B. Ervens, A. Nenes, C. J. Nielsen, E. Swietlicki, J. P. Putaud, Y. Balkanski, S. Fuzzi, J. Horth, G. K. Moortgat, R. Winterhalter, C. E. L. Myhre, K. Tsigaridis, E. Vignati, E. G. Stephanou, and J. Wilson (2005), Organic aerosol and global climate modelling: a review, *Atmos. Chem. Phys.*, *5*, 1053-1123, 10.5194/acp-5-1053-2005.

Karl, M., A. Guenther, R. Köble, and G. Seufert (2009), A new European plant-specific emission inventory of biogenic volatile organic compounds for use in atmospheric transport models, *Biogeosciences*, *6*, 1059-1087, 10.5194/bg-6-1059-2009.

Kautzman, K. E., J. D. Surratt, M. N. Chan, A. W. H. Chan, S. P. Hersey, P. S. Chhabra, N. F. Dalleska, P. O. Wennberg, R. C. Flagan, and J. H. Seinfeld (2010), Chemical composition of gas- and aerosol-phase products from the photooxidation of naphthalene, *J. Phys. Chem. A*, *114*, 913-934, 10.1021/jp908530s.

Keene, W. C., A. A. P. Pszenny, J. R. Maben, E. Stevenson, and A. Wall (2004), Closure evaluation of size-resolved aerosol pH in the New England coastal atmosphere during summer, *J. Geophys. Res.*, *109*, D23307, 10.1029/2004JD004801.

Kessler, E. (1969), On the distribution and continuity of water substance in atmospheric circulation, *Meteorol. Monogr.*, *10*, 88.

Kim, Y. (2011), Modélisation de la qualité de l'air: évaluation des paramétrisations chimiques et météorologiques, Ph.D. thesis, Université Paris-Est.

Kim, Y., K. Sartelet, and C. Seigneur (2009), Comparison of two gas-phase chemical kinetic mechanisms of ozone formation over Europe, *J. Atmos. Chem.*, *62*, 82-119, 10.1007/s10874-009-9142-5.

Kim, Y., F. Couvidat, K. Sartelet, and C. Seigneur (2011a), Comparison of different gas-phase mechanisms and aerosol modules for simulating particulate matter formation, *J. Air Waste Manage. Assoc*, *61*, 1218-1226.

Kim, Y., K. Sartelet, and C. Seigneur (2011b), Formation of secondary aerosols: impact of the gas-phase chemical mechanism, *Atmos. Chem. Phys.*, *11*, 583-598, 10.5194/acp-11-583-2011.

Kleindienst, T. E., M. Lewandowski, J. H. Offenberg, M. Jaoui, and E. O. Edney (2007), Ozone-isoprene reactions: Re-examination of the formation of secondary organic aerosol, *Geophys. Res. Lett.*, *34*, L01805, 10.1029/2006GL027485.

Kleindienst, T. E., M. Lewandowski, J. H. Offenberg, M. Jaoui, and E. O. Edney (2009), The formation of secondary organic aerosols from the isoprene + OH reaction in the absence of NO_X, *Atmos. Chem. Phys.*, *9*, 6541-6558, 10.5194/acp-9-6541-2009.

Koo, B., C. Chien, G. Tonnesen, R. Morris, J. Johnson, T. Sakulyanontvittaya, P. Piyachaturawat, and G. Yarwood (2011), Natural emissions for regional modeling of background ozone and particulate matter and impacts on emissions control strategies, *Atmos. Environ.*, *44*, 2372-2382, 10.1016/j.atmosenv.2010.02.041.

Kourtchev, I., J. Warnke, W. Maenhaut, T. Hoffmann, and M. Claeys (2008a), Polar organic marker compounds in $PM_{2.5}$ aerosol from a mixed forest site in western Germany, *Chemosphere*, *73*, 1308-1314, 10.1016/j.chemosphere.2008.07.011.

Kourtchev, I., T. M. Ruuskanen, P. Keronen, L. Sogacheva, M. Dal Maso, A. Reissell, X. Chi, R. Vermeylen, M. Kulmala, W. Maenhaut, and M. Claeys (2008b), Determination of isoprene and α-/β-pinene oxidation products in boreal forest aerosols from Hyytiälä, Finland: diel variations and possible link with particle formation events., *Plant Biol.*, *10*, 138-149, 10.1055/s-2007-964945.

Kouvarakis, G., K. Tsigaridis, M. Kanakidou, and N. Mihalopoulos (2000), Temporal variations of surface regional background ozone over crete island in the southeast mediterranean, *J. geophys. Res.*, *105*, 4399-4407, 10.1029/1999JD900984.

Kroll, J. H., and J. H. Seinfeld (2008), Chemistry of secondary organic aerosol: Formation and evolution of low-volatility organics in the atmosphere, *Atmos. Environ.*, *42*, 3593-3624, 10.1016/j.atmosenv.2008.01.003.

Kroll, J. H., N. L. Ng, S. M. Murphy, R. C. Flagan, and J. H. Seinfeld (2006), Secondary organic aerosol formation from isoprene photooxidation, *Environ. Sci. Technol.*, *40*, 1869-1877, 10.1021/es0524301.

Kusaka, H., H. Kondo, Y. Kikegawa, and F. Kimura (2001), A simple single-layer urban canopy model for atmospheric models: Comparison with multi-layer and slab models, *Bound.-Lay. Meteorol.*, *101*, 329-358, 10.1023/A:1019207923078.

Lee, J. Y., and D. A. Lane (2009), Unique products from the reaction of naphthalene with the hydroxyl radical, *Atmos. Environ.*, *43*, 4886-4893, 10.1016/j.atmosenv.2009.07.018.

Lee, J. Y., and D. A. Lane (2010), Formation of oxidized products from the reaction of gaseous phenanthrene with the oh radical in a reaction chamber, *Atmos. Environ.*, *44*, 2469-2477, 10.1016/j.atmosenv.2010.03.008.

Lee-Taylor, J., S. Madronich, B. Aumont, A. Baker, M. Camredon, A. Hodzic, G. S. Tyndall, E. Apel, and R. A. Zaveri (2011), Explicit modeling of organic chemistry and secondary organic aerosol partitioning for Mexico City and its outflow plume, *Atmos. Chem. Phys.*, *11*, 13219-13241, 10.5194/acp-11-13219-2011.

Lelieveld, J., H. Berresheim, S. Borrmann, P. J. Crutzen, F. J. Dentener, H. Fischer, J. Feichter, P. J. Flatau, J. Heland, R. Holzinger, R. Korrmann, M. G. Lawrence, Z. Levin, K. M. Markowicz, N. Mihalopoulos, A. Minikin, V. Ramanathan, M. de Reus, G. J. Roelofs, H. A. Scheeren, J. Sciare, H. Schlager, M. Schultz, P. Siegmund, B. Steil, E. G. Stephanou, P. Stier, M. Traub, C. Warneke, J. Williams, and H. Ziereis (2002), Global air pollution crossroads over the mediterranean, *Science*, *298*, 794-799, 10.1126/science.1075457.

Lelieveld, J., P. Hoor, P. Jackel, A. Pozzer, P. Hadjinicolaou, J. P. Cammas, and S. Beirle (2009), Severe ozone air pollution in the persian gulf region, *Atmos. Chem. Phys.*, *9*, 1393-1406, 10.5194/acp-9-1393-2009.

Liggio, J., and S.-M. Li (2006), Organosulfate formation during the uptake of pinonaldehyde on acidic sulfate aerosols, *Geophys. Res. Lett.*, *33*, L13808, 10.1029/2006GL026079.

Liggio, J., S.-M. Li, and R. McLaren (2005), Heterogeneous reactions of glyoxal on particulate matter: Identification of acetals and sulfate esters, *Environ. Sci. Technol.*, *39*, 1532–1541, 10.1021/es048375y.

Lim, B. Y., and P. J. Ziemann (2009a), Chemistry of secondary organic aerosol formation from oh radical-initiated reactions of linear, branched and cyclic alkanes in the presence of NO_x, *Aerosol. Sci. Technol.*, *43*, 604-619, 10.1080/02786820902802567.

Lim, B. Y., and P. J. Ziemann (2009b), Effects of molecular structure on aerosol yields from oh radical-initiated reactions of linear, branched, and cyclic alkanes in the presence of NO_x, *Environ. Sci. Technol.*, *43*, 2328-2334, 10.1021/es803389s.

Lim, H.-J., A. G. Carlton, and B. J. Turpin (2005), Isoprene forms secondary organic aerosol through cloud processing: Model simulations, *Environ. Sci. Technol.*, *39*(12), 4441-4446, 10.1021/es048039h.

Limbeck, A., H. Puxbaum, L. Otter, and M. C. Scholes (2001), Semivolatile behavior of dicarboxylic acids and other polar organic species at a rural background site (Nylsvely, RSA), *Atmos. Environ.*, *35*, 1853-1862, 10.1016/S1352-2310(00)00497-0.

Liousse, C., B. Guillaume, J. M. Grégoire, M. Mallet, C. Galy, V. Pont, A. Akpo, M. Bedou, P. Castéra, L. Dungall, E. Gardrat, C. Granier, A. Konaré, F. Malavelle, A. Mariscal, A. Mieville, R. Rosset, D. Serça, F. Solmon, F. Tummon, E. Assamoi, V. Yoboué, and P. Van Velthoven (2010), Updated African biomass burning emission inventories in the framework of the AMMA-IDAF program, with an evaluation of combustion aerosols, *Atmos. Chem. Phys.*, *10*(19), 9631-9646, 10.5194/acp-10-9631-2010.

Liu, J., D. Jones, J. Worden, D. Noone, M. Parrington, and J. Kar (2009a), Analysis of the summertime buildup of tropospheric ozone abundances over the Middle East and North Africa as observed by the tropospheric emission spectrometer instrument, *J. geophys. Res.*, *114*, D05304, 10.1029/2008JD010993.

Liu, P., and Y. Zhang (2008), A computationally-efficient secondary organic aerosol module for three-dimensional air quality models, *Atmos. Chem. Phys.*, *8*, 3985-3998, 10.5194/acp-8-3985-2008.

Liu, Y., I. El Haddad, M. Scarfogliero, L. Nieto-Gligorovski, B. Temime-Roussel, E. Quivet, N. Marchand, B. Picquet-Varrault, and A. Monod (2009b), In-cloud processes of methacrolein under simulated conditions - Part 1: Aqueous phase photooxidation, *Atmos. Chem. Phys.*, *9*, 5093-5105, 10.5194/acp-9-5093-2009.

Liu, Y., F. Siekmann, P. Renard, A. El Zein, G. Salque, I. El Haddad, B. Temime-Roussel, D. Voisin, R. Thissen, and A. Monod (2012), Oligomer and SOA formation through aqueous phase photooxidation of methacrolein and methyl vinyl ketone, *Atmos. Environ.*, *49*, 123-129, 10.1016/j.atmosenv.2011.12.012.

Louis, J.-F. (1979), A parametric model of vertical eddy fluxes in the atmosphere, *Bound.-Lay. Meteorol.*, *17*, 187-202.

Ludwig, J., and O. Klemm (1990), Acidity of size-fractionated aerosol particles, *Water Air Soil Pollut*, *49*, 35-50, 10.1007/BF00279508.

Luecken, D. J. (2008), Comparison of atmospheric chemical mechanisms for regulatory and research applications, in *Simulation and Assessment of Chemical Processes in a Multiphase Environment*, pp. 95-106, Springer, The Netherlands, 10.1007/978-1-4020-8846-9_8.

Luecken, D. J., S. Phillips, G. Sarwar, and C. Jang (2008), Effects of using the CB05 vs. SAPRC99 vs. CB4 chemical mechanism on model predictions: Ozone and gas-phase photochemical precursor concentrations, *Atmos. Environ.*, *42*, 5805-5820, 10.1016/j.atmosenv.2007.08.056.

Lukács, H., A. Gelencsér, A. Hoffer, G. Kiss, K. Horváth, and Hartyáni (2009), Quantitative assessment of organosulfates in size-segregated rural fine aerosol, *Atmos. Chem. Phys.*, *9*, 231-238, 10.5194/acp-9-231-2009.

Mallet, V., D. Quélo, B. Sportisse, M. Ahmed de Biasi, É. Debry, I. Korsakissok, L. Wu, Y. Roustan, K. Sartelet, M. Tombette, and H. Foudhil (2007), Technical Note: The air quality modeling system Polyphemus, *Atmos. Chem. Phys.*, *7*(20), 5479–5487, 10.5194/acp-7-5479-2007.

Martilli, A., A. Clappier, and M. W. Rotach (2002), An urban surface exchange parameterisation for mesoscale models, *Bound.-Lay. Meteorol.*, *104*, 261-304, 1023/A:1016099921195.

Massoud, R., A. Shihadeh, M. Roumié, M. Youness, J. Gerard, N. Saliba, R. Zaarour, M. Abboud, W. Farah, and N. A. Saliba (2011), Intraurban variability of PM_{10} and $PM_{2.5}$ in an eastern mediterranean city, *Atmos. Res.*, *101*, 893-901, 10.1016/j.atmosres.2011.05.019.

Matthias, V., A. Aulinger, and M. Quante (2008), Adapting CMAQ to investigate air pollution in north sea coastal region, *Environ. Modell. Softw.*, *23*, 356-368, 10.1016/j.envsoft.2007.04.010.

Mauldin III, R., S. Madronich, S. Flocke, and F. Eisele (1997), New insights on oh: Measurements around and in clouds, *Geophys. Res. Lett.*, *24*, 3033-3036.

Mellor, G. L., and T. Yamada (1974), A hierarchy of turbulence closure models for planetary boundary layers, *J. Atmos. Sci.*, *31*, 1791-1806.

Meng, Z., D. Dabdub, and J. H. Seinfeld (1998), Size-resolved and chemically resolved model of atmospheric aerosol, *J. Geophys. Res.*, *103*, 3419–3435, 10.1029/97JD02796.

Menut, L., A. Goussebaile, B. Bessagnet, D. Khvorostiyanov, and A. Ung (2012), Impact of realistic hourly emissions profiles on air pollutants concentrations modelled with CHIMERE, *Atmos. Environ.*, *49*, 233-244, 10.1016/j.atmosenv.2011.11.057.

Meylan, W. M., and P. H. Howard (1991), Bond contribution method for estimating henry's law constants, *Environ. Toxicol. Chem*, *10*, 1283-1293, 10.1002/etc.5620101007.

Meylan, W. M., and P. H. Howard (2000), SRC's EPI suite, v3.20, *Tech. Rep.*, Syracuse Research Corporation.

Michoud, V., A. Kukui, M. Camredon, A. Colomb, A. Borbon, K. Miet, B. Aumont, M. Beekmann, R. Durand-Jolibois, S. Perrier, P. Zapf, G. Siour, W. Ait-Helal, N. Locoge, S. Sauvage, V. Gros, C. Afif, M. Furger, G. Ancellet, and J. F. Doussin (2012), Radical budget analysis in a suburban european site during the MEGAPOLI summer field campaign, *Atmos. Chem. Phys. Discuss.*, *12*, 15883-15943, 10.5194/acpd-12-15883-2012, 2012.

Middleton, P., J. S. Chang, J. C. Del Corral, H. Geiss, and J. M. Rosinski (1988), Comparison of RADM and OSCAR precipitation chemistry data, *Atmos. Environ.*, *22*, 1195-1208, 10.1016/0004-6981(88)90350-2.

Mlawer, E. J., S. J. Taubman, P. D. Brown, M. J. Iacono, and S. A. Clough (1997), Radiative transfer for inhomogeneous atmospheres : RRTM, a validated correlated-k model for the longwave, *J. Geophys. Res.*, *102*, 16663-16682, 10.1029/97JD00237.

MoE (2005), National environmental action plan, *Tech. Rep.*, Ministry of environment, Beirut, Lebanon.

Molders, N. (2008), Suitability of the Weather Research and Forecasting (WRF) model to predict the june 2005 fire weather for interior Alaska, *Weather and Forecasting*, *23*, 953-973, 10.1175/2008WAF2007062.1.

Monahan, E., D. Spiel, and K. Davidson (1986), *Oceanic whitecaps and their role in air-sea exchange processes*, chap. A model of marine aerosol generation via whitecaps and wave disruption, Dordrecht: D. Reidel Pub.

Monod, A., and J. Doussin (2008), Structure-activity relationship for the estimation of oh-oxidation rate constants of aliphatic organic compounds in the aqueous phase: alkanes, alcohols, organic acids and bases, *Atmos. Environ.*, *33*, 7611-7622, 10.1016/j.atmosenv.2008.06.005.

Morris, R. E., B. Koo, A. Guenther, G. Yarwood, D. McNally, T. W. Tesche, G. Tonnesen, J. Boylan, and B. Brewer (2006), Model sensitivity evaluation for organic carbon using two multi-pollutant air quality models that simulate regional haze in the southeastern United States, *Atmos. Environ.*, *40*(26), 4960-4972, 10.1016/j.atmosenv.2005.09.088.

Mueller, S., and J. Mallard (2011), Contributions of natural emissions to Ozone and PM(2.5) as Simulated by the Community Multiscale Air Quality (CMAQ) model, *Environ. Sci. Technol.*, *45*, 4817-4823, 10.1021/es103645m.

Murphy, B. N., and S. N. Pandis (2009), Simulating the formation of semivolatile primary and secondary organic aerosol in a regional chemical transport model, *Environ. Sci. Technol.*, *43*, 4722–4728, 10.1021/es803168a.

Nakanishi, M., and H. Niino (2004), An improved Mellor-Yamada Level-3 model with condensation physics: its design and verification, *Bound.-Lay. Meteorol.*, *112*, 1-31, 10.1023/B:BOUN.0000020164.04146.98.

Nenes, A., S. N. Pandis, and C. Pilinis (1998), ISORROPIA: A new thermodynamic equilibrium model for multiphase multicomponent inorganic aerosols, *Aquat. Geoch.*, *4*, 123-152.

Nenes, A., P. S. N., and C. Pilinis (1999), Continued development and testing of a new thermodynamic aerosol module for urban and regional air quality models, *Atmos. Environ.*, *33*(10), 1553-1560, 10.1016/S1352-2310(98)00352-5.

Ng, N. L., P. S. Chhabra, A. W. H. Chan, J. D. Surratt, J. H. Kroll, A. J. Kwan, D. C. McCabe, P. O. Wennberg, A. Sorooshian, S. M. Murphy, N. F. Dalleska, R. C. Flagan, and J. H. Seinfeld (2007a), Effect of NO_x level on secondary organic aerosol (SOA) formation from the photooxidation of terpenes, *Atmos. Chem. Phys.*, *7*, 5159–5174, 10.5194/acp-7-5159-2007.

Ng, N. L., J. H. Kroll, A. W. H. Chan, P. S. Chhabra, R. C. Flagan, and J. H. Seinfeld (2007b), Secondary organic aerosol formation from m-xylene, toluene, and benzene, *Atmos. Chem. Phys.*, *7*, 3909-3922, 10.5194/acp-7-3909-2007.

Ng, N. L., A. J. Kwan, J. D. Surratt, A. W. H. Chan, P. S. Chhabra, A. Sorooshian, H. O. T. Pye, J. D. Crounse, P. O. Wennberg, R. C. Flagan, and J. H. Seinfeld (2008), Secondary organic aerosol (SOA) formation from reaction of isoprene with nitrate radicals (NO_3), *Atmos. Chem. Phys.*, *8*, 4117-4140, 10.5194/acp-8-4117-2008.

Nguyen, T. B., A. P. Bateman, D. L. Bones, S. A. Nizkorodov, J. Laskin, and A. Laskin (2010), High-resolution mass spectrometry analysis of secondary organic aerosol generated by ozonolysis of isoprene, *Atmos. Environ.*, *44*, 1032-1042, 10.1016/j.atmosenv.2009.12.019.

Odum, J. R., T. Hoffman, F. Bowman, D. Collins, R. C. Flagan, and J. H. Seinfeld (1996a), Gas/particle partitioning and secondary organic aerosol yields, *Environ. Sci. Technol.*, *30*, 2580-2585, 10.1021/es950943+.

Odum, J. R., F. Hoffmann, D. Bowman, D. Collins, R. C. Flagan, and J. H. Seinfeld (1996b), Gas/particle partitioning and secondary organic aerosol yields, *Environ. Sci. Technol.*, *30*, 2580-2585, 10.1021/es950943+.

Offenberg, J. H., M. Lewandowski, E. O. Edney, T. E. Kleindienst, and M. Jaoui (2007), Investigation of a systematic offset in the measurement of organic carbon with a semicontinuous analyzer, *J. Air Waste Manage. Assoc.*, *57*, 596-599.

Ostro, B., and L. Chestnut (1998), Assessing the health benefits of reducing particulate matter air pollution in the United States, *Environ. Res.*, *76*, 94-106, 10.1006/enrs.1997.3799.

Pandis, S. N., S. E. Paulson, J. H. Seinfeld, and R. C. Flagan (1991), Aerosol formation in the photooxidation of isoprene and β-pinene, *Atmos. Environ.*, *25*, 997-1008, 10.1021/es0524301.

Pankow, J. F. (1994a), An absorption model of gas/particle partitioning of organic compounds in the atmosphere, *Atmos. Environ.*, *28A*, 185-188.

Pankow, J. F. (1994b), An absorption model of the gas/aerosol partitioning involved in the formation of secondary organic aerosol, *Atmos. Environ.*, *28A*, 189-193.

Pankow, J. F., and W. E. Asher (2008), SIMPOL.1: a simple group contribution method for predicting vapor pressures and enthalpies of vaporization of multifunctional organic compounds, *Atmos. Chem. Phys.*, *8*, 2773-2796, 10.5194/acp-8-2773-2008.

Paulot, F., J. D. Crounse, H. G. Kjaergaard, A. Kürten, J. St. Clair, J. H. Seinfeld, and P. O. Wennberg (2010), Unexpected epoxide formation in the gas-phase photooxidation of isoprene, *Science*, *325*, 730-733, 10.1126/science.1172910.

Peltier, R. E., R. J. Weber, and A. P. Sullivan (2007), Investigating a liquid-based method for online organic carbon detection in atmospheric particles, *Aerosol. Sci. Technol.*, *41*, 1117-1127, 10.1080/02786820701777465.

Perri, M. J., Y. B. Lim, S. P. Seitzinger, and B. J. Turpin (2010), Organosulfates from glycoladehyde in aqueous aerosols and clouds: Laboratory studies, *Atmos. Environ.*, *44*, 2658-2664, 10.1016/j.atmosenv.2010.03.031.

Polidori, A., B. Turpin, H.-J. Lim, J. C. Cabada, R. Subramanian, S. N. Pandis, and A. L. Robinson (2006), Local and regional secondary organic aerosol : Insights from a year of semi-continuous carbon measurements at Pittsburgh, *Aerosol. Sci. Tech.*, *40*, 861-872, 10.1080/02786820600754649.

Pöschl, U., R. Von Kuhlmann, N. Poisson, and P. J. Crutzen (2000), Development and intercomparison of condensed isoprene oxidation mechanisms for global atmospheric modeling, *J. Atmos. Chem.*, *37*, 29-52, 10.1023/A:1006391009798.

Pouliot, P., H. Denier van der Gon, M. Schaap, M. Moran, and U. Nopmongcol (2012), Comparing emissions inventories and model-ready emissions datasets between Europe and North America for the AQMEII project, *Atmos. Environ.*, *53*, 4-14, 10.1016/j.atmosenv.2011.12.041.

Pozzoli, L., G. Janssens-Maenhout, T. Diehl, I. Bey, M. G. Schultz, J. Feichter, E. Vignati, and F. Dentener (2011), Re-analysis of tropospheric sulfate aerosol and ozone for the period 1980-2005 using the aerosol-chemistry-climate model ECHAM5-HAMMOZ, *Atmos. Chem. Phys.*, *11*, 9563-9594, 10.5194/acp-11-9563-2011.

Presto, A. A., M. A. Miracolo, N. M. Donahue, and A. L. Robinson (2010), Secondary organic aerosol formation from high-NO_x photo-oxidation of low volatility precursors: n-alkanes, *Environ. Sci. Technol.*, *44*, 2029–2034, 10.1021/es903712r.

Prevot, A. S. H., M. Crippa, S. N. Pandis, M. Beekmann, and U. Baltensperger (2011), Organic aerosols and their sources in Paris during the MEGAPOLI campaigns, *Geophysical Research Abstracts*, *13*, EGU2011-4631-2.

Pun, B. K. (2008), Development and initial application of the sesquiversion of MADRID, *J. Geophys. Res.*, *113*, D12212, 10.1029/2008JD009888.

Pun, B. K., and C. Seigneur (2007), Investigative modeling of new pathways for secondary organic aerosol formation, *Atmos. Chem. Phys.*, *7*, 2199-2216, 10.5194/acp-7-2199-2007.

Pun, B. K., and C. Seigneur (2008), Organic aerosol spatial/temporal patterns: Perspectives of measurements and model, *Environ. Sci. Tech.*, *42*(19), 7287-7293, 10.1021/es800500j.

Pun, B. K., C. Seigneur, D. Grosjean, and P. Saxena (2000), Gas-phase formation of water-soluble organic compounds in the atmosphere: A retrosynthetic analysis, *J. Atmos. Chem.*, *35*, 199-223, 10.1023/A:1006261217691.

Pun, B. K., R. J. Griffin, C. Seigneur, and J. H. Seinfeld (2002a), Secondary organic aerosol. 2. Thermodynamic model for gas/particle partitioning of molecular constituents, *J. Geophys. Res.*, *107*, 433, 10.1029/2001JD000542.

Pun, B. K., S.-Y. Wu, and C. Seigneur (2002b), Contribution of biogenic emissions to the formation of ozone and particulate matter in the eastern United States, *Environ. Sci. Technol.*, *36*, 3586-3596, 10.1021/es015872v.

Pun, B. K., S.-Y. Wu, C. Seigneur, J. H. Seinfeld, R. J. Griffin, and S. N. Pandis (2003), Uncertainties in modeling secondary organic aerosols: Three-dimensional modeling studies in Nashville/western Tennessee, *Environ. Sci. Technol.*, *37*, 3647-3661, 10.1021/es0341541.

Pun, B. K., C. Seigneur, and K. Lohman (2006), Modeling secondary organic aerosol formation via multiphase partitioning with molecular data, *Environ. Sci. Technol.*, *40*, 4722-4731, 10.1021/es0522736.

Pye, H. O. T., and J. H. Seinfeld (2010), A global perspective on aerosol from low-volatility organic compounds, *Atmos. Chem. Phys.*, *10*(9), 4377-4401, 10.5194/acp-10-4377-2010.

Rao, S. T., S. Galmarini, and K. Puckett (2011), Air Quality Model Evaluation International Initiative (AQMEII): Advancing the State of the Science in Regional Photochemical Modeling and Its Applications, *Bulletin of the American Meteorological Society*, *92*, 23-30, 10.1175/2010BAMS3069.1.

Raventos-Duran, T., M. Camredon, R. Valorso, and B. Aumont (2010), Structure-activity relationships to estimate the effective henry's law coefficients of organics of atmospheric interest, *Atmos. Chem. Phys. Discuss.*, *10*, 4617-4647, 10.5194/acpd-10-4617-2010.

Real, E., and K. N. Sartelet (2011), Modeling of photolysis rates over europe: impact on chemical gaseous species and aerosols, *Atmos. Chem. Phys.*, *11*, 1711-1727, 10.5194/acp-11-1711-2011.

Robinson, A. L., N. M. Donahue, M. K. Shrivastava, E. A. Weitkamp, A. M. Sage, A. P. Grieshop, T. E. Lane, J. R. Pierce, and S. N. Pandis (2007), Rethinking organic aerosols: Semivolatile emissions and photochemical aging, *Science*, *315*, 1259–1262, 10.1126/science.1133061.

Robinson, N. H., J. F. Hamilton, J. D. Allan, B. Langford, D. E. Oram, Q. Chen, K. Docherty, D. K. Farmer, J. L. Jimenez, M. W. Ward, C. N. Hewitt, M. H. Barley, M. E. Jenkin, A. R. Rickard, S. T. Martin, G. McFiggans, and H. Coe (2011), Evidence for a significant proportion of secondary organic aerosol from isoprene above a maritime tropical forest, *Atmos. Chem. Phys.*, *11*, 1039-1050, 10.5194/acp-11-1039-2011.

Roeckner, E., R. Brokopf, M. Esch, M. Giorgetta, S. Hagemann, L. Kornblüh, L. E. Manzini, U. Schlese, and U. Schulzweida (2006), Sensitivity of simulated climate to horizontal and vertical resolution in the ECHAM5 atmosphere model, *J. Climate*, *19*, 3771-3791, 10.1175/JCLI3824.1.

Rollins, W. A., A. Kiender-Scharr, J. L. Fry, T. Brauers, S. S. Brown, H.-P. Dorn, W. P. Dubé, H. Fuchs, A. Mensah, T. F. Mentel, R. Tillmann, R. Wegener, P. J. Wooldridge, and R. C. Cohen (2009), Isoprene oxidation by nitrate radical: alkyl nitrate and secondary organic aerosol yields, *Atmos. Chem. Phys.*, *9*, 6685-6703, 10.5194/acp-9-6685-2009.

Roustan, Y., K. N. Sartelet, M. Tombette, É. Debry, and B. Sportisse (2010), Simulation of aerosols and gas-phase species over Europe with the Polyphemus system. Part II: Model sensitivity analysis for 2001, *Atmos. Environ.*, *44*, 4219-4229, 10.1016/j.atmosenv.2010.07.005.

Royer, P., P. Chazette, K. Sartelet, Q. J. Zhang, M. Beekmann, and J.-C. Raut (2011), Comparison of lidar-derived pm_{10} with regional modeling and ground-based observations in the frame of MEGAPOLI experiment, *Atmos. Chem. Phys.*, *11*, 10705-10726, 10.5194/acp-11-10705-2011.

Ruppert, L., and K. H. Becker (2000), A product study of the oh radical-initiated oxidation of isoprene: formation of C_5-unsaturated diols, *Atmos. Environ.*, *34*, 1529-1542, 10.1016/S1352-2310(99)00408-2.

Russell, A. G. (2008), EPA Supersites program-related emissions-based particulate matter modeling: initial applications and advances, *J. Air Waste Manage. Assoc.*, *58*, 289-302, 10.3155-1047-3289.58.2.289.

Russell, A. G., and R. Dennis (2000), NARSTO critical review of photochemical models and modeling, *Atmos. Environ.*, *34*, 2283-2324, 10.1016/S1352-2310(99)00468-9.

Russell, M., and D. T. Allen (2005), Predicting secondary organic aerosol formation rates in southeast Texas, *J. Geophys. Res.*, *110*, D07S17, 10.1029/2004JD004722.

Salamanca, F., A. Krpo, A. Martilli, and A. Clappier (2010), A new building energy model coupled with an urban canopy parameterization for urban climate simulations- Part I. formulation, verification, and sensitivity analysis of the model, *Theor. Appl. Climatol.*, *99*, 331-344, 10.1007/s00704-009-0142-9.

Saliba, N. A., S. Moussa, H. Salame, and M. El-Fadel (2006), Variation of selected air quality indicators over the city of Beirut, Lebanon: Assessment of emission sources, *Atmos. Environ.*, *40*, 3263-3268, 10.1016/j.atmosenv.2006.01.054.

Saliba, N. A., H. Kouyoumdjian, and M. Roumié (2007), Effect of local and long-range transport emissions on the elemental composition of $PM_{10-2.5}$ and $PM_{2.5}$ in Beirut, *Atmos. Environ.*, *41*, 6497-6509, 10.1016/j.atmosenv.2007.04.032.

Sartelet, K., E. Debry, K. Fahey, Y. Roustan, M. Tombette, and B. Sportisse (2007), Simulation of aerosols and gas-phase species over Europe with the Polyphemus system. Part I: model-to-data comparison for 2001, *Atmos. Environ.*, *41*, 6116-6131, 10.1016/j.atmosenv.2007.04.024.

Sartelet, K., H. Hayami, and B. Sportisse (2008), MICS Asia Phase II Sensitivity to the aerosol module, *Atmos. Environ.*, *42*(15), 3562-3570, doi:10.1016/j.atmosenv.2007.03.05.

Sartelet, K. N., F. Couvidat, C. Seigneur, and Y. Roustan (2012), Impact of biogenic emissions on air quality over Europe and North America, *Atmos. Environ.*, *53*, 131-141, 10.1016/j.atmosenv.2011.10.046.

Sarwar, G., D. Luecken, G. Yarwood, G. Z. Whitten, and W. P. L. Carter (2008), Impact of an updated carbon bond mechanism on predictions from the CMAQ modeling system: Preliminary assessment, *J. Appl. Meteor. Climatol.*, *47*, 3-14, 10.1175/2007JAMC1393.1.

Saxena, P., L. Hildemann, P. H. McMurry, and J. H. Seinfled (1995), Organics alter hygroscopic behavior of atmospheric particles, *J. Geophys. Res.*, *100*, 18755-18770, 10.1029/95JD01835.

Schauer, J. J., M. J. Kleeman, G. R. Cass, and B. R. T. Simoneit (1999), Measurement of emissions from air pollution sources. 2. C_1 through C_{30} organic compounds from medium duty diesel trucks, *Environ. Sci. Technol.*, *33*, 1578–1587, 10.1021/es980081n.

Schell, B., I. J. Ackermann, H. Hass, F. S. Binkowski, and A. Ebel (2001), Modeling the formation of secondary organic aerosol within a comprehensive air quality model system, *J. Geophys. Res.*, *106*, 28275-28293, 10.1029/2001JD000384.

Sciare, J., O. d'Argouges, Q. J. Zhang, R. Sarda-Estève, C. Gaimoz, V. Gros, M. Beekmann, , and O. Sanchez (2010a), Comparison between simulated and observed chemical composition of fine aerosols in Paris (France) during springtime: contribution of regional versus continental emissions, *Atmos. Chem. Phys.*, *10*, 11987-12004, 10.5194/acp-10-11987-2010.

Sciare, J., O. d'Argouges, Q. J. Zhang, R. Sarda-Estève, C. Gaimoz, V. Gros, M. Beekmann, and O. Sanchez (2010b), Comparison between simulated and observed chemical composition of fine aerosols in Paris (France) during springtime: contribution of regional versus continental emissions, *Atmos. Chem. Phys.*, *10*(24), 11987-12004, 10.5194/acp-10-11987-2010.

Sciare, J., O. D'Argouges, R. Sarda-Estève, C. Gaimoz, C. Dolgorouky, N. Bonnaire, O. Favez, B. Bonsang, and V. Gros (2011), Large contribution of water-insoluble secondary organic aerosols in the region of Paris (France) during wintertime, *J. Geophys. Res.*, *116*, D22203, 10.1029/2011JD015756.

Seigneur, C., and A. M. Wegrecki (1990), Mathematical modeling of cloud chemistry in the Los Angeles basin, *Atmos. Environ.*, *24A*, 989-1006.

Seigneur, C., P. Karamchandani, K. Lohman, K. Vijayaraghavan, and R.-L. Shia (2001), Multiscale modeling of the atmospheric fate and transport of mercury, *J. Geophys. Res.*, *106*, 27795-27809, 10.1029/2000JD000273.

Seinfeld, J. H., and S. N. Pandis (1998), *Atmospheric Chemistry and Physics*, Wiley-interscience.

Shaw, S. L., B. Gantt, and N. Meskhidze (2010), Production and emissions of marine isoprene and monoterpenes: A review, *Advances in Meteorology*, p. 408696, 10.1155/2010/408696.

Shiraiwa, M., M. Ammann, T. Koop, and U. Pöschl (2011), Gas uptake and chemical aging of semisolid organic aerosol particles, *Proc. Natl. Acad. Sci.*, *108*, 11003-11008, 10.1073/pnas.1103045108.

Shrivastava, M., J. Fast, R. Easter, W. I. Gustafson Jr., R. A. Zaveri, J. L. Jimenez, P. Saide, and A. Hodzic (2011), Modeling organic aerosols in a megacity: comparison of simple and complex representations of the volatility basis set approach, *Atmos. Chem. Phys.*, *11*, 6639-6662, 10.5194/acp-11-6639-2011.

Shrivastava, M. K., E. M. Lipsky, C. O. Stanier, and A. L. Robinson (2006), Modeling semivolatile organic aerosol mass emissions from combustion systems, *Environ. Sci. Technol.*, *40*, 2671-2677, 10.1021/es0522231.

Shrivastava, M. K., T. E. Lane, N. M. Donahue, S. N. Pandis, and A. L. Robinson (2008), Effects of gas particle partitioning and aging of primary emissions on urban and regional organic aerosol concentrations, *J. Geophys. Res.*, *113*, D18301, 10.1029/2007JD009735.

Simpson, D., W. Winiwarter, G. Börjesson, S. Cinderby, A. Ferreiro, A. Guenther, C. N. Hewitt, R. Janson, M. A. K. Khalil, S. Owen, T. E. Pierce, H. Puxbaum, M. Shearer, U. Skiba, R. Steinbrecher, L. Tarrason, and M. G. Oquist (1999), Inventorying emissions from nature in Europe, *J. Geophys. Res.*, *104*, 8113-8152, 10.1029/98JD02747.

Simpson, D., K. E. Yttri, Z. Klimont, K. Kupiainen, A. Caseiro, A. Gelencsér, C. Pio, H. Puxbaum, and M. Legrand (2007), Modeling carbonaceous aerosol over Europe: Analysis of the CARBOSOL and EMEP EC/OC campaigns, *J. Geophys. Res.*, *112*, D23S14, 10.1029/2006JD008158.

Skamarock, W. C., J. B. Klemp, J. Dubhia, D. O. Gill, D. M. Barker, M. G. Duda, X. Y. Huang, W. Wang, and J. G. Powers (2008a), A description of the advanced research WRF version 3, *Tech. Rep.*, NCAR Technical note-475+STR available at: `http://www.mmm.ucar.edu/wrf/users/docs/arw_v3.pdf`.

Skamarock, W. C., J. B. Klemp, J. Dudhia, D. O. Gill, D. M. Barker, M. G. Duda, X.-Y. H. W. Wang, and J. G. Powers (2008b), A description of the Advanced Research WRF version 3. NCAR Technical note, -475+STR, *Tech. Rep.*

Smoydzin, L., M. Fnais, and J. Lelieveld (2012), Ozone pollution over the Arabian Gulf: role of meteorological conditions, *Atmos. Chem. Phys. Discuss.*, *12*, 6331-6361, 10.5194/acpd-12-6331-2012.

Song, C., R. A. Zaveri, M. Alexander, J. A. Thornton, S. Madronich, J. V. Ortega, A. Zelenyuk, X.-Y. Yu, A. Laskin, and D. A. Maughan (2007), Effect of hydrophobic primary organic aerosols on secondary organic aerosol formation from ozonolysis of α-pinene, *Geophys. Res. Lett.*, *34*, L20803, 10.1029/2007GL030720.

Spittler, M., I. Barnes, I. Bejan, K. J. Brockmann, B. T., and K. Wirtz (2006), Reactions of NO_3 radicals with limonene and α-pinene: Product and SOA formation, *Atmos. Environ.*, *40*, S116-S127, 10.1016/j.atmosenv.2005.09.093.

Stavrakou, T., J. F. Müller, K. F. Boersma, I. De Smedt, and R. J. van der A (2008), Assessing the distribution and growth rates of NO_x emission sources by inverting a 10-year record of NO_2 satellite columns, *Geophys. Res. Lett.*, *35*, L10801, 10.1029/2008GL033521.

Steinbrecher, R., G. Smiatek, R. Köble, G. Seufert, J. Theloke, K. Hauff, P. Ciccioli, R. Vautard, and G. Curci (2009), Intra- and inter-annual variability of VOC emissions from natural and semi-natural vegetation in europe and neighbouring countries, *Atmos. Environ.*, *43*, 1380-1391, 10.1016/j.atmosenv.2008.09.072.

Stockwell, W. R., F. Kirchner, M. Kuhn, and S. Seefeld (1997), A new mechanism for regional atmospheric chemistry modeling, *J. Geophys. Res.*, *102*(D22), 25847-25879, 10.1029/97JD00849.

Struzewska, J., and J. W. Kaminski (2008), Formation and transport of photooxidants over Europe during the July 2006 heat wave - observations and GEM-AQ model simulations, *Atmos. Chem. Phys.*, *8*, 721-736, 10.5194/acp-8-721-2008.

Stull, R. B. (1988), *An introduction to boundary layer meteorology*, Kluwer Academic Publishers, Dordrecht.

Surratt, J. D., S. M. Murphy, J. H. Kroll, N. L. Ng, L. Hildebrandt, A. Sorooshian, R. Szmigielski, R. Vermeylen, W. Maenhaut, M. Claeys, R. C. Flagan, and J. H. Seinfeld (2006), Chemical composition of secondary organic aerosol formed from the photooxidation of isoprene, *J. Phys. Chem. A*, *110*, 9665-9690, 10.1021/jp061734m.

Surratt, J. D., A. W. H. Chan, N. C. Eddingsaas, M. N. Chan, C. L. Loza, A. J. Kwan, S. P. Hersery, R. C. Flagan, P. O. Wennberg, and J. H. Seinfeld (2010), Reactive intermediates revealed in secondary organic aerosol formation from isoprene, *Proc. Natl. Acad. Sci.*, *107*, 6640-6645, 10.1073/pnas.0911114107.

Suzuki, T., K. Ohtaguchi, and K. Koide (1992), Application of principal components analysis to calculate henry's constant from molecular structure, *Computers Chem.*, *16*, 41-52.

Svendby, T. M., M. Lazaridis, and K. Tørseth (2008), Temperature dependent secondary organic aerosol formation from terpenes and aromatics, *J. Atmos. Chem.*, *59*, 25-46, 10.1007/s10874-007-9093-7.

Szeremeta, E., P. Barzaghi, O. Böge, H. Herrmann, L. Gmachowski, and K. J. Rudzinski (2009), *Atmospheric composition change - Causes and Consequences - Local to Global*, chap. Aqueous-phase reactions of isoprene oxidation products with hydroxyl radicals, Aracne editrice S.r.l.

Szmigielski, R., J. D. Surratt, Y. Gómez-González, P. Van der Veken, I. Kourtchev, R. Vermeylen, F. Blockhuys, M. Jaoui, T. E. Kleindienst, M. Lewandowski, J. H. Offenberg, E. O. Edney, J. H. Seinfeld, W. Maenhaut, and M. Claeys (2007), 3-Methyl-1,2,3-butanetricarboxylic acid: An atmospheric tracer for terpene secondary organic aerosol, *Geophys. Res. Lett.*, *34*, L24811, doi:10.1029/2007GL031338.

Tilgner, A., and H. Herrmann (2010), Radical-drivencarbonyl-to-acid conversion and acid degradation in tropospheric aqueous systems studied by CAPRAM, *Atmos. Environ.*, *44*, 5415-5422, 10.1016/j.atmosenv.2010.07.050.

Troen, I. B., and L. Mahrt (1986), A simple model of the atmospheric boundary layer , sensitivity to surface evaporation, *Bound.-Lay. Meteorol.*, *37*, 129-148.

Tsimpidi, A. P., V. A. Karydis, M. Zavala, W. Lei, N. Bei, L. Molina, and S. N. Pandis (2011), Sources and production of organic aerosol in Mexico City: insights from the combination of a chemical transport model (PMCAMx-2008) and measurements during MILAGRO, *Atmos. Chem. Phys.*, *11*, 5153-5168, 10.5194/acp-11-5153-2011.

Tulet, P., A. Grini, R. J. Griffin, and S. Petitcol (2006), ORILAM-SOA: A computationally efficient model for predicting secondary organic aerosols in three-dimensional atmospheric models, *J. Geophys. Res.*, *111*, D23208, 10.1029/2006JD007152.

Turpin, B. J., and H.-J. Lim (2001), Species contributions to $PM_{2.5}$ mass concentrations: revisiting common assumptions for estimating organic mass, *Aerosol. Sci. Tech.*, *35*, 602-610, 10.1080/02786820119445.

Valorso, R., B. Aumont, M. Camredon, T. Raventos-Duran, C. Mouchel-Vallon, N. L. Ng, J. H. Seinfeld, J. Lee-Taylor, and S. Madronich (2011), Explicit modelling of SOA formation from α-pinene photooxidation: sensitivity to vapour pressure estimation, *Atmos. Chem. Phys.*, *11*, 6895-6910, 10.5194/acp-11-6895-2011.

van Pinxteren, D., A. Plewka, D. Hofmann, K. Müller, H. Kramberger, B. Svrcina, K. Bächmann, W. Jaeschke, S. Mertes, J. L. Collett Jr., and H. Herrmann (2005), Schmücke hill cap cloud and valley stations aerosol characterisation during FEBUKO (II): Organic compounds, *Atmos. Environ.*, *39*, 4305-4320, 10.1016/j.atmosenv.2005.02.014.

Vautard, R., M. D. Moran, E. Solazzo, R. C. Gilliam, V. Matthias, R. Bianconi, C. Chemel, J. Ferreira, B. Geyer, A. B. Hansen, A. Jericevic, M. Prank, A. Segers, J. D. Silver, J. Werhahn, R. Wolke, S. T. Rao, and S. Galmarini (2012), Evaluation of the meteorological forcing used for the Air Quality Model Evaluation International Initiative (AQMEII) air quality simulations, *Atmos. Environ.*, *53*, 15-37, 10.1016/j.atmosenv.2011.10.065.

Verwer, J. G., E. J. Spee, J. G. Bloom, and W. Hundsdorfer (1999), A second-order rosenbrock method applied to photochemical dispersion problems, *SIAM J. Sci. Comput.*, *20*, 1456-1480, 10.1137/S1064827597326651.

Vestreng, V. (2003), Review and revision. emission data reported to CLRTAP Tech. Rep., EMEP MSW-W, *Tech. Rep.*, Norwegian Meteorological Institute, Oslo, Norway.

Vijayaraghavan, K., C. Seigneur, P. Karamchandani, and S.-Y. Chen (2007), Development and application of a multi-pollutant model for atmospheric mercury deposition, *J. Appl. Meteorol. Climatol.*, *46*, 1341-1353, 10.1175/JAM2536.1.

Volkamer, R., P. J. Ziemann, and M. J. Molina (2009), Secondary organic aerosol formation from acetylene (c_2h_2): seed effect on SOA yields due to organic photochemistry in the aerosol aqueous phase, *Atmos. Chem. Phys.*, *9*, 1907-1928, 10.5194/acp-9-1907-2009.

Vutukuru, S., R. J. Griffin, and D. Dabdub (2006), Simulation and analysis of secondary organic aerosol dynamics in the south coast air basin of California, *J. Geophys. Res.*, *111*, D10S12, 10.1029/2005JD006139.

Waked, A., and C. Afif (2012), Emissions of air pollutants from road transport in Lebanon and other countries in the Middle East region, *Atmos. Environ.*, *61*, 446-452, 10.1016/j.atmosenv.2012.07.064.

Waked, A., C. Seigneur, F. Couvidat, Y. Kim, K. Sartelet, C. Afif, A. Borbon, P. Formenti, and S. Sauvage (2012a), Modeling air pollution in Lebanon: evaluation at a suburban site in Beirut, *Submitted to Atmos. Chem. Phys.*

Waked, A., C. Afif, and C. Seigneur (2012b), An atmospheric emission inventory of anthropogenic and biogenic sources for Lebanon, *Atmos. Environ.*, *50*, 88-96, 10.1016/j.atmosenv.2011.12.058.

Wang, L., R. Atkinson, and J. Arey (2007), Formation of 9,10-phenanthrenequinone by atmospheric gas-phase reactions of phenanthrene, *Atmos. Environ.*, *41*, 2025-2035, 10.1016/j.atmosenv.2006.11.008.

Wiedinmyer, C., B. Quayle, C. Geron, A. Belote, D. McKenzie, X. Zhand, S. O'Neill, and K. K. Wynne (2006), Estimating emissions from fires in north america for air quality modeling, *Atmos. Environ.*, *40*, 3419-3432, 10.1016/j.atmosenv.2006.02.010.

WRAP (2008), Western Regional Air Parternship, 2005. Development of 2000-04 baseline period and 2018 projection year emission inventories, Prepared by Air Sciences, Inc. Project No. 178-8, *Tech. Rep.*, Air Sciences, Inc., Golden, CO, USA.

Yarwood, G., S. Rao, M. Yocke, and G. Whitten (2005), Updates to the carbon bond chemical mechanism: CB05 final report to the US EPA, RT-0400675, available at: http://www.camx.com/publ/pdfs/CB05_Final_Report_120805.pdf.

Yasmeen, F., N. Sauret, J.-F. Gal, P.-C. Maria, L. Massi, W. Maenhaut, and M. Claeys (2010), Characterization of oligomers from methylglyoxal under dark conditions: a pathway to produce secondary organic aerosol through cloud processing during nighttime, *atmos. chem. phys.*, *10*, 3803-3812, 10.5194/acp-10-3803-2010.

Yaws, C., and H.-C. Yang (1992), *Henry's law constant for compound in water, in Thermodynamic and Physical Property Data*, C. L. Yaws, ed., Gulf Publishing Company, Houston, TX.

Yu, H., Y. Kaufman, M. Chin, G. Feingold, L. Remer, T. Anderson, Y. Balkanski, N. Bellouin, O. Boucher, S. Christopher, P. DeCola, R. Kahn, D. Koch, N. Loeb, M. Reddy, M. Schulz, T. Takemura, and M. Zhou (2006), A review of measurement-based assessments of the aerosol direct radiative effect and forcing, *Atmos. Chem. Phys.*, *6*, 616-666, 10.5194/acp-6-613-2006.

Yu, S., P. V. Bhave, R. L. Dennis, and R. Marthur (2007), Seasonal and regional variations of primary and secondary organic aerosols over the continental United States: Semi-empirical estimates and model evaluation, *Environ. Sci. Technol.*, *41*, 4690-4697, 10.1021/es061535g.

Zhang, Q., J. L. Jimenez, M. R. Canagaratna, J. D. Allan, H. Coe, I. Ulbrich, M. R. Alfarra, A. Takami, A. M. Middlebrook, Y. L. Sun, K. Dzepina, E. Dunlea, K. Docherty, P. F. De-Carlo, D. Salcedo, T. Onasch, J. T. Jayne, T. Miyoshi, A. Shimono, S. Hatakeyama, N. Takegawa, Y. Kondo, J. Schneider, F. Drewnick, S. Borrmann, S. Weimer, K. Demerjian, P. Williams, K. Bower, R. Bahreini, L. Cottrell, R. J. Griffin, J. Rautiainen, J. Y. Sun, Y. M. Zhang, and D. R. Worsnop (2007a), Ubiquity and dominance of oxygenated species in organic aerosols in anthropogenically-influence northern hemisphere mildlatitudes, *Geophys. Res. Lett.*, *34*, 10.1029/2007GL029979.

Zhang, Y., B. Pun, K. Vijayaraghavan, S.-Y. Wu, C. Seigneur, S. N. Pandis, M. Z. Jacobson, A. Nenes, and J. H. Seinfeld (2004), Development and application of the Model of Aerosol Dynamics, Reaction, Ionization, and Dissolution (MADRID), *J. Geophys. Res.*, *109*, D01202, 10.1029/2003JD003501.

Zhang, Y., P. Liu, B. Pun, and C. Seigneur (2006), A comprehensive performance evaluation of MM5-CMAQ for the summer 1999 southern oxidants study episode. Part I: Evaluation protocols, databases, and meteorological predictions, *Atmos. Environ*, *40*, 4825-4838, 10.1016/j.atmosenv.2005.12.043.

Zhang, Y., J.-P. Huang, D. K. Henze, and J. H. Seinfeld (2007b), Role of isoprene in secondary organic aerosol formation on a regional case, *J. Geophys. Res.*, *112*, D20207, 10.1029/2007JD008675.

Zhang, Y., M. K. Dubey, S. C. Olsen, J. Zheng, and R. Zhang (2009), Comparisons of WRF/Chem simulations in Mexico City with ground-based rama measurements during the 2006-MILAGRO, *Atmos. Chem. Phys.*, *9*, 3777-3798, 10.5194/acp-9-3777-2009.

Zhang, Y., Y. Pan, K. Wang, J. D. Fast, and G. A. Grell (2010a), WRF/Chem-MADRID: Incorporation of an aerosol module into WRF/Chem and its initial application to the TexAQS2000 episode, *J. Geophys. Res.*, *115*, D18202, 10.1029/2009JD013443.

Zhang, Y. Y., L. Müller, R. Winterhalter, G. K. Moortgat, T. Hoffmann, and U. Pöschl (2010b), Seasonal cycle and temperature dependence of pinene oxidation products, dicarboxylic acids and nitrophenols in fine and coarse air particulate matter, *Atmos. Chem. Phys.*, *10*, 7859-7873, 10.5194/acp-10-7859-2010.

Zuend, A., C. Marcolli, T. Peter, and J. H. Seinfeld (2010), Computation of liquid-liquid equilibria and phase stabilities: implications for rh-dependent gas/particle partitioning of organic-inorganic aerosols, *Atmos. Chem. Phys.*, *10*, 7795-7820, doi:10.5194/acpd-10-12497-2010.